

Turkish Journal of

# Analytical Chemistry

Volume 4

Issue 2

December 2022

w w w . t u r k j a c . o r g

Turkish Journal of  
**Analytical  
Chemistry**  
TurkJAC

Volume 4  
Issue 2  
December 2022

**Publication Type:** Peer-reviewed scientific journal

**Publication Date:** December 29, 2022

**Publication Language:** English

Published two times in a year (June, December)

## **Owner**

Prof. Miraç Ocak

Karadeniz Technical University, Faculty of Sciences, Department of Chemistry

## **Executive Editor**

Prof. Ümmühan Ocak

Karadeniz Technical University, Faculty of Sciences, Department of Chemistry

## **Co-Editor**

Ender Çekirge

Karadeniz Technical University, Institute of Forensic Sciences

## **Layout Editor**

Ender Çekirge

Karadeniz Technical University, Institute of Forensic Sciences

## **Editorial Secretary**

Ender Çekirge

Karadeniz Technical University, Institute of Forensic Sciences

## **Language Editors**

Prof. Miraç Ocak

Karadeniz Technical University, Faculty of Sciences, Department of Chemistry

Nurhayat Özbek

Karadeniz Technical University, Faculty of Sciences, Department of Chemistry

Aslıhan Yılmaz Çamoğlu

Karadeniz Technical University, Faculty of Sciences, Department of Chemistry

## **Proofreaders**

Nurhayat Özbek

Karadeniz Technical University, Faculty of Sciences, Department of Chemistry

Aslıhan Yılmaz Çamoğlu

Karadeniz Technical University, Faculty of Sciences, Department of Chemistry

Dr. Abidin Gümrükçüoğlu

Artvin Çoruh University, Faculty of Forestry, Department of Forestry  
Engineering

## **Editors**

Prof. Ümmühan Ocak

Karadeniz Technical University, Faculty of Sciences, Department of Chemistry

Prof. Miraç Ocak

Karadeniz Technical University, Faculty of Sciences, Department of Chemistry

Prof. Selehattin Yılmaz

Çanakkale Onsekiz Mart University, Faculty of Science and Literature,  
Department of Chemistry

Prof. Volkan Numan Bulut

Karadeniz Technical University, Maçka Vocational School, Department of  
Chemistry and Chemical Processing Technologies

Prof. Ali Gündođdu	Karadeniz Technical University, Maça Vocational School, Department of Pharmacy Services
Prof. Dilek Kul	Karadeniz Technical University, Faculty of Pharmacy, Department of Basic Pharmaceutical Sciences
Assoc. Prof. Fatma Ađın	Karadeniz Technical University, Faculty of Pharmacy, Department of Basic Pharmaceutical Sciences

## **Section Editors**

Prof. Salih Zeki Yıldız	Sakarya University, Faculty of Science and Literature, Department of Chemistry
-------------------------	--

## **Editor Board**

Prof. Selehattin Yılmaz	Çanakkale Onsekiz Mart University, Faculty of Science and Literature, Department of Chemistry
Prof. Celal Duran	Karadeniz Technical University, Faculty of Sciences, Department of Chemistry
Prof. Hakan Alp	Karadeniz Technical University, Faculty of Sciences, Department of Chemistry
Prof. Volkan Numan Bulut	Karadeniz Technical University, Maça Vocational School, Department of Chemistry and Chemical Processing Technologies
Prof. Ali Gündođdu	Karadeniz Technical University, Maça Vocational School, Department of Pharmacy Services
Asst. Prof. Aysel Bařođlu	Gümüşhane University, Faculty of Health Sciences, Department of Occupational Health and Safety
Prof. Ayşegül İyidođan	Gaziantep University, Faculty of Science and Literature, Department of Chemistry
Prof. Sevgi Kolaylı	Karadeniz Technical University, Faculty of Sciences, Department of Chemistry
Prof. Hüseyin Serencam	Trabzon University, College of Applied Sciences, Department of Gastronomy and culinary arts
Assoc. Prof. Fatma Ađın	Karadeniz Technical University, Faculty of Pharmacy, Department of Basic Pharmaceutical Sciences
Prof. Duygu Özdeř	Gümüşhane University, Gümüşhane Vocational School, Department of Chemistry and Chemical Processing Technologies
Dr. Mustafa Z. Özel	University of York, Department of Chemistry
Prof. Małgorzata Wiśniewska	University of Maria Curie- Sklodowska, Faculty of Chemistry, Institute of Chemical Sciences, Department of Radiochemistry and Environmental Chemistry
Prof. Dilek Kul	Karadeniz Technical University, Faculty of Pharmacy, Department of Basic Pharmaceutical Sciences

Prof. Sławomira Skrzypek	University of Lodz, Faculty of Chemistry, Department of Inorganic and Analytical Chemistry
Prof. Fatih İslamoğlu	Recep Tayyip Erdoğan University, Faculty of Science and Literature, Department of Chemistry
Asst. Prof. Zekeriyya Bahadır	Giresun University, Faculty of Science and Literature, Department of Chemistry
Asst. Prof. Yasemin Çağlar	Giresun University, Faculty of Engineering, Department of Genetic and Bioengineering
Prof. Agnieszka Nosal-Wiercińska	University of Maria Curie- Sklodowska, Faculty of Chemistry, Institute of Chemical Sciences, Department of Analytical Chemistry
Assoc. Prof. Dr. Halit Arslan	Gazi University, Faculty of Science, Department of Chemistry
Assoc. Prof. Cemalettin Baltacı	Gümüşhane University, Faculty of Engineering and Natural Sciences, Department of Food Engineering
Asst. Prof. Zafer Ocak	Kafkas University, Education Faculty, Mathematics and Science Education
Prof. Mustafa İmamoğlu	Sakarya University, Faculty of Science and Literature, Department of Chemistry
Assoc. Prof. Esra Bağda	Sivas Cumhuriyet University, Faculty of Pharmacy, Department of Basic Pharmaceutical Sciences, Analytical Chemistry Division
Assoc. Prof. Hüseyin Altundağ	Sakarya University, Faculty of Science and Literature, Department of Chemistry
Asst. Prof. Mehmet Başoğlu	Gümüşhane University, Faculty of Engineering and Natural Sciences, Department of Energy Systems Engineering

### **Publishing Board**

Prof. Latif Elçi	Pamukkale University, Faculty of Science and Literature, Department of Chemistry
Prof. Münevver Sökmen	Konya Food and Agriculture University, Faculty of Engineering and Architecture, Department of Bioengineering
Prof. Atalay Sökmen	Konya Food and Agriculture University, Faculty of Engineering and Architecture, Department of Bioengineering
Prof. Kamil Kaygusuz	Karadeniz Technical University, Faculty of Sciences, Department of Chemistry
Prof. Yaşar Gök	Pamukkale University, Faculty of Science and Literature, Department of Chemistry
Prof. Ayşegül Gölcü	İstanbul Technical University, Faculty of Science and Literature, Department of Chemistry
Prof. Mustafa Tüzen	Gaziosmanpaşa University, Faculty of Science and Literature, Department of Chemistry
Prof. Mustafa Soylak	Erciyes University, Faculty of Sciences, Department of Chemistry

Prof. Fikret Karadeniz	Kafkas University, Faculty of Science and Literature, Department of Chemistry
Prof. Mehmet Yaman	Firat University, Faculty of Sciences, Department of Chemistry
Prof. Halit Kantekin	Karadeniz Technical University, Faculty of Sciences, Department of Chemistry
Prof. Esin Canel	Ankara University, Faculty of Sciences, Department of Chemistry
Prof. Dilek Ak	Anadolu University, Faculty of Pharmacy, Department of Basic Pharmaceutical Sciences
Prof. Mustafa Küçükislamođlu	Sakarya University, Faculty of Science and Literature, Department of Chemistry
Prof. Salih Zeki Yıldiz	Sakarya University, Faculty of Science and Literature, Department of Chemistry
Prof. Recai İnam	Gazi University, Faculty of Sciences, Department of Chemistry
Prof. Dr. Durişehvar Ünal	İstanbul University, Faculty of Pharmacy, Department of Basic Pharmaceutical Sciences
Prof. Mehmet Tüfekçi	Avrasya University, Faculty of Science and Literature, Department of Biochemistry
Prof. Hüseyin Kara	Selçuk University, Faculty of Sciences, Department of Chemistry
Prof. Sezgin Bakirdere	Yıldız Technical University, Faculty of Science and Literature, Department of Chemistry
Prof. Hasan Basri Şentürk	Karadeniz Technical University, Faculty of Sciences, Department of Chemistry
Prof. Yusuf Atalay	Sakarya University, Faculty of Science and Literature, Department of Physics
Prof. Salih Zeki Yıldiz	Sakarya University, Faculty of Science and Literature, Department of Chemistry

**Authorship, Originality, and Plagiarism:** The authors accept that the work is completely original and that the works of others have been appropriately cited or quoted in the text with the necessary permissions. The authors should avoid plagiarism. It is recommended that they check the article using appropriate software such as Ithenticate and CrossCheck. The responsibility for this matter rests entirely with the authors. All authors will be notified when the manuscript is submitted. If a change of author is needed, the reason for the change should be indicated. Once the manuscript is accepted, no author changes can be made.

### **Aims and Scope**

“Turkish Journal of Analytical Chemistry” publishes original full-text research articles and reviews covering a variety of topics in analytical chemistry. Original research articles may be improved versions of known analytical methods. However, studies involving new and innovative methods are preferred. Topics covered include:

- Analytical materials
- Atomic methods
- Biochemical methods
- Chromatographic methods
- Electrochemical methods
- Environmental analysis
- Food analysis
- Forensic analysis
- Optical methods
- Pharmaceutical analysis
- Plant analysis
- Theoretical calculations
- Nanostructures for analytical purposes
- Chemometric methods
- Energy

### **ETHICAL GUIDELINES**

TurkJAC follows ethical tasks and responsibilities are defined by the Committee on Publication Ethics (COPE) in publication procedure. Based on this guide, the rules regarding publication ethics are presented in the following sections.

#### **Ethical Approval**

Ethics committee approval must be obtained for studies on clinical and experimental regarding human and animals that require an ethical committee decision, this approval must be stated in the article and documented in the submission. In such articles, the statement that research and publication ethics are complied with should include. Information about the approval such as committee name, date, and number should be included in the method section and also on the first/last page of the article.

#### **Editors**

1. In the preliminary evaluation of a submission, the editor of the journal evaluates the article's suitability for the purpose and scope of the journal, whether it is similar to other articles in the literature, and whether it meets the expectations regarding the language of writing. When it meets the mentioned criteria, the scientific evaluation process is started by assigning a section editor if necessary.
2. A peer-reviewed publication policy is employed in all original studies, taking into full account of possible problems due to related or conflicting interests.

3. Section editors work on the articles with a specific subject and their suggestion is effective in the journal editor's decision about acceptance or rejection of the article.
4. No section editor contacts anyone except the authors, reviewers, and the journal editor about articles in the continued evaluation process.
5. In the journal editor's decision to accept or reject an article, in the addition of section editor's suggestion in consequence of scientific reviewing, the importance of the article, clarity and originality are decisive. The final decision, in this case, belongs to the journal editor.

### **Authors**

1. The authors should actively contribute to the design and execution of the work. Authorship should not be given to a person who does not have at least one specific task in the study.
2. Normally all authors are responsible for the content of the article. However, in interdisciplinary studies with many authors, the part that each author is responsible for should be explained in the cover letter.
3. Before the start of the study, it would be better to determine the authors, contributors, and who will be acknowledged in order to avoid conflict in academic credits.
4. The corresponding author is one of the authors of the article submitted to the journal for publication. All communications will be conducted with this person until the publication of the article. The copyright form will be signed by the corresponding author on all the authors' behalf.
5. It is unacceptable to submit an article that has already been published entirely or partly in other publication media. In such situation, the responsibility lies with all authors. It is also unacceptable that the same article has been sent to TurkJAC and another journal simultaneously for publication. Authors should pay attention to this situation in terms of publication ethics.
6. Plagiarism from others' publications or their own publications and slicing of the same study is not acceptable.
7. All authors agree that the data presented in the article are real and original. In case of an error in the data presented, the authors have to be involved in the withdraw and correction process.
8. All authors must contribute to the peer-reviewed procedure.

### **Reviewers**

1. Peer reviewers worked voluntarily are external experts assigned by editors to improve the submitted article.
2. It is extremely important that the referee performs the review on time so that the process does not prolong. Therefore, when the invitation is agreed upon, the reviewer is expected to do this on time. Also, the reviewer agrees that there are no conflicts of interest regarding the research, the authors, and/or the research funders.
3. Reviewers are expected not to share the articles reviewed with other people. The review process should be done securely.
4. Reviewers are scored according to criteria such as responding to the invitations, whether their evaluations are comprehensive and acting in accordance with deadlines, and the article submissions that they can make to TurkJAC are handled with priority.

# Contents

## Research Articles

- A Simple and High Throughput Methodology for Simultaneous Determination of Levodopa and Carbidopa 52–58  
*İrem Aydın Kırılancı, Kemal Volkan Özdokur\*, Fatma Nil Ertas*
- Electrochemical and liquid chromatographic analysis of triamcinolone acetonide in pharmaceutical formulations 59–66  
*Nuray Denizhan, Selehattin Yılmaz\*, Gülşen Sağlıkoğlu, Emrah Kılınç, Çiğdem Yengin, Fatma Gülay Der*
- Determination of physical, chemical and antioxidant properties of pomegranate sauces sold in Turkish markets 67–75  
*Yunus Emre Kamış, Bülent Akar\*, Cemalettin Baltacı*
- Determination of Ethylenediaminetetraacetic acid (EDTA) levels in surface waters by high performance liquid chromatography (HPLC)-Ultraviolet/Visible (UV/VIS) detector 76–79  
*Oltan Canlı\*, Barış Güzel, Kartal Çetintürk*
- Fast pyrolysis of fig leaves: influence of pyrolysis parameters and characterization of bio-oil 80–87  
*Turgay Kar, Sedat Keleş\*, Zafer Emir, Kamil Kaygusuz*
- Electroanalytical analysis of guaifenesin from pharmaceuticals on boron doped diamond electrode 88–93  
*Fatma Ağın\*, Gökçe Öztürk, Dilek Kul*
- Heavy metal pollution from listwaenitization: In case of Alakeçi Bayramıç-Çanakkale/West Türkiye) 94–102  
*Alaaddin Vural*
- Development and validation of RPLC method for the simultaneous analysis of ACE inhibitors in tablet formulations 103–110  
*Erdem Kuzucanlı, Ebru Çubuk Demiralay\*, Y. Doğan Daldal, Zehra Üstün, İlkay Konçe, Güleren Alsancak*
- The effect of silicon phthalocyanine on cell death and mitochondrial membrane potential in pancreatic cancer cells 111–115  
*Hakkı İsmail Kaya, Ceren Boguslu, Esra Kabak, Çağla Akkol, Ece Tugba Saka\*, Selcen Celik-Uzuner*
- Investigation of interaction of Bismarck Brown Y-palladium complex with AS1411 G-Quadruplex aptamer 116–122  
*Esra Bağda\*, Rümeyza Durak, Efsan Bağda, Didem Duman, Ebubekir Ayhan*
- Determination of LC-MS/MS phenolic profile, antioxidant activity and  $\alpha$ -glucosidase enzyme inhibition of *Linum mucronatum* Bertol. subsp. *armenum* (Bordz.) P.H.Davis 123–130  
*Fatma KILIÇ, Zeynep AKAR\**



# A simple and high throughput methodology for simultaneous determination of levodopa and carbidopa

İrem Aydın Kırlangıç<sup>1</sup> , Kemal Volkan Özdokur<sup>2\*</sup> , Fatma Nil Ertaş<sup>1</sup> 

<sup>1</sup>Ege University, Science Faculty, Chemistry Department, 35100, İzmir, Türkiye

<sup>2</sup>Erzincan Binali Yıldırım University, Science&Letter Faculty, Chemistry Department, 24002, Erzincan, Türkiye

## Abstract

Parkinson's disease (PD) is a degenerative disorder of the central nervous system. The motor symptoms of PD disease result from the death of dopamine-generating cells in a region of the mid brain and the dopamine precursor levodopa (L-Dopa) is used for the treatment. Carbidopa (Car) is administered in association with L-Dopa in pharmaceutical formulation as an inhibitor on the decarboxylase activity. Thus, their simultaneous determination is of great importance because of their co-existence in pharmaceutical preparations. Present study deals with a simple method development for simultaneous voltammetric determination of L-Dopa and Car at a pencil graphite electrode (PGE) via monitoring the reduction peak of L-Dopa and the second oxidation peak of Car. The developed method exhibited a linear range for L-Dopa and Car between 0.29 – 3.06 and 0.22 – 3.3  $\mu\text{M}$  and the limit of detection was calculated as 0.096 and 0.073  $\mu\text{M}$  for L-Dopa and Car, respectively. The sensitivity of the method was found comparable to other methods depending on the sophisticated electrode modifications and the limits of detection were calculated as sub micromolar levels.

**Keywords:** Levodopa, carbidopa, pencil graphite electrode, assay method, differential pulse voltammetry

## 1. Introduction

Pharmaceuticals play an important part in human health; however, these compounds serve their purpose only if they are given in an appropriate amount and do not contain impurities. [1]. Every step of the process, starting with the development of a new molecule, up to clinical trials to reveal the optimum dose, requires analytical methods to monitor drug interaction and quality control purposes. Therefore, pharmaceutical analyzes require fast, precise, and selective methods with high efficiency to analyze trace amounts and screening approaches in mixtures [2].

Chromatographic methods have been widely used for quantitative and qualitative analysis of drug substances in tablets and biological fluids. Recently, liquid chromatography with tandem mass spectrometry (LC-MS/MS) is the method of choice in many laboratories [3]. As an economical alternative to the chromatographic techniques, voltammetric methodologies are emerging that offer high precision, accuracy, and precision for many analytical applications. In the past two decades, several review articles have been presented in the field of drug analysis using solid

electrodes [5] and carbonaceous materials for electrode fabrication [4]. Gupta and co-workers have reviewed the voltammetric techniques for drug analysis to assess the performance of various electrodes and surface-active agents in determination [6]. In particular, pencil graphite electrodes are promising materials for drug analysis [7].

Levodopa (L-Dopa, L-3,4-dihydroxyphenylalanine) is the precursor of catecholamines produced via biosynthesis from L-tyrosine. L-Dopa is commonly known as the drug used for Parkinson's disease, but its activity suffers from its conversion to dopamine by a decarboxylation process [8,9]. Since a small amount of L-Dopa can be transported across the cerebral tissue to the central nervous system, another reagent is required for inhibiting the decarboxylase activity. Car has widely served for this purpose, and it is administered with L-Dopa for the treatment [10]. Consequently, their simultaneous analysis is important task in pharmaceutical quality control purposes.

Due to the electroactive nature of catecholamines, voltammetric methods are widely used for their determinations in pharmaceutical formulations [11].

**Citation:** İ.A. Kırlangıç, K.V. Özdokur, F.N. Ertaş, A simple and high throughput methodology for simultaneous determination of levodopa and carbidopa, Turk J Anal Chem, 4(2), 2022, 52–58.

**\*Author of correspondence:** vozdokur@gmail.com.tr

**Tel:** + 90 (446) 224 30 32 / 40019

**Fax** + 90 (446) 224 30 16

**Received:** May 20, 2022

**Accepted:** August 14, 2022

 <https://doi.org/10.51435/turkjac.1119121>

For complex sample matrices, on the other hand, electrochemical methods are prone to interferences and often require special precautions. In addition, electrochemical behavior of catecholamines may differ significantly due to minor changes in their structure allowing us to determine these compounds simultaneously. Accordingly, carbon paste electrode (CPE) modified by meso-tetrakis (3-methylphenyl) cobalt porphyrin (CP) and TiO<sub>2</sub> nanoparticles was utilized for this purpose [12]. In a more recent study the carbon paste electrode was functionalized with NiFe<sub>2</sub>O<sub>4</sub> nanoparticle and 2-(4-ferrocenyl-[1,2,3]triazol-1-yl)-1-(naphthalen-2-yl) ethanone for simultaneous determination of Car and L-Dopa [13]. For glassy carbon electrode (GCE) this selectivity was maintained by covering the electrode with a Nafion film, which is selective for Car in the presence of L-Dopa [14].

Alternatively, the GCE has been modified with graphene nanosheets by chemically reducing graphene oxide by using hydrazine allowing the simultaneous analysis of L-Dopa and Car in micromolar levels [15]. Chemometric approach can also be a solution for the peak convolution issue and an analytical method based the partial least-squares algorithm enabled the simultaneous determination of L-Dopa, Car and benserazide in pharmaceutical formulations [16]. However, in real sample analysis, other precautions should be considered. Beitollah et al have developed a CPE containing of multiwall carbon nanotubes (MWCNT) and an ionic liquid (1-methyl-3-butylimidazolium bromide) which showed good electrocatalytic effect on Car by shifting the potential in negative direction in comparison to the bare CPE and increasing the peak potential as well [17]. It was also reported that the stability of the CPE was enhanced greatly due to the introduction of ionic liquid as a binder. The sensor was successfully applied for the determination of Car in human urine and serum and the interference of ascorbic acid was minimized by using ascorbic oxidase enzyme.

Although proper modification of the electrodes provides the desired selectivity and sensitivity by changing the peak potentials and enhancing the peak formation, modification procedures are often more complex, and it is rather difficult to maintain reproducible surfaces in fabrication. On the other hand, PGE provides an inexpensive alternative to other carbonaceous electrodes due to its low background current along with high electrochemical reactivity [18]. Since these electrodes can be readily used by eliminating time-consuming cleaning and polishing processes, PGEs are widely utilized in detection of a wide variety of electroactive species [19,20] and in developing genosensors [21].

In this study, a simple and sensitive voltammetric method was developed for the simultaneous determination of L-Dopa and Car in pharmaceutical formulations. To the best of our knowledge, this is the first study dealing with the simultaneous determination of L-Dopa and Car by using the PGEs without any modification and not requiring further chemo-metric modelling for achieving required selectivity. The anodic and cathodic peak were both used for quantification of Car and L-Dopa with aid of Differential pulse voltammetry (DPV) technique. Two different PGEs were utilized for the purpose and their response was evaluated in terms of sensitivity and selectivity.

## 2. Materials and methods

All chemicals were of analytical grade. L-Dopa (99.98%) and Car (99.83%) were purchased from Sigma Aldrich. Stock solutions of L-Dopa and Car were prepared in 0.01 M chloroacetic acid solution. Sinemet 25/250 mg tablets were purchased from a local drug store. The chloroacetic acid was purchased from Merck and 0.01 M chloroacetic acid solution was used for buffer preparation along with the 3.0 M NaOH solution.

The developed sensor was used for the quantification of L-Dopa and Car in Sinemet 25 / 250 mg tablets with the aid of standard addition method. Briefly, Sinemet 25 / 250 mg tablet was ground into fine particles by using agate mortar and a 1.000 g portion of tablets were weighted precisely. Ultrapure water: methanol mixture (1:1, v/v) is added into the beaker and placed into an ultrasonic bath for the extraction of active substances and filtered through the Teflon syringe filter. Then, the filtrate was added into the cell for voltammetric measurement. Subsequently, known amount of standard solution of L-Dopa and Car was added into the same cell three times. The obtained peak currents were plotted against to added concentration and sample concentrations were calculated extrapolated the obtained curve the concentration axis.

Electrochemical measurements were recorded with Metrohm PGST 204 Potentiostat equipped with conventional three electrodes system. In typical experiment, Ag / AgCl (sat'd. KCl), platinum wire was used as the reference and counter electrode, respectively. Faber 0.7 / 2B pencil graphite electrode denoted as PGE-A, and Tombow 0.3 / HB pencil lead denoted as PGE-B were used as the working electrodes. Chloroacetic acid buffer was used during electrochemical measurements. The potential was cycled between -0.5 and 1.0 V at a scan rate of 50 mV/s during the cycling voltammetry scan.

All measurements were tripled for obtaining a steady state current. Differential pulse voltammetric

measurements were carried out in a range of 0 – 1.0 V at a rate of 10 mV/s and pulse amplitude was set as 25 mV.

### 3. Results and Discussion

#### 3.1. Voltammetric behavior of L-Dopa and carbidopa

Initial studies were devoted to reveal voltammetric behavior of L-Dopa and Car at both electrodes at pH 2.0 chloroacetic acid buffer solution. Cyclic voltammograms (CVs) of  $2.54 \times 10^{-4}$  M L-Dopa recorded at PGE-A and PGE-B at a scan rate of 50 mV/s reflect the differences in the chemical composition of both graphite materials (Fig. 1a). CVs recorded at former electrode have revealed a quasi-reversible peak formation at 0.57 V and a corresponding cathodic peak at 0.39 V while, rather small but closer peak formations were observed for the latter electrode having the peak potentials of 0.46 and 0.42 V for anodic and cathodic processes, respectively. The mineral content that gives the hardness of the PGE-B could be responsible for the reversible behaviors of both analytes while the polymeric content of PGE-A results in more analytes to attach onto the surface.

For  $2.21 \times 10^{-4}$  M Car on the other hand, two oxidation peaks with equal heights have been observed at 0.58 V and 0.95 V at PGE-A (Fig. 1b), with a very small cathodic counterpart in agreement with a previous study at a GCE [22]. For PGE-B, the subsequent oxidation peak potentials were 0.44 V and 0.82 V, where the first peak was higher than the second peak. Considering the higher sensitivity for L-Dopa, PGE-A was chosen for further studies.

Since the electrochemical behaviors of L-Dopa and Car are dependent on the pH of the solution, the influence of the medium pH on these peak characteristics was investigated. Fig. 2 has shown that the peak potentials of L-Dopa have shifted into more negative potentials as the pH increases, and irreversible electrode reactions have been observed in alkaline media. For Car, on the other hand, irreversible electrode process has been observed for all pHs and the peak potentials of the anodic peaks have given linear curves with the pH with the slopes of -42 and -64 mV pH<sup>-1</sup>, respectively, suggesting that the reaction mechanism includes equal number of proton and electron evolved during the oxidation processes [23]. The peak currents were also altered with the solution pH as expected. Since the highest peak currents have been observed at pH 2.0 for both compounds, this medium pH was selected for further studies.

Analytical characteristics of the method for L-Dopa and Car were studied by recording DP voltammograms individually at pH 2.0 chloroacetic acid medium.

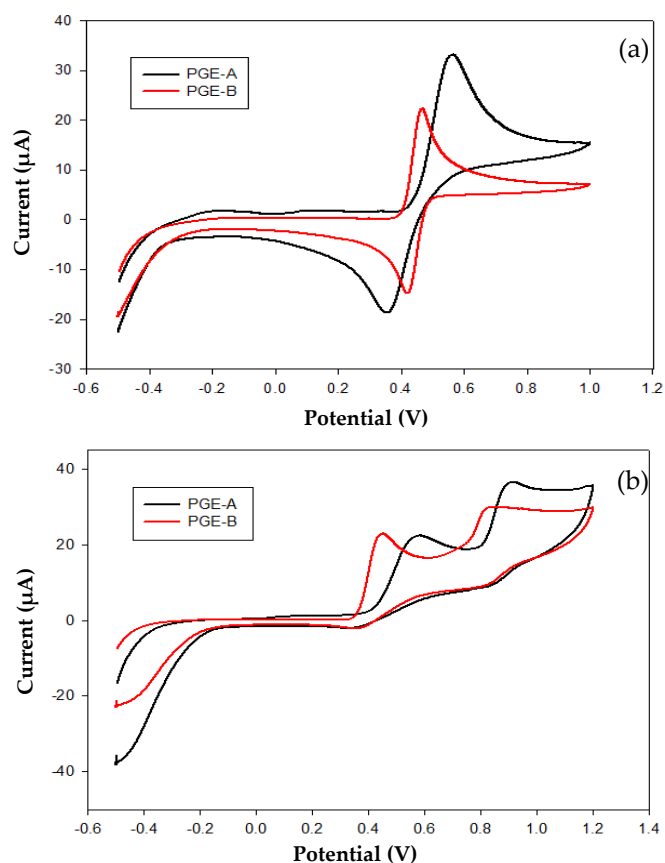


**Figure 1.** Cyclic voltammetric behavior of (a)  $2.54 \times 10^{-4}$  M L-Dopa and (b)  $2.21 \times 10^{-4}$  M Car in pH 2.0 chloroacetic acid buffer at two different PGEs at 50 mV/s scan rate

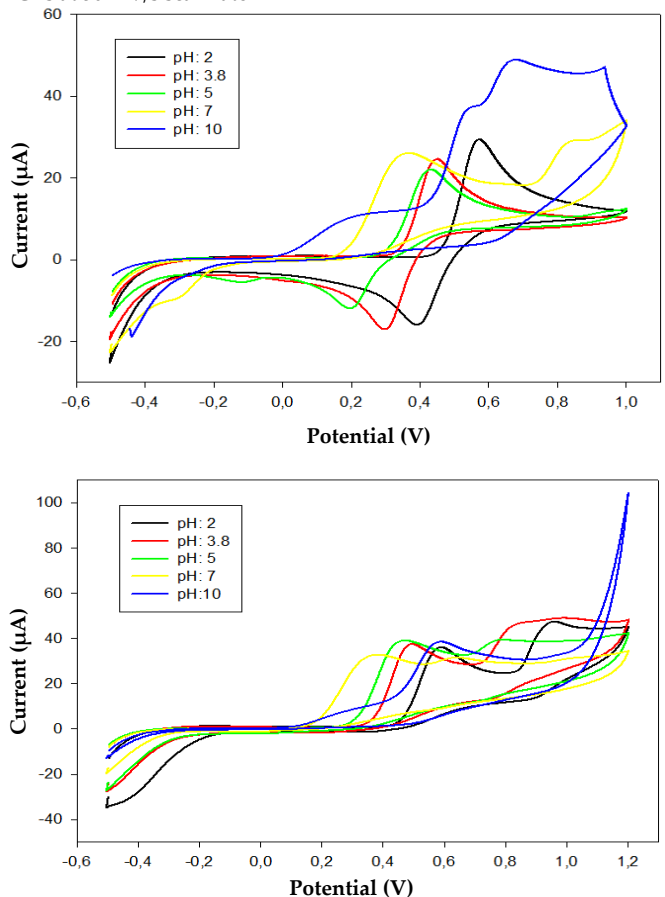


**Figure 2.** The influence of the medium pH on the cyclic voltammetric behaviour of a)  $2.54 \times 10^{-4}$  M L-Dopa and b)  $2.21 \times 10^{-4}$  M Car at PGE-A at a scan rate of 50 mV/s

**Table 1.** Analytical merits of the individual voltammetric analysis of the analytes

	Measured Peak	Dynamic range	Equation	LOD / LOQ	RSD (%)	Recovery
L-Dopa	Anodic peak at 0.42 V	$2.9 \times 10^{-7} - 2.8 \times 10^{-6}$ M	$y = 0.00275x - 0.0034$ $R^2 = 0.9947$	LOD: $0.88 \times 10^{-7}$ M LOQ: $2.90 \times 10^{-7}$ M	$8.26 \times 10^{-7}$ M: 3.54% $1.94 \times 10^{-6}$ M: 4.63%	$8.26 \times 10^{-7}$ M: 86.81% $1.94 \times 10^{-6}$ M: 93.68%
	Cathodic peak at 0.45 V	$2.9 \times 10^{-7} - 3.06 \times 10^{-6}$ M	$y = 0.0011x - 0.0055$ $R^2 = 0.9915$	LOD: $0.88 \times 10^{-7}$ M LOQ: $2.90 \times 10^{-7}$ M	$8.26 \times 10^{-7}$ M: 6.67% $1.94 \times 10^{-6}$ M: 5.08%	$8.26 \times 10^{-7}$ M: 83.75% $1.94 \times 10^{-6}$ M: 90.37%
Car	Anodic peak at 0.46 V	$6.54 \times 10^{-7} - 1.94 \times 10^{-6}$ M	$y = 0.0138x - 0.0012$ $R^2 = 0.9901$	LOD: $1.98 \times 10^{-7}$ M LOQ: $6.54 \times 10^{-7}$ M	$8.26 \times 10^{-7}$ M: 16.8% $1.94 \times 10^{-6}$ M: 7.49%	$8.26 \times 10^{-7}$ M: 76.0% $1.94 \times 10^{-6}$ M: 90.4%
		$2.25 \times 10^{-6} - 3.29 \times 10^{-6}$ M	$y = 0.0293x - 0.0189$ $R^2 = 0.9936$			
	Anodic peak at 0.82 V	$6.54 \times 10^{-7} - 1.60 \times 10^{-6}$ M	$y = 0.0301x + 0.0042$ $R^2 = 0.9758$	LOD: $1.98 \times 10^{-7}$ M LOQ: $6.54 \times 10^{-7}$ M	$8.26 \times 10^{-7}$ M: 0.79% $1.94 \times 10^{-6}$ M: 2.23%	$8.26 \times 10^{-7}$ M: 92.67% $1.94 \times 10^{-6}$ M: 96.23%
		$1.94 \times 10^{-6} - 3.29 \times 10^{-6}$ M	$y = 0.0462x - 0.0311$ $R^2 = 0.9656$			

For L-Dopa, both anodic and cathodic peak currents have been employed for constructing the calibration curve and a linear relation between anodic peak current at 0.42 V in the concentration range of  $2.9 \times 10^{-7} - 2.8 \times 10^{-6}$  M (S-1). The repeatability of the electrode was tested by measuring the samples spiked with  $8.26 \times 10^{-7}$  and  $1.94 \times 10^{-6}$  M L-Dopa with taking account the anodic peak and relative standard deviation (RSD) was found less than 5% (Table 1).

Cathodic scan has also yielded a linear calibration graph for L-Dopa by monitoring the cathodic peak at 0.45 V in the concentration range of  $2.9 \times 10^{-7} - 3.1 \times 10^{-6}$  M (S - 2). Limit of detection (LOD) and limit of quantification (LOQ) was calculated based on a signal-to-noise ratio ( $S / N = 3$ ) and the limit of quantitation (LOQ) was determined to be 3.3 times the LOD. On the other hand, two linear segments were found for two oxidation peaks of Car in the concentration range studied in agreement with former studies [13]. The fact that the decrease in the slope of the second linear segment is likely due to kinetic limitation [18]. For the first anodic peak at 0.46 V, the calibration curve was linear in the range of  $6.54 \times 10^{-7} - 1.94 \times 10^{-6}$  M while the other calibration graph was drawn in a rather narrow concentration range in micromolar level (S-3). The equations and other characteristics of the curve were listed in the Table 1. The accuracy of the individual analysis method was tested by analyzing quality control samples and the satisfactory recoveries were obtained for both analytes.

### 3.2. Simultaneous determination of L-Dopa and carbidopa

As can be deduced from the above studies, the anodic peak of L-Dopa at 0.42 V overlaps with the first anodic peak of Car at 0.46 V, which makes it difficult their simultaneous determination. Considering the irreversible behavior of Car in the potential range studied, L-Dopa can be determined free from the interference of Car in their binary mixture, by monitoring its reduction peak. A previous study utilized

this peak for sensitive determination of L-Dopa without the interference of Car but, they could manage to determine the Car upon coating the electrode with a selective Nafion film. Here, by taking the advantage of sensitive determination of Car through using the both anodic peaks in micromolar levels, the second peak at 0.82 V which is laid down on the potential region was utilized for quantization free from the interference of L-Dopa.

Calibration studies have been repeated with binary mixtures for controlling the selectivity of the method. The cathodic peak of L-Dopa in micromolar level was recorded in pH 2.0 chloroacetic acid buffer solution by scanning the potential in DPV mode between 0.8 and 0 V at a rate of 10 mV/s and Car was added in equal concentrations into the cell to see any interference. No significant change was observed in the cathodic peak of L-Dopa. Here, the concentration ratio of the analytes may be important on the other peak formation. Considering that the method is intended to be applied to commercial formulations which contain 25 mg Carbidopa and 250 mg Dopa in dosages, the ratio of 1:10 was adopted.

The calibration curve was constructed for L-Dopa in a concentration range of  $1.0 \times 10^{-5} - 2.0 \times 10^{-4}$  M ( $R^2$ : 0.9894). Reproducibility was studied for  $5.0 \times 10^{-5}$  M L-Dopa concentration, and the mean signal was calculated as  $0.1183 \pm 0.01607$   $\mu$ A. The RSD value was calculated as 13.58% for the studied concentration. The mean background current was calculated as 0.0055  $\mu$ A and the LOD and LOQ values were calculated as  $3.58 \times 10^{-6}$  M and  $1.19 \times 10^{-5}$  M, respectively.

Fig. 3 shows the DP voltammograms of Car in pH 2.0 chloroacetic acid buffer solution upon addition of standard solution containing tenfold concentration of L-Dopa. The first anodic peak at 0.55 V is the overlapped peak obtained for both L-Dopa and Carbidopa, and the second anodic peak given inset belongs to Car alone.

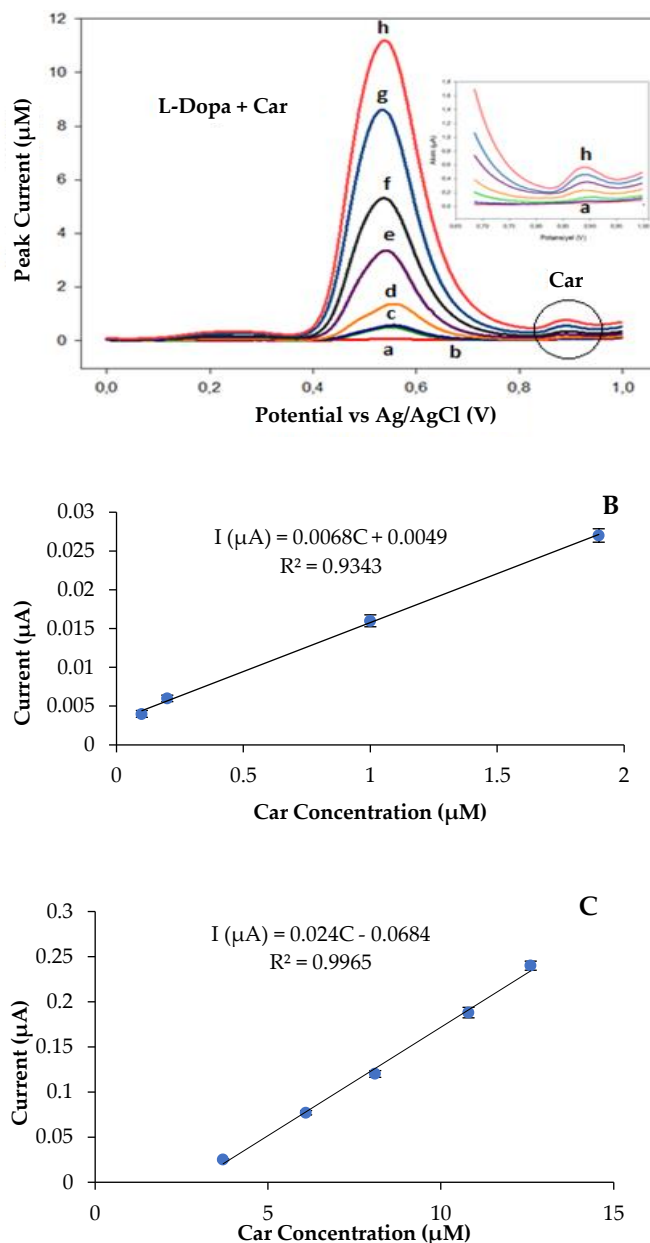


**Figure 3.** A) DP voltammograms recorded at 10 mV/s scan rate in pH 2.0 chloroacetic acid buffer upon addition of standard solution containing tenfold concentration of L-Dopa to be a)  $2.0 \times 10^{-7}$  M, b)  $9.88 \times 10^{-7}$  M, c)  $1.94 \times 10^{-6}$  M, d)  $3.73 \times 10^{-6}$  M, e)  $6.13 \times 10^{-6}$  M, f)  $8.05 \times 10^{-6}$  M, g)  $1.08 \times 10^{-5}$  M, h)  $1.26 \times 10^{-5}$  M Car in the cell and B) the lower range and C) higher range calibration curves drawn for the second anodic peak of Car.

Again, two linear calibration curves have been observed for the Car in the concentration ranges of  $2.0 \times 10^{-7}$ – $1.94 \times 10^{-6}$  M ( $R^2$ : 0.9343) and  $3.73 \times 10^{-6}$ – $1.26 \times 10^{-5}$  M ( $R^2$ : 0.9971). Reproducibility was studied for low, medium and high concentration levels of the calibration graph and for  $3.73 \times 10^{-6}$  M, the RSD was estimated as 6.97% while it was calculated as 6.43% for  $8.05 \times 10^{-6}$  M. Higher concentrations for Car ( $1.26 \times 10^{-5}$  M) has resulted an RSD of % 4.29 which is in the acceptable limits. The LOD and LOQ values were calculated as  $1.24 \times 10^{-7}$  M and  $4.13 \times 10^{-7}$  M, respectively. The accuracy of the method was tested by recovery measurements. Recovery was calculated for 84% for  $3.73 \times 10^{-6}$  M, 97% for  $8.05 \times 10^{-6}$  M and 98% for  $1.26 \times 10^{-5}$  M.

**Table 2.** Analytical merits of the standard addition method for the commercial tablet analysis

Parameter	L-Dopa	Car
Dynamic range	$1.01 \times 10^{-6}$ – $1.81 \times 10^{-4}$ M	$2.9 \times 10^{-7}$ – $1.3 \times 10^{-5}$ M
Equation	$y = 0.4452x + 0.0169$	$y = 0.0314x - 0.0209$
$R^2$	0.9956	0.9849
LOD	$0.3 \times 10^{-7}$ M	$1.0 \times 10^{-7}$ M
LOQ	$1.01 \times 10^{-6}$	$2.9 \times 10^{-7}$ M
Labeled value	$4.80 \times 10^{-6}$ M	$4.20 \times 10^{-7}$ M
Measured value	$5.19 \times 10^{-6}$ M	$3.92 \times 10^{-7}$ M
%Recovery	108.12%	93.33%
Confidence Interval ( $\alpha=0.05$ , $n=3$ )	89.2 – 111.8 %	86.8 – 113.2 %
Precision (RSD%)	( $1.01 \times 10^{-6}$ M)	( $2.9 \times 10^{-7}$ M)
Intraday	6.43	7.21
Interday	7.71	8.95

### 3.3. Method application

Overall results have indicated that a disposable bare pencil lead electrode can be used for simultaneous determination of Car and L-Dopa sensitively and selectively. The performance of developed method was applied for commercial tablets. The tablet was homogenized and prepared as described above. Then, the sample solution was transferred to the electrochemical cell for subsequent determination. The DP anodic scan was initiated from 0.8 to 0.0 V and the cathodic peak signals of L-Dopa was recorded upon standard addition onto the sample solution. In order to avoid the possible matrix effect of Sinemet tablet excipients, standard addition method was used for sample application. Table 2 shows the obtained results and the recovery values for the Sinemet tabled studied.

The comparison of the developed sensor with the literature was given in Table 3. The proposed electrode exhibits great sensitivity towards to L-Dopa and Car. The LOD and LOQ values are comparable with those studies which use electrode modifiers. Since, the other studies have modifiers, the sensor developed is found more economic, less hazardous for environment and ready to use without time consuming fabrication.

## 4. Conclusion

Present study describes a practical solution for the overlapped peaks of Car and L-Dopa which are important to be determined simultaneously in commercial tablets. A disposable pencil graphite electrode was utilized as the electrode via monitoring the reduction peak of L-Dopa and the second oxidation peak of Car without any significant interference. Even though the LOD calculated for individual analytes are sub micromolar levels, in their binary mixtures the electrode performance was found comparable with the modified electrodes as given in Table 3.

**Table 3.** Comparison of the performances of the electrochemical methods developed for simultaneous analysis of Car and / or L-Dopa

Analyte	Matrix	Detection Method	Electrode	Linear Range	LOD	Reference
L-Dopa Car	Water, Urine, Blood serum	DPV	Coumarin derivative / TiO <sub>2</sub> / IL / CPE	0.10 – 900 μM 20.0 – 900 μM	41 nM 0.38 μM	[9]
L-Dopa Car	Water, Urine Blood serum Pharmaceutical tablets	DPV	Meso-tetrakis (3-methyl phenyl) (CP) / TiO <sub>2</sub> NPs / CPE	0.1 – 100 μM —	69 ± 2 nM —	[12]
L-Dopa Car Benserazide	Pharmaceutical tablets	DPV / Multivariate calibration	GCE	110–1300 μM 31– 470 μM 31–620 μM	5.12 μM 2.16 μM 2.77 μM	[16]
L-Dopa Car Tryptophan	Pharmaceutical tablets	CV	EBNBH/CNT CPE	0.2 – 700 μM —	0.094 μM 7.2 μM 12.3 μM	[22]
L-Dopa Car Droxidopa	Urine, Blood serum	SWV	CNT / 5-amino-2'-ethyl-biphenyl-2-ol / CPE	0.2 – 700 μM 0.12 – 225 μM	— 50 nM	[24]
L-Dopa Car Uric acid Folic acid	Pharmaceutical tablets, Urine, Blood serum	SWV	DHB / AuNPs / RGO / GCE	0.05–1200 μM — —	0.018 μM — —	[25]
L-Dopa Car Uric acid Folic acid	Urine	SWV	MWCNT / CPE	0.09– 400 μM — —	0.071 μM — —	[26]
L-Dopa Car	pharmaceutical formulations	DPV	lead dioxide immobilized in a polyester resin	260 – 1200 μM 32 – 150 μM	25 μM 3.7 μM	[27]
L-Dopa Car	Pharmaceutical tablets	DPV	PGE	1.01–18.1 x10 <sup>-5</sup> M 0.98–8.05 μM	2.72 μM 0.44 μM	Present Study

CPE: Carbon paste electrode, EBNBH: 2, 2'-[1,2-ethanediybis (nitriolethylidene)]-bis-hydroquinone, CP: cobalt porphyrin, TiO<sub>2</sub> NPs: Titanium dioxide nanoparticles, IL: ionic liquid, DHB: 2-(3,4-dihydroxyphenyl benzothiazole), AuNPs: Gold nanoparticles, RGO: Reduced graphene oxide, MWCNT: multiwalled carbon nanotube, PGE: Pencil graphite electrode, SWV: Square wave voltammetry, CV: Cyclic voltammetry

## Acknowledgement:

Authors would like to thank Ege University Research Project (2014 FEN 056) for financial support.

## References

- [1] M.R. Siddiqui, Z.A. Al Othman, N. Rahman, Analytical techniques in pharmaceutical analysis: A review, *Arab J Chem*, 10, 2017, 1409–1421.
- [2] M.S. Lee, E.H. Kerns, LC/MS applications in drug development, *Mass Spectrom Rev* 18, 1999, 187– 279.
- [3] L. Ge, S. P. Li, G. Lisak, Advanced sensing technologies of phenolic compounds for pharmaceutical and biomedical analysis, *J Pharm Biomed Anal*, 1795, 2020, 112913.
- [4] S.A. Özkan, B. Uslu, H.Y. Aboul-Enein, Analysis of pharmaceuticals and biological fluids using modern electroanalytical techniques, *Crc Rev Anal Chem*, 33(3), 2003, 155–181.
- [5] B. Uslu, S.A. Ozkan, Electroanalytical application of carbon based electrodes to the pharmaceuticals, *Anal Lett*, 40, 2006, 817–853.
- [6] V.K. Gupta, R. Jain, K. Radhapyari, N. Jadon, S. Agarwal, Voltammetric techniques for the assay of pharmaceuticals--a review, *Anal Biochem*, 408, 2011, 179–196.
- [7] R.R. Sawkar, V.B. Patil, M.M. Shanbhag, N. P. Shetti, S.M. Tuwar, T.M. Aminabhavi, Detection of ketorolac drug using pencil graphite electrode, *Biomed Eng Adv*, 2, 2021, 100009.
- [8] A. Antonini, A. Yegin, C. Preda, L. Bergmann, W. Poewe, Global long-term study on motor and non-motor symptoms and safety of levodopa-carbidopa intestinal gel in routine care of advanced Parkinson's disease patients; 12-month interim outcomes, *Parkinsonism Relat D*, 21, 2014, 231–35.
- [9] M.M. Ardakani, A. Khoshroo, Nano composite system based on coumarin derivative–titanium dioxide nanoparticles and ionic liquid: Determination of levodopa and carbidopa in human serum and pharmaceutical formulations, *Anal Chim Acta*, 798, 2013, 25–32.
- [10] F. Bugamelli, C. Marcheselli, E. Barba, M.A. Raggi, Determination of L-Dopa, carbidopa, 3-O-methyl-dopa and entacapone in human plasma by HPLC–ED, *J Pharmaceut Biomed*, 54, 2011, 562–567.
- [11] K.V. Ozdokur, E. Engin, C. Yengin, H. Ertas, F.N. Ertas, Determination of Carbidopa, Levodopa, and Droxidopa by High-Performance Liquid Chromatography-Tandem Mass Spectrometry, *Anal Lett*, 51(1–2), 2017, 73–82.
- [12] M. Ardakani, Z. Taleat, A. Khoshroo, H. Beitollahi, H. Dehghani, Electrocatalytic oxidation and voltammetric determination of levodopa in the presence of carbidopa at the surface of a nanostructure based electrochemical sensor, *Biosens Bioelectron*, 35 (115), 2012, 75–81.
- [13] S.Z. Mohammadia, H. Beitollahi, M. Kaykhai, N. Mohammadzadeh, S. Tajik, R. Hosseinzadeh, Simultaneous determination of droxidopa and carbidopa by carbon paste electrode functionalized with NiFe<sub>2</sub>O<sub>4</sub> nanoparticle and 2-(4-ferrocenyl-[1,2,3] triazol-1-yl)-1-(naphthalen-2-yl) ethanone, *Measurement*, 155, 2020, 107522.
- [14] M.S.M. Quintino, M. Yamashita, L. Angnes, Voltammetric Studies and Determination of Levodopa and Carbidopa in Pharmaceutical Products, *Electroanal*, 18, 2006, 655–661
- [15] Q. Wang, M.R. Das, M. Li, R. Boukherroub, S. Szunerits, Voltammetric detection of L-Dopa and carbidopa on graphene modified glassy carbon interfaces, *Bioelectrochemistry*, 93, 2013, 15–22.
- [16] C. Zapata-Urzuá, M. Pérez-Ortiz, M. Bravo, A.C. Olivieri, A. Álvarez-Lueje, Simultaneous voltammetric determination of levodopa, carbidopa and benserazide in pharmaceuticals using multivariate calibration, *Talanta*, 82, 2010, 962–968.
- [17] H. Beitollah, M. Goodarziyan, M.A. Khalilzadeh, H. Karimi-Maleh, M. Hassanzadeh, M. Tajbakhsh, Electrochemical behaviors and determination of carbidopa on carbon nanotubes ionic liquid paste electrode, *J Mol Liq*, 173, 2012, 137–143.
- [18] I.G. David, D.E. Popa, M. Buleandra, Pencil graphite electrodes: a versatile tool in electroanalysis, *J Anal Methods Chem*, 2017, 1905968.
- [19] A. Dehnavi, A. Soleymanpour, Highly sensitive voltammetric electrode for the trace measurement of methyl-dopa based on a

- pencil graphite modified with phosphomolibdate/graphene oxide, *Microchem J*, 157, 2020, 104969.
- [20] L. Liv, N. Nakiboğlu, Simple and rapid voltammetric determination of boron in water and steel samples using a pencil graphite electrode, *Turk J Chem*, 40, 2016, 412 – 421.
- [21] M. Özsoz, A. Erdem, K. Kerman, D. Ozkan, B. Tugrul, N. Topcuoglu, H. Ekren, M. Taylan, Electrochemical genosensor based on colloidal gold nanoparticles for the detection of factor v leiden mutation using disposable pencil graphite electrodes, *Anal Chem*, 75 (9), 2003, 2181–2187.
- [22] M.M. Ardakani, B.Ganjipour, H. Beitollahi, M.K. Amini, F. Mirkhalaf, H. Naeimi, M.N. Barzoki, Simultaneous determination of levodopa, carbidopa and tryptophan using nanostructured electrochemical sensor based on novel hydroquinone and carbon nanotubes: Application to the analysis of some real samples, *Electrochim Acta*, 56, 2011, 9113– 9120.
- [23] K.V. Özdokur, Voltammetric determination of isoniazid drug in various matrix by using cuox decorated mw-cnt modified glassy carbon electrode, *Electroanalysis* 2020, 32, 489 –495.
- [24] S. Tajik, M. A. Taher, H. Beitollahi, Simultaneous determination of droxidopa and carbidopa using a carbon nanotube paste electrode, *Sensor Actuat B-Chem*, 188, 2013, 923– 930.
- [25] A. Benvidi, A. D. Firouzabadi, M. M. Ardakani, B. B. F. Mirjalili, R. Zare, Electrochemical deposition of gold nanoparticles on reduced graphene oxide modified glassy carbon electrode for simultaneous determination of levodopa, uric acid and folic acid, *J Electroanal Chem*, 736, 2015, 22–29.
- [26] N. Rastakhiz, H. Beitollahi, A. Kariminik, F. Karimi, Voltammetric determination of carbidopa in the presence of uric acid and folic acid using a modified carbon nanotube paste electrode, *J M Liq*, 172, 2012, 66–70.
- [27] H. C. de Melo-Ana, P. D. S. Wagner, L. Polito, O. Fatibello-Filho, I. C. Vieira, Simultaneous differential pulse voltammetric determination of L-Dopa and carbidopa in pharmaceuticals using a carbon paste electrode modified with lead dioxide immobilized in a polyester resin, *J Braz Chem Soc*, 18, 2007, 797–803.

## Electrochemical and liquid chromatographic analysis of triamcinolone acetonide in pharmaceutical formulations

Nuray Denizhan<sup>1</sup> , Selehattin Yılmaz<sup>1\*</sup> , Gülşen Sağlıkoğlu<sup>1</sup> , Emrah Kılınç<sup>2</sup> , Çiğdem Yengin<sup>3</sup> , Fatma Gülay Der<sup>2</sup> 

<sup>1</sup> Çanakkale Onsekiz Mart University, Faculty of Science, Department of Chemistry, 17020, Çanakkale, Türkiye

<sup>2</sup> Ege University, Faculty of Pharmacy, Department of Analytical Chemistry, 35100, İzmir, Türkiye

<sup>3</sup> Ege University, Faculty of Pharmacy, Department of Pharmaceutical Chemistry, 35100, İzmir, Türkiye

### Abstract

The electrochemical reduction of triamcinolone acetonide on the pencil graphite electrode (PGE) surface was firstly investigated by cyclic voltammetry (CV). The dependence of the cathodic peak current and peak potential on different pHs and scan rates was investigated. The current type was determined as adsorption controlled. 0.067 M phosphate (pH 4.50 to pH 7.50), 0.2 M acetate (pH 3.50 to 5.50) and 0.04 M Britton Robinson (BR; pH 2.00 to 12.00) buffers were employed as supporting electrolytes. The scan rate studies were realized in the range of 25 – 1000 mV/s (vs. Ag/AgCl). The maximum peak current was observed in the 0.04 M BR buffer (pH 3.50). The peak current increased and shifted to more cathodic values with the increasing scan rate. The logarithm of the peak current ( $\log I_p$ ) versus the logarithm of the scan rate ( $\log v$ ) showed linear regression with the equation  $\log I_p (\mu A) = 0.8395 \log v (mV/s) - 0.8386$  and the correlation coefficient ( $r = 0.9761$ ). The slope of the  $\log v$ - $\log I_p$  curve was close to 1.0, which indicated that the electrode reaction was adsorption controlled, as desirable. The linear range was  $1 \times 10^{-7} - 5 \times 10^{-5}$  M, the sensitivity was  $1.3347 \mu A/M$ , and the limit of detection (LOD) and the limit of quantification (LOQ) were  $3.18 \times 10^{-8}$  M and  $1.00 \times 10^{-7}$  M, respectively. HPLC-PDA analysis was performed with H<sub>2</sub>O:MeOH (28:72, v/v) as mobile phases A and B at a flow rate of 1 mL/min at 242 nm. The method validation studies were conducted in accordance with the ICH Q2(R1) guideline, and the corresponding results were summarized in tables. The HPLC-PDA method displayed linearity in the concentration range of 0.1 – 50  $\mu g/mL$  ( $2.3 \times 10^{-7} - 1.15 \times 10^{-4}$  M) with LOD and LOQ values as 0.017  $\mu g/mL$  ( $3.992 \times 10^{-8}$  M) and 0.0561  $\mu g/mL$  ( $1.29 \times 10^{-7}$  M), respectively.

**Keywords:** Triamcinolone acetonide, voltammetry, HPLC-PDA, pencil graphite electrode

### 1. Introduction

Triamcinolone acetonide, 9-fluoro-11,16,17,21-tetrahydroxy-1,4-pregnadien-3,20-dion (TA), is a synthetic halogenated cyclic ketal pregnane corticosteroid used to treat various disorders such as skin inflammations, mouth sores, various joint conditions, and allergic rhinitis (Fig. 1).

The systematic administration of glucocorticoids is on the ban list by the World Anti-Doping Agency (WADA) and the International Olympic Committee (IOC) due to their feature of both creating toxicological risks and enhancing sports performance. Synthetic glucocorticoids, including TA, are also included in the list of the doping agents [1,2]. The analysis of pharmaceutical active substances from commercial forms is preferably conducted by analytical techniques. TA was determined in pharmaceutical dosage forms and

biological samples by liquid chromatography (HPLC and LC-MS/MS) [3–8], gas chromatography (GC) [9], spectrophotometry [10–12], and electrochemical techniques (voltammetry) [13,14].

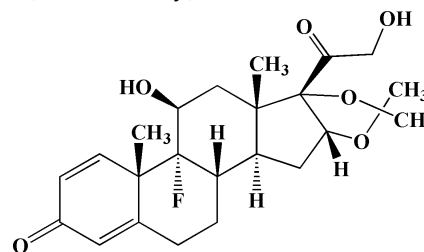


**Figure 1.** Structural formula of TA

It was shown in the literature that corticosteroids had 2 reducible electroactive groups, which are C-3 and C-20 carbonyl groups. Goyal et al. explained that the

**Citation:** N.B. Denizhan, S. Yılmaz, G. Sağlıkoğlu, E.B. Kılınç, Ç. Yengin, F.G. Der, Electrochemical and liquid chromatographic analysis of triamcinolone acetonide in pharmaceutical formulations, Turk J Anal Chem, 4(2), 2022, 59–66.

 <https://doi.org/10.51435/turkjac.1132742>

**\*Author of correspondence:** seleyilmaz@hotmail.com

**Tel:** +90 (286) 218 00 18 → 22191

**Fax** +90 (286) 218 39 17

**Received:** June 16, 2022

**Accepted:** October 2, 2022

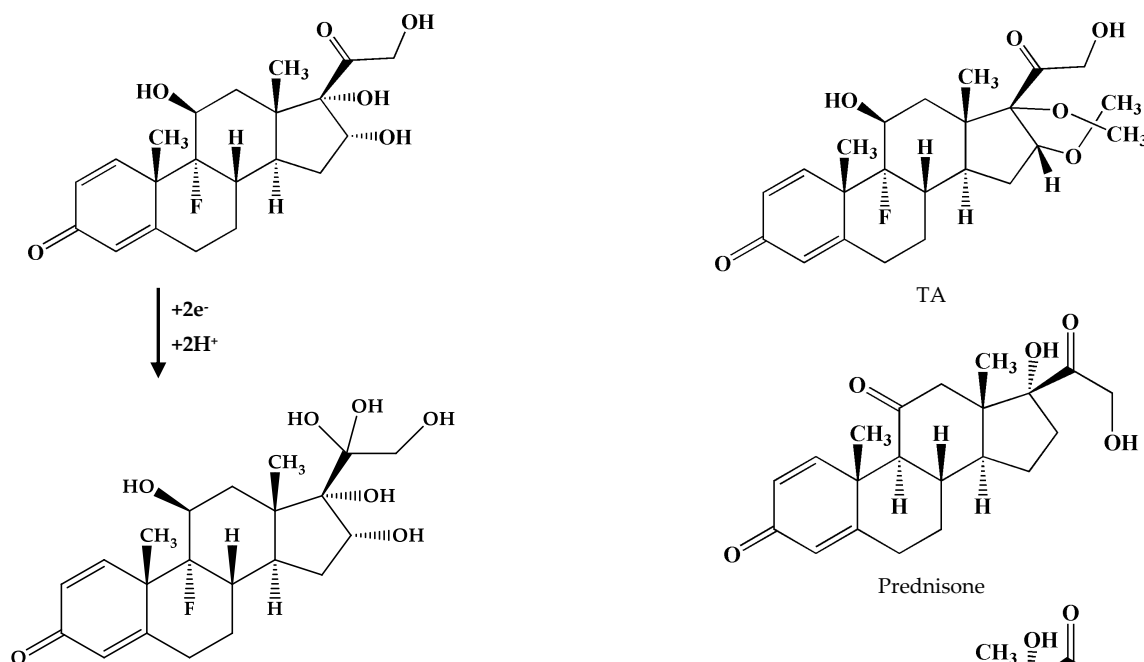


**Figure 2.** Tentative mechanism given in the literature [14,15] for the cathodic reduction of TA

carbonyl group of TA was being reduced and that this group was also activated by the C-16 and C-17 hydroxyl groups. Goyal proposed the following mechanism (Fig. 2), explaining that the reduction occurred with  $2e^-$  and  $2H^+$  as a result of experimental information [14,15].

Many studies were carried out in various supporting electrolyte to explain the reducing properties of corticosteroids. Kabasakalian and McGlotten studied prednisone, prednisolone, cortisone, and hydrocortisone in 50% ethanol solutions at pH of 5.5. They suggested that the value of  $n$  for the reduction of these compounds was between 0.9 and 1.0. In the reduction of the C-3 carbonyl group, dimerization occurred after radical formation [16]. The chemical structures of TA and the other investigated compounds in the literature are given in Fig. 3.

A few studies have been found in the literature for the analysis of TA by electrochemical methods. These are, in summary, as follows:

Hammam [13], have developed a determination of triamcinolone acetonide in pharmaceutical formulation and human serum by adsorptive cathodic stripping voltammetry (AdCSV). Under optimized conditions, the stripping voltammetric peak current of TA showed a linear dependence on TA concentration over the range  $1 \times 10^{-9} - 9 \times 10^{-8}$  M. The detection limit (LOD) was  $3 \times 10^{-10}$  M, and the quantitation limit (LOQ) was  $1 \times 10^{-9}$  M.

Vehdi et al. [14], have developed a determination of triamcinolone acetonide steroid on glassy carbon electrode by stripping voltammetric methods. An adsorption-controlled well-defined reduction peak was observed in all pH conditions. A calibration plots

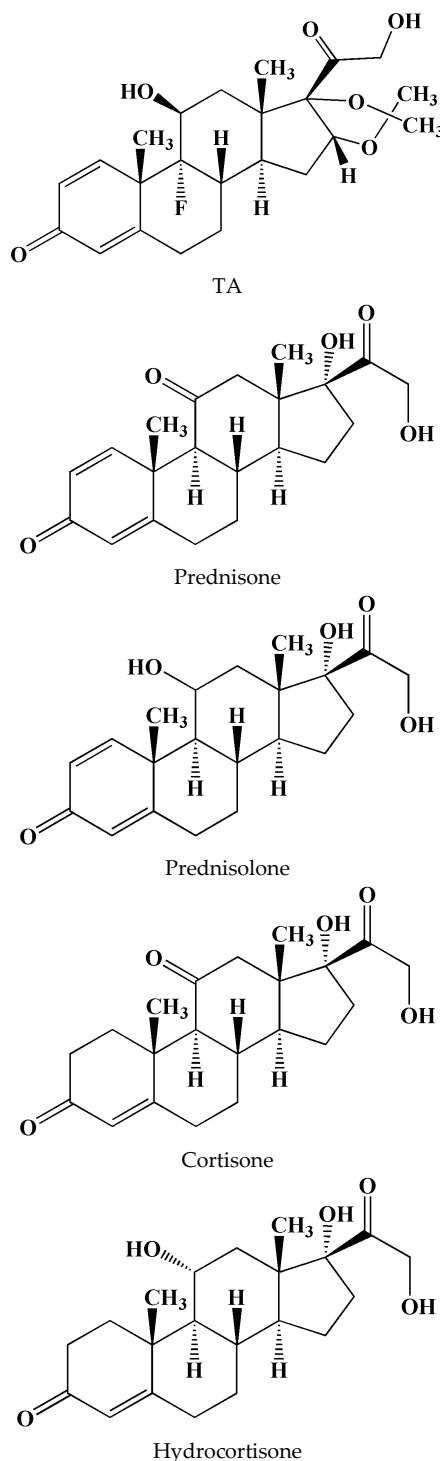


**Figure 3.** The chemical structures of TA and the other investigated compounds in literature

was derived, and the lower limit of determination observed are  $0.1 \mu\text{g/mL}$  from DPSV and  $0.01 \mu\text{g/mL}$  from SWSV.

Zagrzewski et al. [17], have developed an electrochemical behavior of TA on the carbon paste electrodes for its voltammetric determination.

The calibration plot was found linear in the concentration from 2 to  $46 \mu\text{mol/L}$ , the detection limit was  $1.5 \mu\text{mol/L}$ . Unlike the literature, PGE was applied for the first time in this study.

In the current study, the electrochemical and chromatographic analysis of triamcinolone acetonide was carried out in commercial pharmaceutical dosage forms. The aim of the voltammetric study is to determine TA for the first time using a pencil graphite electrode (PGE) because of its advantages such as being easily accessible, inexpensive, disposable, and high reproducibility compared to the literature. The chromatographic method was also applied for the accuracy of the electrochemical method.

## 2. Materials and methods

### 2.1. Reagents

TA standard and its pharmaceutical forms were obtained from DEVA Inc.. All chemicals used were analytical-reagent grade. Methanol, which was used as a HPLC mobile phase component, was of gradient grade for liquid chromatography (LiChrosolv, 99.9%) and was obtained from Merck KGaA (Germany). Ultrapure water used in the preparation of aqueous mobile phase B had a total organic carbon level <10 ppb and a total ion resistance > 18.2 MΩ cm and was produced freshly and used without storage by Elix Milli-Q Gradient A10 Ultrapure Water System (Millipore company).

### 2.2. Apparatus

A Metrohm 757 VA Trace Analyzer (Herisau, Switzerland) model instrument was used for voltammetric measurements, with a three-electrode system consisting of PGE as the working electrode, a platinum wire as the auxiliary electrode, and Ag/AgCl (KCl 3 mol/L, Metrohm) as the reference electrode. Tombow 0.5 mm HB model mechanical pencil refills were used as the PGE working electrode. Argon (Ar) gas was passed from supporting electrolyte solution (5 min) and after addition each sample (60 s) to remove oxygen. pH measurements were carried out with EZDO-5011A model (Herisau, Switzerland) pH-meter at 15 to 20 °C for laboratory temperature.

The HPLC-PDA hardware used during the chromatographic analysis was Ultimate-3000 series HPLC system of Thermo-Dionex Company, and consisted of solvent tray (SR3000), integrated online degasser and high-pressure gradient pump (LPG3400SD), derivative autosampler (WPS3000TSL), column compartment (TCC3000SD) and PDA detector (DAD3000) modules. The HPLC hardware was operated with the Chromeleon (v.6.80 SR13) chromatographic data acquisition software. The analytical column used for separation was Macherey-Nagel MN 250/4.6 Nucleosil C18 100-5μ (Serial No: 2065339, Batch No. 21302092).

### 2.3. Procedure

#### 2.3.1. Electrochemical analysis

The electrochemical properties of TA were investigated by voltammetric techniques. In order to detect the experimental conditions for the analysis of the electrochemical reduction of TA, 0.067 M phosphate (pH 4.50 to pH 7.50), 0.2 M acetate (pH 3.50 to 5.50) and 0.04 M BR (pH 2.00 to 12.00) buffers were used to support the electrolytes. Kenacort-A ampoule was supplied from Deva Inc. (İstanbul, Turkey).  $1 \times 10^{-2}$  and  $1 \times 10^{-3}$  M TA stock solutions were prepared in methanol and stored in the refrigerator. Kenacort-A ampoule was dissolved in methanol.  $1 \times 10^{-2}$ ,  $1 \times 10^{-3}$ , and  $1 \times 10^{-4}$  M of stock solutions were prepared in methanol. The solutions liquor was put into cell. The amount of TA in the Kenacort-A ampoule was calculated from the corresponding equations in the calibration plots. The drug sample analysis was performed by differential pulse adsorptive stripping voltammetry DPAdSV. Pulse amplitude 50 mV, pulse time 0.04 s and voltage step 0.009 V were selected for DPAdSV parameters. Potential step 10 mV and scan rate were selected in the between 25 – 1000 mV/s for CV.

#### 2.3.2. HPLC measurements

Various mobile phase solvent ratios, wavelengths, flow rates and retention time were studied for the optimization of the chromatographic parameters.  $1 \times 10^{-3}$  M stock solution of TA was prepared in methanol. The diluted standard solutions were prepared by diluting the stock solution with appropriate volume of the mobile phase. The optimum conditions among them were determined as A and B during the HPLC-PDA analysis were H<sub>2</sub>O:MeOH (28:72, v/v) at a flow rate of 1 mL/min. 190 – 400 nm spectrums were collected while the absorption was acquired at 242 nm with the PDA detector and the retention time was assigned as 3.52 min. Then, standard solutions in the range of 0.1 – 50 ppm were prepared from stock solutions, and the calibration curve with 9 points (0.1, 0.25, 0.50, 1.0, 2.5, 5.0, 10.0, 25.0, and 50.0 ppm) was plotted. 2D and 3D chromatograms of 5 ppm TA standard is given Fig. 9, where the retention time was assigned as 3.52 min. The developed method was validated in accordance with the ICH Q2(R1) guideline, and the corresponding results were summarized in tables. The HPLC-PDA method displayed linearity in the concentration range of 0.1 – 50 μg/mL ( $2.3 \times 10^{-7}$  –  $1.15 \times 10^{-4}$  M) with limit of detection (LOD) and limit of quantification (LOQ) values as  $3.992 \times 10^{-8}$  and  $1.29 \times 10^{-7}$  M, respectively. Two different products (Kenacort-A ointment and Kenacort-A injection) were used for sample analysis. While preparing the ointment sample, 1.0 grams of ointment was weighed and dissolved in 50 mL of methanol. It was stirred for 3 hours at room temperature with a magnetic

stirrer in a sealed container at 400 rpm. Thus, 20 ppm sample solution was prepared and vialled, and injected into HPLC after filtering through coarse filter paper. While preparing the ampoule sample, 50  $\mu\text{L}$  suspension was taken directly from the prepared ampoule and completed to 50 mL with methanol. Thus, a sample solution of 40 ppm was prepared, and this solution prepared was injected into HPLC. Different extraction methods, such as magnetic stirrer and ultrasonic bath, were used in drug analyzes.

### 3. Results and discussion

#### 3.1. Electrochemical analysis of TA

The electrochemical reduction of TA was studied in various supporting electrolytes (pH 2 – 12). The stock solution of TA ( $1 \times 10^{-3}$  M) was prepared with bi-distilled water. DPAdSV voltammograms of  $5 \times 10^{-5}$  M TA was taken in these electrolytes. The maximum peak signal was observed in the 0.04 M BR buffer (pH 3.50). Therefore, this buffer and pH was chosen for further studies. The CV measurements were performed with  $5 \times 10^{-5}$  mol/L TA at scan-rates of 25 – 1000 mV/s on a PGE in 0.04 mol/L BR buffer at pH 3.50 (Fig. 4) The peak current values increased with the increase of the scan rates. The peak potential values shifted to more positive values with the increase of the scan rate. This indicates that the reduction is easier at higher scan rates. In order to determine the type of current, the logarithm of the peak current ( $\log I_p$ ) versus the logarithm of the scan rate ( $\log v$ ) was plotted. The linear regression equation was obtained as  $\log I_p (\mu\text{A}) = 0.8395 \log v (\text{mV/s}) - 0.8386$  with the correlation coefficient of ( $r$ ) 0.9761. The slope of this equation was close to 1.0. This value indicates that the electrode reaction was adsorption controlled.

#### 3.2. The effect of deposition time and deposition potential

The effect of deposition time and deposition potential on the peak current was given in Fig. 5 and Fig. 6, respectively.

The adsorption parameters were selected for the deposition time as 15 s and for the deposition potential as -250 mV/s according to Fig. 5 and Fig. 6. Subsequent studies were carried out according to these parameters.

#### 3.3. Formation of calibration plots

The DPAdSV voltammograms of TA within the range of  $1 \times 10^{-7} - 5 \times 10^{-5}$  M (0.1 – 15  $\mu\text{M}$ ) in 0.04 BR (pH 3.5) at PGE and the inset calibration plot are given in Fig. 7.

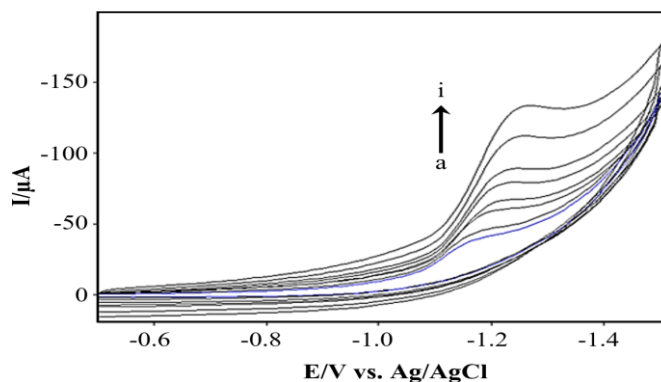


Figure 4. Dependence of cyclic voltammograms of  $5 \times 10^{-5}$  M TA on scan rates blank (a), 75 (b) 100 (c), 200 (d), 300 (e), 400 (f), 500 (g), 750 (h), and 1000 (i) mV/s in 0.04 M BR buffer (pH 3.50) at PGE. Experimental details are given in subsection 2.3.1

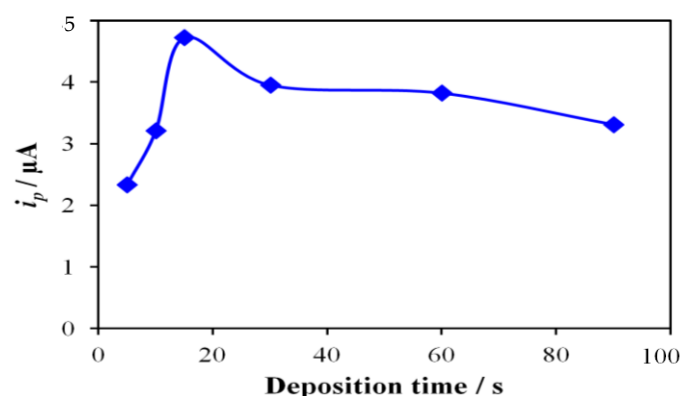


Figure 5. Variation of peak current with deposition time of  $5 \times 10^{-5}$  M TA with CV technique (pH 3.50 BR buffer)

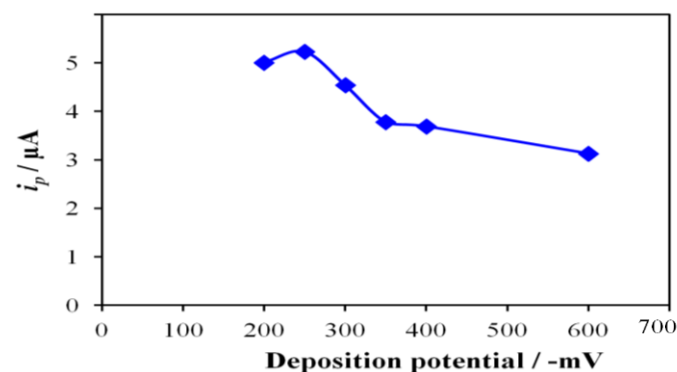


Figure 6. Variation of peak current with deposition potential of  $5 \times 10^{-5}$  M TA with CV technique (pH 3.50 BR buffer)

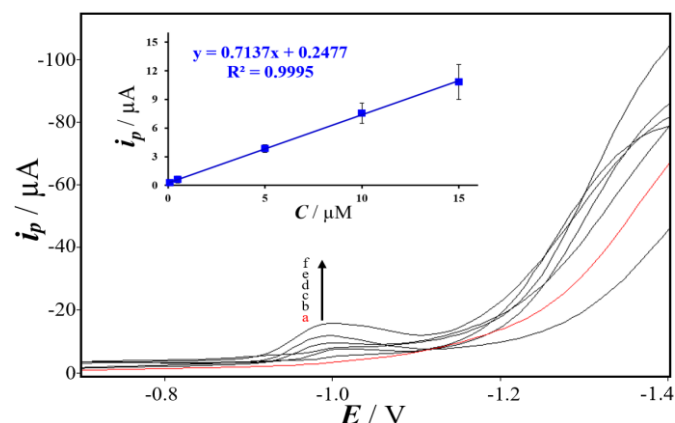


Figure 7. DPAdSV voltammograms of blank (a), and TA within the concentration range of 0.1 (b), 0.2 (c), 5.0 (d), 10 (e), and 15 ( $\mu\text{M}$ ) in pH 3.5 BR buffer at PGE, and inset calibration plot

The validation parameters and recovery data of the studied voltammetric are presented in Table 1.

**Table 1.** Regression data of the calibration curves of TA in pH 3.5 BR buffer at PGE

Validation Parameters	Results
Measurement potential (V)	-1.01
Linear concentration range (M)	$1 \times 10^{-7} - 5 \times 10^{-5}$
Slope ( $\mu\text{A}/\mu\text{M}$ )	0.7137
SD of slope	0.04
Intercept ( $\mu\text{A}$ )	0.2477
SD of intercept	0.06
r	0.9995
N	5
LOD (M)	$3.18 \times 10^{-8}$
LOQ (M)	$1.00 \times 10^{-7}$
Intra-day precision of PC/ RSD%*	1.50
Intra-day precision of PP/ RSD%*	2.00
Inter-day precision of PC/ RSD%*	3.30
Inter-day precision of PP/ RSD%*	2.50

\* RSD%: Relative standard deviation (obtained from 5 measurements)  
r: coefficient of correlation, N: number of measurements, PC: peak current, PP: peak potential

The result of the analysis for TA in pharmaceutical preparations by voltammetry is given Table 2.

**Table 2.** Determination of TA in pharmaceutical preparations (Kenacort-A ampoule form) by DPAdSV

Parameters	Kenacort-A (Ampoule)
Labelled claim (mg)	40.00
Amount found (mg)*	43.00
RSD%	3.00
Amount added (mg)	10.86
Found (mg)*	10.58
Average recovered%*	97.50

The data for the electrochemical determination of TA was found comparable with the literature in terms of LOD, LOQ, and linear range (Table 3).

**Table 3.** Literature data for the electrochemical determination of TA

Method	Linear range ( $\mu\text{M}$ )	LOD ( $\mu\text{M}$ )	LOQ ( $\mu\text{M}$ )	Reference
HMDE	0.001 – 0.009	0.003	0.001	[13]
GCE	0.2 – 50	0.1	—	[14]
CPE	2 – 46	1.5	—	[17]
PGE	1 – 15	0.03	0.1	(This study)

As it was shown in Table 3, the limit of the detection and quantitation of PGE, used for the first time in this application, was close to HMDE and less than GCE and CPE. The advantages of it are that it is easily available, inexpensive, disposable, and highly reproducible.

Additionally, PGE electrode has some important advantages over the mercury electrode. While the mercury electrode is toxic, PGE is non-toxic. The mercury electrode is both expensive and difficult to clean. However, the PGE electrode is both disposable and economical. Therefore, PGE should be preferred.

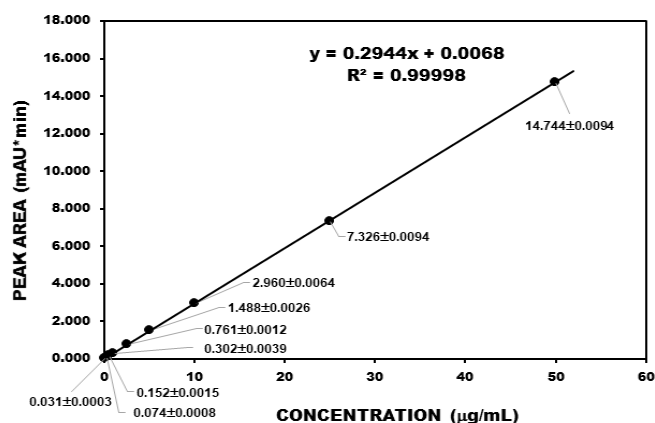


**Figure 8.** Calibration plot of HPCL-PDA method (Experimental details as in HPLC measurements subsection)

### 3.4. HPLC-PDA quantification of TA

The chromatographic analyses were carried out as described in 2.3.2. of the experimental section. Using the peak area, the HPLC calibration curve (Fig. 8) levels of TA in drug formulations were determined.

2D(A) and 3D(B) chromatograms of 5  $\mu\text{g}/\text{mL}$  Triamincinolone acetonide (TA) standard were given in Fig. 9. 2D and 3D chromatogram taken to get a more detailed and clearer image. While 2D (A) gives dimensions such as height and width, depth is given in 3D (B).

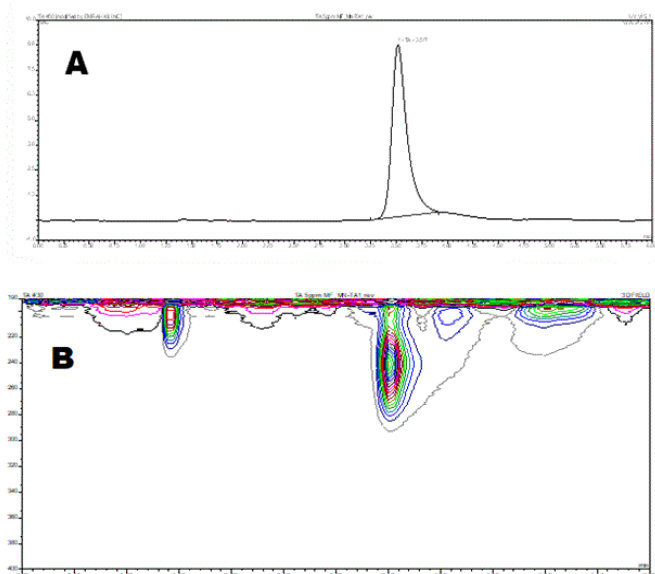


**Figure 9.** 2D (A) and 3D (B) chromatograms of 5  $\mu\text{g}/\text{mL}$  Triamincinolone acetonide (TA) standard (Experimental details as in HPLC measurements subsection)

2D chromatogram of Kenacort-A ointment is given Fig. 10. The active ingredient in the composition of Kenacort-A ointment is 1 mg TA, and the excipients are Orahesive powder (Gelatin powder type-A, pectin, sodium carboxy methyl cellulose) and plastibase (mineral oil and polyethylene bakelite). 3D chromatogram of Kenacort-A ointment sample is given Fig. 10B.

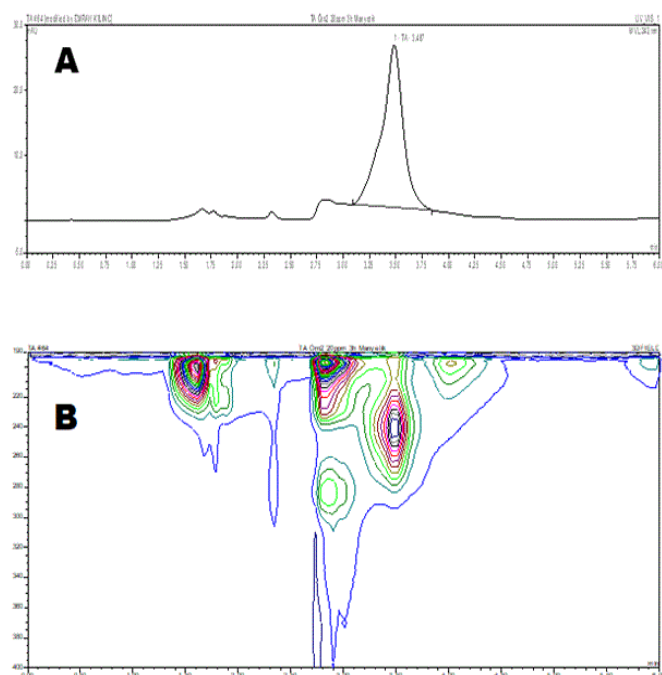


**Figure 10.** 2D (A) and 3D (B) chromatograms of Kenacort-A ointment sample (Experimental details as in *HPLC measurements* subsection)

The other studied commercial pharmaceutical formulation was Kenacort-A ampoule. 2D and 3D chromatograms of Kenacort-A ampoule are given in [Fig. 11A](#) and [11B](#), respectively. In the content of Kenacort-A ampoule, the active ingredient is 40 mg TA in every 1 mL of suspension, and the auxiliary substances are benzyl alcohol, polysorbate 80, sodium carboxymethyl cellulose, sodium chloride, and injectable water.

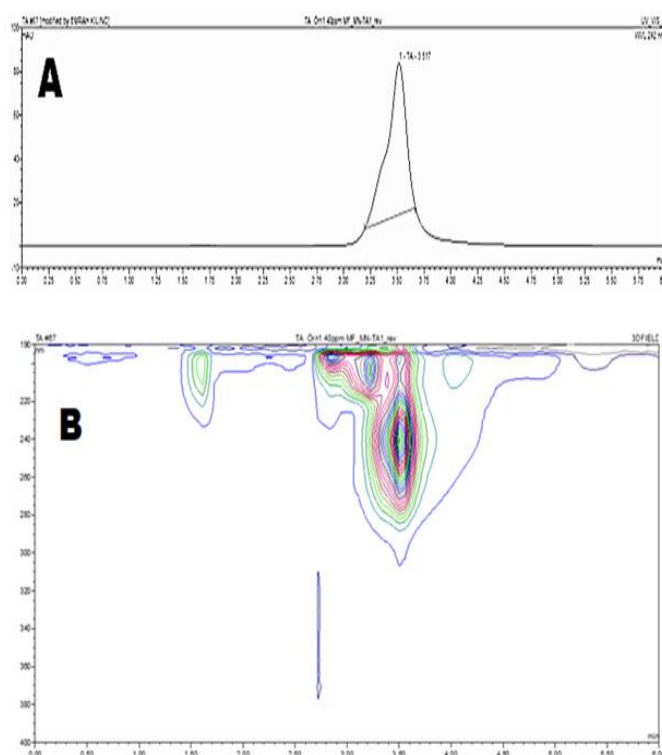


**Figure 11.** 2D (A) and 3D (B) chromatograms of Kenacort-A ampoule sample (Experimental details as in *HPLC measurements* subsection)

Different extraction methods were used for sample preparations prior to the drug analyses, while the optimum was found to be magnetic stirring for Kenacort-A ointment. HPLC results are given for the chromatographic analysis of TA in formulations ([Table 4](#)).

**Table 4.** The assay results of TA in Kenacort-A Ointment and ampoule with HPLC-PDA method (Experimental details as in *Samples preparation and extraction* and *HPLC measurements* subsections)

Dosage Forms	Spiked (ppm TA)	Determined (ppm TA)	Extraction Methods	Recovery (%)
Ointment	20	20.001 ± 0.042	Magnetic stirrer (3 hours at 400 rpm)	100.005
Ointment	20	18.166 ± 0.032	Ultrasonic bath (3 hours at 25°C)	90.83
Ampoule	40	48.736 ± 0.436	Filtered after dilution	121.84

The validation studies of the HPLC-PDA method for TA were executed performed in accordance with the ICH Q2(R1) guideline, and the obtained results were summarized in [Table 5](#).

**Table 5.** Summary of method validation studies according to ICH Q2(R1) guideline

Validation parameters	Results																		
Specificity	R < 1																		
Linearity	Linearity range: 0.1 – 50 µg/mL ( $2.3 \times 10^{-7}$ – $1.15 \times 10^{-4}$ M) Regression equation: $y = 0.2944x + 0.0068$ ( $r = 0.9998$ )																		
	<table border="1"> <thead> <tr> <th>Sample No</th> <th>Determined (%)</th> <th>RSD%</th> </tr> </thead> <tbody> <tr> <td>1</td> <td>100</td> <td>1.6</td> </tr> <tr> <td>2</td> <td>92.8</td> <td>0.8</td> </tr> <tr> <td>3</td> <td>97.2</td> <td>0.7</td> </tr> <tr> <td>4</td> <td>96.0</td> <td>1.6</td> </tr> <tr> <td>5</td> <td>97.6</td> <td>0.5</td> </tr> </tbody> </table>	Sample No	Determined (%)	RSD%	1	100	1.6	2	92.8	0.8	3	97.2	0.7	4	96.0	1.6	5	97.6	0.5
Sample No	Determined (%)	RSD%																	
1	100	1.6																	
2	92.8	0.8																	
3	97.2	0.7																	
4	96.0	1.6																	
5	97.6	0.5																	
Precision (Intra-day, RSD%)	<table border="1"> <thead> <tr> <th>Sample No</th> <th>Determined (%)</th> <th>RSD%</th> </tr> </thead> <tbody> <tr> <td>1</td> <td>101.6</td> <td>0.3</td> </tr> <tr> <td>2</td> <td>101.7</td> <td>0.4</td> </tr> <tr> <td>3</td> <td>100.2</td> <td>0.1</td> </tr> <tr> <td>4</td> <td>99.8</td> <td>0.1</td> </tr> <tr> <td>5</td> <td>99.7</td> <td>0.2</td> </tr> </tbody> </table>	Sample No	Determined (%)	RSD%	1	101.6	0.3	2	101.7	0.4	3	100.2	0.1	4	99.8	0.1	5	99.7	0.2
Sample No	Determined (%)	RSD%																	
1	101.6	0.3																	
2	101.7	0.4																	
3	100.2	0.1																	
4	99.8	0.1																	
5	99.7	0.2																	
Accuracy	$\delta \pm SD$ : $5.1 \pm 0.14$ Rel. Error: +0.2%																		
LOD	0.017 µg/mL = $3.92 \times 10^{-8}$ M																		
LOQ	0.0561 µg/mL = $1.29 \times 10^{-7}$ M																		

The linearity range was obtained as  $2.30 \times 10^{-7}$  –  $1.15 \times 10^{-4}$  M (0.1 – 50 µg/mL). LOD and LOQ were achieved as  $3.92 \times 10^{-8}$  M (0.017 µg/mL) and  $1.29 \times 10^{-7}$  M (0.0561 µg/mL), respectively.

In the literature, there are studies related to HPLC and TA quantification, and their results are in harmony with the HPLC findings of the current paper. Literature and this study are given [Table 6](#).

The chromatographic determination of TA was found comparable with the literature in terms of LOD, LOQ, linear range, and the other parameters are given in [Table 6](#).

As it was shown in [Table 6](#), in this study, retention time was close to that in literature studies.

**Table 6.** Literature data for the chromatographic determination of TA

Method	Linear range (µg/mL)	LOD (µg/mL)	LOQ (µg/mL)	Column	Temperature (°C)	Flow rate (mL/min)	Retention time (min)	Reference
HPLC-PDA	1 – 200	0.14	0.47	C8 (Hypersil 150 × 4.6 mm, 5 µm)	Ambient	1 – 2 (Gradient)	12.45	[18]
HPLC-UV	—	—	0.24	C18 (Nucleosil125 × 4 mm, 5µm)	30	0.8	4.8	[19]
HPLC-UV	1 – 50	0.19	0.62	C18 (Hypersil 150 × 4.6 mm, 5µm)	40	1.5	3.42	[20]
HPLC-UV	6.26 – 100.20	2.63	7.97	Supelcosil LC-ABZ (150 × 4.6 mm, 5µm)	37	—	2.68	[21]
HPLC-PDA	0.1 – 50	0.017	0.0561	C18 (Nucleosil 250 × 4.6 mm, 5 µm)	Ambient	1	3.52	(This study)

However, linear range, LOD and LOQ of HPLC-PDA was less than that of the previous methods. So, this indicates that the applied HPLC method was more suitable than previous HPLC methods.

Electrochemical method displayed the linear range was  $1 \times 10^{-7} - 5 \times 10^{-5}$  M, and LOD and LOQ were  $3.18 \times 10^{-8}$  M and  $1.00 \times 10^{-7}$  M, respectively. The HPLC-PDA method displayed linearity in the concentration range of  $2.3 \times 10^{-7} - 1.15 \times 10^{-4}$  M with LOD and LOQ values as  $3.992 \times 10^{-8}$  M and  $1.29 \times 10^{-7}$  M, respectively. Although these results obtained with both methods are close to each other, the electrochemical method has advantages such as being more economical, easier experimental procedures, working with less samples, taking less time and working with disposable electrodes. However, this study indicates that both techniques are good alternatives to each other.

#### 4. Conclusions

In the current study, the electrochemical properties of TA were simultaneously determined by voltammetric techniques using first time PGE, and HPLC-PDA was developed for its analysis in commercial pharmaceutical dosage forms. Regression data of the calibration curves and analysis of TA were successfully carried out in Kenacort-A Ampoule form (Table 1 and Table 2) at PGE (easily available, inexpensive, disposable and highly reproducible) compared with the other electrodes in the literature. The electrode reactions were found to be adsorption controlled. The TA levels in various pharmaceutical formulations (Kenacort-A ointment and Kenacort-A Ampoule) were determined with HPLC-PDA methods. Different extraction methods were used for the preparation of Kenacort-A ointment samples prior to the analysis, while it was concluded that the optimum method was magnetic stirring (Table 4). Analytical method validation studies were performed, and the obtained experimental results were summarized in Table 5. This study indicates that the developed voltammetric and HPLC methods can be applied for the electrochemical and chromatographic analysis of other drug active materials.

#### Acknowledgement

We would like to thank DEVA Inc. (Istanbul, Turkey) for kindly supplying pure TA and its tablet and ampoule dosage forms. Emrah KILINC acknowledges partial support from Ege University Department of Scientific Research Projects (BAP, Project number: 12/ECZ/031).

#### References

- [1] The International Olympic Committee (IOC) "Anti-Doping Rules Applicable to the Games of the XXIX Olympiad", 2008, 3–9.
- [2] H. Koç, O. Yüksel, Kadınlarda fiziksel ve fizyolojik performansın değerlendirilmesi, Dumlupınar Üniversitesi Sağlık Bilimleri Dergisi, 9, 2007, 1.
- [3] A.J.P. van Heugtena, W. de Boer, W.S. de Vries, C.M.A. Markestijn, H. Vromans, Development and validation of a stability-indicating HPLC-UV method for the determination of triamcinolone acetonide and its degradation products in an ointment formulation, J Pharm Biomed Anal, 149, 2018, 149, 265.
- [4] S. Sudsakorn, L. Kaplan, D.A. Williams, Simultaneous determination of triamcinolone acetonide and oxymetazoline hydrochloride in nasal spray formulations by HPLC, J Pharm Biomed Anal, 40, 2006, 1273.
- [5] G.M. Fernandes-Cunha, J.B. Saliba, R.C. Siqueira, R. Jorge, A. Silva-Cunha, Determination of triamcinolone acetonide in silicone oil and aqueous humor of vitrectomized rabbits' eyes: Application for a pharmacokinetic study with intravitreal triamcinolone acetonide injections (Kenalog®40), J Pharm Biomed Anal, 89, 2014, 24.
- [6] D. De Orsi, M. Pellegrini, S. Pichini, D. Mattioli, E. Marchei, L. Gagliardi, High-performance liquid chromatography – diode array and electrospray-mass spectrometry analysis of non-allowed substances in cosmetic products for preventing hair loss and other hormone-dependent skin diseases, J Pharm Biomed Anal, 48, 2008, 641.
- [7] S.A. Doppenschmitt, B. Scheidel, F. Harrison, J.P. Surmann, Simultaneous determination of triamcinolone acetonide and hydrocortisone in human plasma by high-performance liquid chromatography, J Chromatogr B: Biomed Sci Appl, 682, 1996, 79.
- [8] A.M. di Pietra, V. Andrisano, R. Gotti, V. Cavrini, On-line post-column photochemical derivatization in liquid chromatographic-diode-array detection analysis of binary drug mixtures, J Pharm Biomed Anal, 14, 1996, 1191.
- [9] H. Tokunaga, T. Kimura, J. Kawamura, Gas chromatographic determination of glucocorticoids as trimethylsilyl ether derivatives, Yakugaku Zasshi, 99(8), 1979, 800.
- [10] D. Aghaba, D. Zivanov-Stakic, S. Vladimirov, K. Zubac, Determination of triamcinolone, triamcinolone acetonide and fluocinonide in dosage forms, Acta Pol Pharm, 47(1–2), 1990, 15–18.
- [11] E.R.M. Kedor-Hackmann, E.A.S. Gianotto, M.I.R.M. Santoro, Determination of triamcinolone acetonide in ointment by UV derivative spectrophotometry and high performance liquid chromatography, Anal Lett, 30(10), 1997, 1861.

- [12] Y.S. El-Saharty, N.Y. Hassan, F.H. Metwally, Simultaneous determination of terbinafine HCl and triamcinolone acetonide by UV derivative spectrophotometry and spectrodensitometry, *J Pharm Biomed Anal*, 28(3–4), 2002, 569.
- [13] E. Hammam, Determination of triamcinolone acetonide in pharmaceutical formulation and human serum by adsorptive cathodic stripping voltammetry, *Chem. Anal. (Warsaw, Pol.)*, 52, 2007, 43.
- [14] C. Vedhi, R. Eswar, H.G. Prabu, P. Manisankar, Determination of triamcinolone acetonide steroid on glassy carbon electrode by stripping voltammetric methods, *Int J Electrochem Sci*, 3, 2008, 509.
- [15] R.N. Goyal, V.K. Gupta, S. Chatterjee, A sensitive voltammetric sensor for determination of synthetic corticosteroid triamcinolone, abused for doping, *Biosens Bioelectron*, 24, 2009, 3562.
- [16] P. Kabasakalian, J. McGlotten, The polarographic reduction of prednisone ( $17\alpha,21$ -Dihydroxy- $1,4$ -pregnadiene- $3,11,20$ -trione), prednisolone ( $11\beta,17\alpha,21$ -Trihydroxy- $1,4$ -pregnadiene- $3,20$ -dione) and their precursors, *J Am Chem Soc*, 78(19), 1956, 5032.
- [17] P.M. Zagrzewski, K.N. Belikov, I.A. Zinchenko, The study of the electrochemical behavior of triamcinolone acetonide on the carbon paste electrodes for its voltammetric determination, *Methods Objects Chem Anal*, 13(3), 2018, 136.
- [18] M.M. Baker, T.S. Belal, M.S. Mahrous, H.M. Ahmed, H.G. Daabees, A validated stability-indicating HPLC-DAD method for simultaneous determination of econazole nitrate, triamcinolone acetonide, benzoic acid and butylated hydroxyanisole in cream dosage form, *Analytical Methods*, 9, 2016, 2185.
- [19] M. Sigg, R. Daniels, The effect of alkanediols on the release of triamcinolone acetonide from semisolid dosage forms, *Int J Pharm*, 605, 2021, 120843.
- [20] M.M. Sebaiy, S.M. El-Adl, M.M. Baraka, M.S. Mohram, Y.M. Elkady, Stability indicating HPLC method for the simultaneous estimation of triamcinolone acetonide and benzyl alcohol in pure form and Epirelefan® vial, *Am J Med Chem*, 2(1), 2020, 4.
- [21] M. Márquez Valls, A. Martínez Labrador, L. Halbaut Bellowa, D. Bravo Torres, P.C. Granda, M. Miñarro Carmona, D. Limón, A.C. Calpena Campmany, Biopharmaceutical study of triamcinolone acetonide semisolid formulations for sublingual and buccal administration, *Pharmaceutics*, 13, 2021, 1080.



# Determination of physical, chemical and antioxidant properties of pomegranate sauces sold in Turkish markets

Yunus Emre Kamış<sup>1</sup> , Bülent Akar<sup>2\*</sup> , Cemalettin Baltacı<sup>2</sup> 

<sup>1</sup> Gümüşhane University, Graduate Education Institute, Department of Food Engineering, 29000, Gümüşhane, Türkiye

<sup>2</sup> Gümüşhane University, Faculty of Engineering and Natural Sciences, Department of Food Engineering, 29000, Gümüşhane, Türkiye

## Abstract

This study aimed to determine the physical, chemical and antioxidant properties of pomegranate sauces sold in the Turkish markets. A total of eighteen pomegranate sauces, seventeen of which were purchased from the market, and one produced in a rotary evaporator, were analyzed with respect to antioxidant activity, titratable acidity, brix, hydroxymethylfurfural (HMF), pH, color, and sugar. The antioxidant activities of the samples were analyzed by six different methods, including DPPH (2,2-diphenyl-1-picrylhydrazil) radical scavenging activity, ferric reducing antioxidant power (FRAP), ABTS<sup>•+</sup> radical scavenging capacity, total antioxidant capacity assay (TAC), total phenolic content (TPC), and total flavonoid content (TFC) methods. The highest and lowest antioxidant activity values were as follows, respectively: 5.23 and 822.69 mg AA/kg for the DPPH method, 57.94 and 2380.94 mg FeSO<sub>4</sub>/kg for the FRAP method, 660.47 and 3690.83 mg AA/kg for the TAC method, 23.06 and 11680.71 mg QEE/kg for the TFC method, and 123.54 and 9566.95 mg GAE/kg for the TPC method. In addition, HMF contents of the most samples were below the permissible limit value (50 mg/kg), while some of them showed a heterogeneous distribution between 4.58 and 103.68 mg/kg. Such a heterogeneous distribution of the HMF contents may be due to the factors such as raw materials and additives used in production, applied heat treatments, production processes, and storage conditions. As a result, HMF content in pomegranate sauce can be reduced below the permissible limit if the production conditions comply with the standards.

**Keywords:** Antioxidant activity, hidroxyethylfurfural (HMF), physicochemical analysis, pomegranate sauces

## 1. Introduction

Pomegranate is an ancient fruit that has always been valuable throughout human history [1] and has a high cultural value as well as commercial value. [2]. There is evidence that the plant was cultivated in Egypt after the discovery of agriculture about ten thousand years ago [1]. The pomegranate plant (*Punica granatum* L) in the Punicaceae family is a deciduous shrub and monoecious, it is also grown up to 7 m [3,4]. The flowering time of the plant is usually between March-April and July-August and the flowering time lengthens out up to 10 – 12 weeks [5]. The native of the plant is Iran, which is one of the world's largest commercial producers and exporters of pomegranate fruit [6,7]. Besides Iran, the Southern Caucasus, Afghanistan, Southern Asia, Western Asia, Anatolia, and the Mediterranean are the native of the species [8]. In addition, it is cultivated in countries such as Türkiye, Iraq, Iran, Syria, USA, Italy, Spain, Tunisia, Morocco, Afghanistan, Palestine, Israel, Egypt, Saudi Arabia, India, China, and Thailand [9,10]. As stated,

Türkiye is among the countries that are the native of the pomegranate plant and it is naturally spreads in the provinces of Türkiye such as Siirt, Şırnak, Adıyaman, Antalya, Artvin, Aydın and Samsun [11]. The production of pomegranate fruits in Türkiye is carried out in high quantities in the Mediterranean, Southeastern Anatolia, and Aegean regions [12]. Pomegranate fruit has many positive effects on human health with its bioactive components such as phenolic substances, antioxidants, organic acids, vitamins, polysaccharides, sugars, and minerals [13–15]. It shows biological activity and is a particularly good antioxidant [16,17], also has antiproliferative, antiviral, anti-aging, antimicrobial properties [17]. Because of all these properties, pomegranate fruit has gained common popularity as a functional food and nutraceutical source. Promising results have been obtained from human clinical trials on diabetes, cardiovascular disease, and prostate cancer [18]. Due to these positive effects of

**Citation:** Y.E. Kamış, B. Akar, C. Baltacı, Determination of physical, chemical and antioxidant properties of pomegranate sauces sold in Turkish markets, Turk J Anal Chem, 4(2), 2022, 67–75.

**\*Author of correspondence:** akarblnt@gmail.com

**Tel:** +90 (456) 233 10 00–1854

**Fax:** +90 (456) 233 10 75

**Received:** June 08, 2022

**Accepted:** October 14, 2022

 <https://doi.org/10.51435/turkjac.1127473>

pomegranate on human health, there is an increase in demand for the product in the world [19]. While pomegranate is mostly consumed by people as a fresh fruit, it is also frequently consumed as pomegranate juice, pomegranate jam, pomegranate wine, dried pomegranate seeds, pomegranate molasses, pomegranate syrup or pomegranate sauce. Pomegranate sour is traditionally used in Turkish kitchens for give a sour-sweet taste to some dishes and salads [9]. In recent years, pomegranate sauce is also commercially available. Pomegranate sour is obtained by pressing the pomegranate fruit, and then clarifying and concentrating it in open air or under a vacuum in suitable conditions [20]. Pomegranate sauces are used in salads and many dishes in Türkiye. Therefore, it is important to add sufficient quantities of appropriate sauce ingredients to the pomegranate sour. Although traditional and small-scale companies are contributed to the production, pomegranate sauces are mostly produced by large-scale companies [21]. People show a high demand for pomegranate and pomegranate products because of their positive effects on health. However, incorrect practices in the manufacture of this product may occur food safety problems and this situation gives rise to health problems instead of positive health expectations for this product.

Although there are a few studies to determine the physical and chemical properties of pomegranate sauces produced in Türkiye [21–22]. Numbers of analyzed pomegranate sauce sample and physicochemical properties were limited in these studies unlike the current study. This study aimed to determine and evaluate the physical, chemical and antioxidant properties of pomegranate sauces sold in the Turkish market and to produce a standard quality product.

## 2. Material and methods

### 2.1. Sampling and preparation

A total of eighteen pomegranate sauces, seventeen (different brand products coded in the range of S1 – S17) of which were purchased ready-made from the market and one (coded as S18, the control sample) produced in the laboratory (Gümüşhane University, Faculty of Engineering and Natural Sciences, Department of Food Engineering) with the help of a rotary evaporator, were studied. First, the peels of the pomegranate fruits were removed, then the pomegranate juice was obtained by squeezing the fruit. The juice was evaporated to 70% Brix in the vacuum evaporator and, finally, pomegranate sauce was prepared by using starch, sugar, and lemon.

Each analysis was repeated at least three times and the results are presented as “mean ± standard deviation”. Pomegranate sauces were stored at room

temperature in the laboratory until the analysis studies were completed.

### 2.2. Chemicals and Instrumentation

The chemicals and solvents (analytical or HPLC purity) were purchased from Merck (Darmstadt, Germany) and Sigma-Aldrich (St. Louis., Missouri., USA). The following systems were used for the analyte measurements: Agilent 1200 series HPLC system for the sugar and HMF analysis, Shimadzu UV-1800 spectrophotometer for the antioxidant activity, the Ohaus Starter 3000 Bench pH Meter (Ohaus Corporation, Parsippany, NJ, USA) for the pH measurements, A Anton Paar MCR 102 rheometer (Thermo Scientific, Germany) for the rheological analysis, a Minolta CR-300 colorimeter (Minolta Camera Co., Osaka, Japan) for color analysis (values of  $L^*$ ,  $a^*$ ,  $b^*$ ), an ABBE refractometer (Optic IvymenSystem, Spain) for the water soluble dry matter contents (Brix%), A Heildoph rotary evaporator (Schwabach, Germany) for removing solvents from the solutions, A Shimadzu analytical scales with 0.1 mg sensitivity for weighing the samples.

### 2.3. Analysis

#### 2.3.1. Physicochemical analysis

Water-soluble dry matter contents (Brix%) of the pomegranate sauce samples were determined with a refractometer device. Sample was placed to between two prisms and set to 20 °C and optical refractive index of the pomegranate sauce was read and recorded [23].

For determination of titratable acidity of the samples, the pomegranate sauce samples were homogenized and weighed 10 g. Then 75 mL of distilled water was added. While the suspension was stirred with a magnetic stirrer, at the same time the 0.1 N sodium hydroxide solution was titrated until the pH value reached 8.3 for a maximum of 60 seconds. Titratable acidity was calculated according to the [Formula 1](#).

$$\text{Titratable acidity (\%)} = \frac{V \times N \times 0.064 \times 100}{m} \quad (1)$$

V: Volume of the standard NaOH solution (mL)

N: Normality of the standard NaOH solution

m: Sample mass (g)

0.064: Equivalent factor used to impart the acidity as citric acid

pH measurements were made according to TS 1728 ISO 1842 (fruit and vegetable products - pH determination) [24] with the desktop pH meter.

Color analysis ( $L^*$ ,  $a^*$ ,  $b^*$  values) of the samples were performed using a colorimeter device.  $L^*$ ,  $a^*$ ,  $b^*$  values represent the colors on the food as red-green,

blue-yellow (Among  $b^*$  values,  $-b$  denotes yellow and  $+b$  denotes blue), black to white lightness between 0 and 100, respectively. The measured color values were determined according to Quek [25].

The quantitative determination of HMF was carried out according to TS 6178 - ISO 7466 standard [26] and modified by Baltacı et al [27] and, Baltacı and Akşit [28]. In this method, 2.5 g of each pomegranate sauce samples were weighed and transferred to a 50 mL flask and then 25 mL of distilled water was added to extract the sample at the room temperature. To precipitate the protein, 0.25 mL Carrez I and 0.25 mL Carrez II solutions were added to the mixture for 10 min. Then the volume of the mixture was made up to 100 mL with distilled water and the mixture was filtered through a 0.45  $\mu\text{m}$  injection filter. After that, the prepared extracts were transferred into vials and injected into the conditioned HPLC system. To generate the calibration plot, a series of HMF standard solutions were prepared, injected into the HPLC system and the peak areas were recorded. The HMF concentrations of the samples were determined quantitatively with the help of the standard calibration graph (the HMF concentrations versus the peak areas). The HMF concentrations calculated as mg/L with the calibration equation were converted to mg/kg with the following [Formula 2](#):

$$HMF (mg/kg) = \frac{V_1}{M} \times \frac{1}{V_2} \times \frac{(y - b)}{m} \quad (2)$$

$V_1$ : Final volume (mL)

$V_2$ : Initial sample volume injected into the HPLC system (mL)

$M$ : Sample mass (g)

$y$ : Device signal (pick area value)

$b$ : The intercept value of the calibration equation

$m$ : Slope value of the calibration equation

For sugar analysis, first, approximately 2.5 g of the pomegranate sauce was weighed into a beaker and treated with 40 mL of distilled water. Then, the beaker content was mixed well, transferred to a volumetric flask containing 25 mL of methanol, and the mixture transferred to vials after filtering through a 0.45  $\mu\text{m}$  injection filter. A set of standard calibration solutions were prepared at sequential concentrations from glucose, fructose, and sucrose standards. After the peak areas of all standard and sample solutions were read in HPLC, the total sugar concentrations ( $\mu\text{g/mL}$ ) in the samples were determined with the help of the linear calibration graph [29]. Finally, glucose sucrose and fructose contents of the samples were calculated separately according to the [Formula 3](#) and thus, the % total sugar content was determined.

$$\begin{matrix} \text{Glucose,} \\ \text{fructose,} \\ \text{sucrose (\%)} \end{matrix} = \frac{V_1}{M} \times \frac{1}{V_2} \times \frac{100}{1000} \times \frac{(y - b)}{m} \quad (3)$$

In order to identify the artificial food colors, first, approximately 40 g of the pomegranate sauce was treated with distilled water, and then, filtered. Then, a few drops of concentrated HCl were added to the filtrate and an oil-free sheep wool thread was plunged into the beaker. It was kept in a water bath for one hour and washed with running tap water. It was checked whether the wool thread was dyed or not. If the dye has not been removed from the wool thread by washing, it is placed in a beaker and distilled water and a few drops of  $\text{NH}_3$  (5%) are added and boiled for evaporating  $\text{NH}_3$  in a water bath for half an hour. As a result of this application, if the dye in the wool thread has passed into the solution, it is concluded that the dye in the product is artificial, and if not, it is natural [30].

A rheometer device was used to determine the viscosities of the pomegranate sauce samples at different temperatures. The samples were placed on the rheometer at a constant temperature (15, 25 and 35  $^\circ\text{C}$ ) to plot flow behavior graphs. The graphs were obtained by measuring shear stress in the range of 0 – 100  $\text{s}^{-1}$  shear velocity. The apparent viscosity values of the samples were determined at a shear rate of 50  $\text{s}^{-1}$  based on measured values and plotted graph.

### 2.3.2. Antioxidant activity

#### 2.3.2.1. DPPH radical scavenging activity:

The principle of this method is based on the ability of antioxidant compounds to reduce the intensity of the purple color of the DPPH radical. DPPH radical gives a strong absorption pick at 517 nm [31]. First, 3.0 mL of a methanolic DPPH solution was added to 0.1 mL of the aqueous extract of the pomegranate sauce extract, and the mixture was vortexed. After standing for 30 min, the absorbance of the mixture was read at 517 nm in a UV-Vis spectrophotometer. The same procedure was repeated for the standard ascorbic acid and trolox [32]. The standard calibration curve was plotted to determine the DPPH free radical scavenging activity.

#### 2.3.2.2. Ferric reducing antioxidant power (FRAP):

According to the FRAP method developed by Benzie and Strain [33], first, 0.25 mL of the aqueous extract of each sample was transferred into a test tube and then 2.75 mL of FRAP solution was added to the tube. The mixture was incubated for 30 min after vortexing and finally the absorbance was read at 593 nm. The same procedure was repeated for the standard  $\text{FeSO}_4$  solutions to obtain the standard calibration curve. The total iron

reduction antioxidant capacity was expressed as mg of FeSO<sub>4</sub> equivalent per kg [32].

#### 2.3.2.3. ABTS<sup>•+</sup> radical scavenging capacity:

2.85 mL of the ABTS<sup>•+</sup> solution was added to 0.15 mL of the pomegranate sauce extract in a test tube. Then the mixture was kept for 120 min after vortexed. The same procedures were performed for the standard ascorbic acid and Trolox to obtain the standard calibration curve. All absorbance of the samples and standards were read at 734 nm [32]. Radical scavenging capacity of ABTS<sup>•+</sup> was calculated as Trolox equivalent and the results is expressed as the trolox equivalent antioxidant capacity (TEAC).

#### 2.3.2.4. Determination of total antioxidant capacity (TAC):

0.5 mL of the sample extract was transferred into a test tube and 2.5 mL of distilled water was added. Then, 1.0 mL of the molybdate reagent solution was added to the mixture. The mixture was incubated for 90 min in a water bath at 95 °C after vortexing for 10 min. The absorbance of the mixtures was read at 695 nm [34]. The standard calibration graph was obtained using ascorbic acid (AA) standards. The total antioxidant capacity values were determined as mg AA by comparing with the antioxidant ascorbic acid standard.

#### 2.3.2.5. Total phenolic content (TPC):

Phenolic contents of the pomegranate sauce samples were analyzed using the Folin-Ciocalteu's reagent [35]. First, 3.4 mL of distilled water was added to 0.3 mL of the pomegranate sauce extract. Then, 0.5 mL of methanol and 0.2 mL of the Folin-Ciocalteu's reagent were added to the mixture, and the mixture was incubated for 10 min at room temperature after vortexing. After that, 0.6 mL of 10% Na<sub>2</sub>CO<sub>3</sub> solution was added to the mixture, and the mixture was incubated again in the dark for 120 min at the room temperature. At the end of the incubation period, the absorbance of the mixture was read at 760 nm in the UV-vis spectrophotometer. The results were given as gallic acid equivalents (GAE) using the standard calibration curve.

#### 2.3.2.6. Total flavonoid content (TFC):

First, 3.2 mL of methanol (30% v/v) was added to the pomegranate sauce extract, 0.5 mL of which was pipetted into a test tube, and then the mixture was vortexed. 150 µL of 0.5 M sodium nitrite solution and 150 µL of 0.3 M aluminum chloride solution were added to the mixture. 1.0 mL of 1.0 M NaOH solution was added to the mixture after incubating for 5 min at room temperature. the absorbance of the final mixture was read in the device at 506 nm [34]. The same procedure was repeated for the standard ascorbic acid and Trolox

to plot the calibration graph using the catechin solutions at sequential concentrations ranging from 25 to 400 mg/mL. Total flavonoid quantities were given as mg catechin equivalents/L.

## 2.4. Statistical evaluations

The results obtained from all analyzes were statistically evaluated and interpreted by the Duncan test and principal component analysis (PCA) using the XLSTAT (2010) package program.

## 3. Results and discussion

### 3.1. Physicochemical analysis results

All results from the analysis of the samples are presented in Table 1. Water-soluble dry matter is an important parameter in the quality assessment of fruit, juice, and concentrates because of affecting the taste (especially sweetness) of the fruit and it directly affects the willingness to buy the product [36,37]. The highest water-soluble dry matter (Brix%) content obtained from the analysis of the samples was 76.70% in the S12 coded sample, and the lowest 70% was in the N18 coded sample. The Brix values of all samples were found to be close to each other. Similarly, Yıldız et al. [22] reported that the brix values of nine pomegranate sauces varied between 69.50% and 73.30%. In general, Brix values of fruit concentrates produced by thermal evaporation of some of the water vary between 25% and 60% [38]. Therefore, the Brix values of pomegranate sauces can be greatly affected by the heat treatment applied during production and as a result, differences can be observed between the products.

Titrateable acidity, a better indicator than pH for determining the effect of acids on flavor, was determined in terms of citric acid equivalent in all samples. As seen in Table 1, the highest and lowest titrateable acidity values belong to the samples coded S16 with 7.58% and S15 with 2.65%, respectively. Titrateable acidity values of S5, S8, S9, S14, S16, and S18 coded samples are higher than other samples. This situation can be associated with the raw materials and additives used in the production of pomegranate sauces. Karabiyikli and Kışla [39] reported that titration acidity (as citric acid equivalent) values of traditional pomegranate sauces varied from 8.60 to 9.30%. In another study, it was determined that the acidity values of pomegranate sauces were in the range of 4.30 – 7.97 g/100 g [22]. The results obtained from this study are similar to those in the literature.

pH values of the samples varied between 1.66 (S12) and 2.88 (S18). pH is a decisive factor in processes in all foods, such as color (pigment), texture, water holding capacity, enzymatic, gelation, denaturation, growth, and

inhibition of microorganisms, germination or death of bacterial spores, and some chemical reactions (Maillard reaction) [40]. There is no standard guideline value in Türkiye for the pH values of pomegranate sauces. However, in some studies in the literature, it has been reported that the pH values of pomegranate sauces are in the range of 2.33 – 2.68 [39] and 2.64 – 2.91 [22], close to those in the present study.

As a result of HMF analysis of the pomegranate sauce samples, the lowest and highest values were found as 4.58 mg/kg (S18) and 103.68 mg/kg (S3), respectively. Daily intakes of HMF per person vary between 4 and 30 mg. However, when prune drinks are consumed, up to 350 mg of HMF can be taken into the body daily [41]. It has been found to be responsible for harmful effects such as mutagenic, genotoxic, cytotoxic and enzyme inhibition effects on human health when consumed in high doses [42].

As a result of the total sugar analysis, the highest content was found in the S8 coded sample with 28.70%, and the lowest in the S3 coded sample with 14.84%. Similar results have been reported in the literature. While Kışla and Karabiyıklı [43] reported that the total sugar content of pomegranate sauces ranged from 12.24% to 29.11%, another study reported that the values ranged between 21.89% and 53.44% [22].

From the Table 1, the highest glucose, fructose, and sucrose contents of the samples are 15.40% (S17), 16.41% (S6) and 24.61% (S15), respectively, while the lowest values are <LOQ for glucose and fructose, and 1.93% (S17) for sucrose. Total sugar, glucose, fructose, and sucrose contents of the sample S18 are determined as 26.05%, 8.59%, 12.10%, and 5.36%, respectively.

While glucose could be detected in S8, S9, S10, S11, S12, S14, S16, S17 and S18 coded samples, it could not be detected in other samples. Also, fructose could not be detected in the glucose-free samples except S1, S6 and S13 coded samples. On the other hand, sucrose was determined quantitatively in all samples. On the contrary, as glucose and fructose levels of the pomegranate sauces decreased, sucrose levels increased. The reason for the differences in glucose, fructose and sucrose levels may be attributed to the raw materials and additives.

Color is one of the most important sensory properties of foods. Therefore, minimizing the pigment losses during the processing and storage is an important to maintain the quality [44]. The red color of pomegranate juice is due to the formation of pelargonidin, cyanidin and delphinidin [45]. The highest values of L\*, a\*, b\* and ΔE was determined as 31.31 (S11), 26.48 (S16), 17.58 (S11) and 27.37 (S11), while the lowest values were measured as 15.84 (S18), 9.03 (S12), -4.58 (S4) and 0.00 (S18), respectively (Table 2). Mokrzycki and Tatol [46] reported that a standard observer sense color differences between results as shown below: “0 < ΔE < 1 -the observer does not notice the difference, 1 < ΔE < 2 -only the experienced observer can notice the difference, 2 < ΔE < 3.5 -the inexperienced observer also notices the difference, 3.5 < ΔE < 5 -clear color difference is noticeable, 5 < observer ΔE -observer notices two different colors.”

In addition to the color values of the samples, no artificial food colors were detected in any of the pomegranate sauce samples during the analysis.

Knowing the viscosity of the product in food processing is an important criterion to define the product

**Table 1.** Analysis results of Brix, titratable acidity (as citric acid equivalent), pH, HMF, fructose, glucose, sucrose, and total sugar of the pomegranate sauce samples

Sample	Water soluble dry matter %	Titratable acidity (as citric acid) %	pH	HMF mg/kg	Fructose % (m/m)	Glucose % (m/m)	Sucrose % (m/m)	Total sugar % (m/m)
S1	74.85 ± 1.85 <sup>bcd*</sup>	3.77 ± 0.19 <sup>ef</sup>	1.69 ± 0.06 <sup>i</sup>	26.67 ± 1.90 <sup>ef</sup>	4.78 ± 4.79 <sup>def</sup>	<LOQ	17.00 ± 0.10 <sup>bc</sup>	21.78 ± 4.89 <sup>cde</sup>
S2	76.70 ± 0.02 <sup>a</sup>	3.27 ± 0.17 <sup>h</sup>	2.30 ± 0.02 <sup>d</sup>	12.07 ± 1.35 <sup>gh</sup>	<LOQ**	<LOQ	23.49 ± 2.65 <sup>a</sup>	23.49 ± 2.65 <sup>bcd</sup>
S3	76.40 ± 0.30 <sup>a</sup>	3.37 ± 0.23 <sup>gh</sup>	2.25 ± 0.01 <sup>d</sup>	103.68 ± 1.53 <sup>a</sup>	<LOQ	<LOQ	14.84 ± 3.30 <sup>cd</sup>	14.84 ± 3.30 <sup>g</sup>
S4	76.60 ± 0.80 <sup>a</sup>	3.34 ± 0.4 <sup>gh</sup>	2.03 ± 0.06 <sup>f</sup>	36.84 ± 0.94 <sup>d</sup>	<LOQ	<LOQ	17.65 ± 0.78 <sup>bc</sup>	17.65 ± 0.78 <sup>efg</sup>
S5	74.70 ± 0.004 <sup>bcd</sup>	5.66 ± 0.05 <sup>c</sup>	1.91 ± 0.03 <sup>h</sup>	24.18 ± 5.54 <sup>f</sup>	<LOQ	<LOQ	14.96 ± 0.83 <sup>cd</sup>	14.96 ± 0.83 <sup>fg</sup>
S6	75.10 ± 0.30 <sup>bc</sup>	3.65 ± 0.004 <sup>f</sup>	1.96 ± 0.02 <sup>g</sup>	14.52 ± 0.50 <sup>g</sup>	16.41 ± 5.30 <sup>a</sup>	<LOQ	10.78 ± 0.69 <sup>ef</sup>	27.19 ± 6.00 <sup>ab</sup>
S7	76.45 ± 0.05 <sup>a</sup>	3.37 ± 0.09 <sup>gh</sup>	2.18 ± 0.03 <sup>e</sup>	8.60 ± 0.39 <sup>e</sup>	<LOQ	<LOQ	18.15 ± 1.39 <sup>b</sup>	18.15 ± 1.39 <sup>efg</sup>
S8	73.65 ± 0.45 <sup>ef</sup>	6.70 ± 0.10 <sup>b</sup>	1.70 ± 0.04 <sup>j</sup>	43.40 ± 1.96 <sup>c</sup>	6.72 ± 1.61 <sup>cd</sup>	14.61 ± 0.24 <sup>a</sup>	7.38 ± 1.39 <sup>gh</sup>	28.70 ± 0.02 <sup>a</sup>
S9	72.50 ± 0.40 <sup>g</sup>	6.66 ± 0.14 <sup>b</sup>	2.27 ± 0.01 <sup>d</sup>	16.09 ± 1.01 <sup>g</sup>	2.75 ± 0.24 <sup>efg</sup>	2.90 ± 0.42 <sup>f</sup>	19.41 ± 4.01 <sup>b</sup>	25.06 ± 3.35 <sup>abc</sup>
S10	75.40 ± 0.003 <sup>b</sup>	3.55 ± 0.08 <sup>fg</sup>	2.14 ± 0.02 <sup>e</sup>	24.50 ± 1.03 <sup>f</sup>	5.42 ± 0.003 <sup>cde</sup>	4.05 ± 0.42 <sup>e</sup>	18.18 ± 1.31 <sup>b</sup>	27.64 ± 0.89 <sup>ab</sup>
S11	73.00 ± 0.003 <sup>fg</sup>	4.46 ± 0.09 <sup>d</sup>	2.03 ± 0.06 <sup>f</sup>	67.02 ± 1.83 <sup>b</sup>	8.19 ± 0.41 <sup>c</sup>	8.21 ± 1.48 <sup>c</sup>	5.55 ± 0.48 <sup>h</sup>	21.95 ± 2.36 <sup>cde</sup>
S12	73.90 ± 0.003 <sup>def</sup>	3.93 ± 0.17 <sup>e</sup>	1.66 ± 0.02 <sup>j</sup>	16.07 ± 1.96 <sup>g</sup>	6.01 ± 0.13 <sup>cd</sup>	4.22 ± 0.17 <sup>e</sup>	7.95 ± 0.73 <sup>gh</sup>	18.18 ± 0.77 <sup>efg</sup>
S13	70.15 ± 0.65 <sup>h</sup>	3.25 ± 0.12 <sup>h</sup>	2.06 ± 0.01 <sup>f</sup>	23.44 ± 0.56 <sup>f</sup>	13.30 ± 0.21 <sup>b</sup>	0.00 ± 0.00 <sup>g</sup>	12.77 ± 0.56 <sup>de</sup>	26.07 ± 0.36 <sup>abc</sup>
S14	70.30 ± 0.10 <sup>h</sup>	7.42 ± 0.20 <sup>a</sup>	2.52 ± 0.02 <sup>b</sup>	22.14 ± 1.55 <sup>f</sup>	4.75 ± 0.05 <sup>d</sup>	10.16 ± 1.13 <sup>b</sup>	10.82 ± 0.28 <sup>ef</sup>	25.73 ± 0.91 <sup>abc</sup>
S15	73.00 ± 0.30 <sup>fg</sup>	2.65 ± 0.11 <sup>i</sup>	1.90 ± 0.02 <sup>h</sup>	24.54 ± 1.49 <sup>f</sup>	<LOQ	<LOQ	24.61 ± 0.96 <sup>a</sup>	24.61 ± 0.96 <sup>abc</sup>
S16	74.30 ± 0.10 <sup>cde</sup>	7.58 ± 0.16 <sup>a</sup>	2.38 ± 0.01 <sup>c</sup>	44.19 ± 5.70 <sup>c</sup>	4.52 ± 0.25 <sup>def</sup>	6.93 ± 0.84 <sup>d</sup>	8.74 ± 0.90 <sup>fg</sup>	20.20 ± 0.18 <sup>de</sup>
S17	74.30 ± 0.10 <sup>cde</sup>	3.73 ± 0.11 <sup>ef</sup>	1.91 ± 0.02 <sup>h</sup>	29.33 ± 4.31 <sup>e</sup>	1.98 ± 0.07 <sup>fg</sup>	15.40 ± 0.40 <sup>a</sup>	1.93 ± 0.00 <sup>i</sup>	19.31 ± 0.48 <sup>def</sup>
S18***	70.00 ± 0.004 <sup>h</sup>	5.58 ± 0.08 <sup>c</sup>	2.88 ± 0.03 <sup>a</sup>	4.58 ± 0.18 <sup>i</sup>	12.10 ± 0.28 <sup>b</sup>	8.59 ± 0.20 <sup>c</sup>	5.36 ± 0.69 <sup>h</sup>	26.05 ± 0.22 <sup>abc</sup>

\*The different letters in the same column mean that the difference between the results is statistically significant at  $p < 0.05$  according to the Duncan test.

\*\*The values of LOQ: % 0.10 for fructose, 0.15 for glucose, 0.5 for sucrose; The values of LOD: % 0.03 for fructose, 0.05 for glucose, 0.17 for sucrose

\*\*\*Control sample

**Table 2.** Color analysis results of the pomegranate sauce samples

Sample	L	a	b*	ΔE
S1	16.68 ± 0.68 <sup>ghi*</sup>	12.45 ± 1.35 <sup>hi</sup>	-3.38 ± 0.43 <sup>fgh</sup>	1.39 ± 0.93 <sup>ij</sup>
S2	23.56 ± 0.51 <sup>bc</sup>	17.83 ± 0.36 <sup>cd</sup>	7.33 ± 1.18 <sup>c</sup>	14.89 ± 1.30 <sup>c</sup>
S3	18.61 ± 2.74 <sup>efgh</sup>	9.47 ± 1.44 <sup>j</sup>	-3.55 ± 0.66 <sup>fgh</sup>	4.09 ± 2.83 <sup>ghi</sup>
S4	16.12 ± 0.11 <sup>hi</sup>	9.35 ± 0.10 <sup>j</sup>	-4.58 ± 0.06 <sup>h</sup>	2.93 ± 0.22 <sup>ghij</sup>
S5	16.46 ± 0.66 <sup>ghi</sup>	11.75 ± 3.02 <sup>hi</sup>	-4.21 ± 0.21 <sup>h</sup>	2.24 ± 1.09 <sup>ghij</sup>
S6	16.67 ± 0.87 <sup>ghi</sup>	10.85 ± 0.59 <sup>ij</sup>	-3.71 ± 0.80 <sup>gh</sup>	2.06 ± 0.29 <sup>hij</sup>
S7	17.28 ± 0.76 <sup>fghi</sup>	13.32 ± 0.88 <sup>hfg</sup>	-2.35 ± 0.58 <sup>fgh</sup>	2.63 ± 1.35 <sup>ghij</sup>
S8	25.11 ± 0.33 <sup>b</sup>	22.97 ± 0.31 <sup>b</sup>	9.99 ± 0.51 <sup>b</sup>	20.01 ± 0.56 <sup>b</sup>
S9	18.91 ± 0.70 <sup>efg</sup>	18.80 ± 1.31 <sup>c</sup>	-0.60 ± 0.58 <sup>c</sup>	8.10 ± 0.99 <sup>d</sup>
S10	20.06 ± 3.22 <sup>de</sup>	9.38 ± 1.19 <sup>j</sup>	-3.32 ± 0.72 <sup>fgh</sup>	5.26 ± 3.27 <sup>efg</sup>
S11	31.31 ± 0.95 <sup>a</sup>	18.53 ± 0.26 <sup>c</sup>	17.58 ± 1.17 <sup>a</sup>	27.37 ± 1.38 <sup>a</sup>
S12	21.97 ± 2.16 <sup>cd</sup>	9.03 ± 2.15 <sup>j</sup>	-2.42 ± 0.24 <sup>fgh</sup>	7.21 ± 2.70 <sup>def</sup>
S13	17.37 ± 0.17 <sup>fghi</sup>	13.88 ± 0.68 <sup>fgh</sup>	-2.58 ± 0.37 <sup>fgh</sup>	2.77 ± 0.71 <sup>ghij</sup>
S14	17.28 ± 0.15 <sup>fghi</sup>	15.93 ± 0.50 <sup>def</sup>	-2.17 ± 0.23 <sup>f</sup>	4.45 ± 0.63 <sup>fgh</sup>
S15	19.65 ± 1.43 <sup>ef</sup>	16.21 ± 1.10 <sup>de</sup>	1.26 ± 0.55 <sup>d</sup>	7.81 ± 0.75 <sup>de</sup>
S16	22.80 ± 1.40 <sup>c</sup>	26.48 ± 1.56 <sup>a</sup>	7.35 ± 1.94 <sup>c</sup>	19.59 ± 2.77 <sup>b</sup>
S17	17.73 ± 0.54 <sup>efghi</sup>	15.29 ± 0.80 <sup>efg</sup>	-0.76 ± 0.83 <sup>c</sup>	4.95 ± 1.02 <sup>fgh</sup>
S18**	15.84 ± 0.20 <sup>i</sup>	12.21 ± 0.41 <sup>hi</sup>	-4.09 ± 0.23 <sup>h</sup>	0.00 ± 0.00 <sup>i</sup>

\*The different letters in the same column mean that the difference between the results is statistically significant at  $p < 0.05$  according to the Duncan test

\*\* Control sample

quality, that is, the texture of the product is based on viscosity [47].

Viscosity and shear stress values obtained from the rheology analysis of the samples are given in Table 3. From the table, the viscosity values at 50 shear rates are the highest in the sample S7 with 3311.63 value (mPa.s), and the lowest in the sample S14 with 574.29 (mPa.s). There is a direct proportionality between shear stress and viscosity (Table 3). The samples with the highest viscosity values also have high Brix and sucrose values. Brix and sucrose values were decisive for viscosity in the pomegranate sauces. Hidayanto et al [47] reported that viscosity increased with the increase of the sucrose concentration in the solution.

### 3.2. Antioxidant activity results

Antioxidants, one of the important components of the body defense system, protect organisms against the harmful effects of free radicals. Therefore, interest in natural foods, especially plants, which contain high amounts of antioxidants, has been increasing recently [48]. Analysis results of DPPH, FRAP, ABTS, TAC, TPC, TFC of the pomegranate sauce are given in Table 4. As a result of all antioxidant analysis methods applied, all results of the N18 coded sample produced in the laboratory were found to be the highest compared to the others. The highest antioxidant activity values of the pomegranate sauce samples were determined as 2822.69 ± 3.01 mg AA/kg for DPPH, %92.58 for DPPH (% inhibition), 2380.94 mg FeSO<sub>4</sub>/kg for FRAP, 719.42 mg AA/kg for ABTS, %98.71 for ABTS % inhibition, 3690.83 mg AA/kg for TAC, 9566.95 mg GAE/kg for TPC, 11680.71 mg QEE/kg for TFC.

**Table 3.** Rheology values of the pomegranate sauce samples

Sample	Shear rate (1/s)	Viscosity (mPa.s)	Shear stress (Pa)
S1	50	2086.57 ± 58.28 <sup>f</sup>	104.33 ± 2.91 <sup>def</sup>
S2	50	2131.60 ± 25.24 <sup>e</sup>	106.58 ± 1.26 <sup>de</sup>
S3	50	2464.13 ± 162.83 <sup>c</sup>	123.21 ± 8.14 <sup>c</sup>
S4	50	2864.93 ± 118.94 <sup>b</sup>	143.24 ± 5.94 <sup>b</sup>
S5	50	1519.10 ± 115.44 <sup>hi</sup>	75.96 ± 5.77 <sup>fgh</sup>
S6	50	1852.20 ± 51.22 <sup>gh</sup>	92.61 ± 2.56 <sup>ef</sup>
S7	50	3311.63 ± 177.60 <sup>a</sup>	165.58 ± 8.88 <sup>a</sup>
S8	50	722.54 ± 24.49 <sup>j</sup>	36.13 ± 1.22 <sup>hi</sup>
S9	50	793.93 ± 24.74 <sup>ij</sup>	39.70 ± 1.24 <sup>gh</sup>
S10	50	2263.80 ± 95.26 <sup>d</sup>	113.19 ± 4.76 <sup>cd</sup>
S11	50	889.30 ± 18.34 <sup>i</sup>	44.46 ± 0.92 <sup>g</sup>
S12	50	2178.70 ± 60.79 <sup>ef</sup>	108.94 ± 3.04 <sup>d</sup>
S13	50	760.39 ± 6.52 <sup>j</sup>	38.02 ± 0.33 <sup>h</sup>
S14	50	574.29 ± 30.58 <sup>k</sup>	28.71 ± 1.53 <sup>ij</sup>
S15	50	1565.07 ± 24.66 <sup>h</sup>	78.25 ± 1.23 <sup>fg</sup>
S16	50	1861.00 ± 25.72 <sup>g</sup>	93.05 ± 1.28 <sup>e</sup>
S17	50	1710.17 ± 9.26 <sup>ghi</sup>	85.51 ± 0.46 <sup>f</sup>
S18**	50	586.93 ± 115.05 <sup>i</sup>	29.35 ± 5.75 <sup>i</sup>

\* The different letters in the same column mean that the difference

\*\*Control sample

The activity values measured in the sample N18 are considerably higher than the others. For example, the lowest TFC value determined was 23.06 mg QEE/kg in the N17 coded sample, while it was 11680.71 mg QEE/kg in the N18 coded sample, that is, N18 is approximately 500 times higher than N17. Tehranifar et al. [7] reported that pomegranate fruit shows high antioxidant activity due to the phenolic content. Therefore, the more pomegranate juice is added to the pomegranate sauce, the higher the antioxidant activity.

Principal component analysis (PCA) was performed to evaluate the relationship between 18 pomegranate sauces according to their physical and chemical properties. PCA can be described as the most popular method for determining correlations between both variables and observations. In this method, the considering data and all variables can be analyzed on a line chart simultaneously. Principal component analysis (PCA) was applied to all results obtained from the analysis of the pomegranate sauce samples using the XLSTAT (2010) package statistical program, and the resulting graph is shown in Fig. 1.

It is seen that F1 and F2 plots explains 65.97% of the. While the F1 variation explains 43.74%, the F2 variation explains 22.24%. According to the results, the pomegranate sauce samples formed four different groups. The samples S8, S9, S14, S11, and S16 formed one separate group because their antioxidant contents are higher than the other samples except S18. However, the sample S18 is in a separate group alone because it has a very high antioxidant content compared to all other samples. Except for the samples in these two groups, all other samples are grouped together because they have similar results.

**Table 4.** Analysis results of DPPH, FRAP, ABTS, TAC, TPC, TFC of the pomegranate sauce samples

Sample	DPPH mg AA/kg	DPPH % Inhibition	FRAP mg FeSO <sub>4</sub> /kg	ABTS mg AA/kg	ABTS % Inhibition	TAC mg AA/kg	TPC mg GAE/kg	TFC mg QEE/kg
S1	304.73 ± 106.94 <sup>g</sup>	10.19 ± 3.58 <sup>g</sup>	556.90 ± 6.58 <sup>cd</sup>	69.99 ± 7.76 <sup>ef</sup>	9.79 ± 1.08 <sup>ef</sup>	742.93 ± 10.72 <sup>ghi</sup>	210.07 ± 0.95 <sup>fgh*</sup>	235.71 ± 18.73 <sup>hi</sup>
S2	5.23 ± 2.62 <sup>k</sup>	0.17 ± 0.09 <sup>k</sup>	608.77 ± 5.33 <sup>b</sup>	24.05 ± 6.28 <sup>ef</sup>	3.30 ± 0.86 <sup>f</sup>	660.47 ± 11.06 <sup>i</sup>	123.54 ± 10.83 <sup>h</sup>	251.68 ± 66.23 <sup>hi</sup>
S3	49.74 ± 22.82 <sup>jk</sup>	1.63 ± 0.75 <sup>jk</sup>	606.91 ± 8.47 <sup>b</sup>	27.22 ± 9.99 <sup>ef</sup>	3.73 ± 1.36 <sup>ef</sup>	714.39 ± 14.39 <sup>hi</sup>	175.41 ± 23.01 <sup>fgh</sup>	196.74 ± 50.65 <sup>hi</sup>
S4	147.01 ± 62.28 <sup>hi</sup>	4.85 ± 2.05 <sup>hi</sup>	609.96 ± 3.56 <sup>b</sup>	16.95 ± 4.19 <sup>f</sup>	2.34 ± 0.58 <sup>f</sup>	782.23 ± 5.69 <sup>ghi</sup>	202.79 ± 21.55 <sup>fgh</sup>	797.44 ± 37.94 <sup>efg</sup>
S5	265.91 ± 18.25 <sup>g</sup>	8.73 ± 0.60 <sup>g</sup>	544.24 ± 28.70 <sup>d</sup>	98.02 ± 33.84 <sup>e</sup>	13.47 ± 4.65 <sup>e</sup>	917.47 ± 31.48 <sup>fgh</sup>	207.14 ± 26.25 <sup>fgh</sup>	361.04 ± 38.13 <sup>ghi</sup>
S6	24.00 ± 7.42 <sup>k</sup>	0.80 ± 0.25 <sup>k</sup>	580.12 ± 30.54 <sup>bc</sup>	45.60 ± 36.00 <sup>ef</sup>	6.35 ± 5.02 <sup>ef</sup>	776.60 ± 12.82 <sup>ghi</sup>	233.01 ± 17.44 <sup>fgh</sup>	573.23 ± 32.57 <sup>ghi</sup>
S7	107.33 ± 9.75 <sup>ji</sup>	3.57 ± 0.33 <sup>ji</sup>	580.87 ± 7.43 <sup>bc</sup>	46.02 ± 8.77 <sup>ef</sup>	6.40 ± 1.22 <sup>ef</sup>	708.82 ± 6.29 <sup>hi</sup>	163.75 ± 1.66 <sup>gh</sup>	378.49 ± 32.63 <sup>ghi</sup>
S8	1740.02 ± 22.24 <sup>c</sup>	56.96 ± 0.73 <sup>c</sup>	57.94 ± 9.35 <sup>h</sup>	631.85 ± 59.28 <sup>b</sup>	86.53 ± 8.12 <sup>b</sup>	2411.09 ± 429.39 <sup>b</sup>	717.61 ± 56.43 <sup>c</sup>	638.24 ± 19.12 <sup>fgh</sup>
S9	1484.24 ± 58.32 <sup>d</sup>	48.34 ± 1.90 <sup>d</sup>	88.56 ± 6.96 <sup>gh</sup>	571.27 ± 129.60 <sup>b</sup>	77.84 ± 17.66 <sup>b</sup>	1211.40 ± 14.41 <sup>e</sup>	774.87 ± 114.03 <sup>c</sup>	1218.59 ± 33.30 <sup>e</sup>
S10	190.52 ± 57.58 <sup>h</sup>	6.22 ± 1.88 <sup>h</sup>	555.05 ± 4.90 <sup>cd</sup>	89.49 ± 5.77 <sup>ef</sup>	12.23 ± 0.79 <sup>ef</sup>	1033.62 ± 13.27 <sup>f</sup>	270.80 ± 19.58 <sup>def</sup>	971.94 ± 69.13 <sup>ef</sup>
S11	752.57 ± 40.82 <sup>e</sup>	24.66 ± 1.33 <sup>e</sup>	380.02 ± 26.67 <sup>f</sup>	293.36 ± 31.45 <sup>c</sup>	40.21 ± 4.31 <sup>c</sup>	2247.56 ± 31.54 <sup>bc</sup>	351.80 ± 97.30 <sup>d</sup>	858.37 ± 76.44 <sup>ef</sup>
S12	440.32 ± 61.95 <sup>f</sup>	14.33 ± 2.02 <sup>f</sup>	477.31 ± 16.59 <sup>e</sup>	183.84 ± 19.56 <sup>d</sup>	25.02 ± 2.66 <sup>d</sup>	782.07 ± 6.43 <sup>ghi</sup>	255.97 ± 4.27 <sup>efg</sup>	953.26 ± 57.73 <sup>ef</sup>
S13	459.94 ± 9.48 <sup>f</sup>	14.98 ± 0.31 <sup>f</sup>	491.30 ± 27.81 <sup>e</sup>	166.45 ± 32.78 <sup>d</sup>	22.68 ± 4.47 <sup>d</sup>	904.31 ± 13.30 <sup>fgh</sup>	247.20 ± 23.11 <sup>efg</sup>	2394.72 ± 19.22 <sup>d</sup>
S14	1869.84 ± 29.91 <sup>b</sup>	62.04 ± 0.99 <sup>b</sup>	86.06 ± 8.35 <sup>hg</sup>	627.18 ± 15.11 <sup>b</sup>	87.06 ± 2.10 <sup>b</sup>	1877.48 ± 70.19 <sup>d</sup>	1526.21 ± 80.78 <sup>b</sup>	3636.59 ± 75.48 <sup>b</sup>
S15	500.18 ± 32.73 <sup>d</sup>	16.47 ± 1.08 <sup>f</sup>	378.20 ± 24.43 <sup>f</sup>	291.96 ± 28.80 <sup>c</sup>	40.21 ± 3.97 <sup>c</sup>	763.70 ± 37.55 <sup>ghi</sup>	338.95 ± 18.07 <sup>de</sup>	338.19 ± 211.78 <sup>ghi</sup>
S16	1744.37 ± 38.01 <sup>c</sup>	57.25 ± 1.25 <sup>c</sup>	96.45 ± 4.37 <sup>g</sup>	616.01 ± 21.50 <sup>b</sup>	84.57 ± 2.95 <sup>b</sup>	2142.69 ± 16.51 <sup>c</sup>	1448.38 ± 49.34 <sup>b</sup>	3070.88 ± 212.44 <sup>c</sup>
S17	320.58 ± 13.14 <sup>g</sup>	10.45 ± 0.43 <sup>g</sup>	609.78 ± 9.02 <sup>b</sup>	26.63 ± 10.63 <sup>ef</sup>	3.63 ± 1.45 <sup>ef</sup>	684.45 ± 13.29 <sup>i</sup>	124.17 ± 19.02 <sup>h</sup>	23.06 ± 5.36 <sup>i</sup>
S18**	2822.69 ± 3.01 <sup>a</sup>	92.58 ± 0.10 <sup>a</sup>	2380.94 ± 46.69 <sup>a</sup>	719.42 ± 0.00 <sup>a</sup>	98.71 ± 0.01 <sup>a</sup>	3690.83 ± 41.00 <sup>a</sup>	9566.95 ± 108.09 <sup>a</sup>	11680.71 ± 1042.63 <sup>a</sup>

\* The different letters in the same column mean that the difference between the results is statistically significant at  $p < 0.05$  according to the Duncan test

\*\* Control sample

Principal component analysis (PCA) was performed to evaluate the relationship between 18 pomegranate sauces according to their physical and chemical properties. PCA can be described as the most popular method for determining correlations between both variables and observations. In this method, the considering data and all variables can be analyzed on a line chart simultaneously. Principal component analysis (PCA) was applied to all results obtained from the analysis of the pomegranate sauce samples using the XLSTAT (2010) package statistical program, and the

resulting graph is shown in Fig. 1. It is seen that F1 and F2 plots explains 65.97% of the. While the F1 variation explains 43.74%, the F2 variation explains 22.24%. According to the results, the pomegranate sauce samples formed four different groups. The samples S8, S9, S14, S11, and S16 formed one separate group because their antioxidant contents are higher than the other samples except S18. However, the sample S18 is in a separate group alone because it has a very high antioxidant content compared to all other samples. Except for the

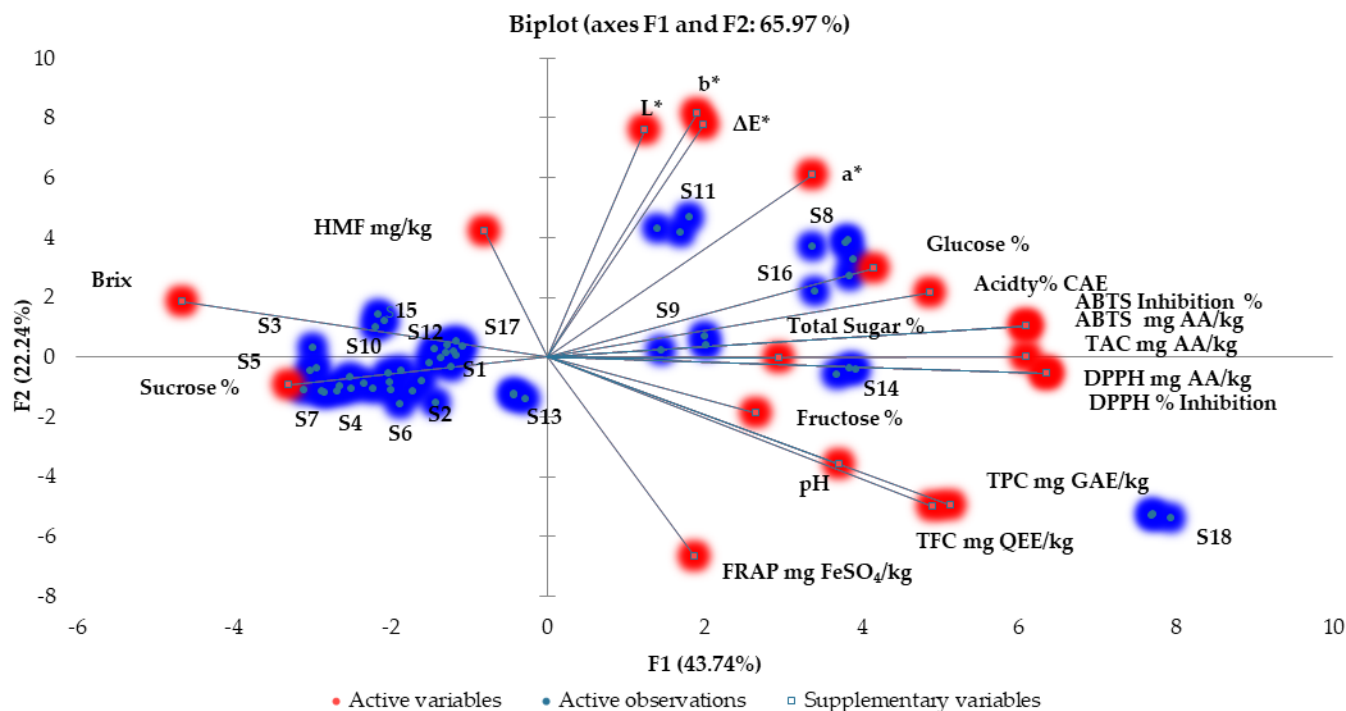


**Figure 1.** Results of the principal component analysis (PCA) for the pomegranate sauces

samples in these two groups, all other samples are grouped together because they have similar results.

#### 4. Conclusions

This study was carried out to determine the some physicochemical and antioxidant properties of the pomegranate sauces. In terms of many parameters, the analysis results of the samples were different from each other due to raw materials, additional additives, applied heat treatments, and production process. The antioxidant content of the sample N18 (produced in the laboratory) is very high compared to all other samples as it is obtained from fresh pomegranate juice, and contains no additives except starch, sugar, and lemon. Because of the positive effects of pomegranate and pomegranate products on human health, its consumption should be increased. However, antioxidant activity and HMF contents are important in the production of pomegranate products.

#### References

- [1] D. Heber, R.N. Schulman, N.P. Seeram, Pomegranates: ancient roots to modern medicine (1st edition). 2006, Boca Raton, USA: CRC Press.
- [2] H. Kurt, G. Şahin, Bir ziraat coğrafyası çalışması: Türkiye’de nar (*Punica granatum* L.) tarımı. Marmara Coğrafya Dergisi, 27, 2013, 551–574 (in Turkish).
- [3] D. Narzary, T.S. Rana, S.A. Ranade, Genetic diversity in inter-simple sequence repeat profiles across natural populations of Indian pomegranate (*Punica granatum* L.), Plant Biol, 12(5), 2010, 806–813.
- [4] E. Shaygannia, M. Bahmani, B. Zamanzad, M. Rafieian-Kopaei, A review study on *Punica granatum* L., Evid-Based Compl Alt Med, 21(3), 2016, 221–227.
- [5] M. Mars, Pomegranate plant material: Genetic resources and breeding, a review, Options Mediterr Serie A, 42, 2000, 55–62.
- [6] A. Sarkhosh, Z. Zamani, R. Fatahi, H. Ghorbani, J.A.V.A.D. Hadian, A review on medicinal characteristics of pomegranate (*Punica granatum* L.), J Med Plant Res, 6(22), 2007, 13–24.
- [7] A. Tehranifar, M. Zarei, Z. Nemati, B. Esfandiari, M.R. Vazifeshenas, Investigation of physico-chemical properties and antioxidant activity of twenty Iranian pomegranate (*Punica granatum* L.) cultivars, Sci Hort, 126(2), 2010, 180–185.
- [8] A. İkinci, I. Bolat, M. Şimşek, International pomegranate trade and pomegranate standard, In International Gap Agriculture and Livestock Congress, Şanlıurfa, Turkey, 2005, 607–613.
- [9] N. Erbil, M. Arslan, Geleneksel yöntemlerle üretilen nar ekşisinin antibakteriyel ve antimutajenik etki potansiyeli, Erzincan Üniversitesi Fen Bilimleri Enstitüsü Dergisi, 12, 2019, 957–965 (in Turkish).
- [10] R. Gunnaiah, R.C. Jagadeesha, S. Cholin, G. Prabhuling, A.G. Babu, B. Fakrudin, P. Pujer, S.B.N. Murthy, Genetic diversity assessment and population structure analysis of pomegranate cultivars from different countries and Himalayan wild accessions, J Hort Sci Biotech, 96(5), 2021 614–623.
- [11] Tübives, *Punica granatum* L., 2022, <http://www.tubives.com/>
- [12] A.I. Özgüven, C. Yılmaz, Pomegranate growing in Turkey, Options Mediterr Serie A: Seminaires Mediterraneennes, 42, 2000, 41–48.
- [13] M. Maskan, Production of pomegranate (*Punica granatum* L.) juice concentrate by various heating methods: colour degradation and kinetics, J Food Eng, 72(3), 2006, 218–224.
- [14] M. Viuda-Martos, J. Fernández-López, J.A. Pérez-Álvarez, Pomegranate and its many functional components as related to human health: a review, Compr Rev Food Sci, 9(6), 2010, 635–654.
- [15] Z. Kalaycıoğlu, F.B. Erim, Total phenolic contents, antioxidant activities, and bioactive ingredients of juices from pomegranate cultivars worldwide, Food Chem, 221, 2017, 496–507.
- [16] M. Ozgen, C. Durgaç, S. Serçe, C. Kaya, Chemical and antioxidant properties of pomegranate cultivars grown in the Mediterranean region of Turkey, Food Chem, 111(3), 2008, 703–706.
- [17] S.Ö. Ergin, Nar meyvesi (*Punica granatum* L.) ile farklı nar ürünlerinin antioksidan özellikleri, Akademik Gıda, 17(2), 2019, 243–251 (in Turkish).
- [18] S.D. Johanningsmeier, G.K. Harris, Pomegranate as a functional food and nutraceutical source, Annu Rev Food Sci Tech, 2, 2011, 181–201.
- [19] F. Muradoglu, M.F. Balta, K. Ozrenk, Pomegranate (*Punica granatum* L.) genetic resources from Hakkari, Turkey, J Agric Biol Sci, 2(6), 2006, 520–25.
- [20] Ö. Taştan, T. Baysal, Nar ürünleri ve üretimi, Nar sağlıkta yıldız, Editors: E. Akççek H, Kayalar, Ö, Semih, 2018, Gece Kitaplığı, Türkiye (in Turkish).
- [21] B. Dayi, H.A. Akdoğan, A. Akdoğan, Nar sosunda kromatografik yöntemle bazı polisiklik aromatik hidrokarbonların analizi, Akademik Gıda, 15(3), 2017, 269–273.
- [22] H. Yildiz, M. Sengul, B. Cetin, N. Karatas, S. Ercisli, Z. Okcu, S. Hadziabulic, Antioxidant and antimicrobial activities of pomegranate (*Punica granatum* L.) sour sauce extracts, CR Acad Bulg Sci, 67(1), 2014, 145–156.
- [23] TS 1562, Çay-Rutubet Tayini, 1990, Türk Standartları Enstitüsü, Ankara.
- [24] TS 1728 ISO 1842, Meyve ve Sebze Ürünleri- pH Tayini, 2001, Türk Standartları Enstitüsü, Ankara.
- [25] S.Y. Quek, N.K. Chok, P. Swedlund, The physicochemical properties of spray dried watermelon powders, Chem Eng Process: Process Intensif, 46(5), 2007, 386–392.
- [26] TS 6178 ISO 7466, Meyve ve Sebze Ürünleri- 5-Hidroksimetilfurfural (5-HMF) İçeriğinin Tayini, 2002, Türk Standartları Enstitüsü, Ankara.
- [27] C. Baltacı, H. İlyasoglu, A. Gundogdu, O. Ucuncu, Investigation of hydroxymethylfurfural formation in herle. Int J Food Prop, 19(12), 2016, 2761–2768.
- [28] C. Baltacı, Z. Akşit, Validation of HPLC method for the determination of 5-hydroxymethylfurfural in pestil, köme, jam, marmalade and pekmez, Hittite J Sci Eng, 3(2), 2016, 91–97.
- [29] IHC, International Honey Commission, 2009, (<http://www.ihc-platform.net/ihcmethods2009.pdf>)
- [30] İ. Tosun, Standardı olan bazı reçel çeşitlerinin bileşimi üzerine araştırmalar. Yüksek Lisans Tezi, Ondokuz Mayıs Üniversitesi, Fen Bilimleri Enstitüsü, 1991.
- [31] W. Brand-Williams, M.E., Cuvelier, C.L.W.T. Berset, Use of a free radical method to evaluate antioxidant activity, LWT-Food Sci Tech, 28(1), 1995, 25–30.
- [32] D. Ahmed, M.M. Khan, R. Saeed, Comparative analysis of phenolics, flavonoids, and antioxidant and antibacterial potential of methanolic, hexanic and aqueous extracts from adiantum caudatum leaves, Antioxidants, 4(2), 2015, 394–409.
- [33] I.F. Benzie, J.J. Strain, The ferric reducing ability of plasma (FRAP) as a measure of “antioxidant power”: the FRAP assay, Anal Biochem, 239(1), 1996, 70–76.
- [34] P. Kantangana, P.S. Haddad, T. Stevanovic, Study of polyphenol content and antioxidant capacity of myrianthus arboreus (cecropiaceae) root bark extracts, Antioxidants (Basel), 4(2), 2015, 410–426.

- [35] V.L. Singleton, K. Slinkard, Total phenol analysis: automation and comparison with manual methods, *Am J Enol Vitic*, 28(1), 1977, 49–55.
- [36] H. Sun, S. Zhang, C. Chen, C. Li, S. Xing, J. Liu, J. Xue, Detection of the soluble solid contents from fresh jujubes during different maturation periods using NIR hyperspectral imaging and an artificial bee colony, *J Anal Methods Chem*, 2019, 5032950.
- [37] Kusumiyati, Y. Hadiwijaya, I.E. Putri, S. Mubarak, J.S. Hamdani, Rapid and non-destructive prediction of total soluble solids of guava fruits at various storage periods using handheld near-infrared instrument. In *IOP Conference Series: Earth and Environmental Science*; IOP Publishing: Bristol, UK, 2020; pp. 1–7
- [38] P.S.R., Kesters, K.W. Waldron, Production of high-value functional vegetable juices from food co-products. In *Handbook of Waste Management and Co-Product Recovery in Food Processing*, Editor: K. Waltron, 2009, UK, Woodhead Publishing.
- [39] S. Karabiyikli, D. Kışla, Inhibitory Effect of Sour Pomegranate Sauces on Some Green Vegetables and Kisir, *Int J Food Microbiol*, 155(3), 2012, 211–216.
- [40] A. Andrés-Bello, V. Barreto-Palacios, P. García-Segovia, J. Mir-Bel, J. Martínez-Monzó, Effect of pH on color and texture of food products, *Food Eng Rev*, 5(3), 2013, 158–170.
- [41] K. Abraham, R. Gürtler, K. Berg, G. Heinemeyer, A. Lampen, K.E. Appel, Toxicology and risk assessment of 5-Hydroxymethylfurfural in food, *Mol Nutr Food Res*, 55(5), 2011, 667–678.
- [42] M.R. Farag, M. Alagawany, M. Bin-Jumah, S.I. Othman, A.F. Khafaga, HM, Shaheen, D. Samak, A.M. Shehata, A.A. Allam, E.A.E.H. Mohamed, The toxicological aspects of the heat-borne toxicant 5-hydroxymethylfurfural in animals: a review, *Molecules*, 25(8), 2020, 1941.
- [43] D. Kışla, Ş. Karabiyikli, Antimicrobial effect of sour pomegranate sauce on *Escherichia coli* O157: H7 and *Staphylococcus aureus*, *J Food Sci*, 78(5), 2013, 715–718.
- [44] Ö. Turfan, M. Türkyılmaz, O. Yemiş, M. Özkan, Anthocyanin and colour changes during processing of pomegranate (*Punica granatum* L., cv. Hicaznar) juice from sacs and whole fruit, *Food Chem*, 129(4), 2011, 1644–1651.
- [45] E. Shaygannia, M. Bahmani, B. Zamanzad, M. Rafieian-Kopaei, A review study on *Punica granatum* L., *Evid. Based Complementary Altern Med*, 21(3), 2016, 221–227.
- [46] W.S. Mokrzycki, M. Tatol, Colour difference  $\Delta E$ -A survey, *Mach. Graph. Vis*, 20(4), 2011, 383–411.
- [47] E. Hidayanto, T. Tanabe, J. Kawai, Measurement of viscosity and sucrose concentration in aqueous solution using portable Brix meter, *Berk Fis*, 13(2), 2010, 23–28.
- [48] Z. Akar, A. Karakurt, F. Okumuş, S. Cinemre, A.Ö. Düzgün, B. Akar, Z. Can, RP-HPLC-UV Analysis of the Phenolic Compounds, Antimicrobial Activity Against Multi-Drug Resistant Bacteria and Antioxidant Activity of Fruit and Seed of *Diospyros lotus* L., *Int J Second Metab*, 7(4), 2020, 237–246.



# Determination of ethylenediaminetetraacetic acid (EDTA) levels in surface waters by high performance liquid chromatography (HPLC)-Ultraviolet/Visible (UV/VIS) detector

Oltan Canlı<sup>1\*</sup> , Barış Güzel<sup>1</sup> , Kartal Çetintürk<sup>2</sup> 

<sup>1</sup> Water Management and Treatment Technologies Research Group, Climate Change and Sustainability Vice Presidency, TUBITAK Marmara Research Center, 41470, Kocaeli, Türkiye

<sup>2</sup> İstanbul University, Institute of Marine Science and Management, 34470, İstanbul, Türkiye

## Abstract

Ethylenediaminetetraacetic acid (EDTA), a chemical harmful to human health with its high solubility in water, is used as a metal chelating agent in various sectors. Thus, it is necessary to be monitored in surface waters taken from dams supplying drinking and utility water. This work presents the applicability of the HPLC-UV/VIS system for the quantification of EDTA in surface waters based on the limit values of national and international legislations. The applicability of EDTA quantification in surface water was checked with validation study. The method validation consisted of selectivity, calibration curve linearity, limit of detection (LOD) and limit of quantification (LOQ), accuracy (recovery), and precision. The linearity of EDTA was obtained ranging from 10 µg/L to 200 µg/L concentrations with the correlation coefficient of 0.9985 and the calibration curve equation of  $y = 4659.4x - 50223$ . The LOD and LOQ values of EDTA were 2.85 µg/L and 9.51 µg/L with the RSD of 5.36. In accuracy, the mean recovery of EDTA in surface water has been determined as 87.51 percent with an RSD of 6.11. The repeatability (RSD, %) varied from 5.44% to 7.02% with concentrations of  $35.19 \pm 1.91$  µg/L and  $17.11 \pm 1.20$  µg/L, whereas the reproducibility (RSD, %) was obtained at 3.45% with the concentration of  $34.13 \pm 1.18$  µg/L. In this study, the presence of EDTA was investigated in approximately 300 surface water samples and EDTA was found as positive in the concentration range of 11.17 µg/L to 52.14 µg/L in eleven real samples.

**Keywords:** EDTA, HPLC, pollution, water

## 1. Introduction

Ethylenediaminetetraacetic acid (EDTA) is an aminopolycarboxylic acid with multiple bonded -COOH groups and -NH<sub>2</sub> bonded in its structure (Fig. 1). It is a white, water-soluble solid commonly used to bind acid, iron, and calcium ions. Most of the EDTA available in general is in the form of the free acid and disodium salt. The free acid form is insoluble in water. Depending on the pH value, metals form stable complexes with EDTA. It is in the form of chelating agents in the pharmaceutical, food, personal care product, agricultural industries, and household [1,2]. The polarity, chelating ability towards metal ions, high solubility, and low biodegradability properties of EDTA in water allow it to be identified as a persistent organic pollutant in the aquatic environment [3,4]. The use and sustainable management of land and water resources have been made important with increasing environmental awareness recently. The widespread use

and diversification of EDTA usage in industrial areas along with the developing technology have brought about an increase in environmental concerns. Therefore, the monitoring of EDTA presence especially in the environment is critical for human health and the environment [5].

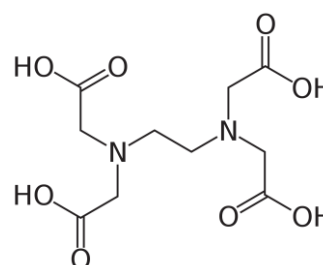


**Figure 1.** The chemical structure of EDTA

Its physical and chemical properties can lead to spread easily on the environment and may have carcinogenic,

**Citation:** O. Canlı, B. Güzel, K. Çetintürk, Determination of Ethylenediaminetetraacetic acid (EDTA) levels in surface waters by high performance liquid chromatography (HPLC)-Ultraviolet/Visible (UV/VIS) detector, Turk J Anal Chem, 4(2), 2022, 76–79.

 <https://doi.org/10.51435/turkjac.1124687>

**\*Author of correspondence:** oltan.canli@tubitak.gov.tr

**Tel:** +90 (262) 677 2922

**Fax** +90 (262) 641 2309

**Received:** June 06, 2022

**Accepted:** October 16, 2022

mutagenic, and toxic effects on humans and aquatic organisms [2]. Thus, the release of EDTA has been monitored and controlled in the world continuously with national and international lists and regulations. In this context, there is national and international legislation such as the Turkish Regulation on the Management of Surface Water Quality [6] and the EU Water Framework Directive (2008/105/EC on Environmental Quality Standards) [7] for monitoring EDTA concentration in surface waters. According to Table 4 of the Annexes of the Surface Water Quality Regulation in Turkey, the environmental quality standard limit for EDTA in lakes, rivers, and coastal and transitional waters is 39 µg/L.

From the past to the present, there are many studies that reported the determination of EDTA in water samples in different analytical methods and systems such as HPLC [8], ion chromatography/mass spectrometry (IC/MS) [4,9], gas chromatography/mass spectrometry (GC/MS) [1,2,10], and liquid chromatography/tandem spectrometry (LC-MS/MS) [11]. The aim of the current work was to investigate the applicability of the HPLC-UV/VIS system for the quantification of EDTA in surface waters based on the limit values of national and international legislation such as the Turkish Regulation on the Management of Surface Water Quality. In the literature, studies conducted on samples prepared with the use of solvents in GC/MS are contrary to the "Green Chemistry Approach", which is based on the protection of human and environmental health. In this regard, this study is important in terms of obtaining fast and precise EDTA results and savings on time and solvent cost.

## 2. Materials and methods

### 2.1. Reagents and chemicals

Ethylenediaminetetraacetic acid disodium salt dehydrate was purchased from Sigma-Aldrich (St. Louis Missouri, USA). HPLC grade methanol was supplied from Merck (Darmstadt, Germany). The purification of water used to prepare the solutions was done with a Milli-Q Plus system (EMD Millipore, Billerica, MA). To draw the calibration graphs, calibration solutions were prepared from 10 mg/L concentrations of stock standard solution, respectively. They were preserved in a freezer (-20 °C) at 1.5 mL vials and were prepared once a month again.

### 2.2. HPLC-UV/VIS analytical condition

All the measurements were performed on an HPLC-UV/VIS instrument consisting of a binary pump (Shimadzu LC-10AD HPLC Binary Pump model), Shimadzu automatic injector (SIL-10AF model), and a

column oven (CTO-10AS model). Shimadzu UV/VIS detector (SPD-10AV model, Light source: D2 deuterium lamp) was used. Column possessing Symmetry C8 150 mm × 3.9 mm id, 5-µm particle size (Waters Technologies, Ireland) as an analytical column was used. The HPLC method used gradient mobile phases containing LC grade distilled water (mobile phase A) and methanol (mobile phase B). The column temperature was set at 25 °C with a flow rate of 0.3 mL/min. The gradient profile was programmed as follows: 0 – 2 min 20% B; 2 – 9 50% B; hold at 20% B 1 min (total run time 10 min). The injection volume was 100 µL. Data acquisition and processing were done with Shimadzu LabSolutions/LCsolution GPC software version 2.1.

### 2.3. Surface water samples and sample preparation

Surface water samples were collected from five lakes including Naipköy lake (Tekirdağ), Alibey lake (İstanbul), Omerli lake (İstanbul), Elmalı lake (İstanbul) and Sapanca lake (Sakarya) on January 4–18, 2021. They were fully filled in 500 mL glass bottles and were preserved in pursuant to International Organization for Standardization (ISO) standard [12]. The stability of samples was provided by storing below 5 °C. All samples were analyzed by HPLC within 36 hours of reaching the laboratory. Their pH values changed from 7.28 to 7.68.

The preparation of water samples for measurement in HPLC does not contain solvent and consists of a single step. All the samples were taken into a vial by filtering through a 0.22 µm filter.

### 2.4. Analytical performance of HPLC-UV/VIS method

The applicability of EDTA quantification in surface water was checked with validation study consisting of selectivity, calibration curve linearity, limit of detection (LOD) and limit of quantification (LOQ), accuracy (recovery), and precision according to the EURACHEM Guideline [13] and Guidelines for Standard Method Performance Requirements [14].

## 3. Results and discussions

### 3.1. Selectivity, linearity and sensitivity (LOD and LOQ)

The selectivity study of EDTA was done with the investigation of blank samples consisting of only ultrapure (deionized organic-free) water. As a result of eight measurements sequentially, no peaks belonging to interfering compounds that would cause false-positive results were found in the chromatograms at the retention time of EDTA (5.773 min.) (Fig. 2).

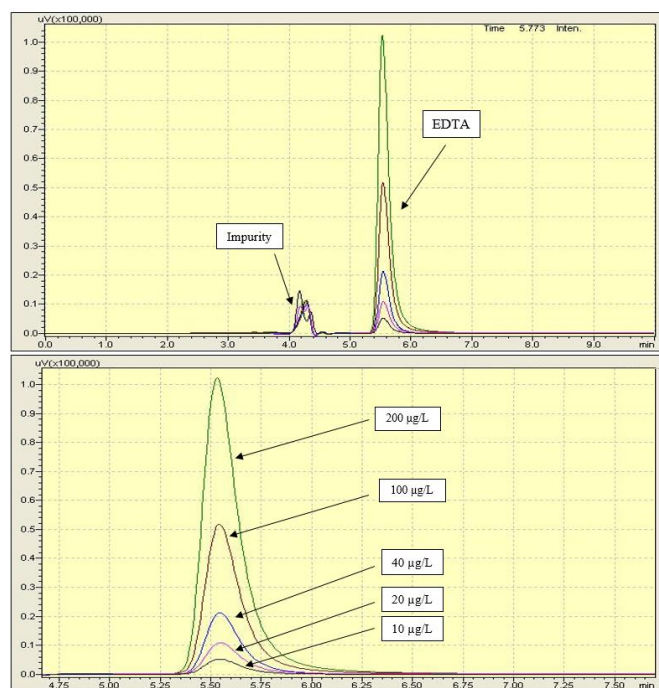


**Figure 2.** The view of the concentration levels of EDTA in the chromatogram of HPLC-UV/VIS

The linearity of EDTA was obtained ranging from 10 µg/L to 200 µg/L concentrations at five concentration levels prepared by using the necessary amount of stock standard solution in 10 mL of ultra-deionized water (Fig. 2). In the validation study, acceptable linearity of any substance is linear regression with a correlation coefficient better than 0.99 [15–18]. Fig. 3 shows that the correlation coefficient of EDTA with the calibration curve equation of  $y = 4659.4x - 50223$  was 0.9985 which defines as excellent in pursuance of the correlation coefficient.

The measurement sensitivity (LOD and LOQ) study of EDTA in HPLC-UV/VIS was done by seven measurements in the solutions prepared by spiking stock standard solution of EDTA to ultra-deionized pure water to have a concentration of 20 µg/L. The calculations of LOD and LOQ were actualized by multiplying the average noise value obtained from the chromatogram by three and ten, respectively. As can be seen in Table 1, the LOD and LOQ values of EDTA were 2.85 µg/L and 9.51 µg/L with the relative standard deviation (RSD) of 5.36. Also, LOD and LOQ values of this method are similar and comparable with the results of Kuran and co-workers [2].

### 3.2. Accuracy and precision

The reliability of the HPLC-UV/VIS method was checked with accuracy, which is defined as the recovery results of the concentration of 20 µg/L in seven measurements, and precision (repeatability and reproducibility studies). The repeatability was made at two concentrations of 20 µg/L and 40 µg/L and the reproducibility was only done at the concentration of 40 µg/L in six measurements.

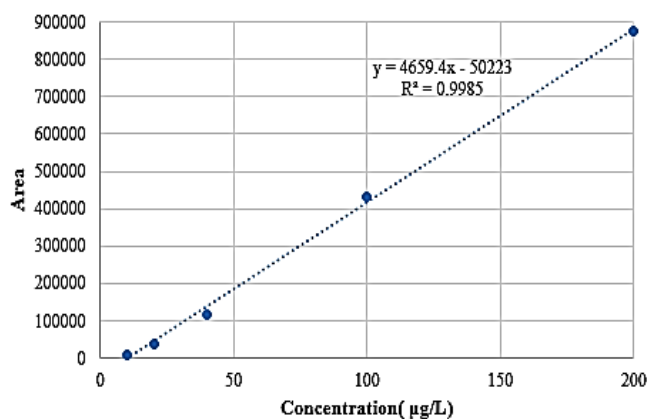


**Figure 3.** The linearity of EDTA from 10 µg/L to 200 µg/L concentrations

The studied concentrations were prepared by spiking the surface water samples. In Table 1, the mean recovery of EDTA in surface water has been determined as 87.51 percent with an RSD of 6.11%. The repeatability (RSD, %) varied from 5.44% to 7.02% with concentrations of  $35.19 \pm 1.91$  µg/L and  $17.11 \pm 1.20$  µg/L, whereas the reproducibility (RSD, %) was obtained at 3.45% with the concentration of  $34.13 \pm 1.18$  µg/L. As seen in Table 1, the accuracy and precision results of the study show that the method meets the requirements for the rapid and accurate determination of EDTA in surface waters according to the validation guidelines for Standard Method Performance Requirements [14].

**Table 1.** LOD-LOQ, accuracy, and precision (repeatability and reproducibility) of EDTA

Analytical performance/compound		EDTA	
LOD-LOQ	LOD (µg/L)	2.85	
	LOQ (µg/L)	9.51	
	RSD (n=7 %)	5.36	
Accuracy	Recovery (%)	87.51	
	RSD (%)	6.11	
Repeatability	20 µg/L	$17.11 \pm 1.20$	
	RSD (%)	7.02	
	40 µg/L	$35.19 \pm 1.91$	
	RSD (%)	5.44	
Reproducibility	Area 1	211788	
	Area 2	217604	
	Area 3	218364	
	Day 1	Area 4	209254
		Area 5	197523
		Area 6	195509
	Mean	208340	
	Day 2	Area 1	196714
		Area 2	200018
		Area 3	201487
		Area 4	198455
		Area 5	201114
Area 6		209525	
Mean	201219		
40 µg/L	$34.13 \pm 1.18$		
RSD (%)	3.45		

### 3.3. Real samples

In this study, the presence of EDTA was investigated in approximately three hundred surface water samples taken from the dams mentioned in Section 2.3. As a result of the analysis of the relevant samples, the presence and amount of EDTA were determined according to the areas of the standards included in the calibration and the retention time in the chromatogram. EDTA was found as positive in the concentration range of  $11.17 \pm 0.28 \mu\text{g/L}$  to  $52.14 \pm 0.21 \mu\text{g/L}$  in eleven real samples. In Table 4 of Annexes to the Surface Water Quality Regulation in TURKEY,  $39 \mu\text{g/L}$  EDTA concentration in lakes, rivers, coastal and transitional waters is the environmental quality standard limit. This limit value was exceeded in two of the samples obtained with a positive EDTA result.

### 4. Conclusions

This paper was presented rapid, simple (solvent-free pre-treatment) and reliable HPLC-UV/VIS analytical method for the determination of presence of EDTA in surface waters. Applicability of the related method in the analysis of EDTA in surface waters was checked with the parameters of selectivity, calibration curve linearity, the limit of detection (LOD) and limit of quantification (LOQ), accuracy (recovery), and precision according to the related documents/guidelines [13,14]. EDTA ranging from  $10 \mu\text{g/L}$  to  $200 \mu\text{g/L}$  concentrations at five concentration levels had excellent linearity with a correlation coefficient of 0.9985. The LOD and LOQ values of EDTA were  $2.85 \mu\text{g/L}$  and  $9.51 \mu\text{g/L}$  with the RSD of 5.36. The related method was applied to approximately three hundred surface water samples and was obtained successful results.

### Acknowledgements

The authors would like to thank Hüseyin Demir for his support in the laboratory studies.

### References

- [1] R. Kubota, M. Tahara, K. Shimizu, N. Sugimoto, T. Nishimura, Determination of EDTA in water samples by SPE-gas chromatography/mass spectrometry, *J. Water Environ Technol*, 8, 2010, 347–353.
- [2] P. Kuran, D. Pilnaj, M. Dzurkova, M. Smaha, Method development for determination of EDTA in water by using traditional split/splitless injector-Comparing external and internal standard methods of quantification, *IOP Conf Ser: Earth Environ Sci*, 221, 2019, 012126, 1–6.
- [3] F.G. Kari, W. Giger, Speciation and fate of ethylenediaminetetraacetate (EDTA) in municipal wastewater treatment, *Water Res*, 30, 1996, 122–134.
- [4] T.P. Knepper, A. Werner, G. Bogenschütz, Determination of synthetic chelating agents in surface and wastewater by ion chromatography-mass spectrometry, *J. Chromatogr. A*, 1085, 2005, 240–246.
- [5] C. Oviedo, J. Rodríguez, EDTA: The chelating agent under environmental scrutiny, *Quim Nova*, 26(6), 2003, 901–905.
- [6] SWR, The Turkish Regulation on the Management of Surface Water Quality, 2012, Official Gazette: 30.11.2012. Number: 28483.
- [7] WFD, Council Directive 2008/105/EC of the European Parliament and of the Council of 16 December 2008 on Environmental Quality Standards in the Field of Water Policy, 2008.
- [8] T. Kemmei, S. Kodama, T. Muramoto, H. Fujishima, A. Yamamoto, Y. Inoue, K. Hayakawa, Study of solidphase extraction for the determination of sequestering agents in river water by high-performance liquid chromatography, *J Chromatogr A*, 1216, 2009, 1109–1114.
- [9] K.H. Bauer, T.P. Knepper, A. Maes, V. Schatz, M. Voihsel, Analysis of polar organic micropollutants in water with ion chromatography-electrospray mass spectrometry, *J Chromatogr A*, 837, 1999, 117–128.
- [10] Y. Nishikawa, T. Okumura, Determination of nitrilotriacetic acid and ethylenediaminetetraacetic acid in environmental samples as their methyl ester derivatives by gas chromatography-mass spectrometry, *J Chromatogr A*, 690, 1995, 109–118.
- [11] J.B. Quintana, T. Reemtsma, Rapid and sensitive determination of ethylenediaminetetraacetic acid and diethylenetriaminepentaacetic acid in water samples by ion-pair reversed-phase liquid chromatography-electrospray tandem mass spectrometry, *J Chromatogr A*, 1145, 2007, 110–117.
- [12] ISO, Guide to the Expression of Uncertainty in Measurements. International Organization for Standardization (ISO), Geneva, Switzerland, 1993. <https://www.iso.org/standard/45315.html>.
- [13] EURACHEM, The Fitness for Purpose of Analytical Methods: A Laboratory Guide to Method Validation and Related Topics. 2nd edn., LGC, Teddington, 2014. [https://www.eurachem.org/images/stories/Guides/pdf/MV\\_guid\\_e\\_2nd\\_ed\\_EN.pdf](https://www.eurachem.org/images/stories/Guides/pdf/MV_guid_e_2nd_ed_EN.pdf)
- [14] AOAC, Guidelines for Standard Method Performance Requirements. Appendix F., Association of Official Analytical Chemists, aVirginia, aUSA, a2016. [http://www.eoma.aoac.org/app\\_f.pdf](http://www.eoma.aoac.org/app_f.pdf)
- [15] J.A. Ferreira, J.M.S Ferreira, V. Talamini, J. F. Facco, T.M. Rizzetti, O. D. Prestes, M.B. Adaime, R. Zanella, C.B.G. Bottoli, Determination of pesticides in coconut (*Cocos nucifera* Linn.) water and pulp using modified QuEChERS and LC-MS/MS, *Food Chem*, 213, 2016, 616–624.
- [16] B. Güzel, O. Canlı, Method validation and measurement uncertainty of possible thirty volatile organic compounds (VOCs) presented in the polyethylene present in bottled drinking waters sold in Turkey, *J Anal Sci Technol*, 11 (44), 2020, 1–17.
- [17] B. Güzel, O. Canlı, E. Oktem-Olgun, Gas chromatography method validation study for sensitive and accurate determination of volatile aromatic hydrocarbons (VAHs) in water, *Cumhuriyet Sci J*, 39 (4), 2018, 970–982.
- [18] B. Güzel, O. Canlı, Applicability of purge & trap GC-MS method for sensitive analytical detection of naphthalene and its derivatives in waters, *J Mass Spectrom*, 55, 2020, 12.



# Fast pyrolysis of fig leaves: Influence of pyrolysis parameters and characterization of bio-oil

Turgay Kar , Sedat Keleş\* , Zafer Emir , Kamil Kaygusuz 

Karadeniz Technical University, Faculty of Science, Department of Chemistry, 61080, Trabzon, Türkiye

## Abstract

Liquid yields achieved by fast pyrolysis of ligno-cellulosic biomass can be used in the production of chemical raw materials or as an energy source. Pyrolysis product yields generally depend on the type of biomass, temperature, retention time, heating rate, sweeping gas flow rate and particle size. In this study, fast pyrolysis of fig leaves selected as biomass was carried out in a fixed bed pyrolysis reactor. Fig leaves used in fast pyrolysis experiments in this study as an agricultural by-product can be obtained in large quantities from Türkiye. In the experiments, the effect of temperature, entraining gas flow rate, and particle size on pyrolysis product yields were investigated. The experiments were carried out at 400, 500, 600, 700 °C, four different particle sizes. The highest liquid product yield was obtained at 600 °C, while the heating rate was 200 cm<sup>3</sup>/min and the particle size was < 0.150 mm. According to the test results, the most effective parameter on liquid product yield is temperature. Based on the results of this analysis the H/C molar ratio (1.71) and the high calorific value (14.25 MJ/kg) indicate that FL can be used the source of raw materials in obtaining liquid fuel. Instrumental techniques such as FT-IR, SEM-EDS, TG/DTG and GC-MS were used for the characterization of bio-oil. The bio-oil contains alkenes, aldehydes, carboxylic acids, and aromatic structures such as indole derivative as well as alkanes. The heating value of the bio-oil is 32.16 MJ/kg which is close to those of petroleum fractions.

**Keywords:** Renewable energy, biomass, fast pyrolysis, fig leaves, bio-oil

## 1. Introduction

There are two major problems that have occupied the world agenda in recent years. One is environmental problems and the other is increasing energy demand. Meeting the rising energy demand from fossil fuels in large quantities brings with it the environmental pollution and the energy crisis. As fossil fuels burn, gasses such as carbon dioxide, methane, sulfur oxides, nitrogen oxides are released to the environment, which causes global warming. Unless that gases emissions are limited, humans will face more threats from global warming and climate change. Moreover, the fact that existing fossil fuel resources will not meet future demand will lead to an increase in energy prices, bringing about the energy crisis and wars. With the awareness of the environment becoming more apparent after the second half of the 20th century, mankind has begun to recognize and diminish the damage it inflicts on the environment. Recently, the increase in energy demand has led to the search for alternative energy sources for fossil energy sources with an increase in environmental awareness [1]. Renewable and clean

energy is a type of energy derived from continuous and sustainable sources of energy, such as solar, geothermal, biomass, wind, hydropower, which are not exhaustible, such as fossil fuels [2]. Clean energy investments have some of advantages that reducing dependence on foreign energy sources, reducing greenhouse gases and conventional pollutants, and creating new business areas [3]. The three main components of biomass are cellulose, hemicellulose, and lignin. Moreover, there are a few amounts of minor components, minerals, and organic extracts in the structure of the biomass. Before the use biomass should be converted into more valuable products (i.e., liquid fuels). Among the biomass conversion technologies, the most preferred thermal conversion technologies. One of the most important of the thermal conversion technologies is pyrolysis.

Biomass secondary fuels and chemical by-products are obtained as a result of pyrolysis processes with heating and partial combustion. The raw materials used in pyrolysis process are composed of wood, coal, biomass residues and local wastes while gasses, liquids,

**Citation:** T. Kar, S. Keleş, Z. Emir, K. Kaygusuz, Fast pyrolysis of fig leaves: Influence of pyrolysis parameters and characterization of bio-oil, Turk J Anal Chem, 4(2), 2022, 80–87.

**\*Author of correspondence:** sedat@ktu.edu.tr

**Tel:** +90 (462) 377 42 75

**Fax** +90 (462) 325 31 96

**Received:** July 11, 2022

**Accepted:** October 18, 2022

tars, chars, oils and ashes are formed as a result of this process. Fuel products from pyrolysis are much more suitable for cleaning, handling and transporting fuel products obtained from the original biomass. The fast pyrolysis has become increasingly popular in recent years [4]. By means of fast pyrolysis, more liquid products (bio-oil) can be obtained compared to traditional pyrolysis methods [5]. While low vapor residence time, high heating rate and medium temperatures are required to increase liquid product efficiency, slower heating rate is required to increase solid product efficiency [6,7]. After cooling and condensing the pyrolysis vapors a dark brown liquid is formed which has a heating value about half that of conventional fuel oil [8]. Liquid yield is dependent on biomass type, temperature, retention time, char separation and raw material ash content. Char and ash content shows a catalytic effect for cracking of the formed steam [9,10]. Due to decreased fossil fuel reserves, increased fuel demand and CO<sub>2</sub> emission problems, interest in bio-oil as a sustainable liquid hydrocarbon fuel source is constantly increasing [11,12]. Bio-oil contains hundreds of kinds of compounds such as carboxylic acids, aldehydes, ketones, furans [13,14]. In this case, bio-oil causes some negative properties such as high viscosity, thermal instability and corrosivity [15]. Both methods are not useful because they negatively affect cellulose. Stainless steel and polyolefin materials are suitable for storage. High acidity can be reduced by esterification reactions or by using magnesium alloy and powder [16]. Aging is one of the major problems that negatively affect the structure of bio-oil. This problem is usually caused by the ongoing degradation reactions in the bio-oil [17,18]. Polar solvent addition is generally used as a simple method to reduce the viscosity of liquid fuels obtained by pyrolysis of biomass. Addition of 10% by weight of methanol to the bio-oil significantly decreased the viscosity increase [19,20]. All types of biomasses usually contain ash which is dominated by alkali metals such as sodium and potassium [21]. Potassium and some other alkali metals catalyze secondary degradation reactions [22]. These negative factors result in reduced liquid product yield, phase separation because of higher water content and loss of surfactant. Bio-oil's viscosity is one of the most important parameters for direct combustion applications and combustion efficiencies in engines and turbines requiring atomization [23]. Tests of bio-oil in engines and combustors are available in the literature. [24]. The preferred viscosity in engine applications with high pressure is 17 cSt. In conventional fuels, preheating is carried out to reduce the viscosity. However, because of the non-recyclable changes in the properties of bio-oil at temperatures above 55 °C, one-time heating is performed in very short retention [25].

As discussed in Diobold's review, the viscosity is most swayed by the temperature and water content. Bio-oil contains only a small amount of sulfur, so there is not much work to regulate or reduce the sulfur content [26]. A number of studies have shown that bio-oil does not pose a significant risk to living health and the environment [27,28].

In this study, the samples of fig leaves (FL) separated into different particle sizes were burned in a fixed bed pyrolysis reactor. Türkiye is the world's leading country in terms of production figs. In this respect, figs, which are an agricultural by-product, constitute an important raw material potential for clean energy production. Using a fixed bed reactor, the effects of pyrolysis temperature, particle size and sweeping gas flow rate on pyrolysis product yields were studied. In addition, the properties of bio-oil obtained from FL were investigated. This study is a unique study to examine the pyrolysis behavior of fig leaf and to investigate the characterization of bio-oil.

## 2. Materials and methods

### 2.1. Materials

The FL used in the present study was obtained from Trabzon located in the Black Sea region, in the northern part of Türkiye.

### 2.2. Methods

#### 2.2.1. Biomass preparation

Prior to use, sample was dried in an electrical oven for 24 h at 105 °C to ensure the reduction of free moisture. Before pyrolysis, the biomass was passed through in high-speed rotary cutting mill and then screened to give fractions of  $0.425 < D_p < 1.000$  mm,  $0.250 < D_p < 0.425$  mm,  $0.150 < D_p < 0.250$  mm and  $D_p < 0.150$  mm particle sizes.

#### 2.2.2. Pyrolysis experiments

The fixed bed reactor used in this study has also been used in previous research [1,29]. The experimental set up consists of reactor, liquid collecting system, and power supply. During the experiments, pyrolysis temperature was controlled by a PT100 temperature controller. A liquid nitrogen trap was used to condensed pyrolysis vapors. Three groups of experiments were realized to determine the effect of pyrolysis conditions on solid, liquid and gas product yields. The first is to determine the effect of pyrolysis temperature on pyrolysis yield. In this part experiments, 3 grams of air-dried sample was placed in the reactor. After placing the sample, it was heated to the desired final temperature (400, 500, 600 and 700 °C) at 200 °C/min heating speeds. In the second

group of experiments, the effect of particle size on pyrolysis yields was investigated by selecting four different particle sizes. In the last group of experiments, the effect of sweeping gas flow rate (100, 200, 300 and 400 cm<sup>3</sup>/min) on product yield was examined.

The pyrolysis vapors are sent to the liquid collection unit where they are liquefied. The non-liquefied part was sent to outside with the aid of a discharge hose. The pyrolysis liquid accumulated in the liquid collection unit. The amount of solid part is calculated by weighing the solid product while the amount of gas is determined by the difference.

### 2.2.3. Characterization of biomass and pyrolysis products

The pyrolysis liquid was kept in dichloromethane to separate the aqueous and oil phase. Both separated phases are weighed. Then, dichloromethane was blown on a rotary evaporator to determine the bio-oil yield. The resulting bio-oil was kept in *n*-pentane overnight and divided into two phases, soluble and insoluble (asphaltenes) in *n*-pentane. *n*-pentane soluble fraction was used in the characterization of bio-oil. Several instrumental techniques have been used to illuminate the structure of the biomass and its bio-oil, obtained under appropriate conditions (600 °C, 200 cm<sup>3</sup>/min, D<sub>p</sub> ≤ 0.250 mm particle size). Proximate (moisture content, ash content, fixed carbon and volatile matter) and ultimate (elemental composition) analyzes of FL and its bio-oil were carried out. The ultimate analysis was performed using an elemental analyzer (Leco/TrueSpec Micro). The gross calorific values of the raw material and bio-oil are calculated by Dulong-Berthelot's formula given below:

$$QGCV (kJ/g) = 0.3491C + 1.1783H + 0.1005S - 0.1034O - 0.0151N - 0.0211ASH \quad (1)$$

To determine the water content of bio-oil, Karl-Fischer titration was applied with METTLER TOLEDO COULOMETER DL 39. An FT-IR spectrometer (Spectrum 400, Perkin-Elmer, USA) examined the functional groups and fingerprints of the bio-oil from the fast pyrolysis. The HHV of the bio-oil was analyzed on a bomb calorimeter (Model: IKA C 200) according to ASTM D2015. The inorganic elemental compositions of the biomass were determined using SEM-EDS analysis. TG and DTG experiments of the biomass and its bio-oil were carried out using a TG analyzer (TagongsiSDTQ600, USA), under nitrogen atmosphere, heated from room temperature to 800 °C. The GC-FID analysis was carried out on an Agilent 7890A-(5975C inert MSD).

## 3. Results and discussion

### 3.1. Physicochemical characteristics of FL

Table 1 shows the physicochemical characteristics of the FL, prepared for fast pyrolysis experiments. The FL contained 11.07 wt% cellulose, 33.73 wt% hemicellulose, and 13.12 wt% lignin. During the pyrolysis of biomass, organic vapors are formed by breaking down this lignocellulosic content at high temperatures. These vapors are liquefied to produce bio-oil. The remaining solid residual is left as bio-char. Considering the characteristics of FL used as biomass samples, it is seen that H/C ratio (1.68) which is an important parameter is very close to that of traditional crude oil (1.82). The H/C molar ratio of biomass is between 1.0 and 2.0, indicating the potential for producing liquid fuel from the biomass [30,31]. In this study, the high heating value of the fig leaf samples was found to be 14.73 kJ/g and this value is among the thermal values that should be the typical biomass samples that can be used for liquid fuel production [32].

In Fig. 1 the SEM images of raw material are compared with different magnifications (×200, ×1000, ×2000 and ×5000). The morphological structure of FL showed long uniform fibrous lignocellulosic structures. The morphological structure help to predict their agglomeration properties. Images revealed that FL show a fibrous pattern on their surface. Fig leaves exhibited a compact morphology, complex and very ordered in macrofibrils. Lignocellulosic blends interact via intermolecular hydrogen bonding, preventing the material to self-assemble [33].

Table 1. Main characteristics of FL samples

Characteristics	Values
Moisture content <sup>a</sup> (%)	9.11
Holocellulose content <sup>a</sup> (%)	44.80
Cellulose content <sup>a</sup> (%)	11.07
Hemicellulose content <sup>a</sup> (%)	33.73
Lignin content <sup>a</sup> (%)	13.12
Organic extractive <sup>a</sup> (%)	20.72
<b>Proximate analysis (%)</b>	
Volatiles	62.44
Fixed carbon	16.89
Ash	11.56
<b>Ultimate analysis <sup>b</sup>(%)</b>	
Carbon	39.68
Hydrogen	5.57
Nitrogen	2.37
Oxygen <sup>c</sup>	52.38
H/C molar ratio	1.68
O/C molar ratio	0.99
Empirical formula	C <sub>20</sub> H <sub>34</sub> O <sub>20</sub> N
Higher calorific value (MJ/kg)	14.73

<sup>a</sup> weight percentage on dry basis

<sup>b</sup> weight percentage on dry and ash-free basis

<sup>c</sup> by difference

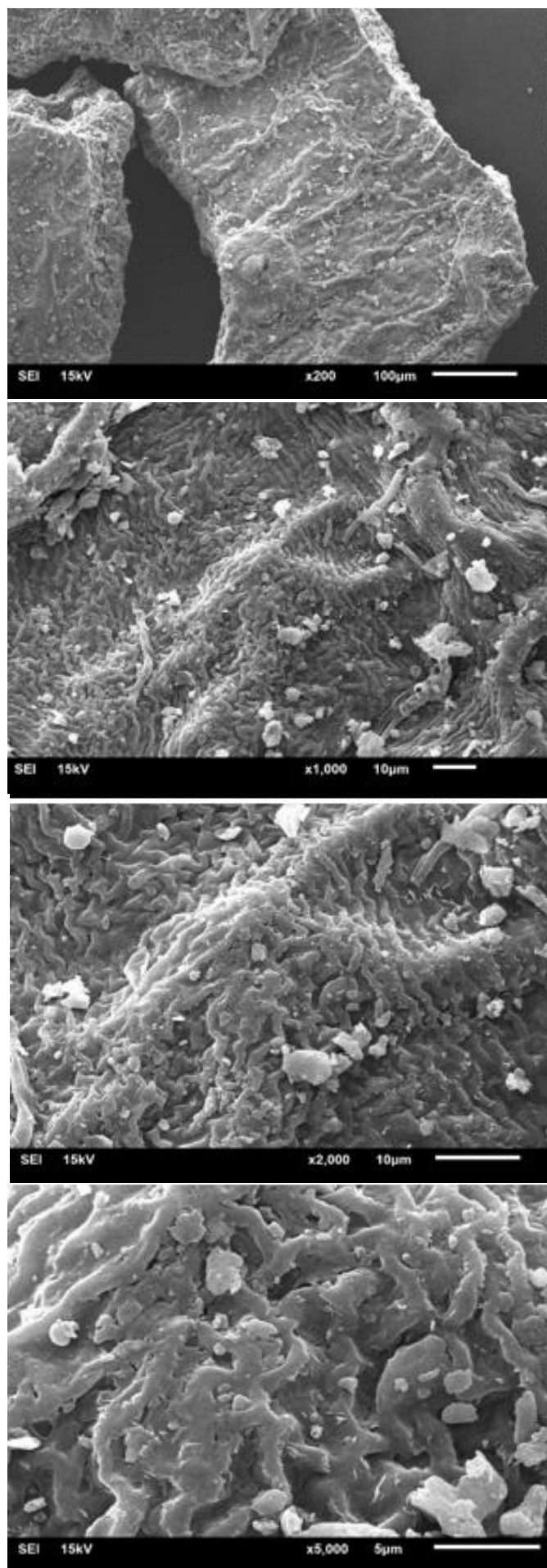


**Figure 1.** Scanning electron microscopy (SEM) images of raw FL, where A, B, C and D shows different

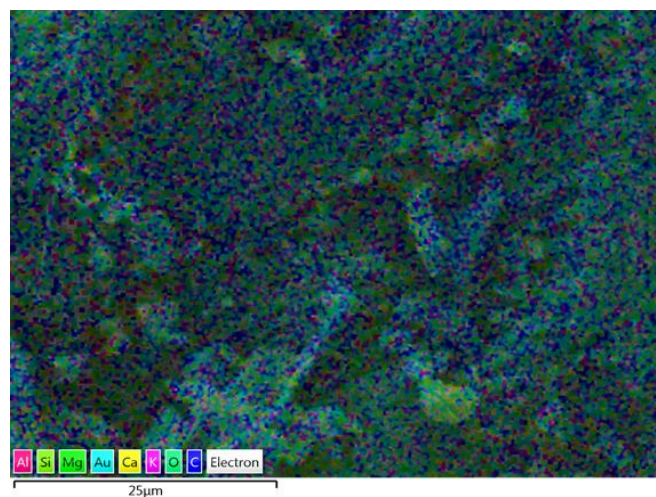


**Figure 2.** SEM-EDS photograph of the FL

**Fig. 2** shows SEM-EDS photograph of the FL. **Fig. 3** shows the inorganic elements (C and O are removed) present of the FL. When the inorganic element contents of FL are examined, Ca and K are the major elements. Si, Mg and Al were also found in large quantities.

### 3.2. Product Yields

#### 3.2.1. Effect of temperature on pyrolysis product yields

Four different pyrolysis temperatures were used in the experiments. According to the obtained results, the highest liquid product yield was achieved in particle size  $\leq 0,150$  mm and nitrogen flow rate of  $200 \text{ cm}^3/\text{min}$ . **Fig. 4** shows the effect of pyrolysis temperature on the product yields and pyrolysis conversion for four different temperatures (400, 500, 600 and 700 °C). The optimum temperature was 600 °C, producing the maximum bio-oil yield of 41.82%. The result shows that as the temperature begins to increase from 400 to 600 °C, the liquid yield increases to the maximum from 30.37 wt% to 41.82 wt%. An increase in temperature up to a certain temperature increases the yield of liquid products. The pyrolysis conversion efficiency increases with rising temperature; this is owing to increase in gas and liquid product yield. The highest pyrolysis conversion was obtained at a temperature of 600 °C, and this result was 79.21% by weight. When the temperature rises from 400 °C to 600 °C, a steady decrease in char product yield is observed. Contrary to expectations, the yield of the solid product increased with the increase of the temperature to 700 °C. This unexpected increase in char product yield is due to the fact that small particle size biomass prevents heat transfer by agglomeration at high temperature. Gas product yields increased with increasing temperature and reached the highest with 50.75 wt% at 700 °C.

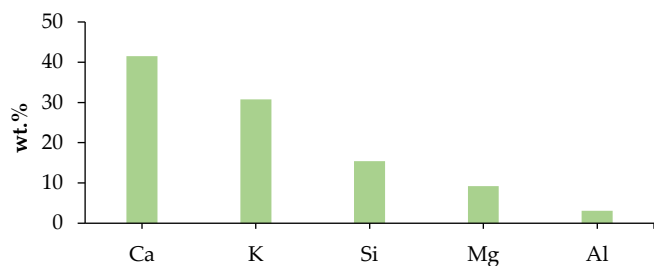


Figure 3. Inorganic elements (wt.%) present of the FL determined using SEM-EDS

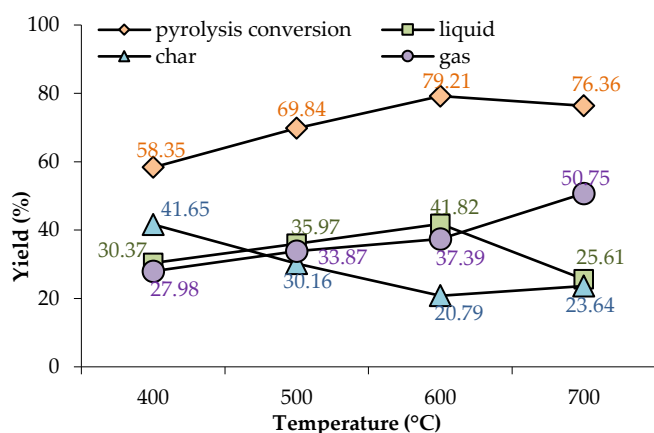


Figure 4. Effect of pyrolysis temperature on product yields (Particle size of  $D_p < 0.150$  mm and nitrogen flow rate of  $200 \text{ cm}^3/\text{min}$ )

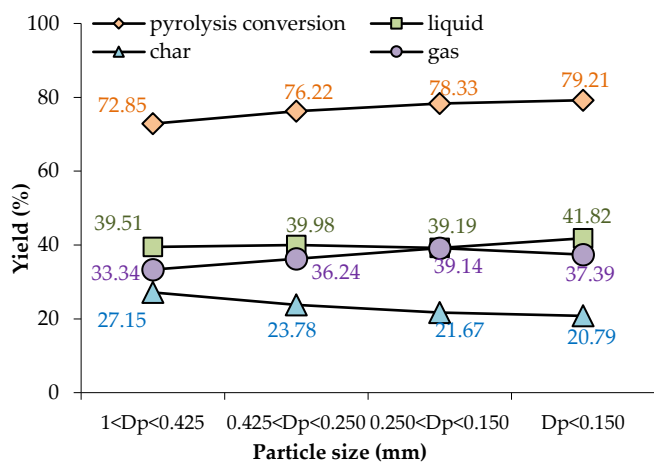


Figure 5. Effect of particle size on product yields (Pyrolysis temperature of  $600 \text{ }^\circ\text{C}$  and nitrogen flow rate of  $200 \text{ cm}^3/\text{min}$ )

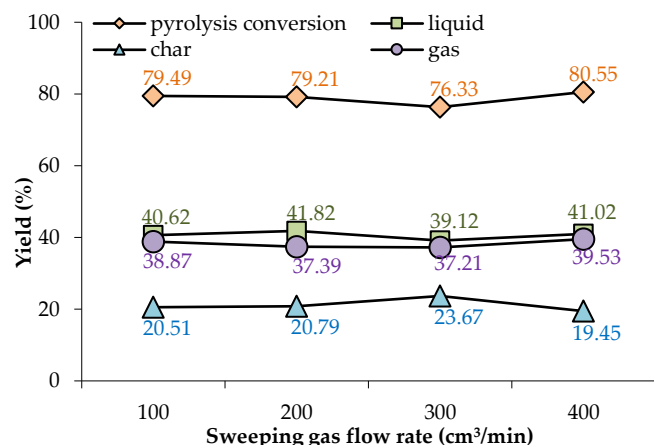


Figure 6. Effect of sweeping gas flow rate on product yields (Particle size of  $D_p < 0.150$  mm and pyrolysis temperature of  $600 \text{ }^\circ\text{C}$ )

### 3.2.2. Effect of particle size on pyrolysis product yields

Fig. 5 shows the effect of particle size on pyrolysis product yields at four different particle sizes. In this group of experiments, the temperature of the pyrolysis was  $600 \text{ }^\circ\text{C}$  degrees and the flow rate of the sweeping gas was  $200 \text{ cm}^3/\text{min}$ . These selected values of the temperature and the sweeping gas flow rate are the values at which the liquid product yield is optimum. The highest liquid product yield was achieved with a minimum particle size of  $D_p < 0.150$  mm, even though there was no significant change in the liquid product yields with the change in particle size. Generally, in cases where particle size is less than 2 mm, there is no significant change in liquid product yields if heat transfer is not adversely affected by agglomeration in biomass. If the pyrolysis conversion yields of Fig. 5 are considered, the pyrolysis conversion efficiencies are increased with the reduction of the particle size. This increase in pyrolysis conversion was due to the increase in gas product yield up to  $0.150 < D_p < 0.250$  mm. The increase in pyrolysis conversion after this particle size is due to the increase in liquid product yield. Finally, the graph in Fig. 5 also shows that the char product yield decreases continuously as the particle size decreases. As mentioned above, if the agglomeration reactions were realized, there would be a significant increase in the yield of char products as the particle size decreased.

### 3.2.3. Effect of sweeping gas flow rate on pyrolysis product yields

In this section, the effect of sweeping gas (nitrogen) flow rate on product yield was investigated. In the experiments, FL with a particle size of  $< 0.150$  mm were selected. The values obtained from the experimental results are shown in the graph in Fig. 6. It is seen that there is no significant change in the liquid and gas productions by increasing the entraining gas flow rate from  $100 \text{ cm}^3/\text{min}$  to  $400 \text{ cm}^3/\text{min}$ . The gas flow rates, which are optimal for liquid and gas product yields, are determined as  $200 \text{ cm}^3/\text{min}$  and  $400 \text{ cm}^3/\text{min}$  respectively. When the nitrogen flow rate increases to  $400 \text{ cm}^3/\text{min}$ , the solid product yield is the lowest. High heating rates and temperatures often lead to a decrease in solid product yields, while the situation in gas product yields is quite the opposite. The highest gas product yield seen in the graph in Fig. 6 was obtained at a gas flow rate of  $400 \text{ cm}^3/\text{min}$ , while the lowest solid product yield was also obtained at this flow rate.

### 3.3. The properties of the bio-oil

The properties of bio-oil are presented in Table 2. From Table 2, it can be seen that the energy content of bio-oil is more than twice that of the FL and It is also seen that bio-oil contains 6.68% nitrogen.

**Table 2.** Main properties of bio-oil from FL

Characteristics	Values
Water (%)	15.46
Carbon (%)	67.86
Hydrogen (%)	7.60
Nitrogen (%)	6.68
Oxygen <sup>a</sup> (%)	17.86
H/C molar ratio	1.34
O/C molar ratio	0.55
Empirical formula	C <sub>75</sub> H <sub>98</sub> O <sub>15</sub> N <sub>6</sub>
Higher calorific value (MJ/kg)	32.16

<sup>a</sup> by difference

The water content of bio-oil is 15.46%. This ratio shows that bio-oil does not contain a lot of water. The average chemical composition of the bio-oil is C<sub>75</sub>H<sub>98</sub>O<sub>15</sub>N<sub>6</sub>. The bio-oil contains a small amount of oxygen content than FL. Due to the increase in the percentage of carbon and hydrogen and the decrease in the oxygen content, the higher calorific value of the bio-oil increased to 32.16 MJ/kg. The TG and DTG curves of the thermal decomposition of FL at heating rate of 5 °C /min under inert atmosphere are shown in Fig. 7. When bio-oil's thermal analysis curves are examined, it can be seen that it can be divided into three stages. The first stage reached from room temperature to 300 °C. The onset thermal temperature of thermal decomposition is therefore 21 °C corresponding to about 16.547 mg and the final decomposition temperature is 290 °C with the amount of residue being 7.488 mg. This means that almost half of the content of bio-oil goes away at this step. This shows that the bio-oil losses weight very fast, a characteristic of water and lighter organic products. The second stage went from 300 °C to the temperature of 450 °C. Bio-oil starts with 7.488 mg at 300 °C and decreases to 4.144 mg when the temperature rises to 450 °C. At this stage, only 20% of the initial bio-oil is broken down. The third stage reached from 450 °C to 600 °C. Bio-oil starts with 4.144 mg at 450 °C and decreases to 0.080 mg when the temperature rises to 600 °C. In this last stage, the carbonaceous and other residues continuously were decomposed at a very fast rate and a severely continued loss of weight was shown in the weight loss curve. The Ar-H stretching vibration at 3013 cm<sup>-1</sup> indicate the presence of aromatic structures. The C–H stretching vibrations at 2958, 2918 and 2850 cm<sup>-1</sup> indicate the presence of alkanes. The C=O stretching vibrations with absorbance at 1707 cm<sup>-1</sup> and indicate the presence of aldehydes, ketones, and carboxylic acids. The C–O stretching vibrations at 1377 and 1260 cm<sup>-1</sup> indicate the presence of alcohols and carboxylic acids. The stretching vibration at 1514 represent C–C stretching vibrations indicative of alkenes and aromatics.

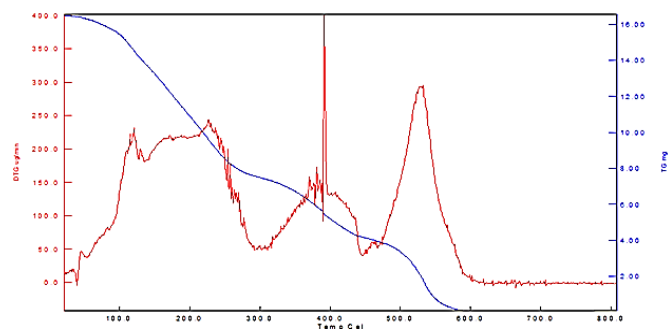


**Figure 7.** TG and DTG curves of the bio-oil at a heating rate of 5 °C /min. Left hand side y axis: DTG curve; right hand side y axis: TG curve

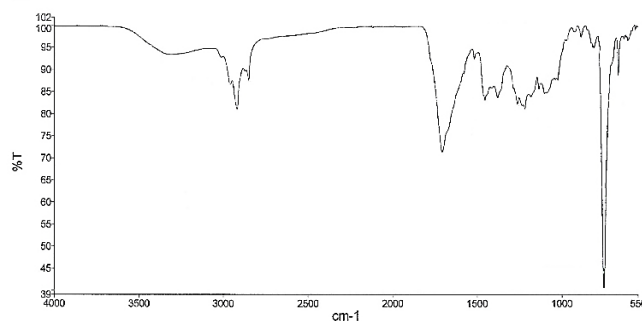


**Figure 8.** IR spectra of the bio-oil from fast pyrolysis of FL

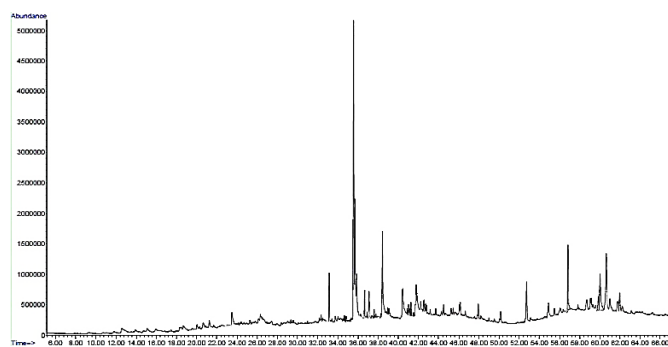


**Figure 9.** Gas chromatogram of the bio-oil

**Table 3.** Compositions of bio-oil from FL

No	Compound	Retention Time (s)	Area (%)
1	1H-Indole, 5-methyl	23.49	2.10
2	1-Heptene, 2-isohexyl-6-methyl	33.14	2.68
3	Psoralene	35.56	25.11
4	Ficusin	35.71	8.91
5	Isopsoralen	35.86	4.02
6	(E)-2,4-Phytadiene	36.67	2.14
7	2-Heptadecanone	37.08	2.66
8	n-Hexadecanoic acid	38.43	7.60
9	7H-Furo[3,2-g][1]benzopyran-7-one	40.41	5.50
10	9-Octadecenoic acid, methyl ester	41.01	1.59
11	2-Hexadecen-1-ol	41.27	0.93
12	9-Octadecenoic acid	41.79	5.84
13	Cyclopropaneoctanal, 2-octyl-	42.23	1.72
14	Hexadecanamide	42.53	0.92
15	Eicosane	46.14	2.67
16	Docosane	47.94	1.32
17	Tetracosane	52.72	3.55
18	Octacosane	54.91	1.79
19	Nonadecane	56.82	4.97
20	1H-Indole, 5-methyl-2-phenyl-	59.85	1.17
21	3-O-Acetyl-6-methoxy-cycloartenol	60.02	4.50
22	Stigmastan-3,5-diene	60.63	6.43
23	14.alpha.-Cheilanth-12-enic Methyl	61.97	1.87

Fig. 9 shows the gas chromatogram of bio-oil obtained from FL. When this chromatogram was examined, it was observed that bio-oil contains a large number of components. The most important of these components are given in Table 3. Both non-aromatic and aromatic hydrocarbon compounds were determined in organic phase of liquid product. When Table 3 is examined, it can be seen that the bio-oil obtained from FL contains different alkanes from 20 carbons to 29 carbons. We can see that bio-oil contains alkenes, aldehydes, carboxylic acids, and aromatic structures such as indole derivative as well as alkanes. It can be seen from the table that bio-oil contains a very high percentage of psoralene. This compound results from the breakdown of lignin and hemicellulose in the FL. FL can be an important source of raw materials for the production of this compound.

#### 4. Conclusions

In this study, fast pyrolysis of FL was performed in a fixed bed pyrolysis reactor. The effects of pyrolysis temperature, sweeping gas flow rate and particle size on the product yield were researched.

In the research findings, it was found that the most important parameter in the change of pyrolysis product yields was temperature and the optimum temperature for liquid product yield was determined to be 600 °C. The liquid yield was decrease after 600 °C because of secondary reactions that produced more gases. When the main component analysis results of FL were examined, it was determined that the holocellulose ratio was high. This means that it will form a liquid product with a high aliphatic content. The 13.6 wt% lignin found in FL shows the presence of phenolic and aromatic compounds in the structure. Especially the H/C ratio of 1.71 is an important parameter in the use of the liquid product obtained from FL as an alternative and clean energy source. Instrumental techniques such as FT-IR, SEM-EDS, TG / DTG and GC-MS were used for the characterization of bio-oil obtained by fast pyrolysis of FL. The heating values of raw material and bio-oil were determined as 14.73 and 32.16 MJ/kg, respectively. Considering these rates, it is seen that the energy content of bio-oil is more than two times higher than the raw material. The energy content of bio-oil is thought to be close to the energy content of petroleum-derived fuels. Bio-oil contains alkenes, aldehydes, carboxylic acids, and aromatic structures such as indole derivative as well as alkanes. Türkiye ranks first in the world fig production. For this reason, FL poured on the ground constitute a significant potential both as a chemical raw material and as a waste. The liquid of FL from fast pyrolysis has good properties for a potential biofuel candidate or as a source of chemicals.

#### Acknowledgment:

Authors would like to thank the Turkish Academy of Sciences for financial funding. Authors would thank the KTU due to the experimental set-up and instrumentation facilities.

#### References

- [1] S. Keleş, T. Kar, M. Akgun, K. Kaygusuz, Catalytic fast pyrolysis of hazelnut cupula: Characterization of bio-oil, *Energ Source Part A*, 39, 2017, 2216–2225.
- [2] C. Acar, I. Dinçer, A Review on Clean Energy Solutions for Better Sustainability, *Int J Energ Res*, 39, 2015, 585–606.
- [3] A.J. Kirkpatrick, L.S. Bennear, Promoting Clean Energy Investment: An Empirical Analysis of Property Assessed Clean Energy, *J Environ Econ Manag*, 68, 2014, 357–375.
- [4] X. Ying, W. Tiejun, M. Longlong, C. Guanyi, Upgrading of fast pyrolysis liquid fuel from biomass over Ru/ $\gamma$ -Al<sub>2</sub>O<sub>3</sub> catalyst, *Energ Convers Manage*, 55, 2012, 172–177.
- [5] Q. Sohaib, M. Habib, S.F.A. Shah, U. Habib, S. Ullah, Fast pyrolysis of locally available green waste at different residence time and temperatures, *Energ Source Part A*, 39, 2017, 1639–46.
- [6] S. Papari, K. Hawboldt, P. Fransham, Study of selective condensation for woody biomass pyrolysis oil vapours, *Fuel*, 245, 2019, 233–239.
- [7] Z. Luo, S. Wang, Y. Liao, J. Zhou, Y.K. Gu, K. Cen, Research on biomass fast pyrolysis for liquid fuel, *Biomass Bioenerg*, 26, 2004, 455–462.
- [8] P.S. Marathe, R.J.M. Westerhof, S.R.A. Kersten, Fast pyrolysis of lignins with different molecular weight: Experiments and modeling, *Appl Energ* 236, 2019, 1125–1137.
- [9] A.V. Bridgwater, Review of fast pyrolysis of biomass and product upgrading, *Biomass Bioenerg*, 38, 2012, 68–94.
- [10] F. Guo, X. Li, Y. Liu, K. Peng, C. Guo, Z. Rao, Catalytic cracking of biomass pyrolysis tar over char-supported catalysts, *Energ Convers Manage*, 167, 2018, 81–90.
- [11] G.W. Huber, S. Iborra, C. Corma, Synthesis of transportation fuels from biomass: chemistry, catalysts, and engineering, *Chem Rev*, 106, 2006, 4044–4098.
- [12] S. Hansen, A. Mirkouei, L. A. Diaz, A comprehensive state-of-technology review for upgrading bio-oil to renewable or blended hydrocarbon fuels, *Renew Sust Energ Rev*, 118, 2020, 109548.
- [13] M. Bertero, J.R. Garcia, M. Falco, U. Sedran, Equilibrium FCC catalysts to improve liquid products from biomass pyrolysis, *Renew Energ*, 132, 2019, 11–18.
- [14] S.U. Chang, Rice Husk and Its Pretreatments for Bio-oil Production via Fast Pyrolysis: a Review, *Bioenerg Res*, 13, 2020, 23–42.
- [15] L.D. Ingram, M. Mohan, P. Bricka, P. Steele, D. Strobel, D. Crocker, B. Mitchell, J. Mohammad, K. Cantrell, C.U. Pittman, Pyrolysis of wood and bark in an auger reactor: physical properties and chemical analysis of the produced bio-oils, *Energ Fuel*, 22, 2008, 614–625.
- [16] I. Nemoto, N. Kouno, E. Sato, Method for treating bio-oil, US Pat Applic, 2008 20080178521.
- [17] J.P. Diebold, A review of the chemical and physical mechanisms of the storage stability of fast pyrolysis bio-oils in Fast Pyrolysis of Biomass: A Handbook, vol. 2 (ed. A.V. Bridgwater), CPL Press, Newbury, 2002, pp. 243–292.
- [18] C. Wang, H. Ding, Y. Zhang, X. Zhu, Analysis of property variation and stability on the aging of bio-oil from fractional condensation, *Renew Energ*, 148, 2020, 720–728.
- [19] J.P. Diebold, S. Czernik, Additives to lower and stabilize the viscosity of pyrolysis oils during storage, *Energ Fuel*, 11, 1997, 1081–1091.

- [20] Y. Mei, M. Chai, C. Shen, B. Liu, R. Liu, Effect of methanol addition on properties and aging reaction mechanism of bio-oil during storage, *Fuel*, 244, 2019, 499–507.
- [21] A. Mlonka-Mędrala, A. Magdziarz, M. Gajek, K. Nowińska, W. Nowak, Alkali metals association in biomass and their impact on ash melting behavior, *Fuel*, 261, 2020, 116421.
- [22] M. Zhao, M.Z. Memon, G. Ji, X. Yang, A.K. Vuppaladadiyam, Y. Song, A. Raheem, J. Li, W. Wang, H. Zhou, Alkali metal bifunctional catalyst-sorbents enabled biomass pyrolysis for enhanced hydrogen production, *Renew Energ*, 148, 2020, 168–175.
- [23] M. Broumand, S. Albert-Green, S. Yun, Z. Hong, M. Thomson, Spray combustion of fast pyrolysis bio-oils: Applications, challenges, and potential solutions, *Prog Energ Combust Sci*, 79, 2020, 100834.
- [24] A. Oasmaa, M. Kytö, K. Sipilä, Pyrolysis oil combustion tests in an industrial boiler, in *Progress in Thermochemical Biomass Conversion* (ed. A.V. Bridgwater), Blackwell Science, Oxford, pp. 2001, 1468–1481.
- [25] D. Chiamonti, A. Oasmaa, Y. Solantausta, Power generation using fast pyrolysis liquids from biomass, *Renew Sust Energ Rev*, 11, 2007, 1056–1086.
- [26] D.Y. Hopa, N. Yılmaz, O. Alagoz, M. Dilek, A. Helvacı, U. Durupınar, Pyrolysis of poppy capsule pulp for bio-oil production, *Waste Manage Res*, 34, 2016, 1316–1321.
- [27] G.V.C. Peacocke, Transport handling and storage of fast pyrolysis liquids, in *Fast Pyrolysis of Biomass: A Handbook*, vol. 2 (ed A.V. Bridgwater), CPL Press, Newbury, 2002, pp. 293–338.
- [28] J. Wang, S. You, Z. Lu, R. Chen, F. Xu, Life cycle assessment of bio-based levoglucosan production from cotton straw through fast pyrolysis, *Bioresour Technol*, 307, 2020, 123179.
- [29] T. Kar, S. Keleş, Fast pyrolysis of chestnut cupulae: yields and characterization of the bio-oil, *Energ Explor Exploit*, 31, 2013, 867–878.
- [30] T. Bridgwater, Review Biomass for Energy. *J Sci Food Agr* 86, 2006, 1755–1768.
- [31] T. Kar, S. Keleş, Characterisation of bio-oil and its sub-fractions from catalytic fast pyrolysis of biomass mixture, *Waste Manage Res* 37, 2019, 674–685.
- [32] J. Lehto, A.A. Oasmaa, Y. Solantausta, M. Kytö, D. Chiamonti, Review of fuel oil quality and combustion of fast pyrolysis bio-oils from lignocellulosic biomass, *Appl Energ*, 116, 2014, 178–190.
- [33] D. Al-shahrani, A.S. Love, D. Salas-de la Cruz, The role of reduced graphene oxide toward the self-assembly of lignin-based bio composites fabricated from ionic liquids, *Int J Mol Sci*, 19, 2018, 1–13.

## Electroanalytical analysis of guaifenesin from pharmaceuticals on boron doped diamond electrode

Fatma Ađın\* , Gökçe Öztürk , Dilek Kul 

Karadeniz Technical University, Faculty of Pharmacy, Department of Analytical Chemistry, 61080, Trabzon, Türkiye

### Abstract

Electrochemical analysis of the expectorant drug guaifenesin was performed on boron doped diamond electrode by cyclic voltammetry, differential pulse voltammetry, and square wave voltammetry techniques. The results of cyclic voltammetry studies indicated that the reaction mechanism of guaifenesin in the anodic direction was irreversible, and diffusion controlled. The linearity ranges of the peak currents versus guaifenesin concentration were between 0.4 and 100  $\mu\text{M}$  with a detection limit of 1.47 nM for differential pulse voltammetry and between 0.8 and 100  $\mu\text{M}$  with a detection limit of 2.92 nM for square wave voltammetry. Quantitative analysis of guaifenesin from the pharmaceuticals was performed using the proposed methods without any pre-separation. Sensitive voltammetric methods with good recovery, high sensitivity and accuracy were developed for the electroanalytical analysis of guaifenesin.

**Keywords:** Boron doped diamond electrode, guaifenesin, pharmaceuticals, validation, voltammetry

### 1. Introduction

Guaifenesin (GFN) is an orally used expectorant drug for the treatment of symptoms of the cold, allergy, and upper respiratory tract infections [1]. It is thought to exert its pharmacological action by increasing the hydration of mucus in the gastric mucosa and decreasing the viscosity of mucus secretion [2,3]. GFN (Fig. 1), 3-(*o*-methoxyphenoxy)-1,2-propanediol, is a highly water-soluble white powder with an empirical formula of  $\text{C}_{10}\text{H}_{14}\text{O}_4$  and a molecular weight of 198.22 g/mol.

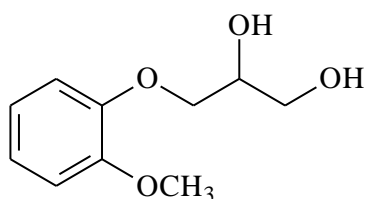


**Figure 1.** Structure of guaifenesin

Drug analysis is carried out at various stages as formulation, stability studies, toxicology, quality control, and pharmacological testing in humans and animals. In hospitals, drug analyzes are performed on patients to support clinical, pharmacokinetic, and bioavailability studies and to monitor abuse of therapeutic drugs. These studies require reliable and

validated analytical methods to quantify drugs in complex media such as formulation and biological samples [4]. Sensitive determination of GFN is important both to monitor the effectiveness of the treatment applied and to minimize its side effects such as nausea, vomiting, kidney stone formation, diarrhea, and constipation [5].

Determination studies of GFN with different methods such as spectrophotometric [6,7], chromatographic [8–10], and voltammetric [11–14] methods are available in the literature. Spectrophotometric and chromatographic methods are more time-consuming and expensive than electrochemical methods due to the need for complex sample preparation. Voltammetry, which is one of the electrochemical methods, is a very advantageous method compared to other analytical methods because it requires a minimum amount of organic solvent, uses low-cost equipment, and does not require a pre-separation process for the samples to be analyzed [15]. While cyclic voltammetry (CV), which is one of the most commonly used voltammetric methods, is suitable for qualitative analysis, differential pulse voltammetry (DPV) and square wave voltammetry (SWV) techniques

**Citation:** F. Ađın, G. Öztürk, D. Kul, Electroanalytical analysis of guaifenesin from pharmaceuticals on boron doped diamond electrode, Turk J Anal Chem, 4(2), 2022, 88–93.

\***Author of correspondence:** fagin@ktu.edu.tr

**Tel:** +90 (462) 377 88 22

**Fax** +90 (462) 325 67 17

**Received:** June 06, 2022

**Accepted:** October 16, 2022

allow high-sensitivity quantitative analysis. The use of boron-doped diamond electrode (BDDE) in voltammetry has become widespread and attractive in recent years [16,17]. As a member of carbon-based materials, BDDE has several unique properties such as good mechanical and electrochemical stability in both acidic and alkaline media, high thermal conductivity, wide potential range, low background current, and low sensitivity to dissolved oxygen in aqueous solutions [18].

The aim of this study is to develop validated voltammetric methods for the electroanalytical analysis of GFN from its pharmaceutical dosage forms using BDDE as the working electrode. Quantitative determination of GFN was accomplished using the validated voltammetric techniques proposed in this study, with high sensitivity, low detection limits, and good recovery.

## 2. Experimental

### 2.1. Chemicals and reagents

GFN was purchased from Sigma-Aldrich (USA) and used as a standard without further purification. Vicks Vapo expectorant® syrup (200 mg/15 mL), the pharmaceutical form of GFN, was purchased from the local pharmacy. Stock solutions of GFN ( $1.0 \times 10^{-3}$  M) were prepared daily with ultrapure water and stored at  $+4^\circ\text{C}$  in the dark. Working solutions of GFN were prepared daily by direct dilution of the GFN stock solution with the selected supporting electrolyte.

Britton-Robinson buffer (BRB) solutions (0.04 M), pH 2.0 – 12.0, were prepared from 0.04 M  $\text{CH}_3\text{COOH}$  (Merck, Germany), 0.04 M  $\text{H}_3\text{BO}_3$  (Aldrich, USA), and 0.04 M  $\text{H}_3\text{PO}_4$  (Merck, Germany). Phosphate buffer (PB) solutions (0.1 M) were prepared using  $\text{H}_3\text{PO}_4$  (Merck, Germany) for pH 2.0 – 4.0 and  $\text{Na}_2\text{HPO}_4$  (Aldrich, USA) and  $\text{NaH}_2\text{PO}_4$  (Merck, Germany) for pH 5.5 – 8.0. Acetate buffer (AB, 0.5 M) solutions at pH 3.5, 4.5, and 5.5 were prepared from  $\text{CH}_3\text{COOH}$  (Aldrich, Germany). 5 M NaOH (Aldrich, USA) solution was used for all pH adjustments. Analytical reagents and Sartorius Arium proUV nanopure water (resistivity  $\geq 18$  M $\Omega$  cm) were used to prepare the solutions.

### 2.2. Apparatus and measurements

All voltammetric measurements were performed using Autolab PGSTAT128N potentiostat/galvanostat (Metrohm-Autolab, The Netherlands) with Nova 11.0 software. All electrochemical studies were carried out with an electrochemical cell consisting of three electrodes, a BDDE (Windsor Scientific  $\phi$ : 3mm) as the working electrode, a platinum wire as the counter electrode, and an Ag/AgCl electrode (Bioanalytical Systems, 3.0 M KCl) as the reference.

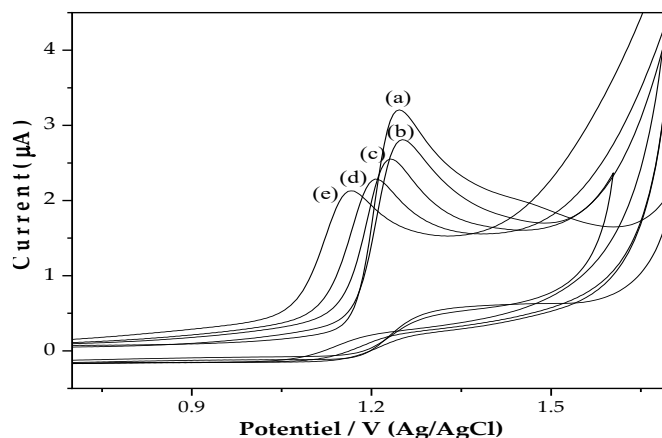


**Figure 2.** Cyclic voltammograms of 60.0  $\mu\text{M}$  GFN in (a) pH 2.0 PB, (b) pH 3.5 AB, (c) pH 5.5 PB, (d) pH 7.0 BRB, and (e) pH 9.0 BRB solutions, Scan rate: 100 mV/s

Hanna HI2211 (Romania) pH meter was used to adjust the pH values of the buffer solutions. All electrochemical measurements were carried out at room temperature ( $25 \pm 1^\circ\text{C}$ ).

### 2.3. Preparation of pharmaceutical dosage forms

Determination studies from pharmaceuticals were performed with a stock solution ( $1.0 \times 10^{-3}$  M) prepared daily using the syrup formulation of GFN (VICKS® expectorant syrup, 200 mg/15 mL). For this purpose, an adequate volume of syrup was transferred to a 10 mL calibrated flask and the volume was made up with bi-distilled water. Working solutions were prepared fresh daily by diluting the stock solution prepared from the syrup with the selected supporting electrolyte and used for the voltammetric determination of GFN.

## 3. Results and discussion

The electrochemical behavior of GFN on BDDE was investigated by CV, DPV, and SWV techniques. Voltammograms of 100  $\mu\text{M}$  GFN solution on BDDE were obtained by CV at a scan rate of 100 mV/s in the pH 2.0–12.0 range (Fig. 2). As can be seen from the cyclic voltammograms in Fig. 2, GFN gave a sharp oxidation peak on BDDE. The absence of any peaks in the direction of reduction in cyclic voltammograms at all buffers and pH indicated that the redox reaction of GFN on BDDE was irreversible.

$$E_p \text{ (mV)} = 1324.5 - 18.0 \text{ pH} \quad (1)$$

$$(r = 0.997) \text{ (pH } 4.5\text{--}11.0, n = 9 \text{ for CV)}$$

$$E_p \text{ (mV)} = 1259.4 - 18.5 \text{ pH} \quad (2)$$

$$(r = 0.995) \text{ (pH } 4.5\text{--}11.0, n = 9 \text{ for DPV)}$$

$$E_p \text{ (mV)} = 1281.9 - 17.7 \text{ pH} \quad (3)$$

$$(r = 0.993) \text{ (pH } 4.5\text{--}11.0, n = 9 \text{ for SWV)}$$

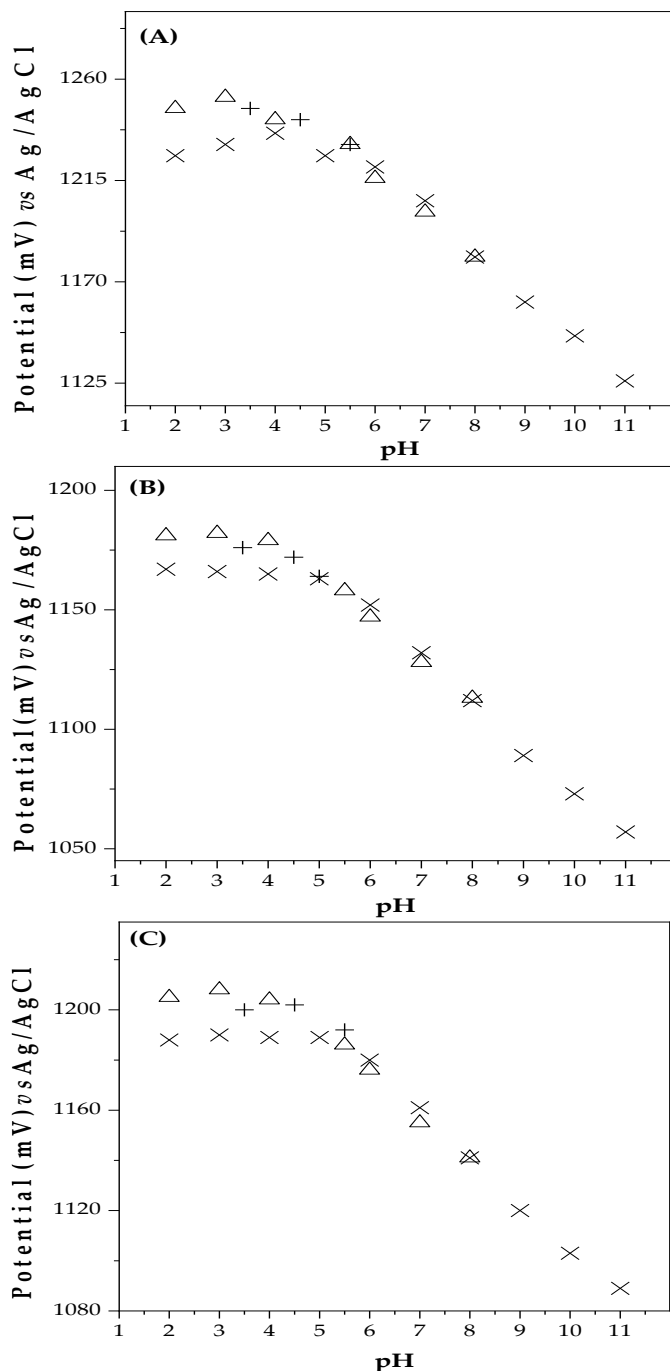


**Figure 3.**  $E_p$ -pH graphs of 60.0  $\mu$ M GFN on BDDE by (A) CV, (B) DPV, and (C) SWV techniques. x: BRB, +: AB,  $\Delta$ : PB solutions

The effect of pH on the peak potential ( $E_p$ ) and peak current ( $I_p$ ) of GFN was investigated on BDDE by CV, DPV, and SWV techniques in different buffer solutions (Figs. 3 and 4). In Fig. 3, it can be seen that the GFN peak potential decreases linearly as the pH value increases. This indicates that as the pH increases, the oxidation reaction of GFN occurs more easily [19].

$E_p$  values obtained with varying pH showed a good linear relationship with the Equations (1 – 3) for CV, DPV, and SWV between pH 4.5 and 11.0. At pHs lower than 4.5, the peak potential of GFN was pH independent for all techniques (Fig. 3).

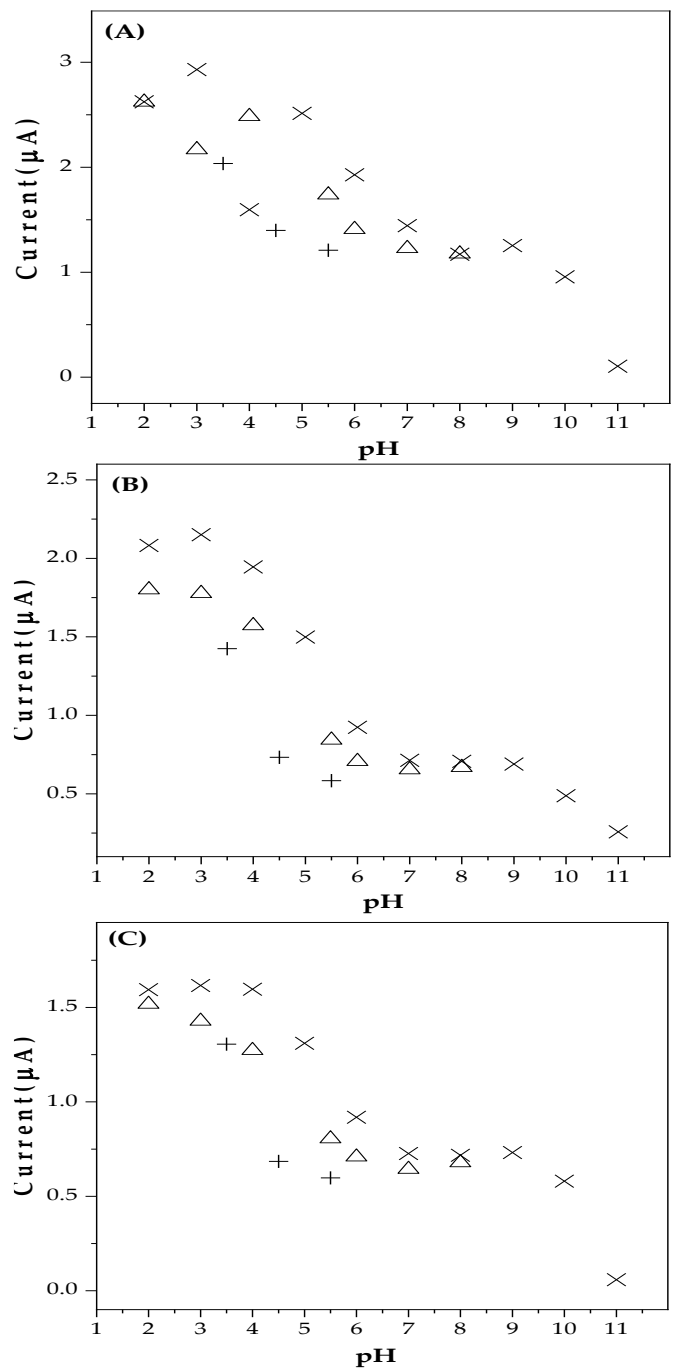


**Figure 4.**  $I_p$ -pH graphs of 60.0  $\mu$ M GFN on BDDE by (A) CV, (B) DPV, and (C) SWV techniques. x: BRB, +: AB,  $\Delta$ : PB solutions

The slope values of -18.0, -18.5, and -17.7 were not close to the theoretical -59.0 mV/pH value [20,21], indicating that the number of protons involved in the oxidation reaction of GFN was not equal to the number of transferred electrons. It is postulated that the oxidation of GFN may occur via the primary alcohol group in the molecule, as suggested in some studies in the literature [22,23].

The peak currents obtained by the CV, DPV, and SWV techniques were plotted against pH as shown in Fig. 4. The most symmetrical peak and the highest peak current (Fig. 4) were obtained in pH 3.5 AB solution, therefore, this solution was chosen as the most suitable supporting electrolyte for further studies.

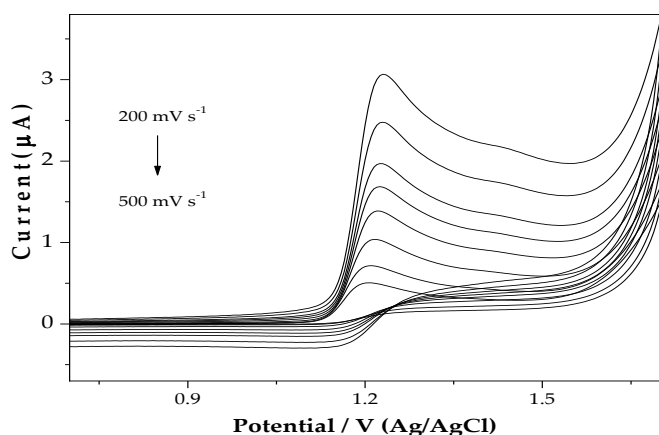


**Figure 5.** Cyclic voltammograms of 60  $\mu\text{M}$  GFN in pH 3.5 AB solution at scan rates of 5, 10, 25, 50, 75, 100, 150, and 200 mV/s on BDDE

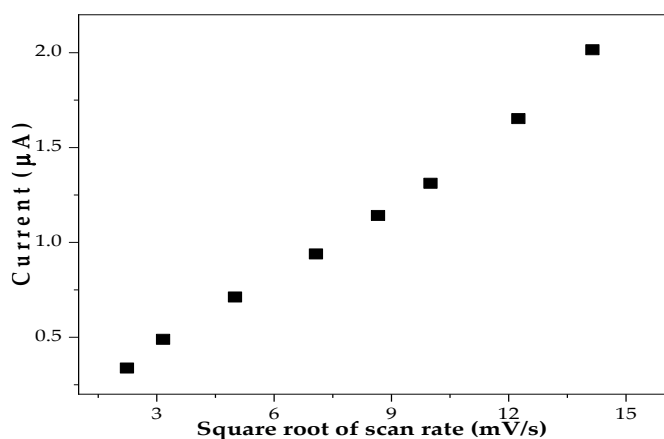


**Figure 6.**  $I_p$ - $v^{1/2}$  graph of 60.0  $\mu\text{M}$  GFN in pH 3.5 AB solution

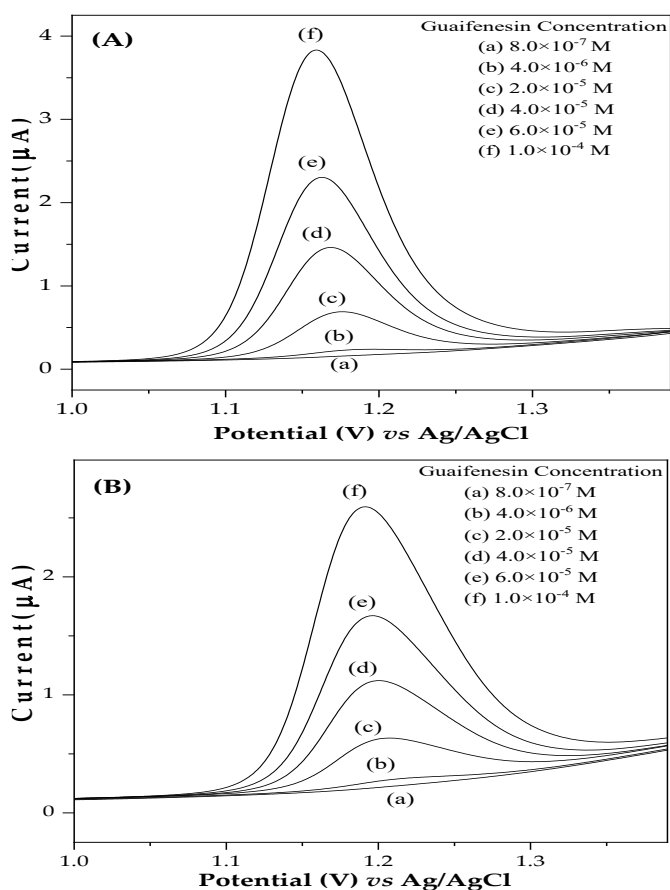


**Figure 7.** (A) DP and (B) SW voltammograms of GFN in pH 3.5 AB solution on BDDE

**Table 1.** Calibration data of GFN obtained by DPV and SWV techniques on BDDE

	DPV	SWV
Measured potential (mV)	1184	1184
Linearity range ( $\mu\text{M}$ )	0.4 – 100	0.8 – 100
Slope ( $\mu\text{A}/\mu\text{M}$ )	$3.63 \times 10^{-2} \pm 5.24 \times 10^{-4}$	$2.41 \times 10^{-2} \pm 4.39 \times 10^{-4}$
Intercept ( $\mu\text{A}$ )	$-7.60 \times 10^{-2} \pm 2.09 \times 10^{-2}$	$-5.40 \times 10^{-2} \pm 1.89 \times 10^{-2}$
Correlation coefficient (r)	0.997	0.996
LOD ( $\mu\text{M}$ )	$1.47 \times 10^{-3}$	$2.92 \times 10^{-3}$
LOQ ( $\mu\text{M}$ )	$4.44 \times 10^{-3}$	$8.84 \times 10^{-3}$
Intra-day precision of peak current (RSD%)*	0.53	0.58
Inter-day precision of peak current (RSD%)*	0.80	1.27

\*Obtained from five measurements

**Table 2.** Results of recovery studies from pharmaceutical dosage form

	DPV	SWV
Labeled amount (mg)	200.00	200.00
Amount found (mg)	199.45	200.35
Relative standard deviation%	0.64	0.48
Bias%	-0.28	0.18
Added amount (mg)	0.039643	0.039643
Found amount (mg)	0.039342	0.039813
Average recovered%	99.24	100.43
Number of experiments	5	5
RSD% of recovery	0.68	0.39
Bias%	-0.76	0.43

**Table 3.** Comparison of parameters obtained with different electrodes for GFN determination

Electrode	Method	Medium	Linear Range ( $\mu\text{M}$ )	LOD ( $\mu\text{M}$ )	Ref.
PtE	DPV	pH 2.0 BRB	100 – 303	—	[11]
PCFE	DPV	pH 7.0 PB	0.1 – 25	0.023	[12]
MWCNT/ILGCE	DPV	pH 7.0 PB	1.5 – 480	0.85	[13]
Au-Pt/NH/CNE	DPV	pH 2.2 BRB	0.05 – 300	0.0175	[14]
PBP/GCE	DPV	pH 3.0 PB	0.1 – 20	0.00366	[27]
PAO/GCE	DPSV	pH 7.0 BRB	0.2 – 100	0.0578	[28]
BDDE	DPV	pH 3.5 AB	0.4 – 100	0.00147	This study
	SWV	pH 3.5 AB	0.8 – 100	0.00292	

PtE: Platinum electrode

PCFE: Anodized nanocrystalline graphite-like pyrolytic carbon film electrode

MWCNT/ILGCE: Multiwalled carbon nanotube-ionic liquid modified glassy carbon electrode

Au-Pt/NH/CNE: Carbon nanotube bimetallic Au-Pt inorganic-organic nanofiber hybrid nanocomposite electrode

PBP/GCE: Poly(bromocresol purple) modified glassy carbon electrode

PAO/GCE: Poly(acridine orange) modified glassy carbon electrode

Scan rate study was performed by CV technique to understand whether the electro-oxidation reaction mechanism of GFN is diffusion-controlled or adsorption-controlled. For this purpose, the electrochemical behavior of 60.0  $\mu\text{M}$  GFN in AB solution at pH 3.5 was investigated in the range of 5 – 200 mV/s (Fig. 5).

The plot of the peak current of GFN versus the square root of the scan rate showed linearity with a slope of 0.1348 (Equation 4), as shown in Fig. 6. Also, the regression equation from the  $\log I_p - \log v$  plot gave a slope of 0.464, which is very close to the theoretical value of 0.5 (Equation 5), which indicates diffusion-controlled process [24,25]. This result indicated that the electro-oxidation process of GFN was controlled by the diffusion on the BDDE surface [24].

$$I_p (\mu A) = 0.1348 v^{1/2} (mV/s) + 0.0212 \quad (4)$$

$$(r = 0.993, n = 8)$$

$$\log I_p (\mu A) = 0.464 \log v (mV/s) - 0.795 \quad (5)$$

$$(r = 0.995, n = 8)$$

Quantitative analysis of GFN was performed using DPV and SWV techniques. Because of their high sensitivity, selectivity, low detection limits, and rapid response, these techniques were used for the determination of GFN. DP and SW voltammograms for different concentrations of GFN were given in Fig. 7. Linear ranges were obtained between 0.40 and 100.0  $\mu M$  for DPV and between 0.80 and 100.0  $\mu M$  for SWV. Characteristics of calibration equations and the validation parameters for both DPV and SWV are reported in Table 1. Limit of detection (LOD) and limit of quantification (LOQ) values were calculated from  $3s/m$  and  $10s/m$ , respectively; where  $s$  is the standard deviation of the response and  $m$  is the slope of the calibration curve [26].

Quantitative determination of GFN from the pharmaceutical dosage form was carried out by DPV and SWV techniques on BDDE using the corresponding calibration equation. For this purpose, syrup form of GFN containing 200 mg of GFN and inactive ingredients per 15 mL was used and recovery studies were performed. The results obtained are given in Table 2.

The data obtained in this study for GFN were compared with the data from other voltammetric studies in the literature (Table 3). The linearity range obtained with platinum electrode [11] was much narrower than the linearity ranges obtained for both techniques in this study. Linearity ranges obtained in the studies with multiwalled carbon nanotube-ionic liquid modified glassy carbon electrode [13], carbon nanotube bimetallic Au-Pt inorganic-organic nanofiber hybrid nanocomposite electrode [14], and poly(acridine orange) modified glassy carbon electrode [28] were wider than the linearity ranges obtained in this study. The linearity range of the DPV technique in this study is the same as that of the anodized nanocrystalline graphite-like pyrolytic carbon film electrode [12] and almost the same as that obtained with poly(bromocresol purple)

modified glassy carbon electrode[27]. Although the linearity ranges vary according to the electrodes used and the developed techniques, the LOD values obtained by DPV and SWV techniques in this study were found to be much lower than the LOD values of other studies in the literature in Table 3. In addition, GFN analysis was performed in a very practical process with bare BDDE without any modification.

## 4. Conclusion

The electro-oxidation behavior of GFN was investigated on BDDE by voltammetric techniques. As a result of voltammetric studies, it was observed that GFN had an irreversible and diffusion-controlled oxidation reaction on the surface of BDDE. Developed DPV and SWV techniques enabled rapid, sensitive, selective, inexpensive, and simple determination of GFN from its pharmaceutical formulation. As a result, accurate and precise voltammetric techniques were developed for GFN analysis using unmodified BDDE.

## Conflicts of interest

The authors declare no conflict of interest.

## References

- [1] W.W. Storms, J.E. Miller, Daily use of guaifenesin (Mucinex) in a patient with chronic bronchitis and pathologic mucus hypersecretion: A case report, *Respiratory Med Case Rep*, 23, 2018, 156–157.
- [2] H.H. Albrecht, P.V. Dicipinigitis, E.P. Guenin, Role of guaifenesin in the management of chronic bronchitis and upper respiratory tract infections, *Multidiscip Respir Med*, 12, 2017, 31.
- [3] J.A. Ohar, J.F. Donohue, S. Spangenthal, The role of guaifenesin in the management of chronic mucus hypersecretion associated with stable chronic bronchitis: A comprehensive review, *Chronic Obstr Pulm Dis*, 6, 2019, 341–349.
- [4] N.A. El-Maali, Voltammetric analysis of drugs, *Bioelectrochemistry*, 64, 2004, 99–107.
- [5] Martindale. Guaifenesin. In *Martindale: The Complete Drug Reference*. Edited by S. Sweetman, 2016, London, The Pharmaceutical Press.
- [6] A.A. Bankar, S.R. Lokhande, R. Sawant, and A.R. Bhagat, Spectrophotometric estimation of guaifenesin and salbutamol in pure and tablet dosage form by using different methods, *Der Pharma Chemica*, 5, 2013, 92–97.
- [7] N.C. Patel, D.B. Patel, P.K. Chaudhari, Spectrophotometric estimation of ambroxol hydrochloride, guaifenesin and levosalbutamol sulphate in syrup, *AJRC*, 6, 2013, 407–414.
- [8] H. Patil, S. Sonawane, P. Gide, Determination of guaifenesin from spiked human plasma using RP-HPLC with UV detection, *J Anal Chem*, 69, 2014, 390–394.
- [9] H.M. Maher, S.M. Al-Taweel, M.M. Alshehri, N.Z. Alzoman, Novel stereoselective high-performance liquid chromatographic method for simultaneous determination of guaifenesin and ketorolac enantiomers in human plasma, *Chirality*, 26, 2014, 629–639.

- [10] O.A. Saleh, A.M. Yehia, A.A.-E.S. El-Azzouny, H.Y. Aboul-Enein, A validated chromatographic method for simultaneous determination of guaifenesin enantiomers and ambroxol HCl in pharmaceutical formulation, *RSC Adv*, 5, 2015, 93749–93756.
- [11] I. Tapsobab, J.E. Belgaieda, K. Boujlel, Voltammetric assay of guaifenesin in pharmaceutical formulation, *J Pharm Biomed Anal*, 38, 2005, 162–165.
- [12] M. Hadi, Electrochemical determination of guaifenesin in a pharmaceutical formulation and human urine based on an anodized nanocrystalline graphite-like pyrolytic carbon film electrode, *Anal Methods*, 7, 2015, 8778–8785.
- [13] M.B. Gholivand, M. Khodadadian, Simultaneous voltammetric determination of theophylline and guaifenesin using a multiwalled carbon nanotube-ionic liquid modified glassy carbon electrode, *Electroanalysis*, 26, 2014, 1975–1983.
- [14] M.B. Gholivand, A. Azadbakht, A. Pashabadi, An electrochemical sensor based on carbon nanotube bimetallic Au-Pt inorganic-organic nanofiber hybrid nanocomposite electrode applied for detection of guaifenesin, *Electroanalysis*, 23, 2011, 2771–2779.
- [15] M.J. Arcos, M. Alonso, M.C. Ortiz, Genetic-algorithm-based potential selection in multivariate voltammetric determination of indomethacin and acetaminophen by partial least squares, *Electrochim Acta*, 43, 1988, 479–485.
- [16] J.H.T. Luong, K.B. Maleb, J.D. Glennon, Boron-doped diamond electrode: synthesis, characterization, functionalization and analytical applications, *Analyst*, 134, 2009, 1965–1979.
- [17] S.J. Cobb, Z.J. Ayres, J.V. Macpherson, Boron doped diamond: A designer electrode material for the twenty-first century, *Annu Rev Anal Chem*, 11, 2018, 463–484.
- [18] P. Talay Pınar, Electrochemical behaviour of ofloxacin in pharmaceutical and biological samples using a boron-doped diamond electrode in using anionic surfactant, *GU J Sci*, 31, 2018, 66–80.
- [19] Ö. Selçuk, C. Erkmen, B. Bozal-Palabıyık, B. Uslu, Electroanalytical investigation and simultaneous determination of etodolac and thiocolchicoside at a non-modified glassy carbon electrode in anionic surfactant media, *Electroanalysis*, 33, 2021, 1290–1298.
- [20] J. Wang, *Electroanalytical Techniques in Clinical Chemistry and Laboratory Medicine*, 1988, New York: VCH Publishers.
- [21] P.T. Kissinger, and W.R. Heineman, *Laboratory Techniques in Electroanalytical Chemistry* (2nd edition), 1984, New York, Markel Dekker.
- [22] S. Shi-Gang, S. Hong-Mei, S. Han-Wen, Mechanism and kinetics of guaifenesin oxidation by bis(hydrogenperiodato)argentate(III) complex anion, *Acta Phys -Chim Sin*, 23, 2007, 409–413.
- [23] Puttaswamy, A. Sukhdev, Oxidation of mephensin and guaifenesin with chloramine-B in hydrochloric acid medium: Design of kinetic model, *Ind J Chem*, 48A, 2009, 339–345.
- [24] E. Laviron, L. Roullier, C. Degrand. A multilayer model for the study of space distributed redox modified redox modified electrodes: Part II. Theory and application of linear potential sweep voltammetry for a simple reaction, *J Electroanal Chem Interfacial Electrochem*, 112, 1980, 11–23.
- [25] D.K. Gosser, Jr., *Cyclic Voltammetry, Simulation and Analysis of Reaction Mechanisms*, 1993, New York, VCH Publishers, pp. 43, 97–99.
- [26] I.R. Berry, and D. Harpaz. *Validation of Active Pharmaceutical Ingredients* (2nd edition), 2001, Washington, CRC Press.
- [27] F. Ağın, Voltammetric determination of guaifenesin in pharmaceuticals and urine samples based on poly(bromocresol purple) modified glassy carbon electrode, *Curr Pharm Anal*, 16, 2020, 633–639.
- [28] H. Işık, G. Öztürk, F. Ağın, D. Kul, Electroanalytical analysis of guaifenesin on poly(acridine orange) modified glassy carbon electrode and its determination in pharmaceuticals and serum samples, *Comb Chem High T Scr*, 24, 2021, 376–385.



# Heavy metal pollution from listwaenitization: In case of Alakeçi (Bayramiç - Çanakkale / West Türkiye)

Alaaddin Vural 

Gümüşhane University, Faculty of Natural Sciences and Engineering, Department of Geological Engineering, 29100, Gümüşhane, Türkiye

## Abstract

This study aimed to investigate the risk of element / heavy metal pollution caused by listwaenitization. In this context, the heavy metal pollution risk of listwaenite-derived soils in the region where listwaenitized ultrabasic rocks are present as a result of hydrothermal alterations in the vicinity of Alakeçi (Bayramiç Çanakkale / Western Türkiye) was investigated with pollution index, geoaccumulation index and integrated pollution risk parameters. For this purpose, Cu, Zn, Pb element concentrations of 350 soil samples collected from the field were determined, and Pollution Index (PI) and Geo-accumulation Index (Igeo) parameters for each element and Integrated Pollution Index (IPI) parameters for each sampling point were calculated. In addition, distribution maps of PI, Igeo and IPI parameters were plotted. When the site is considered in terms of IPI parameter, it has been determined that the site has medium and high pollution risk. When the field is considered in terms of PI and Igeo parameters, a remarkable level of pollution has been detected in the field, especially by Ni, Co and As elements. When the distribution maps of the PI, Igeo and IPI parameters are examined, it has been determined that the pollution risk is higher than the other areas, especially in the areas where hydrothermal alteration is intense and in the tectonic line areas. Although listwaenitizations and listwaenite zones are important target areas especially for epithermal gold mineralizations, this study has shown that listwaenitization areas are also areas at risk of heavy metal pollution. Therefore, listwaenitization zones are areas that should be investigated in terms of heavy metal pollution risk as well as epithermal gold mineralization potentials.

**Keywords:** Listwaenite / listwaenitization, heavy metal pollution, pollution Index (PI), integrated pollution index (IPI), geo-accumulation index (Igeo)

## 1. Introduction

The concept of listwaenitization / listwaenite was first used for the Ural gold fields of Russia located in the Livtenya region [1–3]. Although the concept of listwaenite entered the literature a long time ago, the associated mineralization models are still controversial [1,4–7]. However, the concept of listwaenite has been accepted by many researchers and has been used in many studies [1,8–16]. Listwaenite is a hydrothermal alteration process and the end products of the process are soil zones developed over listwaenitization zones [6,17,18]. Although listwaenitization zones are the subject of mineral exploration, they are also products of hydrothermal alteration, and as a result of alteration, some elements are enriched in the environment, while others are depleted. When evaluated in this context, the listwaenitization zones and the soil developments in

these zones may be exposed to metal enrichment / pollution. Metal enrichment in soils started to attract the attention of the society especially after the second quarter of the last century and many studies were carried out for this purpose [19–21]. Heavy metal pollution has many negative effects not only in the soil, but also in the aquatic environment, together with the food chain, and therefore on human health. [22,23].

The aim of this study is to investigate the risk of heavy metal pollution in developed soils over the Alakeçi (Bayramiç / Çanakkale - Western Türkiye) listwaenitization occurrences. Soil samples collected from the field for mineral exploration purposes in the past [2,22] were evaluated in terms of heavy metal pollution risk by using different pollution parameters in this study.

**Citation:** A. Vural, Heavy metal pollution from listwaenitization: In case of Alakeçi (Bayramiç-Çanakkale/West Türkiye), Turk J Anal Chem, 4(2), 2022, 94–102.

**\*Author of correspondence:** alaaddinvural@hotmail.com

**Tel:** +90 (456) 233 17 13

**Fax** +90 (456) 233 10 75

**Received:** October 18, 2022

**Accepted:** November 21, 2022

## 2. Material and methods

### 2.1. Geological characteristics of the area

In the Biga peninsula, within the borders of Bayramiç (Çanakale-Türkiye) Alakeçi village and its vicinity, a listwaenitization development of approximately 1 km<sup>2</sup> is observed within the Alakeçi mylonitic zone [2,22,24]. The basement rocks of the region are Sakarya Zone, Ayvack-Karabiga Zone and Ezine Zone from southeast to northwest [24].

In the study area, Kazdağ Group metamorphics (consisting of gneiss, amphibolite, and marbles) (Sakarya Zone), ophiolitic mélangé (Ayvack-Karabiga Zone) and mylonitic gneiss unit and meta serpentinites (These two units are called Alakeçi Mylonitic zone) developed between these two zones are observed. All these units are cut by Tertiary magmatic rocks and covered by Tertiary volcanic and sedimentary rocks (Fig. 1 and 2a). The Alakeçi Mylonitic Zone formed between the ophiolitic mélangé and the Kazdağ Group is in east-northeast orientation in accordance with the main foliation of the Kazdağ Group [24]. Along this zone, 1.5–2 km long and approximately 400–500 meters wide, a listwaenite zone extends in the northwest-southeast direction and is interrupted by strike-slip faults in the northeast-southwest direction. (Fig. 1 and 2a). Listwaenite zone consists mainly of Fe-Mg carbonate, quartz, and fuchsite (mica mineral). These minerals are accompanied by scattered chromite and lesser amounts of pyrites. Listwaenite zone is covered with medium-well developed soil derived from listwaenites.

### 2.2. Sampling and analytical procedure

The study was carried out on 350 soil samples collected from the listwaenite zone and its vicinity, and the sampling and analytical procedure of the study are given in detail in the studies of [2] and [1]. Soil samples were taken from the B profile of the soil zone and from approximately 15–30 cm depths, from grid points equally spaced across the field. (Fig. 1, 2a). The collected samples were sifted through an 80 mesh sieve in accordance with routine sample preparation procedures

[25], dried in an oven at 60 °C for 24 hours to remove their natural moisture and analyzed by flame atomic absorption spectrometry (FAAS) for As, Sb, Cu, Pb, Zn, Ni and Co in at the General Directorate of Mineral Research and Exploration (MTA) Laboratory (Ankara-Türkiye). In the MTA Analysis, Technology and Calibration Laboratories, service is provided at the level and quality that meets the requirements of the TS EN ISO / IEC 17025 Standard, in accordance with the impartiality and confidentiality statements. MTA laboratory processes and MTA laboratory standards were used in the analytical procedures.

The method's accuracy has been proven by the analysis of standard reference materials. It was determined by the *t*-test that there was no statistically significant difference between the results obtained and the results were quite satisfactory ( $p \leq 0.05$ ) [26]. The precision of the method was evaluated with the relative standard deviation (RSD). RSD values for the studied elements were calculated to be between %1.2 (for Mo) and 3.2% (for Mo).

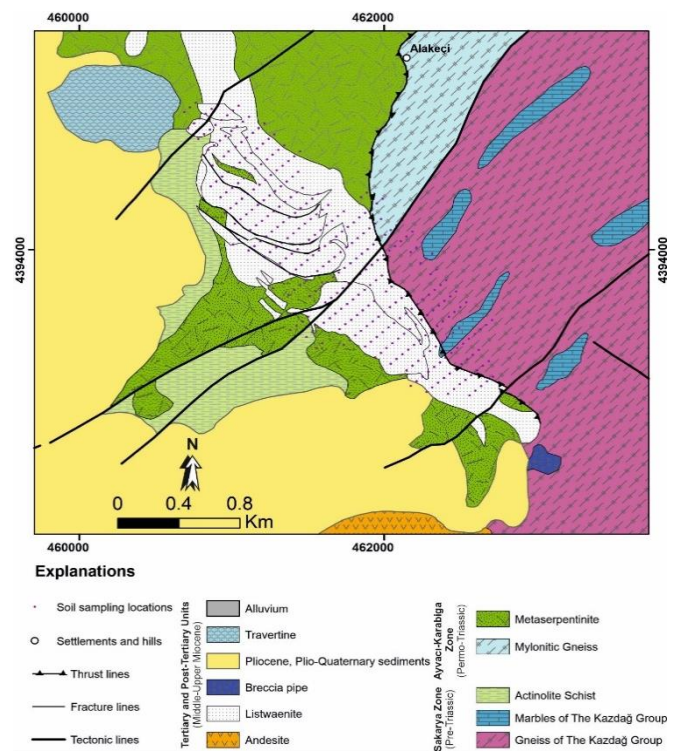


Figure 1. Geology of the study area and sampling map [1,2]

Table 1. Descriptive statistics of elements in soil samples

	Number*	Upper crust value**	Mean	Median	Geometric Mean	Minimum	Maximum	Standard deviation
Cu	342	28	38.3	33.0	32.9	10	265	29.1
Pb	340	17	24.4	20.0	22.3	10	90	10.4
Zn	342	67	64.2	55.0	58.3	15	545	38.8
As	325	4.8	93.3	50.0	61.4	5	800	86.1
Sb	220	0.4	4.8	4.0	3.5	2	60	6.2
Ni	340	47	1517.3	1250.0	916.5	10	6300	1271.1
Co	338	17.3	104.2	80.0	78.4	15	1255	98.1

\* It represents the number of samples measured above the detection limit for the element under investigation

\*\* Upper crust element concentrations from [33]

**Table 2.** Correlation coefficients of the elements

	Cu	Pb	Zn	As	Sb	Ni	Co
Cu	1						
Pb	0.42	1					
Zn	0.75	0.44	1				
As	-0.03	0.05	0.08	1			
Sb	0.08	0.06	0.12	0.65	1		
Ni	-0.26	-0.10	-0.01	0.36	0.18	1	
Co	-0.19	-0.03	0.02	0.37	0.20	0.73	1

### 2.3. Evaluation of the data

Statistical and spatial statistical evaluation of all data was evaluated with IBM SPSS 21 and ArcMap 10.8, respectively. Descriptive statistics and correlation coefficients of data belonging to 7 elements are given in [Tables 1](#) and [2](#) respectively.

Many different pollution parameters are used in the evaluation of heavy metal pollution [19]. In this study, Pollution Index (PI), Integrated Pollution Index (IPI) and Geo-accumulation Index (Igeo) parameters, which are the most well-known ones, were used to investigate heavy metal pollution in soils. The Pollution Index (PI) and the Integrated Pollution Index (IPI) are also widely used to assess media quality [27–31]. PI is obtained by dividing the element concentration in the soil with the average values in the upper crust and / or the earth's soil. In this study, PI was calculated for each element and classified as low ( $PI \leq 1$ ), medium ( $1 < PI \leq 3$ ), or high ( $PI > 3$ ). IPI is obtained by calculating the geometric mean of the PI measurements of the relevant point for each element examined, and the results are classified as low ( $IPI \leq 1$ ), medium ( $1 < IPI \leq 2$ ) and high risk ( $IPI > 2$ ) [27].

Igeo was first proposed by [32] to compare pre-industrial and current heavy metal concentrations and is calculated by the following formula:

$$Igeo = \log_2 Cn / 1.5Bn$$

In the formula, Cn corresponds to the element concentration in the sample studied, and Bn corresponds to the average value in the upper crust / earth soil for the same element. In this study, upper crustal averages from [33] were used. A coefficient of 1.5 was proposed by [32] to balance possible effects on soils. [32] divided the Igeo parameter into seven classes between 0 – 6. According to this;

- < 0 = practically uncontaminated
- 0 – 1 = uncontaminated to moderately contaminated
- 1 – 2 = moderately contaminated
- 2 – 3 = moderately to strongly contaminated
- 3 – 4 = strongly contaminated
- 4 – 5 = strongly to extremely contaminated and
- > 5 = extremely contaminated

## 3. Results and discussion

### 3.1. Statistical evaluation of the data

[Table 1](#) presents the descriptive statistics of the 7 elements in the soil (mean, median, geometric mean, minimum, maximum and standard deviation). Elemental concentrations in soil are 10–265 ppm, 10–90 ppm; 15–545 ppm; 5–800 ppm; 2–60 ppm, 10 to 6300, and 15–1255 ppm for Cu, Pb, Zn, As, Sb, Ni and Co, respectively. The resulting concentrations generally exceed the expected upper crust values and uncontaminated soil values. The high concentrations at the sampling points are thought to be due to the Listwaenitization of ultramafic rocks because of hydrothermal alteration and metasomatism processes. The fact that the standard deviation values are different and larger than zero indicate that the sample populations deviate from the normal distribution, that is, there is a metal enrichment in the field. The environmental effects of element enrichment are discussed below with relevant pollution parameters.

Correlation coefficients were calculated ( $p \leq 0.05$  and  $p \leq 0.01$ ) in order to understand the co-behavior tendencies of the elements in the soil, and the multi-element correlation coefficients in the soil samples are given in [Table 2](#). Considering the multi-element correlation coefficients calculated for the elements, a positive significant relationship was found between Cu and Zn (0.75), between Sb and As (0.65), and between Ni and Co (0.73). The correlations detected between the elements were also found to be compatible with the behavioral associations of the elements.

### 3.2. Evaluation of the site with pollution parameters

Different assumptions can be used to calculate the IPI values of sampling points. For example, different IPI values are calculated for the elements related to each other by calculating the correlation coefficients, and IPI values are also calculated by considering the elements within the same factors by performing factor analysis for the examined elements, so that IPI values depending on the factors affecting the pollution in the researched area are determined. But, in this study, the IPI values of the sampling points were calculated by considering all the investigated elements / heavy metals.

Considering the IPI values calculated for the area, it has been determined that most of the sampling points in the area have a high risk of pollution, while relatively few sampling points have moderate pollution ([Fig. 2b](#)).

When the site was evaluated in terms of Cu according to the PI index, moderate pollution was detected in a significant part of the sampling points ([Fig. 2c](#)). Due to intense alteration, especially in areas close to tectonic

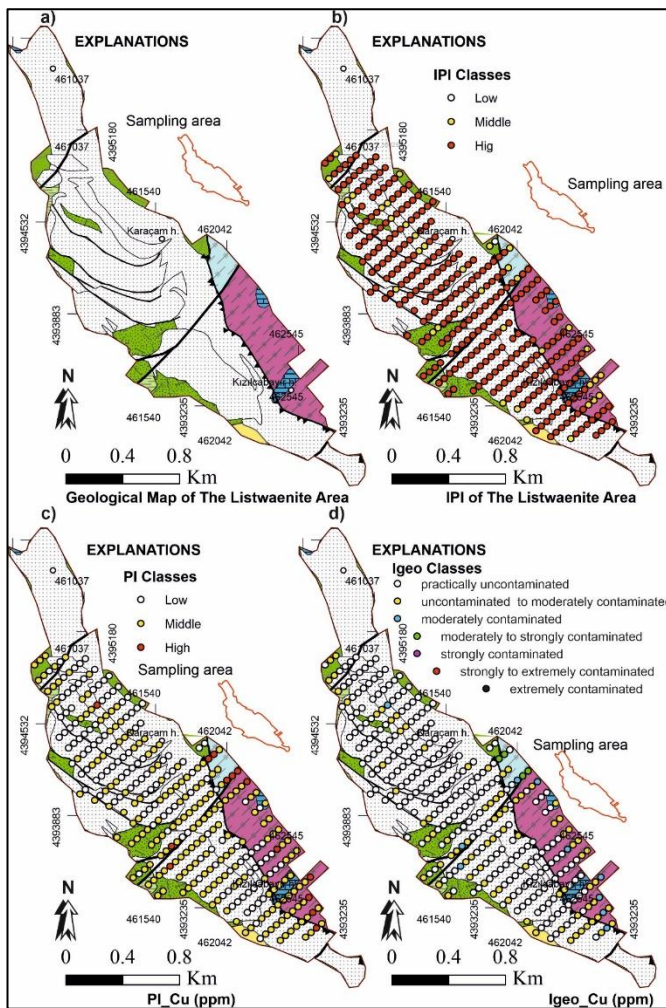


**Figure 2.** a) Study site geology map; b) Study site IPI dot map; c) PI Cu dot map; d) Igeo Cu dot map (See Fig. 1 for Figure explanation)

lines, high pollution, albeit limited, has been determined. Considering the Igeo index for copper, most of the site is practically uncontaminated, while the second plurality of sampling points falls into the uncontaminated to moderately polluted class. A small number of sampling points are in the moderately polluted class and a very small sampling point is in the moderate to severely polluted class (Fig. 2d).

When the site is evaluated with the PI parameter in terms of Pb element, it is seen that most of the sampling points are at the medium pollution level (Fig. 3a). High pollution was detected at only a few sampling points. When the site is evaluated with the Igeo index for Pb, most sampling points fall into the practically uncontaminated class, while a significant portion of the sampling points are in the uncontaminated to moderately polluted class. Only a few sampling points are moderately contaminated (Fig. 3b).

When the site is evaluated according to the PI index in terms of Zn, the southern part of the listwaenite zone is mostly observed in the medium pollution class, while the pollution level is mostly in the low class except for a few sampling points (Fig. 3c). There is high pollution at

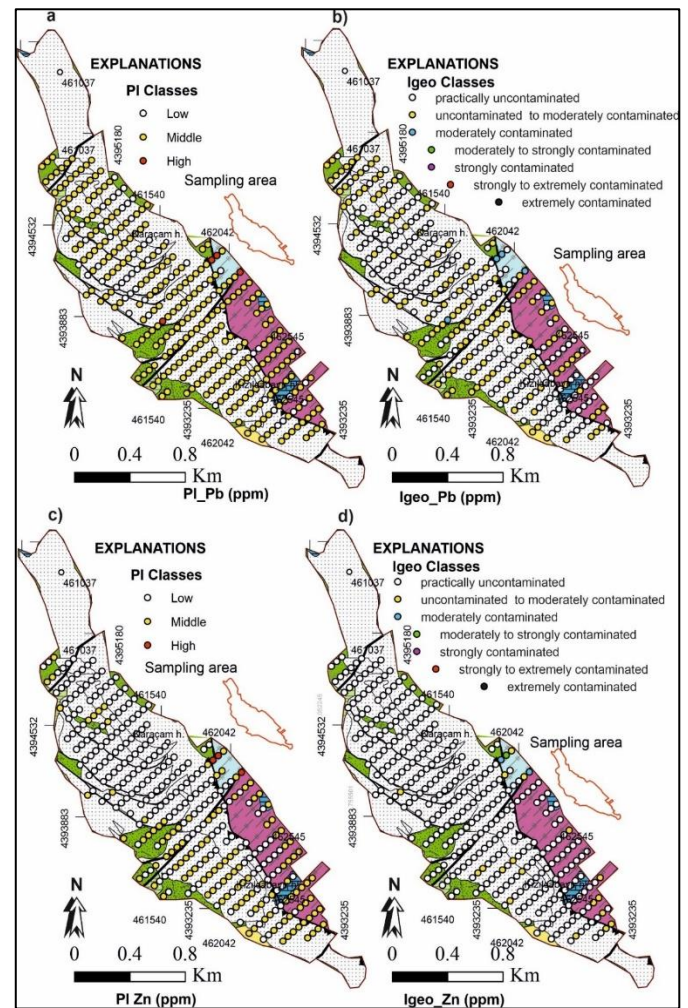


**Figure 3.** a) PI Pb dot map; b) Igeo Pb dot map; c) PI Zn dot map; d) Igeo Zn dot map (See Fig. 1 for Figure explanations)

only 3 points associated with tectonic lines, and when the site is evaluated in terms of Igeo index, most of the site is in the practically unpolluted class, while a small number of sampling points are in the unpolluted to moderately polluted class (Fig. 3d). Moderate pollution was determined at 2 sampling points and moderate to severely polluted class at one sampling point.

According to the PI parameter, the site is in the high pollution class in terms of arsenic (As) at many sampling points. It is seen that very few sampling points are in the medium pollution class (Fig. 4a). When the site is evaluated with the Igeo parameter for As, very few sampling points are in the practically uncontaminated class, with a few sampling points falling into the uncontaminated to moderately polluted class. Most of the sampling points fall into strongly to extremely contaminated class and extremely contaminated. A few sampling points are in the extremely contaminated class (Fig. 4b). In the light of these data, it has been determined that the site is remarkable in terms of pollution in terms of arsenic, and it is recommended to conduct a more detailed multi-purpose investigation in the area.

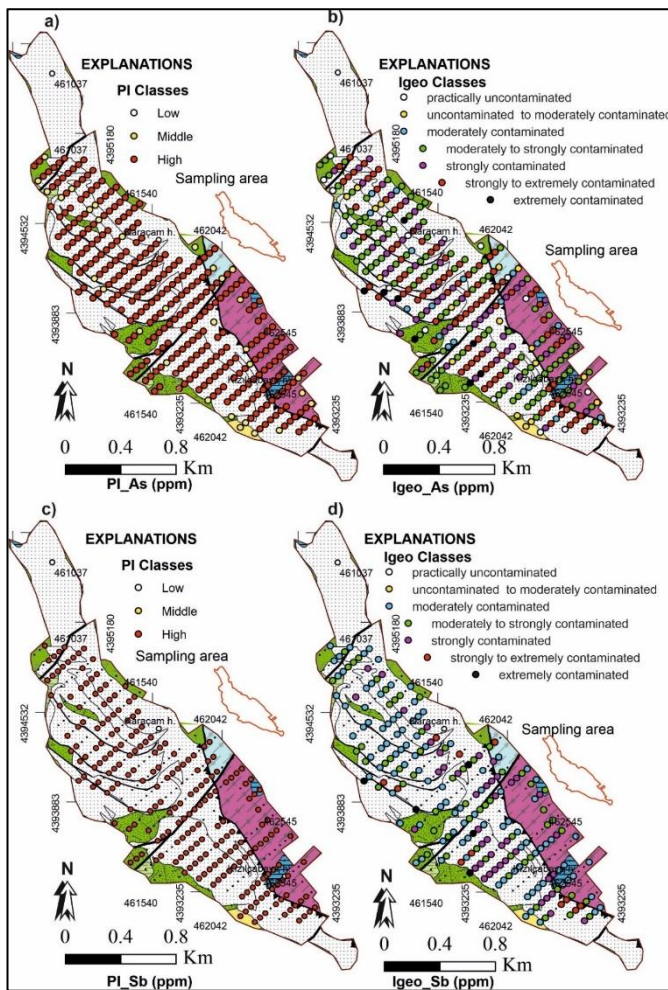


**Figure 4.** a) PI As dot map; b) Igeo As dot map; c) PI Sb dot map; d) Igeo Sb dot map (See Fig. 1 for Figure explanations)

When the study area is examined in terms of antimony, although the Sb was detected above the detection limit in fewer sampling points than the other elements, all sampling points are at high pollution level according to the PI parameter (Fig. 4c). When the Sb values in the field are evaluated with the Igeo parameter, most of the sampling points are in the moderately polluted class, while the remaining sampling points are respectively in the medium-strongly polluted, strongly polluted, and strongly-extremely polluted class (Fig. 4d). For Sb, only 5–6 sampling points are in the extremely polluted class.

When the site was evaluated with the PI index in terms of Ni element, high Ni pollution was detected at the points other than very few sampling points (Fig. 5a). Moderate contamination was detected at only a few sampling points. When the field is examined for Ni element in terms of Igeo parameter, it is determined that only a few sampling points are in the practically uncontaminated class and many sampling points in the south of the field fall into the extremely contaminated class (Fig. 5b). Other sampling points fall into the strongly to extremely contaminated class.

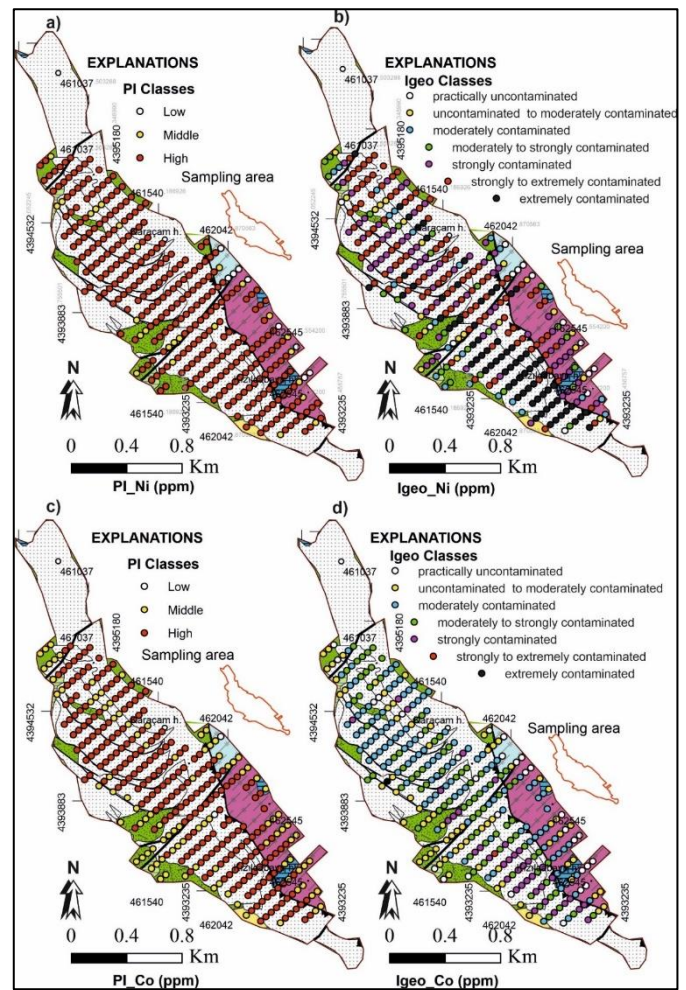


**Figure 5.** a) PI Ni dot map; b) Igeo Ni dot map; c) PI Co dot map; d) Igeo Co dot map (See Fig. 1 for Figure explanations)

When the study area is evaluated with the PI parameter in terms of Co, approximately 80% of the sampling point falls into the high pollution class. Only a few sampling points are in the low pollution class and about 15% of the sampling points are in the medium pollution class (Fig. 5c). When the field soils were evaluated with the Igeo parameter for Co contamination, it was determined that many of the sampling points were in the moderately polluted class and approximately 25% and 15% of the sampling points were moderately to strongly contaminated and strongly contaminated, respectively. Only 1–2 sampling points were found to be strongly to extremely contaminated and extremely contaminated (Fig. 5d).

### 3.3. Pollution parameters distribution maps

It was predicted that it would be useful to prepare distribution maps of pollution parameters for better evaluation of heavy metal pollution in the region, and thus distribution maps for PI, Igeo and IPI parameters of the listwaenite field were plotted. There are many methods in the plotting of distribution maps in spatial statistics studies. Considering the field conditions, the Kriging method was preferred for the study area. The Kriging method was first proposed by [34] and

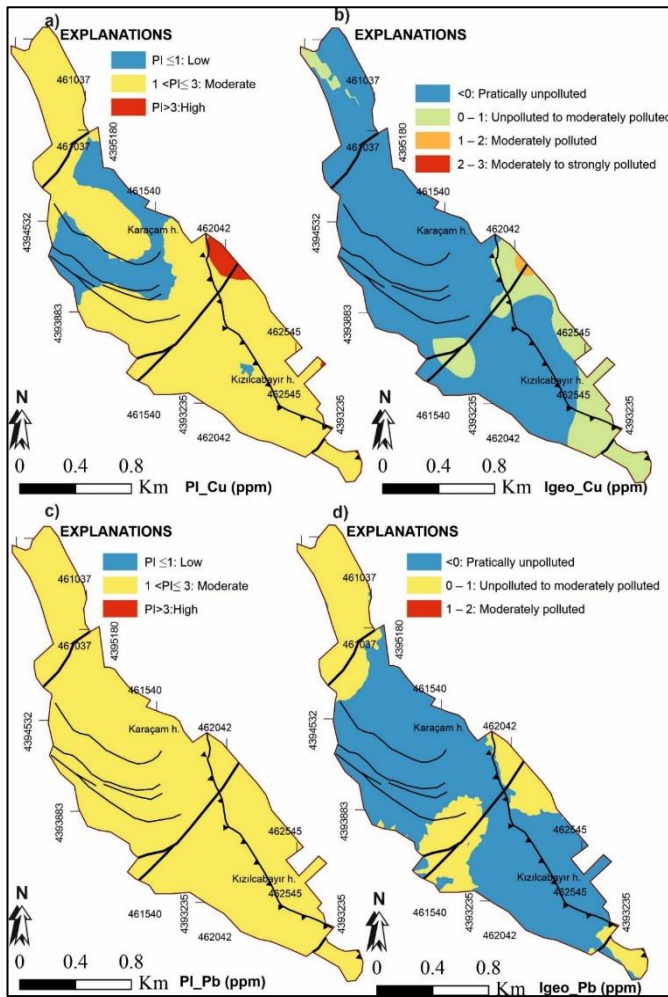


**Figure 6.** a) Distribution map of PI for Cu; b) Distribution map for Igeo of Cu; c) Distribution map of PI for Pb; d) Distribution map of Igeo for Pb (See Fig. 1 for Figure explanations)

developed by [35,36] and is widely used in spatial geostatistical interpolation studies. Kriging method is a flexible method that can be adjusted according to the situation by considering many parameters. It attempts to estimate unsampled point values using the information underlying the areal autocorrelation provided by the semi-variograms to find the most appropriate weighting sets to predict points and surfaces at sampling points. Because the semi-variogram is a function of distance, the weights vary according to the spatial distribution of the samples. Low weights are assigned to distant samples and higher weights are assigned to nearby samples. The Kriging method also considers the relative positions of the samples with respect to each other. Ordinary Kriging is the most reliable and can be easily used for many datasets. Although the transitions of the contours are smoother and more aesthetic in the Simple Kriging method, it is relatively less reliable. The Universal Kriging method, on the other hand, requires experience as well as having more data about the field. Considering all these data, Ordinary Kriging method was used to plot distribution maps of pollution parameters in the area.

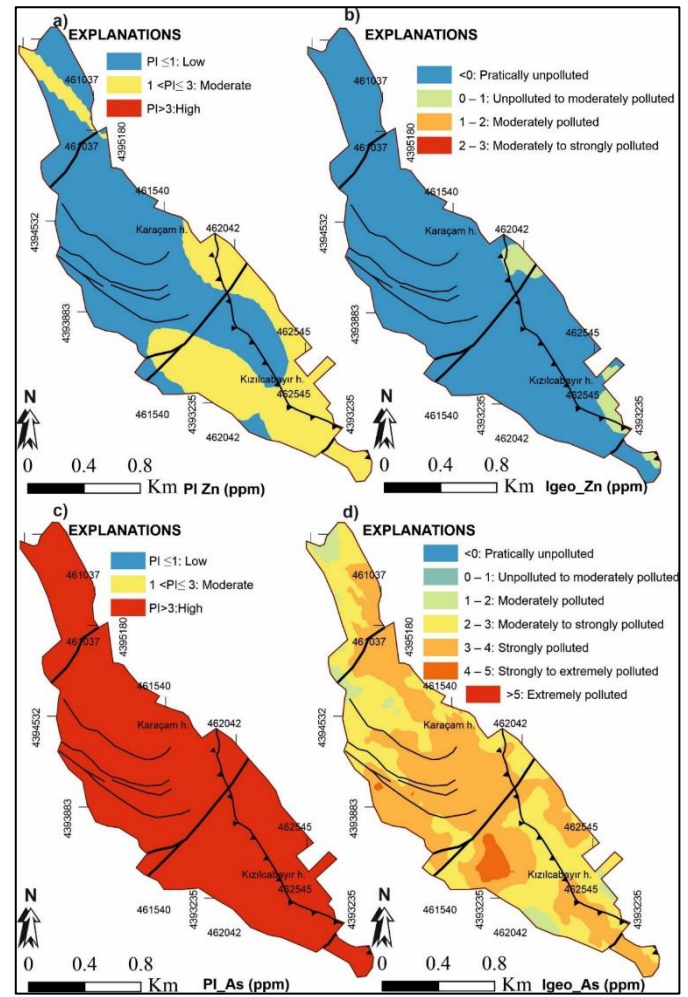


**Figure 7.** a) Distribution map of PI for Zn; b) Distribution map of Igeo for Zn; c) Distribution map of PI for As; d) Distribution map of Igeo for As (See Fig. 1 for Figure explanations)

Cross validation is used to investigate the accuracy of Kriging methods and to evaluate the performance of models used on the Kriging surface. In the studies carried out by many researchers, it has been seen that Kriging and Inverse Distance Weighting methods give the best performance in the studies where the number of points is not frequent and irregular sampling is performed, although most of the interpolation techniques give results close to each other and with high accuracy in regions with frequent sampling [37–46]. In this study, sampling points were organized regularly and frequently for heavy metals, distribution maps of PI, Igeo, and IPI parameters were plotted using the Ordinary Kriging and Constant method (Figs. 6–9).

When the PI distribution map of the copper element is examined (Fig. 6a), it is seen that a small part of the study area (Karaçam hill and its surroundings) shows low pollution, while a significant part of the area has medium pollution. It is seen that the immediate surroundings of the faulted contact separating the Kazdağ metamorphics and mylonitic gneiss have a high pollution risk. When the Igeo distribution map of Cu is examined, it is seen that most of the area is in the

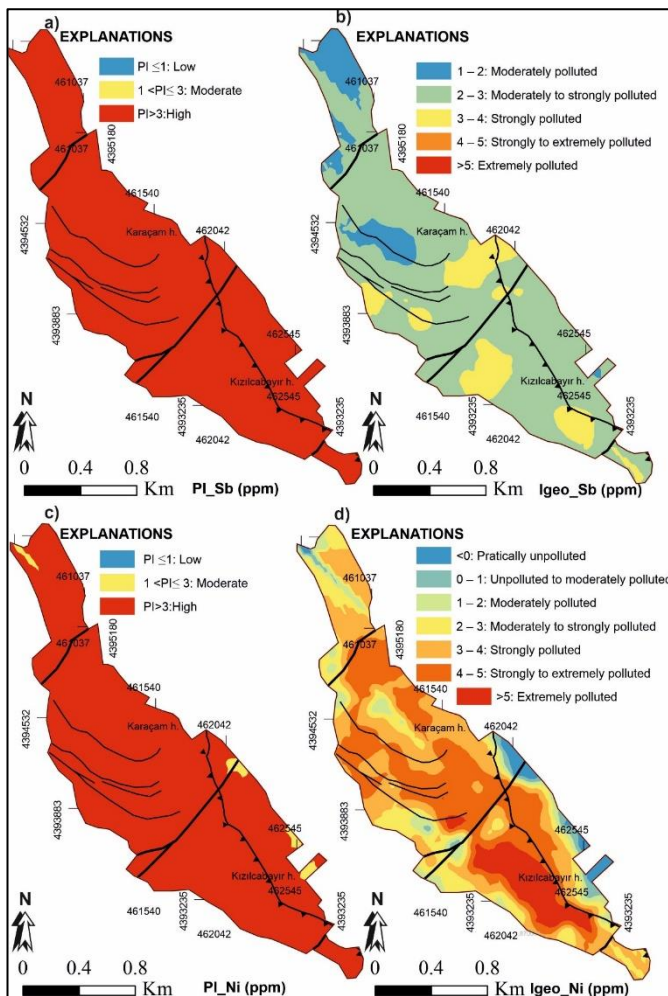


**Figure 8.** a) Distribution map of PI for Sb b) Distribution map of Igeo for Sb c) Distribution map of PI for Ni d) Distribution map of Igeo for Ni (See Fig. 1 for Figure explanations)

practically uncontaminated class, the southwestern part of the listwaenite zone, especially the part bordering the Kazdağ Group metamorphics, falls into the uncontaminated to moderately contaminated class, and the section with the fault contact separating the mylonitic gneiss and Kazdağ metamorphics is in the moderately contaminated class (Fig. 6b). This area partially coincides with the area falling into the high pollution risk class according to the PI parameter. When the PI distribution map for Pb is examined, the whole area is in the moderately polluted class (Fig. 6c). According to the distribution map of the Igeo parameter for Pb, it is seen that the sections with fault lines and relatively more severe alteration (northwest, southeast and middle part of the site) fall into the uncontaminated to moderately contaminated class. (Fig. 6d). According to the Igeo parameter, the areas remaining in the unpolluted to moderately polluted class for Cu and Pb are relatively overlapping areas (Fig. 6b and Fig. 6d).

When the PI distribution map for the Zn was examined, it was seen that a small area in the northwest and southeast of the field showed a medium pollution risk, while the rest had a low pollution risk (Fig. 7a).

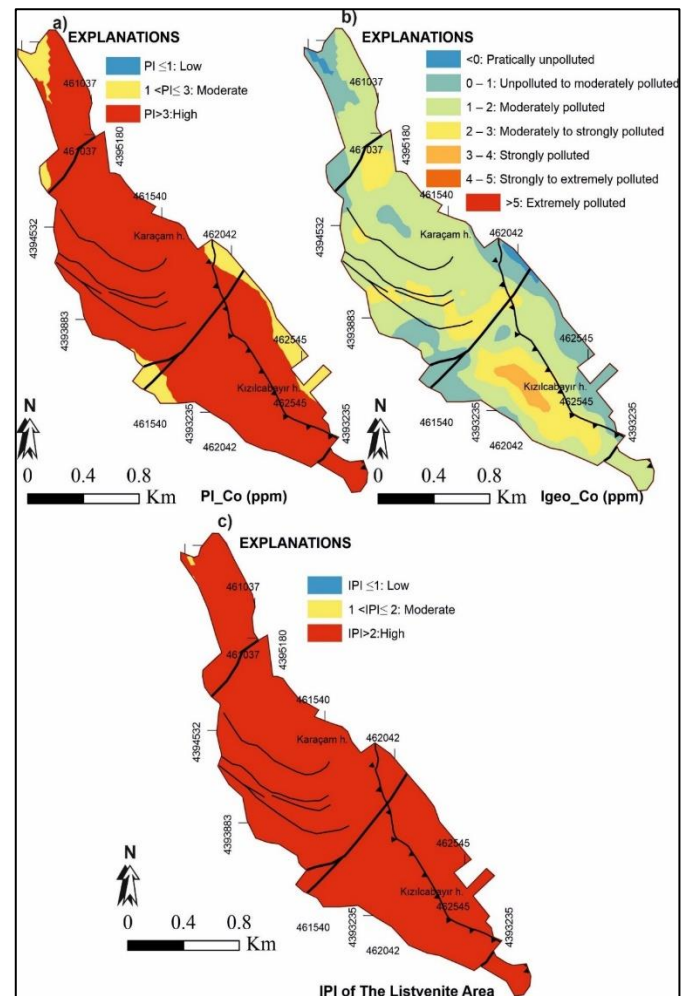


**Figure 9.** a) Distribution map of PI for Co, b) Distribution map of Igeo for Co, c) IPI distribution map for heavy metals (See Fig. 1 for Figure explanations)

According to the Igeo parameter for Zn, the distribution map shows that the limited areas in the southeast of Karaçam hill and east-southeast of Kızılcabayır hill are in the uncontaminated to moderately contaminated class, and the rest is in the practically uncontaminated class (Fig. 7b). According to the arsenic PI distribution map, the entire area shows a remarkably high pollution risk (Fig. 7c). According to the distribution map of the Igeo parameter, small areas in the northwest of the area and in the northwest of Karaçam hill fall into the moderately polluted class, while a significant part of the field falls into the moderately to strong polluted class and strongly polluted class. An area in the northwest of Kızılcabayır hill is classified as strongly to extremely polluted. Considering the PI and Igeo parameters for the field together, it is thought that it would be beneficial to study the field in more detail in terms of arsenic, both in soil and aquatic environments and in medical geology perspectives.

When the area was evaluated in terms of Sb, it was seen that the whole area fell into the high pollution risk class according to the PI distribution map (Fig. 8a). According to the distribution map of the Igeo parameter,

the field falls into the classes between moderately polluted and strongly polluted, and most of the field is in the moderately to strongly polluted class (Fig. 8b). When the field is examined in terms of Ni, almost all the field falls into the highly polluted class in the PI distribution map, while a very small portion falls into the moderate pollution risk class (Fig. 8c). According to the Igeo distribution map, very few parts of the area are in the practically unpolluted class, while the rest of the field falls between the moderately polluted and extremely polluted class. These remarkable pollution values observed in terms of Ni are related to the fact that the main rocks in the area are ultrabasic rocks in origin and the Ni element is not separated from the environment much and enriched in situ with the effect of lateritic processes. Especially since tectonic lines allow the movement of fluids, Ni pollution parameters are high in these areas (Fig. 8d).

When the Co PI distribution map is examined, it is determined that there is a medium pollution risk in small areas in the areas where listwaenite is bordered in other rocks, and a high pollution risk in the remaining section. In the Igeo distribution map, a very small part (northwest of the field, also southeast of Karaçam hill) is practically unpolluted, while most of the field is moderately polluted. Particularly in some parts close to tectonic lines, moderately to strongly polluted class was observed (Fig. 9b). To the west of Kızılcaşayır hill, there is an area that falls into the strongly polluted class. This area also partially overlaps with the Ni Igeo distribution map (Fig. 8d and Fig. 9b). This overlap is due to the similarity of the geochemical behavior characteristics of Ni and Co elements.

When the IPI distribution map of the study area is examined, it is seen that the entire area is in the highly polluted class (Fig. 9c). Therefore, the risk of heavy metal pollution caused by listwaenitization in the area was also confirmed by the IPI parameter. The IPI distribution map also confirms the need for more detailed investigation of the behavior and environmental effects of the elements in the field.

#### 4. Conclusions

The listwaenitization process, which is especially important for gold mineralization in terms of spatial and temporal, is also an enrichment for certain elements, in other words, it is a suitable environment for natural element pollution in relation to the hydrothermal events it is exposed to. Although there have been limited studies on the gold mineralization potential of the Alakeçi listwaenite field, there has been no study on the element / heavy metal pollution of the listwaenite in the

area. In this study, Cu, Pb, Zn, As, Sb, Ni and Co element concentrations of listwaenite-derived soils at Alakeçi listwaenite zone (Bayramiç / Çanakkale / Western Türkiye) were determined using flame atomic absorption spectrometry and the area was investigated in terms of heavy metal pollution with the help of PI, IPI and Igeo parameters, which are the most used in the evaluation of heavy metal pollution in soils. In addition, distribution maps of PI, Igeo and IPI parameters calculated for each element were plotted with the ordinary kriging constant method. As a result of the data obtained, it has been determined that there is a risk of pollution in the field in terms of PI and Igeo parameters, especially in the context of Ni, Co and As. Considering the IPI parameter, it has been determined that some of the sampling points in the field have a medium pollution risk, while many of the sampling points have a high pollution risk. When the distribution maps of the pollution parameters of the investigated elements are examined, it is seen that the pollution areas overlap in general, although the PI and Igeo pollution classifications of the elements differ. It has been determined that the areas showing pollution risk in the field correspond to tectonic lines and intense hydrothermal alteration areas. Element / heavy metal pollution caused by listwaenitization in the field poses risks both for terrestrial and aquatic environments and for human health through the food chain, especially in terms of As, Co and Ni. Therefore, it will be useful to carry out detailed research for environmental and medical geological purposes in the listwaenitization area.

#### Acknowledgements

The data used in this study were obtained within the scope of the mineral exploration project carried out by MTA and are the data used by the author in his doctoral thesis. The author would like to thank MTA and its project staff. The author also thanks Prof Dr Abdullah Kaygusuz for his encouragement in the preparation of this article on heavy metal pollution due to listwaenitization.

#### References

- [1] A. Vural, D. Aydal, Soil geochemistry study of the listwaenite area of Ayvacık (Çanakkale, Turkey), *Casp J Environ Sci*, 18, 2020, 205–215.
- [2] A. Vural, Bayramiç (Çanakkale) ve Çevresindeki Altın Zenginleşmelerinin Araştırılması, Ankara Üniversitesi, 2006.
- [3] R. Murchission, E. de Verneuil, A. Von Seyserling, The geology of Russia in Europe and the Ural Mountains. Geology, John Murray, 1845, London, UK.

- [4] B. Zoheir, Transpressional zones in ophiolitic melange terranes: Potential exploration targets for gold in the South Eastern Desert, Egypt, *J. Geochemical Explor*, 111, 2011, 23–38.
- [5] D. Béziat, M. Dubois, P. Debat, S. Nikiéma, S. Salvi, F. Tollon, Gold metallogeny in the Birimian craton of Burkina Faso (West Africa), *J African Earth Sci*, 50, 2008, 215–233.
- [6] E.V. Belogub, I.Y. Melekestseva, K.A. Novoselov, M. V. Zabolina, G.A. Tret'yakov, V.V. Zaykov, A.M. Yuminov, Listvenite-related gold deposits of the South Urals (Russia): A review, *Ore Geol Rev*, 85, 2017, 247–270.
- [7] A. Aftabi, M.H. Zarrinkoub, Petrogeochemistry of listvenite association in metaophiolites of Sahlabad region, eastern Iran: Implications for possible epigenetic Cu-Au ore exploration in metaophiolites, *Lithos*, 156–159, 2013, 186–203.
- [8] Ş. Koç, Y. Kadioğlu, Mineralogy, geochemistry and precious metal content of Karacakaya listwaenites, Turkey, *Ophioliti*, 21, 1996, 125–130.
- [9] D. Aydal, Gold-bearing listwaenites in the Arac Massif, Kastamonu, Turkey, *Terra Nov*, 2, 1990, 43–52.
- [10] T. Hinsken, M. Bröcker, H. Strauss, F. Bulle, Geochemical, isotopic and geochronological characterization of listvenite from the Upper Unit on Tinos, Cyclades, Greece, *Lithos*, 282–283, 2017, 281–297.
- [11] B. Zoheir, B. Lehmann, Listvenite-lode association at the Barramiya gold mine, Eastern Desert, Egypt, *Ore Geol Rev*, 39, 2011, 101–115.
- [12] B.R. Frost, K.A. Evans, S.M. Swapp, J.S. Beard, F.E. Mothersole, The process of serpentinization in dunite from new caledonia, *Lithos*, 178, 2013, 24–39.
- [13] M. Yusuf, M. Kumar, M.A. Khan, M. Sillanpa, H. Arafat, Hydrothermal listvenitization and associated mineralizations in Zagros Ophiolites: Implications for mineral exploration in Iraqi Kurdistan, *J Geochemical Explor*, 2019, 102036.
- [14] M. Ahankoub, M.A. Mackizadeh, Mineralogy and geochemistry of the Dehshir listvenites, central Iran, *Neues Jahrb Fur Mineral Abhandlungen*, 196, 2019, 1–18.
- [15] C. Hall, R. Zhao, Listvenite and related rocks: perspectives on terminology and mineralogy with reference to an occurrence at Cregganbaun, Co. Mayo, Republic of Ireland, *Miner Deposita*, 30, 1995, 303–313.
- [16] H.A. Gahlan, M.K. Azer, P.D. Asimow, K.M. Al-Kahtany, Formation of gold-bearing listvenite in the mantle section of the Neoproterozoic Bir Umq ophiolite, Western Arabian Shield, Saudi Arabia, *J African Earth Sci*, 190, 2022, 104517.
- [17] A.D. Kiliç, M. İnceöz, Mineralogical, geochemical and isotopic effect of silica in ultramaphic systems, eastern Anatolian Turkey, *Geochemistry Int*, 53, 2015, 369–382.
- [18] Y. Yang, L. Zhao, R. Zheng, Q. Xu, Evolution of the early Paleozoic Hongguleleng–Balkybye Ocean: Evidence from the Hebukesaier ophiolitic mélange in the northern West Junggar, NW China, *Lithos*, 324–325, 2019, 519–536.
- [19] A. Vural, Contamination assessment of heavy metals associated with an alteration area: Demirören Gumushane, NE Turkey, *J. Geol Soc India*, 86, 2015, 215–222.
- [20] G. Külekçi, Investigation of gamma ray absorption levels of composites produced from copper mine tailings, fly ash, and brick dust, *J Mater Cycles Waste Manag*, 24, 2022, 1934–1947.
- [21] G. Külekçi, Investigation of fly ash added light concretes with respect to gamma radiation transmission properties of <sup>133</sup>Ba and <sup>137</sup>Cs, *Radiat Eff Defects Solids*, 176, 2021, 833–844.
- [22] A. Vural, D. Aydal, Determination of lithological differences and hydrothermal alteration areas by remote sensing studies: Kısacık (Ayvacık-Çanakkale, Biga Peninsula, Turkey), *J Eng Res Appl Sci*, 9, 2020, 1341–1357.
- [23] G. Külekçi, <sup>60</sup>Co Radyoaktif Nokta Kaynağı ile Uçucu Külün Gama Radyasyon Koruma Özellikleri, *Avrupa Bilim ve Teknol Derg*, 27, 2021, 145–151.
- [24] A.İ. Okay, M. Siyako, K.A. Burkan, Geology and tectonic of the Biga Peninsula, *Turk Assoc Pet Geol Bull*, 2, 1990, 83–121.
- [25] A.W. Rose, H. Hawkes, J. Webs, *Geochemistry in Mineral Exploration*, 2nd ed., Academic Press, 1991, London, England.
- [26] D. Skoog, D. West, F. Holler, S. Crouch, *Fundamentals of analytical chemistry*, 8th ed., Brooks/Cole-Thomson Learning, Belmont, CA 94002, 2004, USA.
- [27] C.W. Chen, C.M. Kao, C.F. Chen, C. Di Dong, Distribution and accumulation of heavy metals in the sediments of Kaohsiung Harbor, Taiwan, *Chemosphere*, 66, 2007, 1431–1440.
- [28] B.T. Sany, A. Salleh, A.H. Sulaiman, A. Mehdinia, G.H. Monazami, *Geochemical Assessment of Heavy Metals Concentration in Surface Sediment of West Port, Malaysia*, 5(8), 2011, 411–415.
- [29] Ü. Gemici, Evaluation of the water quality related to the acid mine drainage of an abandoned mercury mine (Alaşehir, Turkey), *Environ Monit Assess*, 147, 2008, 93–106.
- [30] A. Sungur, M. Soylak, H. Özcan, Chemical fractionation, mobility and environmental impacts of heavy metals in greenhouse soils from Çanakkale, Turkey, *Environ Earth Sci*, 75, 2016, 1–11.
- [31] G. Yaylali-Abanuz, Determination of anomalies associated with Sb mineralization in soil geochemistry: A case study in Turhal (northern Turkey), *J Geochemical Explor*, 132, 2013, 63–74.
- [32] G. Muller, Index of geoaccumulation in sediments of the Rhine River, *Geol J*, 2, 1969, 108–118.
- [33] R. Rudnick, S. Gao, Composition of the Continental Crust, in: H. Holland, K. Turekian (Eds.), *Readings of Treatise on Geochemistry*, 2nd ed., Elsevier, 2010, London, England.
- [34] D.G. Krige, A stastical Approach to Some Basic Mine Valuation Problems on the Witwatersrand, *J Chem Metall Soc South Min Africa*, 52, 1951, 119–139.
- [35] G. Matheron, Principles of geostatistics, *Econ Geol*, 58, 1963, 1246–1266.
- [36] G. Matheron, *The Theory of Regionalized Variables and Its Applications*, École nationale supérieure des mines, 1971, Paris.
- [37] M. Akçay, A. Lermi, A. Van, Biogeochemical exploration for massive sulphide deposits in areas of dense vegetation: An orientation survey around the Kankoy Deposit, *J Geochemical Explor*, 63, 1998, 173–187.
- [38] N. Ağca, Spatial distribution of heavy metal content in soils around an industrial area in Southern Turkey, *Arab J Geosci*, 8, 2015, 1111–1123.
- [39] C. Patinha, E. Correia, E. Ferreira da Silva, A. Simões, P. Reis, F. Morgado, E. Cardoso Fonseca, Definition of geochemical patterns on the soil of Paul de Arzila using correspondence analysis, *J Geochemical Explor*, 98, 2008, 34–42.
- [40] G. Buttafuoco, A. Tallarico, G. Falcone, I. Guagliardi, A geostatistical approach for mapping and uncertainty assessment of geogenic radon gas in soil in an area of southern Italy, *Environ Earth Sci*, 61, 2010, 491–505.
- [41] M. Basaran, G. Erpul, A.U. Ozcan, D.S. Saygin, M. Kibar, I. Bayramin, F.E. Yilman, Spatial information of soil hydraulic conductivity and performance of cokriging over kriging in a semi-arid basin scale, *Environ Earth Sci*, 63, 2011, 827–838.
- [42] R. Webster, M.A. Oliver, *Geostatistics for Environmental Scientists*, 2nd ed., Jhon Wiley&Sons Ltd., 2007.
- [43] T. Hengl, *A Practical Guide to Geostatistical Mapping of Environmental Variables*, 2007.
- [44] A. Vural, M. Erdoğan, Eski Gümüşhane Kırkpavli alterasyon sahasında toprak jeokimyası, *Gümüşhane Üniversitesi Fen Bilim Enstitüsü Derg*, 4, 2014, 1–15.
- [45] A. Vural, B. Çiçek, Çevreleşme Sahasında Gelişmiş Topraklardaki Ağır Metal Kirliliği, *Düzce Üniversitesi Bilim ve Teknol Derg*, 8, 2020, 1533–1547.
- [46] V. Chaplot, F. Darboux, H. Bourennane, S. Leguédois, N. Silvera, K. Phachomphon, Accuracy of interpolation techniques for the derivation of digital elevation models in relation to landform types and data density, *Geomorphology*, 77, 2006, 126–141.

## Development and validation of RPLC method for the simultaneous analysis of ACE inhibitors in tablet formulations

Erdem Kuzucanli<sup>1</sup> , Ebru Çubuk Demiralay<sup>2\*</sup> , Y. Doğan Daldal<sup>3</sup> , Zehra Üstün<sup>4</sup> , İlkey Konçe<sup>5</sup> , Güleren Alsancak<sup>1</sup> 

<sup>1</sup> Süleyman Demirel University, Faculty of Science and Literature, Department of Chemistry, 32260, Isparta, Türkiye

<sup>2</sup> Süleyman Demirel University, Faculty of Pharmacy, Department of Analytical Chemistry, 32260, Isparta, Türkiye

<sup>3</sup> Kahramanmaraş İstiklal University, Elbistan Vocational School of Health Services, 46300, Kahramanmaraş, Türkiye

<sup>4</sup> Süleyman Demirel University, Atayalvaç Vocational School of Health Services, 32400, Isparta, Türkiye

<sup>5</sup> Süleyman Demirel University, Faculty of Pharmacy, Department of Pharmaceutical Research and Development, 32200, Isparta, Türkiye

### Abstract

This study aimed to develop and validate an HPLC method for the determination of ACE inhibitors benazepril, cilazapril and quinapril in tablet formulation. To determine the optimum liquid chromatographic separation condition, a systematic approach based on the relationship between mobile phase pH and retention time was used. ACE inhibitors were separated on a YMC Triart C18 (3 µm, 150 × 4.6 mm I.D.) column in an acetonitrile-water binary mixture containing 45% (v/v) acetonitrile adjusted to pH 3. Flow rate 0.5 mL/min, column temperature 37 °C and UV detector wavelength 210 nm were determined as optimum chromatographic conditions for the study. The method showed excellent linearity in the concentration range of 5 – 35 µg/mL for benazepril and cilazapril and 0.5 – 85 µg/mL for quinapril. Mean recovery values were found to be 98.663 ± 1.203 for cilazapril, 99.404 ± 0.864 for benazepril and 99.264 ± 0.626 for quinapril. The proposed method is suitable for the simultaneous separation and quantitative determination of drugs.

**Keywords:** Hypertension, ACE inhibitors, RPLC, pKa

### 1. Introduction

Hypertension can be defined as an increase in arterial blood pressure above normal limits. When this condition is not well controlled, it seriously affects the structure and functions of many organs in the body. In hypertensive patients who are effectively treated, significant reductions in the risk of stroke, heart failure, and myocardial infarction occur [1]. Many drug groups are used in the treatment of hypertension. However, the most preferred groups of these drugs are angiotensin-converting enzyme (ACE) inhibitors [2]. ACE inhibitors can be divided and classified into three broad groups based on chemical structure: (1) ACE inhibitors that are structurally sulfhydryl-containing (e.g. captopril) (2) ACE inhibitors that are dicarboxylic-containing (e.g. cilazapril, quinapril, lisinopril, moexipril, benazepril, ramipril,trandolapril, perindopril) and (3) ACE inhibitors that are phosphorus-containing (e.g. fosinopril) [3–5]. Benazepril, cilazapril, and quinapril selected for this study are ACE inhibitors containing carboxyl groups (Fig. 1).

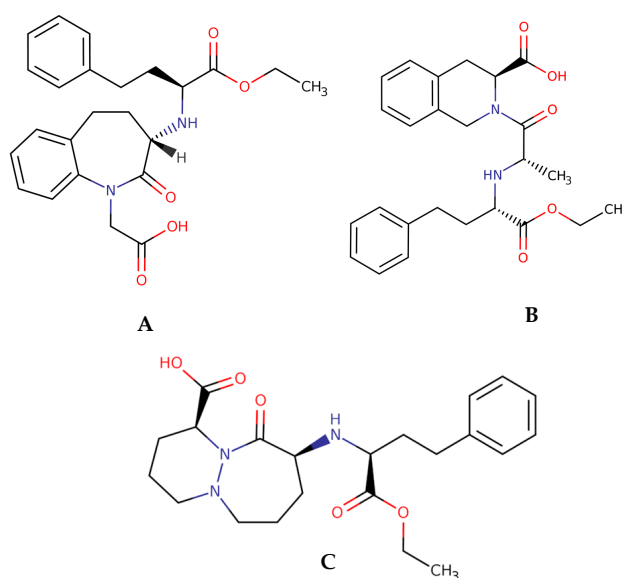


**Figure 1.** Chemical structure of studied compounds (A) benazepril, (B) quinapril, and (C) cilazapril

**Citation:** E. Kuzucanli, E.Ç. Demiralay, Y.D. Daldal, Z. Üstün, İ. Konçe, G. Alsancak, Development and validation of RPLC method for the simultaneous analysis of ACE inhibitors in tablet formulations, Turk J Anal Chem, 4(2), 2022, 103–110.

 <https://doi.org/10.51435/turkjac.1176649>

**\*Author of correspondence:** ebrucubukdemiralay@gmail.com

**Tel:** +90 (246) 211 03 42

**Fax** +90 (246) 237 03 30

**Received:** September 17, 2022

**Accepted:** November 11, 2022

Benazepril is a potent ACE inhibitor in its group that is converted to benazeprilat with cleavage of the ester group by hepatic esterase. Quinapril is a prodrug that is converted to quinaprilat. This drug is almost as potent as benazeprilat by liver esterase with cleavage of the ester groups. Cilazapril is a new ACE inhibitor that does not contain thiol and sulfhydryl groups in the same group as these two compounds [3].

The discovery and design of a compound used as a drug in pharmaceutical chemistry, and the development of effective analytical methods for chemical analysis and quality control are important. Capillary electrophoresis (CE), high performance liquid chromatography (HPLC), and electrochemical methods are widely used for the analysis of compounds in drug formulations and biological fluids [6]. Among these methods, reverse phase liquid chromatography (RPLC) is more preferred due to its advantages such as accuracy, precision, and reproducibility of the measurements [7–10]. The primary purpose of RPLC studies is to ensure that the studied compounds are separated from each other as soon as possible or to make simultaneous determinations provided that certain validation conditions ICH parameters are met [11,12].

In the RPLC method, the parameters known to affect the retention factor ( $k$ ) values of the compounds are changed individually or randomly to determine the optimum separation condition in most studies. While this situation causes unnecessary time and material loss, in some cases, it is insufficient in determining the separation condition [13–17]. To determine the chromatographic working conditions, it is necessary to optimize the chromatographic conditions (column temperature, mobile phase pH and mobile phase organic modifier concentration, etc.) in the developed method instead of this trial-and-error method [14–18].

Solvent optimization in the RPLC method is commenced by selecting a binary mobile phase of the correct solvent strength to elute the compound with an acceptable range of  $k$  values ( $1 < k < 10$ ) and selectivity factor ( $\alpha \geq 1.15$ ). Solvents such as methanol, acetonitrile, and tetrahydrofuran, which are commonly used in RPLC, are mixed with water at different ratios to ensure sufficient retention and chromatographic separation can be easily estimated. At very low water content the properties of the mobile phase depend largely on the properties of the organic modifier. Thus, the  $k$  value can be adjusted to the desired value by changing the mobile phase composition or solvent strength. The change in mobile phase pH also affects the selectivity in the separation of compounds. If the compounds are acidic or basic, the change in selectivity can be easily predicted. While temperature change has a minor effect on the retention of neutral compounds, it has a significant effect

on the retention factor for ionizable compounds. In finding the best separation condition, the temperature change acts as an organic solvent [19].

In this study, the selected ACE inhibitors cilazapril, benazepril, and quinapril were determined by the RPLC method alone or simultaneously [18–23]. In addition, there are few studies on the determination of optimum conditions of compounds with the experimental design method related to ACE inhibitors [24–26]. In this study, the change in  $k$  values depending on the pH of the mobile phase and the organic modifier concentration in the mobile phase was investigated at two different column temperatures (25 – 37 °C) to determine the optimum separation conditions of the selected compounds. With this study, the simultaneous determination of the compounds was made without trial and error. In addition, the method developed was validated according to the International Conference on Harmonization (ICH) and Association of Official Analytical Chemists (AOAC) parameters [12,27] and then quantitative determinations in drug formulations were performed.

## 2. Materials and methods

### 2.1. Apparatus

The Shimadzu HPLC system (Shimadzu Technologies, Kyoto, Japan) was used for the liquid chromatographic study. The system consists of a pump (LC-20AD), UV detector (SPD-20A), column oven (CTO-20A), and degassing unit (DGU-20A3). pH measurements of the RPLC mobile phase were performed using Mettler Toledo MA 235 pH/Ion analyzer (Schwerzenbach, Switzerland) and InLab 413 Ag/AgCl combined glass electrode.

### 2.2. Chemicals

In this study, benazepril, cilazapril, quinapril, pravastatin, and uracil were purchased from Sigma-Aldrich (USA). Acetonitrile was used as an organic solvent in the preparation of the mobile phase, o-phosphoric acid and sodium hydroxide were used as buffer components in the mobile phase, and potassium hydrogen phthalate was used as the primary standard reference in electrode calibration was supplied from Merck (Darmstadt, Germany). All chemicals used in the study are of analytical purity.

### 2.3. Chromatographic study

In this study, the acetonitrile-water binary mixture containing 45% (v/v) acetonitrile was prepared as a mobile phase for the chromatographic determination of the compounds. o-phosphoric acid (85%, w/w) was added to the mobile phase medium at 25 mM and 1 M

NaOH solution was added to reach the desired mobile pH. Six mobile phases with pH ranging between 2.5 and 5.0 were prepared. The mobile phases were used after degasification in an ultrasonic bath. Chromatographic separation was carried out in a YMC Triart C18 column (3 $\mu$ m, 150  $\times$  4.6mm I.D.). The column oven temperature was set at 37  $^{\circ}$ C, the flow rate was 0.5 mL/min, and the injection volume was 20  $\mu$ L. The UV detector was set at 210 nm wavelength.

#### 2.4. Preparation of standard solutions

Stock solutions of compounds were prepared by dissolving in the mobile phase at a concentration of 100  $\mu$ g/mL for qualitative analysis and 50  $\mu$ g/mL for calibration. The internal standard (IS) pravastatin (20  $\mu$ g/mL) was prepared in the same way. For the calibration study, the stock solutions prepared for the working concentration range of each compound were diluted with the mobile phase. The IS concentration was kept constant at 0.5  $\mu$ g/mL throughout the study. Benazepril and cilazapril were prepared in a concentration range of 1 – 15  $\mu$ g/mL and quinapril 0.5 – 8  $\mu$ g/mL.

#### 2.5. Robustness test

The robustness of the method was evaluated according to the system suitability parameter data by analyzing the studied compounds after changing the flow rate ( $\pm$  0.2), organic modifier content ( $\pm$  0.5), pH of the mobile phase ( $\pm$  0.5), and column temperature.

#### 2.6. Analysis of tablets

For quantitative determination of benazepril, cilazapril, and quinapril tablet analysis was performed. In this method, ten tablets were finely powdered and weighted in an equivalent amount to 1 tablet. Then, the powder in the amount of one tablet was put into the volumetric flask and by adding the mobile phase, its volume was made up to 100 mL. To dissolve the active ingredients of the drugs determined in the prepared sample solutions, the solutions were kept in an ultrasonic bath for 20 minutes. The insoluble part in the prepared solution was removed by filtration. Finally, the solution was prepared at different dilution ratios according to the concentration in the calibration range specified for each compound.

#### 2.7. Recovery experiment

A recovery study was conducted to determine the reliability and suitability of the proposed method. Both sample and recovery processes were performed in five replications. This study was carried out by adding a known amount of pure standard and selected internal

standard to the tablet sample containing the analyzed active substance. Recovery percentages were calculated using the obtained data.

### 3. Results and discussion

Benazepril, cilazapril, and quinapril are compounds containing both acidic and basic functional groups. In the chemical structure of these compounds, there is a carboxylic acid as an acidic functional group and a secondary amine as a basic functional group. The retention of compounds with ionizable functional groups in the HPLC column varies according to the pH value of the mobile phase. Determination of ionization/protonation constant ( $pK_a$ ) values is necessary to predict the ionization of the compound at a given pH [28]. Lipophilicity expressed as  $\log P$ , must be known in chromatographic analyses. The increase in this value is a result of the compound's high affinity in the RPLC column [19]. The calculated  $pK_a$  and  $\log P$  values for the studied compounds are given in Table 1.

In this study, a mobile phase optimization study was performed to determine the optimum separation condition in the quantitative determination of cilazapril, benazepril, and quinapril used in the treatment of hypertension by the RPLC method. With knowing the  $pK_a$  values of the compounds, it is possible to determine the pH values at which they are in molecular or ionized form. For this, pH values above and below 1.5 units of  $pK_a$  value are determined as working pH ranges. For this, the effects of column temperature, acetonitrile concentration of the mobile phase, and pH change on the retention factors of the compounds were investigated by keeping the chromatographic conditions constant. The  $t_0$  value used in the calculation of the  $k$  value was determined using the standard uracil solution used as the non-retained species in the column. The  $k$  values at each pH value (2.5 – 5.0) studied were calculated by using the  $t_R$  and  $t_0$  values of the compounds in the acetonitrile water binary mixture containing %40 (v/v), 45% (v/v) and %50 (v/v) acetonitrile. Compounds were highly retained on the HPLC column in 40% acetonitrile medium at 37  $^{\circ}$ C. The  $k$  values are higher than the 45% acetonitrile medium. In a 50% acetonitrile medium,  $k$  values of cilazapril were calculated below 1 in the pH range studied. The  $k$  values at 25  $^{\circ}$ C are greater than at 37  $^{\circ}$ C. In liquid chromatographic studies, it is aimed to complete the analyses as soon as possible. Also, the  $k$  value must be  $\geq$  1.

**Table 1.**  $pK_a$  and  $\log P$  values of compounds [29]

Compounds	$pK_a$		$\log P$
Benazepril	$pK_{a1}$ : 3.04	$pK_{a2}$ : 4.74	1.11
Quinapril	$pK_{a1}$ : 3.71	$pK_{a2}$ : 5.12	1.38
Cilazapril	$pK_{a1}$ : 3.26	$pK_{a2}$ : 4.49	-0.23

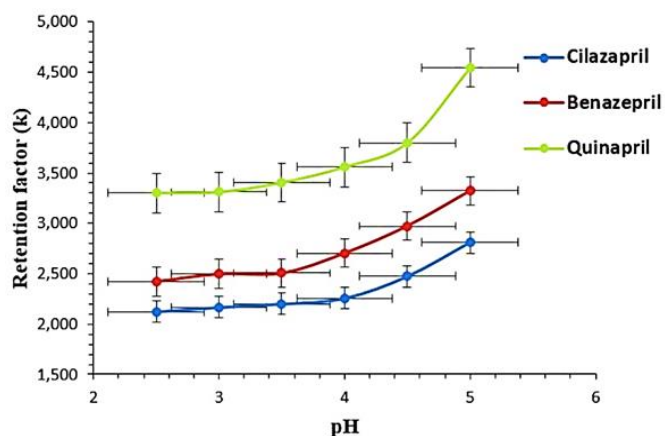


**Figure 2.** Sigmoidal behavior showing the relationship between mobile phase pH and  $k$  values of compounds

For this purpose, according to the results of acetonitrile concentration in three different concentrations, the analyzes performed at 40% (v/v) acetonitrile and 37 °C were chosen as the appropriate conditions. In this condition, the sigmoidal behavior of the basic functional group was observed when the  $k$  values of the Compounds were plotted against the mobile phase pH values (Fig. 2).

Mid-point of sigmoidal curves gives the  $pK_a$  value of the compound in the water-acetonitrile binary mixture studied. The situation where  $pH = pK_a$  is not the optimum condition for separation. At this pH value, tailing is observed in the peaks of the compounds. This is undesirable for quantitative determination [7]. At pH 2.5, where ionization takes place, the compounds are retained little in the HPLC column. Therefore, pH values of the mobile phase are preferred for separation. In addition, optimum chromatographic separation occurs if the  $k$  values of the compounds are in the range of  $1 \leq k \leq 10$ , the selectivity factor ( $\alpha$ ) is greater than 1.15 and the peak resolution ( $R_s$ ) value is greater than 1.5. The selectivity factor is calculated by dividing the retention factor ( $k_2$ ) of the second peak by the retention factor of the first peak ( $k_1$ ). When Fig. 3 is examined, the  $\alpha$  value is below 1.15 at pH 2.5 and 3.5. Benazepril and cilazapril did not differ from each other at these pH values. Separation should occur as soon as possible in a chromatographic assay. For this, an acetonitrile-water binary mixture containing 45% (v/v) acetonitrile adjusted to pH 3.0 was determined as the condition in which the specified chromatographic parameters were met.

The Purnell equation (Eq. 1) shows the relationship between the  $\alpha$ ,  $R_s$ , and  $k$  values.

$$R_s = \frac{1}{4} \sqrt{N} \left[ \frac{(\alpha - 1)}{\alpha} \right] \left[ \frac{k_2}{(1 + k_2)} \right] \quad (1)$$

For this reason, the  $R_s$  value between the two peaks must be calculated using this equation in the qualitative

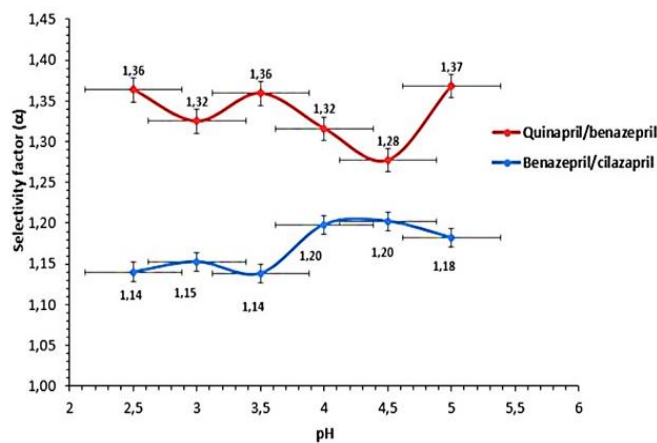


**Figure 3.** Variation in  $\alpha$  values for compound pairs with mobile phase pH

determination. The values calculated according to the Purnell equation under this mobile phase condition are given in Table 2.

Since cilazapril is a more hydrophilic compound compared to quinapril and benazepril (Table 1), it cannot be determined simultaneously with hydrophobic compounds in conventional C18 and C8 columns. YMC Triart C18 column (3  $\mu m$ , 150 x 4.6 mm I.D.) chosen in this study is a column with moderate hydrogen bonding capacity and provides simultaneous separation of both hydrophobic and hydrophilic compounds. In addition, it is a column that has a better peak shape than conventional C18 columns [30].

After the optimization of the liquid chromatographic method developed in the study, method validation was performed for the quantitative determination of the compounds. A widely used technique of quantitation involves the addition of an internal standard (IS) to compensate for errors in the analytical measurements [31,32]. The IS method is preferred to exclude systematic and random errors such as additives in drug formulations and volume errors during sample injection. When the internal standard is selected, it must be chromatographically separated from the compounds determined under optimal separation conditions. In this study, pravastatin was selected as the IS. Under the selected optimal separation conditions, pravastatin could be retained in this column because it was present in its molecular form. The chromatogram obtained under the optimal separation conditions is shown in Fig. 4.

**Table 2.** Calculated data of compounds at optimum separation condition

Compounds	$k_2$	$\alpha$	$k_2/k_2 + 1$	$(\alpha - 1)/\alpha$	$\left(\frac{1}{4}\right)\sqrt{N}$	$R_s$
Pravastatin (I.S)	1.009					
Cilazapril	2.168	2.149	0.684	0.535	14.703	5.379
Benazepril	2.499	1.153	0.714	0.132	18.668	1.766
Quinapril	3.311	1.325	0.768	0.245	14.389	2.710

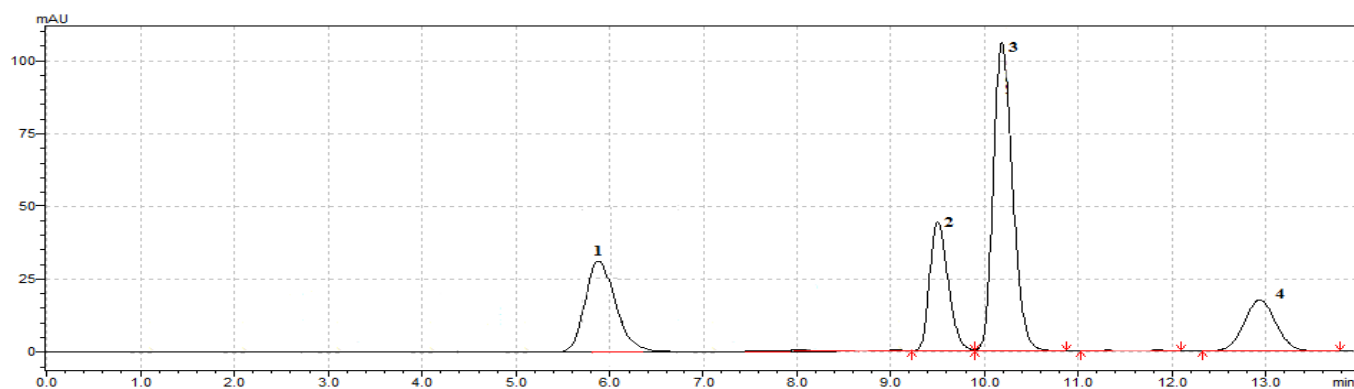


**Figure 4.** The chromatogram obtained according to the optimum separation condition determined: (1) pravastatin (I.S), (2) cilazapril, (3) benazepril, (4) quinapril

**Table 3.** System suitability parameters for compounds

Parameters	P (I.S)	C	B	Q	R.V.
$t_R$	6.017	9.503	10.186	12.934	—
Tailing factor ( $T_i$ )	1.183	1.113	1.159	1.051	$\leq 2$
Retention factor ( $k$ )	1.009	2.116	2.373	3.241	$\geq 1$
Peak resolution ( $R_s$ )	—	5.221	2.109	2.548	$\geq 2$
Theoretical plates ( $N$ )	6540	10630	11398	6821	$\geq 2000$
Separation factor ( $\alpha$ )	—	2.097	1.188	1.289	$>1$
RSD% ( $t_R$ , for retention time)	0.992	0.126	0.160	0.189	$\leq 1$
RSD% (for peak area)	0.537	0.294	0.398	0.245	$\leq 1$

P: Pravastatin, C: Cilazapril, B: Benazepril, Q: Quinapril, R.V.: Recommended value

Once the optimal separation conditions were determined, the suitability of the chromatographic system was determined according to the U.S. Pharmacopoeia 24<sup>th</sup> (USP) and AOAC guidelines [12,33]. For this purpose, chromatographic parameters were calculated by injecting the compounds into the HPLC system (Table 3).

The results of system suitability parameters according to USP (Table 3) showed that the developed chromatographic method was suitable for the analysis and analytical method validation part [33].

In the system suitability test according to the AOAC guideline, the retention times and %RSD of the peak areas of the three compounds are below 2%. This indicates that the change in repeatable injections is small [12]. The tailing factor showing the symmetry of the analyte peak is also below 2%.

A calibration curve was prepared to determine the linearity of the developed method. Linear regression

**Table 4.** Calibration curve parameters for the analysis of compounds

Parameters	Cilazapril	Benazepril	Quinapril
Regression Equation	$y = 1.848x - 0.376$	$y = 4.498x - 0.855$	$y = 3.244x - 0.093$
Standard error of slope	0.013	0.033	0.022
Standard error of intercept	0.111	0.293	0.084
Correlation Coefficient ( $r$ )	0.999	0.999	0.999
Linearity Range ( $\mu\text{g/mL}$ )	1 – 15	1 – 15	0.5 – 8
Limit of Detection (LOD) ( $\mu\text{g/mL}$ )	0.277	0.299	0.158
Limit of Quantification (LOQ) ( $\mu\text{g/mL}$ )	0.838	0.906	0.478

parameters of the peak area ratios versus concentrations of benazepril, cilazapril, and quinapril were presented in Table 4. The limit of detection (LOD) and limit of quantitation (LOQ) were measured for studied compounds. These parameters were determined according to 3.3:1 and 10:1 signal / noise ratios. The described method was linear for the three compounds. The results meet the acceptance criteria according to the ICH and AOAC guidelines, which stated that the coefficient of determination should be  $> 0.999$  [11,12].

Intraday (**repeatability**) and interday (**reproducibility**) precision were determined by injecting two different concentrations at three different times on the same day and these same concentrations on three different days. These results are reported in Table 5. The results are sufficiently accurate and the relative standard deviation (% RSD) values of the results calculated from the analyzes performed with five replicates are below 2% [11].

**Table 5.** Intraday and interday precision analysis results of the analysis method of compounds

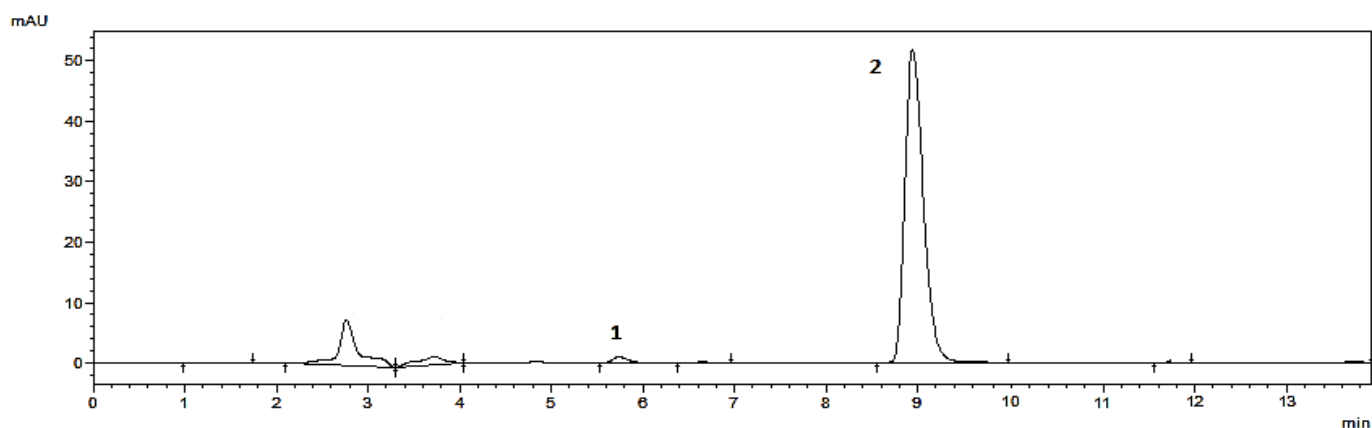
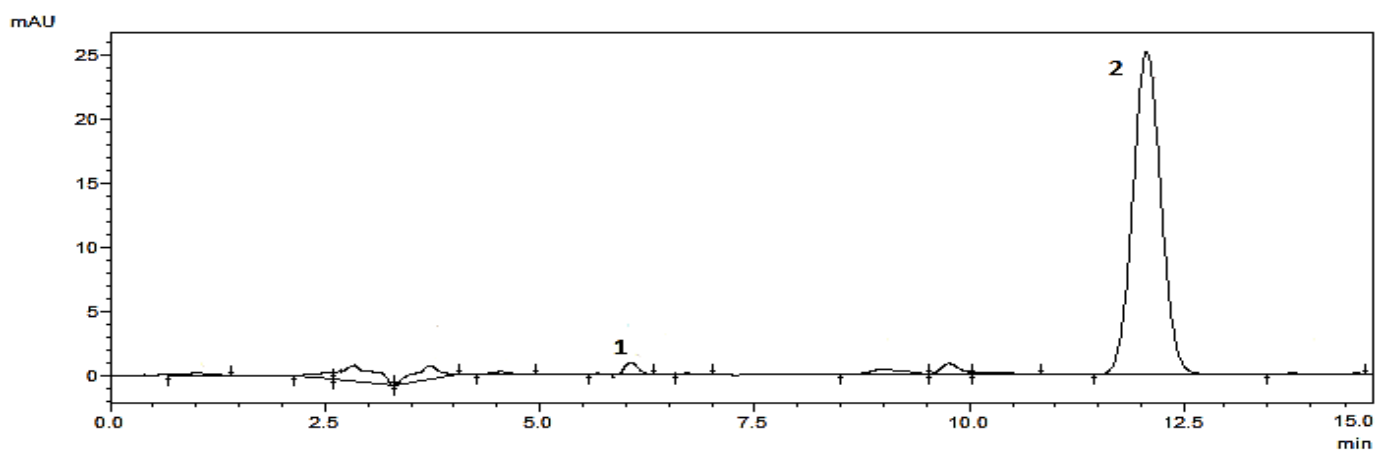
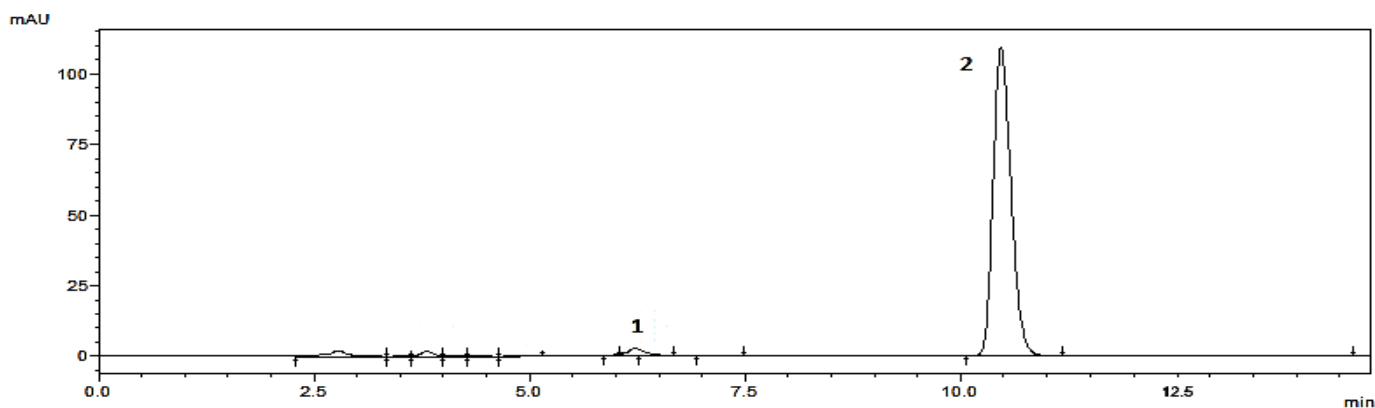
Compounds	Theoretical concentration	Intraday measured concentration			Interday measured concentration		
	( $\mu\text{g/mL}$ )	mean ( $\mu\text{g/mL}$ )	% RSD	Hor <sup>1</sup>	mean ( $\mu\text{g/mL}$ )	% RSD	Hor <sup>2</sup>
Cilazapril	2.500	2.571	0.830	0.060	2.787	1.240	0.089
	12.000	12.321	0.560	0.051	12.838	1.553	0.361
Benazepril	2.500	2.515	0.552	0.035	2.678	1.227	0.077
	12.000	12.457	0.799	0.065	12.671	1.017	0.083
Quinapril	1.000	0.892	0.152	0.011	0.932	1.089	0.078
	6.000	6.550	0.938	0.085	6.691	0.754	0.068

<sup>1</sup>Horrat ratio for repeatability

<sup>2</sup>Horrat ratio for reproducibility

**Table 6.** Robustness results of the developed method

Parameter	Retention time (tr)			Peak area (mAu)		
	Cilazapril	Benazepril	Quinapril	Cilazapril (5 µg/mL)	Benazepril (5 µg/mL)	Quinapril (5 µg/mL)
Optimize condition	9.503	10.186	12.934	354856	861931	259040
Increased organic modifier (50:50)	6.211	7.598	9.775	360048	874221	260064
Decreased organic modifier (40:60)	14.225	15.004	17.066	352064	861277	260448
Increased pH of the mobile phase (pH 3.5)	9.749	10.366	13.147	360447	866288	260412
Decreased pH of the mobile phase (pH 2.5)	9.348	9.938	12.251	355200	860882	258136
Increased flow rate (0.8 mL/min)	7.105	8.433	10.004	354926	862006	258611
Decreased temperature (25 °C)	10.245	11.587	14.688	355706	864072	260449

**Figure 5.** Chromatogram of Inhibace (2.5 mg) tablet sample containing cilazapril. (1) Pravastatin (I.S.) (0.5 µg/mL) and (2) Cilazapril (5 µg/mL)**Figure 6.** Chromatogram of Cibacen (10 mg) tablet sample containing benazepril. (1) Pravastatin (0.5 µg/mL) (I.S.) and (2) Benazepril (5 µg/mL)**Figure 7.** Chromatogram of Cibacen (10 mg) tablet sample containing benazepril. (1) Pravastatin (0.5 µg/mL) (I.S.) and (2) Benazepril (5 µg/mL)

**Table 7.** Result of assay and the recovery analysis of studied compound in tablet formulations

	Cilazapril		Benazepril		Quinapril	
	Quantity found (mg)	Recovery (%)	Quantity found (mg)	Recovery (%)	Quantity found (mg)	Recovery (%)
1	2.490	99.616	9.999	99.992	4.956	99.124
2	2.437	97.473	9.894	98.940	4.960	99.207
3	2.474	98.942	9.882	98.824	4.951	99.018
4	2.512	99.122	9.905	99.144	5.009	100.030
5	2.488	98.164	9.942	99.404	4.957	99.264
Mean±CI*	2.480± 0.039	98.663 ± 1.203	9.942 ± 0.096	99.404 ± 0.864	4.957 ± 0.050	99.264 ± 0.626
SD	0.028	0.846	0.068	0.608	0.035	0.440
% RSD	1.118	0.857	0.680	0.611	0.704	0.443
% Bias	-0.792	-1.337	-0.580	-0.596	-0.852	-0.736

\* Confidence interval at 95% confidence level

In addition, precision values are calculated from the Horwitz (HorRat) equation [34], which represents an empirical relation between the acceptable precision and the corresponding analyte concentration in the sample. HorRat value was calculated in accordance with AOAC guidelines. HorRat(r), HorRat values for repeatability is calculated as  $RSD_r/PRSD(R)$ , HorRat(R), HorRat values for reproducibility is calculated as  $RSD_R/PRSD(R)$  ( $PRSD(R) = 2^{(1-0.5\log C)}$ , C is the mass concentration expressed in the power of 10, i.e  $1 \mu\text{g/g} = 10^{-6}$ ). The AOAC Guidelines suggested that HorRat values  $< 2$ . The repeatability and reproducibility results for studied compounds showed HorRat values of  $< 2$ , which complied with the AOAC guidelines.

For the quantification of cilazapril, benazepril, and quinapril in tablet formulations, tablet solutions were prepared as described in the "Material and Method" section, and the ratio of the peak area of the analyzed compounds to the peak area values of pravastatin because of the analysis was evaluated in the corresponding calibration functions. Then, the number of active compounds contained in the tablets was calculated (Table 7). Chromatograms showing the analysis of the tablet samples were given in Fig. 5 for cilazapril, Fig. 6 for benazepril, and Fig. 7 for quinapril.

The robustness of an analytical procedure refers to its ability to remain unaffected by small changes in method parameters and changes in quantitative results. None of the changes caused a significant change in the peak area and tailing factor of the compounds (Table 6). Quantitative determination of compounds is possible, although changes in retention times are more significant. The reproducibility of the results obtained because of the small changes in this study has proven the method to be robust.

The accuracy of an analytical method refers to the closeness of agreement between the accepted reference value and the found value. Accuracy studies were performed by adding the standard determined at a certain concentration. Accuracy is expressed as percent recovery and is calculated from the slope and intercept values of the calibration curve. The calculated data were

given in Table 7. The calculated average recovery values show that the accuracy of the method is high and that the excipients in the sample medium have no effect.

The average % recovery of three compounds complied with the AOAC Guidelines, which stated that this value should be between 92 – 105% [12].

Experimental results of the amount of benazepril, cilazapril, and quinapril in the selected commercial tablets, expressed as a percentage of label claims were in good agreement with the label claims. The calculated percent recoveries show that the sample preparation and preparation techniques developed for the quantification of the compounds studied are not affected by interferences.

#### 4. Conclusion

The mobile phase was optimized for the quantitative study under the chromatographic conditions determined in this study. In the studies conducted in the literature, the trial-and-error method has been widely used, apart from the experimental design method. In this study, the mobile phase was optimized for the chromatographic separation of ionizable compounds using the pH-*k* relationship. For this, the retention time of cilazapril, benazepril, and quinapril and the suitability of other chromatographic parameters were determined based on the effect of the percentage of organic solvent and pH of the mobile phase. The developed method was validated, and sufficient results were obtained for all the controlled validation parameters. RSD value was calculated below 2% in determining the precision in quantitative analysis of compounds in tablet formulations by RPLC analysis. The evaluation of the obtained results showed that the developed method is suitable for routine use.

#### Acknowledgment

This work was supported by Süleyman Demirel University Scientific Research Projects Coordination (Project 4578-YL2-16).

## References

- [1] I. Maraj, J.N. Makaryus, A. Ashkar, S.I. McFarlane, A.N. Makaryus, Hypertension management in the high cardiovascular risk population, *Int. J. Hypertens*, 2013, 2013, 1–7.
- [2] N.J. Brown, D.E. Vaughan, Angiotensin-converting enzyme inhibitors, *Circulation*, 97, 1998, 1411–1420.
- [3] L. Brunton, B. Chabner, B. Knollman, Goodman and Gilman's The Pharmacological Basis of Therapeutics (9. edition), 1996, New York, McGraw-Hill.
- [4] R. Kumar, R. Sharma, K. Bairwa, R. Kumar Roy, A. Kumar, A. Baruwa, Modern development in ACE inhibitors, *Der Pharmacia Lettre*, 2(3), 2010, 388–419.
- [5] B.G. Katzung, Basic & Clinical Pharmacology (12. edition), 2011, San Francisco, The McGraw-Hill Companies.
- [6] S.D. Firke, K.R. Bhoi, K.R. Patil, S.D. Jayswal, A.R. Tekade, S.S. Chalikwar, A state-of-the-art review on applications of different analytical techniques for some ace inhibitors, *Anal. Chem. Lett.*, 10(1), 2020, 60–79.
- [7] Y. Kazakevich, Y. Lobrutto, HPLC for Pharmaceutical Scientists (1. edition), 2007, Canada, Wiley-Interscience.
- [8] V.R. Meyer, Practical High-Performance Liquid Chromatography (16. edition), 2010, United Kingdom, John Wiley and Sons, Ltd.
- [9] Y.D. Daldal, E.Ç. Demiralay, S.A. Ozkan, Effect of organic solvent composition on dissociation constants of some reversible acetylcholinesterase inhibitors, *J. Braz. Chem. Soc.*, 27(3), 2016, 493–499.
- [10] Y.D. Daldal, E.Ç. Demiralay, Chromatographic and UV-visible spectrophotometric pKa determination of some purine antimetabolites, *J. Mol. Liq.*, 317, 2020, 1–8.
- [11] ICH, Validation of Analytical Procedures: Text and Methodology Q2 (R1) Harmonized Tripartite Guideline 2005.
- [12] AOAC International (2016) Guidelines for Standard Method Performance Requirements AOAC Official Methods of Analysis. Appendix F, 1-18.
- [13] E.Ç. Demiralay, D. Koç, Y.D. Daldal, C. Çakır, Determination of chromatographic and spectrophotometric dissociation constants of some beta lactam antibiotics, *J. Pharm. Biomed. Anal.*, 71, 2012, 139–143.
- [14] E.Ç. Demiralay, Z. Üstün, Y.D. Daldal, Estimation of thermodynamic acidity constants of some penicillinase-resistant penicillins, *J Pharm Biomed Anal.*, 91, 2014, 7–11.
- [15] E.Ç. Demiralay, An experimental design approach to optimization of the liquid chromatographic separation conditions for the determination of metformin and glibenclamide in pharmaceutical formulation, *Acta Chim Slov*, 59(2), 2012, 307–314.
- [16] T. Lundsted, E. Seifert, L. Abramo, B. Thelin, A. Nyström, J. Pettersen, R. Bergam, Experimental design and optimization, *Chemom Intell Lab Syst*, 42, 1998, 3–40.
- [17] S. Bolton, C. Bon, Pharmaceutical Statistics Practical and Clinical Application (4. edition), 2004, Boca Raton, CRC Press.
- [18] D. Bonazzi, R. Gotti, V. Andrisano, V. Cavrini, Analysis of ace inhibitors in pharmaceutical dosage forms by derivative uv spectroscopy and liquid chromatography (hplc), *J Pharm Biomed Anal.*, 16(3), 1997, 431–438.
- [19] F. Colin, K. Poole, Chromatography today. Elsevier Science, First Edition, Amsterdam, 1991
- [20] A. Gumieniczek, H. Hopkala, High-performance liquid chromatographic assay of quinapril in tablets, *Pharm Acta Helv*, 73(4), 1998, 183–185.
- [21] J.A. Prieto, R.M. Jiménez, R.M. Alonso, Quantitative determination of the angiotensin-converting enzyme inhibitor cilazapril and its active metabolite cilazaprilat in pharmaceuticals and urine by high-performance liquid chromatography with amperometric detection, *J Chromatogr B Biomed Appl*, 714(2), 1998, 285–292.
- [22] L. Manna, L. Valvo, S. Alimonti, A liquid chromatographic ion-pairing method for simultaneous determination of benazepril hydrochloride, fosinopril sodium, ramipril and hydrochlorothiazide in pharmaceutical formulations. *Chromatographia*, 53(1), 2001, 271–275.
- [23] F. Elsebaei, Y. Zhu, Fast gradient high performance liquid chromatography method with uv detection for simultaneous determination of seven angiotensin converting enzyme inhibitors together with hydrochlorothiazide in pharmaceutical dosage forms and spiked human plasma and urine. *Talanta*, 85(1), 2011, 123–129.
- [24] S. Kiran, T.Y. Pasha, M. Asif, M. Kamal, T. Jawaid, M.A. Alossaimi, B. Ramesh, M. Majumder, Development and validation of a reverse phase-high performance liquid chromatography method for the assay of benazepril hydrochloride using a quality-by-design approach, *Lat Am J Pharm*, 41(5), 2022, 931–943.
- [25] B. Otašević, J. Šljivić, A. Protić, N. Maljurić, A. Malenović, M. Zečević, Comparison of aqbd and grid point search methodology in the development of micellar hplc method for the analysis of cilazapril and hydrochlorothiazide dosage form stability, *Microchem J*, 145, 2019, 655–663.
- [26] S.M. Auwal, M. Zarei, C.P. Tan, M. Basri, N. Saari. Enhanced physicochemical stability and efficacy of angiotensin i-converting enzyme (ace) - inhibitory biopeptides by chitosan nanoparticles optimized using box-behnken design, *Sci Rep*, 8, 2018, 1–11.
- [27] ICH, International Conference on Harmonization of Technical Requirements for Registration of Pharmaceuticals for Human Use, Validation of analytical procedure: Text and Methodology Q2 (R1), 2005
- [28] D.T. Manallack. The pKa distribution of drugs: application to drug, *Perspect Medicin Chem*, 1, 2007, 25–38.
- [29] M. Remko, Acidity, lipophilicity, solubility, absorption, and polar surface area of some ace inhibitors. *Chem Zvesti CHEM PAP*, 61(2), 2007, 133–141.
- [30] Y.D. Daldal, E.Ç. Demiralay, Development of liquid chromatographic and uv-visible spectrophotometric methods for determination of pKa values of folic acid antimetabolites, *J Pharm Biomed Anal*, 212, 2022, 1–8.
- [31] A. Vonaparti, M. Kazanis, I. Panderi, Development and validation of a liquid chromatographic/electrospray ionization mass spectrometric method for the determination of benazepril, benazeprilat and hydrochlorothiazide in human plasma, *J Mass Spectrom*, 41, 2006, 593–605.
- [32] S.K. Paszun, B. Stanis, W. Pawlowski, Rapid and simple stability indicating hplc method for the determination of cilazapril in pure substance and pharmaceutical formulation in comparison with classic and derivative spectrophotometric methods, *Acta Pol Pharm*, 69(2), 2012, 193–201.
- [33] R. McNally, The United States Pharmacopoeia, 24th revision, Q5 Taunton, M.A, 2000.
- [34] W. Horwitz, L.R. Kamps, K.W. Boyer, Quality assurance in the analysis of foods and trace constituents, *J Assoc Anal Chem*, 63, 1980, 1344–1354.

## The effect of silicon phthalocyanine on cell death and mitochondrial membrane potential in pancreatic cancer cells

Hakkı İsmail Kaya<sup>1</sup> , Ceren Boguslu<sup>1</sup> , Esra Kabak<sup>1</sup> , Cagla Akkol<sup>2</sup> , Ece Tugba Saka<sup>2\*</sup> ,  
Selcen Celik-Uzuner<sup>1</sup> 

<sup>1</sup> Department of Molecular Biology and Genetics, Karadeniz Technical University, 61080, Trabzon, Türkiye

<sup>2</sup> Department of Chemistry, Faculty of Science, Karadeniz Technical University, 61080, Trabzon, Türkiye

### Abstract

Silicon phthalocyanines (SiPcs) are advantageous inorganic molecules because they do not aggregate due to their special structural features. To deal with these structural obstacles, SiPcs have been widely used in a range of disciplines associated with chemical and biological technology. One of the common applications is the use of phthalocyanines as cytotoxic agents in cancer therapies. Cancer is the disease threatening human life and reducing life span and quality, and pancreas cancer is one of the most aggressive cancers with a high rate of mortality around the world. In this study, we therefore aimed to investigate the potential effects of SiPc molecule synthesized for the first time in our previous study on cytotoxicity and mitochondrial activity on pancreatic cancer cells. The results showed the significantly selective cytotoxic effect of SiPc (with a high selective index as 2.5 – 5) on cancer cells compared to normal cells. Mitochondrial membrane potential was not different in cancer cells after SiPc treatment, but interestingly mitochondrial membrane potential of normal cells significantly changed after the treatments. Pre-incubation time (24h) of SiPc before light irradiation induced more significant cytotoxicity in pancreatic cancer cells but not in normal cells compared to prolonged pre-incubation (48h). This study revisited the biological function of previously synthesized SiPc, and the results conclude the cytotoxic activity of SiPc on pancreas cancer. Findings in this work can be extended for other cancer types and detailed with in vivo models in the future.

**Keywords:** Silicon phthalocyanine, cancer, cytotoxicity, mitochondrial membrane potential

### 1. Introduction

Phthalocyanines (Pcs) are a large family of hetero-cyclic conjugated compounds with strong chemical stability. These characteristics make phthalocyanines a significant structural material that can be utilized in many applications such as systems of optical data storage, gas sensors, switching devices and photosensitisers in medical applications [1–5]. One limitation of Pcs applications in solutions is that phthalocyanines are characterized by a very high tendency to aggregate, which reduces their photosensitizing ability through self-quenching. The aggregation of phthalocyanines results in some difficulties in purification and characterization. The lowering of aggregation behaviour can be achieved by the bulky groups to the central metals which have more than four coordination numbers. Axially substituted phthalocyanines are much less likely

to aggregate because of steric hindrance of the non-planar substituents to the central atom [6–10] that is why axially 1-benzyl-4-oxy units substituted silicon phthalocyanines has been chosen in this work (Fig. 1).

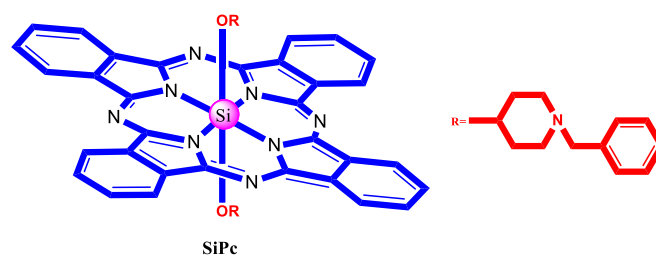


**Figure 1.** Axially 1-benzyl-4-oxy substituted silicon phthalocyanine

In our previous work, we investigated electrochemical, photocatalytic and aggregation behaviour of 1-benzyl-4-oxy substituted silicon highly soluble in most of the organic solvents and are investigated aggregation

**Citation:** H.İ. Kaya, C. Boguslu, E. Kabak, C. Akkol, E.T. Saka, S. Celik-Uzuner, The effect of silicon phthalocyanine on cell death and mitochondrial membrane potential in pancreatic cancer cells, Turk J Anal Chem, 4(2), 2022, 111–115.

 <https://doi.org/10.51435/turkjac.1150201>

**\*Author of correspondence:** ece\_t\_saka@hotmail.com

**Tel:** +90 (462) 377 24 92

**Fax:** +90 (462) 325 31 96

**Received:** July 29, 2022

**Accepted:** November 09, 2022

behaviour in different common organic solvents. The photocatalytic activity of SiPc 3 was examined for *p*-nitrophenol degradation using photochemical reactor. The results indicated that the catalyst showed good activity for *p*-nitrophenol degradation to the corresponding hydroquinone as major product in 1h at 25 °C. Voltametric studies suggested that SiPc displays reversible/quasi reversible/irreversible redox processes, which are the main requirement for the technological usage of this compound [11].

Cancer is one of the most serious health problems worldwide with high mortality. One of the cancer types with the lowest survival rate is pancreatic cancer. Pancreatic ductal adenocarcinoma (PDAC) is the sub-type observed in more than 90% of patients [12]. Phthalocyanines and their derivatives are the molecules with strong absorption in near-infrared regions, chemical and thermal stability, and low toxicity in the dark, in general use to cancer therapy [13]. Phthalocyanines are used as individual cytotoxic agents with the high selectivity for cancer cells [14] or combined with other drugs [15].

Mitochondrion is an organelle serving as the main producer of ATP, and the metabolites necessary to produce macromolecules and reactive oxygen species (ROS). Abnormalities in mitochondrial function and oxidative stress have been associated with the pathologies of some diseases. Mitochondrial membrane potential ( $\Delta\psi_m$ ) is a parameter indicating the proper physiology of the cell. A shift of energy metabolism from oxidative phosphorylation to active glycolysis and an increase in the generation of reactive oxygen species are observed in many cancer cells. These metabolic changes are usually associated with the formation of NAD(P)H oxidase. Mitochondria-dependent metabolic reprogramming in cancer cells is associated with oncogenic signals [16]. In this study we aimed to reveal the cytotoxic effect of our previously synthesized silicon phthalocyanine molecule as well as the potential effect on mitochondrial membrane potential in pancreatic cancer cells.

## 2. Experimental

### 2.1. Materials

SiPc was designed and prepared in our previous work (Fig. 1) [11]. All solvents were dried and purified as described by the reported procedure [17]. 4-Nitrophthalonitrile was purchased from commercial suppliers.

AR42J pancreas cancer (ATCC, Cat No CRL-1492™) and Sol8 normal myoblast (ATCC, Cat No CRL-2174™)

cell lines were cultured in RPMI and DMEM media, respectively. All complete media included 20% FBS and 1% penicillin/streptomycin.

The light source used was red light at a wavelength of 680 nm at an energy density of 10 j/cm<sup>2</sup>.

### 2.2. Methods

After cells reached full confluency (so the cells were almost 100% confluent on culture vessel), cells were treated with different concentrations of SiPc at 1.5, 3, 6 and 12 μM SiPc. Upon treatment with SiPc at 24h or 48h, cells were exposed with 680 nm light for 1 hour at room temperature. Some cells were not treated with light, therefore 4 experimental groups included are as follows:

Group 1; 24h incubation followed by light exposure

Group 2; 24h incubation followed by dark exposure

Group 3; 48h incubation followed by light exposure

Group 4; 48h incubation followed by dark exposure

The day after light exposures MTT assay and mitochondrial membrane potential analyses were performed.

#### 2.2.1. Activation of SiPc with light in cells

PDT was applied according to the formula;  $J = W \times S$  ( $J$  = desired amount of light energy,  $W$  = Light power received by the sensor and  $S$  = Time period (hour) to be applied depending on desired light energy and light power). Therefore, cells were treated with red light at a wavelength of 680 nm at an energy density of 10 j/cm<sup>2</sup> for 1 hour. After light activation cells were incubated at 37 °C with 5% CO<sub>2</sub> for further 24h.

#### 2.2.2. MTT method

After drug treatments and light exposures, media was removed, and cells were washed with 100 μl PBS containing Ca<sup>2+</sup> and Mg<sup>2+</sup>. 10 μl of MTT and 190 μl of complete media were added to each well, and the cells were kept at 37 °C for 2 hours. After 2 hours, media containing MTT was withdrawn, and 200 μl of DMSO was added. Plates were incubated on a shaker overnight at room temperature followed by reading absorbances at 570 nm in the spectrophotometer [18].

#### 2.2.3. Mitochondrial membrane potential ( $\Delta\psi_m$ )

After drug treatments and light exposures, media was removed, and cells were washed with PBS containing 100 μl of Ca<sup>2+</sup> and Mg<sup>2+</sup>. Cells in each well were incubated in 200 μM complete media containing 400 nM Mitotracker red dye, at 37 °C for 45 minutes, followed by

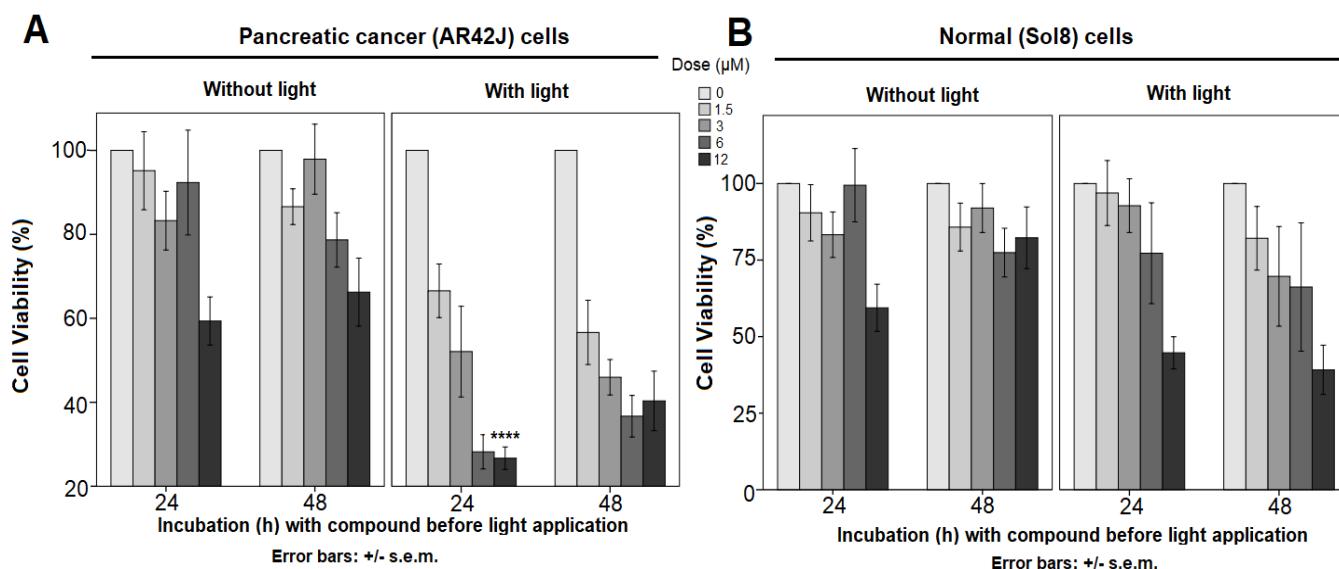


**Figure 2.** A) Cell viability of pancreatic cancer cells (AR42J) after SiPc and B) cell viability of normal muscle cells (Sol8) after SiPc

reading fluorescence at a wavelength of 579 – 599 nm the spectrophotometer [18].

#### 2.2.4. Statistical analyses

Cell viability (%) and mitochondrial membrane potential were analysed by UNIANOVA (univariate analysis of variance) using SPSS software, Version 23. Data was shown with +/- standard errors of the means of experimental repeats (including inter- and intra-repeats). *p* values less than 0.05 were considered as significant.

### 3. Results and discussion

SiPc treatments both for 24h and 48h only after light exposure induced cell death in pancreatic cancer (AR42J) cells ( $p < 0.0001$ ) (Fig. 2A). Although the lowest dose (1.5  $\mu\text{M}$ ) induced cell death on cancer cells (after light), the highest dose (12  $\mu\text{M}$ ) only induced significant cell death on normal cells after light (Fig. 2B). However, there was no significant difference between incubation time with drugs before light exposure ( $p > 0.05$ ). Consistently,  $\text{IC}_{50}$  values were more in Sol8 normal cells than in AR42J pancreatic cancer cells after light exposure (Table 1). SiPc had a cytotoxic effect on cells even if no light activation, but this effect was rather low (Table 1). Phthalocyanines are advantageous as they are applied locally to be activated by light irradiation. This local activation leads to specific targeting of cancer cells [19]. In this study SiPc showed a selective cytotoxic effect on cancer cells with selective indexes around 2.5 – 5 in treated cells at 24h before light application (Table 1). PDT has been shown to selectively affect cancer cells with increased cytotoxicity [20–22]. Cancer is a curable abnormality but one of the main drawbacks of current cancer therapies is low selectivity of cytotoxic agents

therefore the treatment may be harmful for non-cancerous cells by inducing cell death or differentiation mediated by new mutations in normal cells [23]. This handicap is overcome by the discovery of selective cytotoxic agents which affect cancer cells only at the applied conditions. These advantageous agents are supposed to target cancer-specific molecular changes.

Another limitation in drug design is the solubility properties of the candidate compounds. Almost all organic and inorganic compounds are dissolved in dimethylsulfoxide (DMSO) and ethanol but especially the high doses of DMSO itself can trigger toxicity in the cells. Therefore solubility is preferred in safety drug applications and many methodologies are used to enhance the solubility of the compounds [19,24–28] and the SiPc molecule examined in this study was highly soluble therefore it can be considered as solvent-safe for the cells. But these results should be extended for detailed investigation using mice models and other molecular techniques. The used SiPc can be also substituted with other drug molecules, such enzyme inhibitors [29]. Zinc and silicon Pcs were previously shown to have cytotoxic effects on cholangiocarcinoma, the second common type of hepatic cancer [30].

Mitochondrial membrane potential (MMP) ( $\Delta\psi\text{m}$ ) reflecting the functional effectiveness of mitochondria is a biomarker in cell death which tends to decline in

**Table 1.**  $\text{IC}_{50}$  values after SiPc treatments in AR42J and Sol8 cells and selective indexes

Cell Line	Pre-Incubation (h)	Average $\text{IC}_{50}$ ( $\mu\text{M}$ )	
		+ Light	- Light
AR42J	24	3.54	23.30
	48	1.98	20.75
Sol8	24	17.52	22.20
	48	4.95	209.53
Selective index (SI)	24	4.94 ± 2.73	0.95 ± 0.22
	48	2.5 ± 0.78	10 ± 5.41

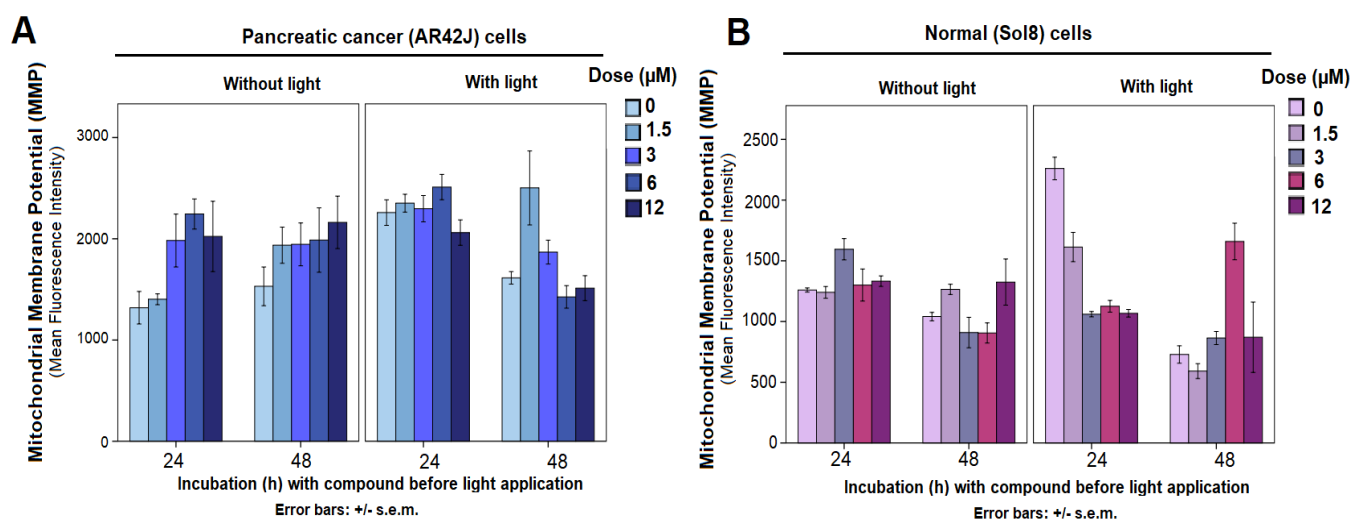


**Figure 3.** A) Mitochondrial membrane potential in pancreatic cancer cells (AR42J) after SiPc and B) mitochondrial membrane potential in normal muscle cells (Sol8) after SiPc

concordance with apoptosis. MMP has been shown to be highly positively associated with cancer malignancy. Especially cancer stem cells have mitochondrial metabolism variability and targeting mitochondria therefore come forward in cancer research [31]. It has been shown that targeting mitochondria increased the effect of photodynamic therapy [32]. Mitochondria are the organelles where oxygen levels are high so that reactive oxygen species can be easily produced, and apoptosis is commonly initiated. This suggests that an ideal photodynamic therapy agent could be a potent photosensitizer that can naturally accumulate in mitochondria. Therefore, the capacity of the new phthalocyanine molecule to be used in this study to target mitochondria was investigated. Some nanoparticles were shown to induce both cell death and the loss of MMP [33]. Hyaluronic acid formulated nanoparticles containing a platinum(II) conjugated silicon(IV) phthalocyanine (SiPc-Pt-HA) were shown to accumulate in mitochondria of MDA-MB-231 breast cancer cells compared to non-cancerous cells [34]. In this study, MMP was not significantly changed in cancer cells at 24h (Fig. 3A) but decreased in normal cells (Fig. 3B). In principle, during PDT the molecular oxygens within the cell are converted into singlet (stimulated) oxygen by stimulating the cytotoxic agent, the photosensitizer, after light applied at the appropriate wavelength. Therefore, mitochondrial membrane potential is supposed to be changed. Normal cells used in this study were muscle cells, and muscle cells are a type of cells with a high number of mitochondria. Therefore, Sol8 cells might be more sensitive to the used silicon phthalocyanine in terms of mitochondrial function. Nevertheless, both types of cells treated with SiPc for prolonged incubation (48h) before light activation did show inaccurate changes on MMP.

## 4. Conclusion

In conclusion, photosensitizer potential of axially 1-benzyl-4-oxy units substituted silicon phthalocyanine on cell death and mitochondrial membrane potential in pancreatic cancer cells was investigated. Our previous work reported that SiPc used in study is highly soluble and has a photocatalytic activity. In this work, previously synthesized SiPc was investigated in terms of cancer therapeutic potential, and it was shown that SiPc had a selective cytotoxic effect (with high selective indexes from 2.5 to 5) but not significant effect on mitochondrial activity on pancreas cancer cells. Normal muscle cells were more sensitive to SiPc in terms of the changes in MMP than normal cells due to most probably their ontological mitochondrial content. Lower pre-incubation of SiPc before light resulted in higher rate of cell death than longer incubation. These results indicate the anti-cancer activity of SiPc, but its molecular mechanism of action should be detailed by extensive molecular and cellular methods.

## References

- [1] R. Ao, L. Kümmerl, D. Haarer, Present limits of data storage using dye molecules in solid matrices, *Adv Mater*, 7, 1995, 495–499.
- [2] J.W. Gardner, M.Z. Iskandari, B. Bott, Effect of electrode geometry on gas sensitivity of lead phthalocyanine thin films, *Sens Actuat B Chem*, B9, 1992, 133–142.
- [3] R. Rellaa, A. Rzzob, A. Licciullic, P. Sicilianoa, L. Troisid, L. Vallic, Tests in controlled atmosphere on new optical gas sensing layers based on TiO<sub>2</sub>/metal-phthalocyanines hybrid system, *Mater Sci Eng C*, 22(2), 2002, 439–443.
- [4] F.Z. Henari, Optical switching in organometallic phthalocyanines, *J. Opt. A, Pure Appl Opt*, 3, 2001, 188–190.
- [5] M. A. El Sallam, H.M. Mallah, D.G. Damhogi, E. Elesh, Thermal analysis, dielectric response and electrical conductivity of silicon phthalocyanine dichloride (SiPcCl<sub>2</sub>) thin films, *J Electron Mater*, 50, 2021, 562–570.

- [6] I. Omeroglu, M. Goksel, V. Kussovski, V. Mantareva, M. Durmus, Novel water-soluble silicon (IV) phthalocyanine for photodynamic therapy and antimicrobial inactivations, *Macrocyclics*, 12, 2019, 255–263.
- [7] G. Dilber, A. Nas, Z. Biyiklioglu, New octa-benzothiazole substituted metal free and metallophthalocyanines: Synthesis, characterization and electrochemical studies, *Turkish J Anal Chem*, 3, 2021, 33–38.
- [8] E. Bagda, The recent studies about the interaction of phthalocyanines with DNA, *Turkish J Anal Chem*, 3, 2021, 9–18.
- [9] G. Sarki, H. Yalazan, H. Kantekin, Synthesis and aggregation properties of 2,9,16,23-tetrakis(chloro)-3,10,17,24-tetrakis[2-(4-allyl-2-methoxyphenoxy)ethoxy]phthalocyaninato cobalt(II), manganese(III), zinc(II), *Turkish J Anal Chem*, 2, 2020, 75–80.
- [10] Y. Caglar, E.T. Saka, A novel silicone phthalocyanines for the preconcentration and spectrophotometric determination of copper by ionic liquid-based dispersive liquid-liquid microextraction, *Turkish J Anal Chem*, 1, 2019, 21–25.
- [11] E.T. Saka, H. Yalazan, Z. Biyiklioglu, H. Kantekin, K. Tekintas, Synthesis, aggregation, photocatalytic and electrochemical properties of axially 1-benzylpiperidin-4-oxy units substituted siliconphthalocyanine, *J Mol Struct*, 1199, 2020, 126994.
- [12] J. Huang, V. Lok, C.H. Ngai, L. Zhang, J. Yuan, X. Q. Lao, K. Ng, C. Chong, Z.J. Zheng, M.C.S. Wong, Worldwide burden of, risk factorsfor, and trends in pancreatic cancer, *Gastroenterology*, 160(3), 2021, 744–754.
- [13] L.B. Oliveirade Siqueira, A.P. Santos Matos, M. R. Mattosda Silva, S. Rocha Pinto, R. S. Oliveira, E. R. Júnior, Pharmaceutical nanotechnology applied to phthalocyanines for the promotion of antimicrobial photodynamic therapy: A literature review, *Photodiagn Photodyn*, 39, 2022, 102896.
- [14] C. Sari, A. Nalcaoğlu, İ. Değirmencioğlu, F. Celep Eyüboğlu, Tumor-selective new piperazine-fragmented silicon phthalocyanines initiate cell death in breast cancer celllines, *J Photoch Photobio B*, 216, 2021, 112143.
- [15] E.C. Aniogo, B.P.A. George, H. Abrahamse, Phthalocyanine induced phototherapy coupled with doxorubicin; a promising novel treatment for breast cancer, *Expert Rev Anticanc*, 17, 2017, 693–702.
- [16] Q. Cui, S. Wen, P. Huang, Targeting cancer cell mitochondria as a therapeutic approach: recent updates, *Future Med Chem*, 9, 2017, 929–949.
- [17] M.J. Stillman, T. Nyokong, *Phthalocyanines: Properties and Applications*, Editor: C. C. Leznoff, 1989, USA, VCH Publishers.
- [18] D.D. Perrin, W.L.F. Armarego, *Purification of Laboratory Chemicals*, second ed., Pergamon Press, Oxford, 1989.
- [19] S. Celik-Uzuner, E. Birinci, S. Tetikoğlu, C. Birinci, S. Kolaylı, Distinct epigenetic reprogramming, mitochondrial patterns, cellular morphology, and cytotoxicity after bee venom treatment, *Recent Pat Anti Canc*, 16.3, 2021, 377–392.
- [20] K. Mitra, M.C.T. Hartman, Silicon phthalocyanines: synthesis and resurgent applications, *Org Biomol Chem*, 6, 2021, 1168–1190.
- [21] A.F. Santos, L.F. Terra, R.A.M. Wailemann, T.C. Oliveira, V.M. Gomes, M.F. Mineiro, F.C. Meotti, A.B. Cardoso, M.S. Baptista, L. Labriola, Methyleneblue photodynamic therapy induces selective and massive cell death in human breast cancer cells, *BMC Cancer*, 17, 2017, 194–209.
- [22] L.A. Muehlman, M.C. Rodrigues, J.P.F. Longo, M.P. Garcia, K.R. Daniel, A.B. Veloso, P.E.N. Souza, S.W. Silva, R.B. Azevedo, Aluminium-phthalocyaninechloride nanoemulsions for anticancer photodynamic therapy: Development and in vitro activity against mono layers and spheroids of human mammaryadenocarcinoma MCF-7 cells, *J Nanobiotechnol*, 13, 2015, 36–47.
- [23] J.M. Pietrasik, A. Witucka, M. Pakula, B.B. Krasinska, A. Niklas, A. Tykarski, K. Ksiazek, Comprehensive review on how platinum- and taxane-based chemotherapy of ovarian cancer affects biology of normal cells, *Cell Mol Life Sci*, 76, 2019, 681–697.
- [24] Q. Liu, M. Pang, S.H. Tan, J. Wang, Q.L. Chen, K. Wang, W.J. Wu, Z.Y. Hong, Potent peptide-conjugated silicon phthalocyanines for tumor photodynamic therapy, *J Cancer*, 9, 2018, 310–320.
- [25] K. Li, W. Dong, Q. Liu, G. Lv, M. Xie, X. Sun, L. Qui, J. Lin, A biotin receptor-targeted silicon(IV) phthalocyanine for in vivo tumor imaging and photodynamic therapy, *J Photoch Photobio B*, 190, 2019, 1–7.
- [26] P. Sen, T. Nyokong, A novel axially palladium(II)-Schiff base complex substituted silicon(IV) phthalocyanine: Synthesis, characterization, photophysical properties and photodynamic antimicrobial chemotherapy activity against *Staphylococcus aureus*, *Polyhedron*, 173, 2019, 114135.
- [27] W.Y. Dong, K. Li, S.J. Wang, L. Qui, M.H. Xie, J.G. Lin, Targeted Photodynamic Therapy (PDT) of Lung Cancer with Biotinylated Silicon (IV) Phthalocyanine, *Current Pharmaceutical Biotechnology*, 22, (2021) 414–422.
- [28] J.P. Taquet, C. Frochot, V. Manneville, M. Heyop-Barberi, Phthalocyanines covalently bound to biomolecules for a targeted photodynamic therapy, *Curr Med Chem*, 14, 2007, 1673–1687.
- [29] B. Aru, A. Günay, E. Senkuytu, G. Yanikkaya-Demirel, A.G. Gürek, D. Atilla, A translational study of a silicon phthalocyanine substituted with a histone deacetylase inhibitor for photodynamic therapy, *ACS Omega*, 40, 2020, 25854–25867.
- [30] J. Schmidt, W. Kuzyniak, J. Berkholtz, G. Steinemann, R. Ogbodu, B. Hoffmann, G. Nouailles, A.G. Gürek, B. Nitzsche, M. Höpfner, Novelzinc-and-silicon-phthalocyanines as photosensitizers for photodynamic therapy of cholangiocarcinoma, *Int J Mol Med*, 42, 2018, 534–546.
- [31] B. Zhang, D. Wang, F. Guo, C. Xuan, Mitochondrial membrane potential and reactive oxygen species in cancer stem cells, *Fam Cancer*, 14(1), 2015, 19–23.
- [32] S.M. Malahingam, J.D.Ordaz, P.S. Low, Targeting of a photosensitizer to the mitochondrion enhances the potency of photodynamic therapy, *ACS Omega*, 6, 2018, 6066–6074.
- [33] A. Al Fraj, A.S. Shaik, S. Afzal, S. Al-Muhsen, R. Halwani, Specific targeting and noninvasive magnetic resonance imaging of an asthma biomarker in the lung using polyethylene glycol functionalized magnetic nanocarriers, *Contrast Media Mol I*, 11, 2016, 172–183.
- [34] K. Mitra, M. Samsó, C.E. Lyons, M.C.T. Hartman, Hyaluronicacid grafted nanoparticles of a platinum(ii)-silicon(iv) phthalocyanines conjugate for tumor and mitochondria-targeted photodynamic therapy in redlight, *J Mater Chem B*, 6, 2018, 7373–7377.



# Investigation of interaction of Bismarck Brown Y-palladium complex with AS1411 G-Quadruplex aptamer

Esra Bağda<sup>1\*</sup> , Rümeyşa Durak<sup>2</sup> , Efkan Bağda<sup>2</sup> , Didem Duman<sup>2</sup> , Ebubekir Ayhan<sup>2</sup> 

<sup>1</sup> Sivas Cumhuriyet University, Faculty of Pharmacy, Department of Basic Pharmaceutical Sciences, 58140, Sivas, Türkiye

<sup>2</sup> Sivas Cumhuriyet University, Faculty of Science, Department of Molecular Biology and Genetics, 58140, Sivas, Türkiye

## Abstract

Increased metabolic activity and metastasis are the main and most known characteristics of cancer cells. Increased activity of the cells results in an increase in the transcription, translation, and replication rate of DNA, hence the probability of the formation of G-quadruplex structures increases. The stabilization or destabilization of G-quadruplex with various ligands may cause disruptions in cell proliferation. So, stabilization or destabilization of these secondary structures is important cancer therapy approach. In the present study, Bismarck brown Y-Pd complex was formed in an easy, one-step mixing method. The spectral characteristics and stoichiometry of the BBY-Pd<sub>2</sub> were investigated UV-Vis spectrophotometrically. The interaction of the BBY-Pd<sub>2</sub> complex with the AS1411 G-quadruplex structure was investigated with spectrophotometric titration. The binding constants were found as  $4.38 (\pm 1.96) \times 10^4 \text{ M}^{-1}$ . The effect of the complex on the G-quadruplex conformation of AS1411 was investigated by using circular dichroism (CD) spectrophotometer. The existence of interactions was further supported by DNA polymerase stop assay using a high-sensitivity LED-induced fluorescence detector Qsep100 capillary gel electrophoresis system.

**Keywords:** G-quadruplex DNA, AS1411, Bismarck brown Y, Palladium, CD spectroscopy, capillary gel electrophoresis

## 1. Introduction

Cancer is one of the difficult-to-treat diseases with high morbidity and mortality values that occur as a result of the disruption of the mechanisms regulating the basic functions of the cell. It was stated that cancer cases are expected to increase by 60% within 20 years by the World Health Organization on Cancer Day 2020 [1]. The studies carried out for the treatment of cancer are followed closely and supported by health institutions such as the World Health Organization and the NIH. Cancer occurs as a result of uncontrolled growth and proliferation of cells. Cancer cells also have the ability to evade apoptosis and exhibit metastasis [2,3]. The process of carcinogenesis is a series of changes that enable cancerous cells to differentiate from normal cells. Changes in gene expression profiles depending on cancer cell types are the main pathway in carcinogenesis [4]. Actually, DNA, which plays an active role in the proliferation of cancerous cells, is a suitable target for cancer treatment [5,6]. Disrupting the functions of DNA in cell proliferation is a promising approach for cancer treatment [7].

DNA regions directly involved in carcinogenesis, such as telomeres and promoters of oncogenes, have guanine-rich sequences. Guanine-rich single-stranded DNA molecules form G-quadruplex conformations in the presence of monovalent cations both *in vitro* and *in vivo*. G-quadruplex structures become stable in the presence of cations such as potassium [8].

The stabilization of these secondary structures, named G-quadruplex DNAs has been proven to inhibit telomerase activity. The ligands showing high selectivity and affinity to G-quadruplex DNA have the potential to be used as anti-cancer drugs [9–12]. Therefore, the design, synthesis, and interaction of G-quadruplex DNA interacting ligands are of scientific value.

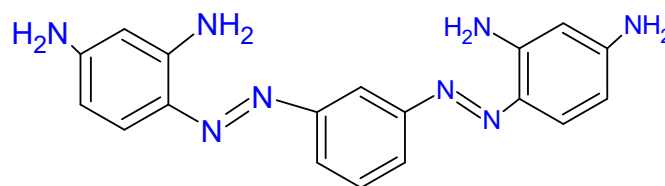


**Figure 1.** Structure of Bismarck Brown compound Y

**Citation:** E. Bağda, R. Durak, E. Bağda, D. Duman, E. Ayhan, Investigation of interaction of Bismarck Brown Y-Palladium complex with AS1411 G-Quadruplex aptamer, Turk J Anal Chem, 4(2), 2022, 116–122.

 <https://doi.org/10.51435/turkjac.1203081>

**\*Author of correspondence:** esraer@cumhuriyet.edu.tr

**Tel:** +90 (346) 478 00 00

**Fax** +90 (346) 219 16 34

**Received:** November 12, 2022

**Accepted:** November 30, 2022

There is a high amount of a multifunctional protein called nucleolin on the surface of cancer cells. Nucleolin is highly expressed both intracellularly and on the cell surface in cancer cells compared to normal cells. Therefore, nucleolin is considered a potential target for diagnosis and cancer treatment in recent years [13]. AS1411 is a 26-base Guanine-rich DNA oligonucleotide that forms G-quadruplexes [14]. AS1411, a nucleolin aptamer, is water soluble and is used as a probe for the detection of various cancer cells. AS1411 has high affinity and binds to nucleolin before uptake by cells [15]. If these G-quadruplex structures are stabilized with appropriate ligands and prevented from unfolding, interruptions occur in DNA replication, transcription, and translation processes [11].

In the present study, the interaction of BBY-Pd<sub>2</sub> complex with nucleolin-targeted AS1411 G-quadruplex aptamer was investigated. Bismarck Brown Y is a water-soluble compound. Due to its solubility in water, it can easily be taken into metabolism and transported in and removed from biological systems. It contains a conjugated  $\pi$  electron system in its structure (Fig. 1). A conjugated  $\pi$  system is an important and desirable property for interaction with DNA species [16]. However, for an effective  $\pi$ - $\pi$  stacking of the Bismarck Brown Y structure with AS1411, it is necessary to provide the appropriate extended- $\pi$  system and planarity of the structure. The complexation with Pd metal will increase the structural rigidity and binding ability of BBY to G-quadruplex DNA providing planarity of the structure. Besides, as stated by Liu et al., palladium-based nanomaterials have shown significant potential for biomedical applications because of their unique optical properties, excellent biocompatibility, and high stability in the physiological environments [17].

Considering all this information, in the present study, the formation of the Bismarck Brown Y-palladium complex in an aqueous solution and the interaction of the formed complex with AS1411 G-quadruplex aptamer were investigated by UV-Vis and CD spectroscopic methods. In addition, the interaction of the formed complex with AS1411 was further tested with DNA polymerase stop assay and monitored by capillary gel electrophoresis system.

## 2. Experimental

### 2.1. Materials and methods

Distilled water was used for the preparation of buffer solutions and in all experimental steps. The solutions used in the experiments were prepared in pH 7.4 Tris buffer containing 150 mM KCl (Trisma base-HCl, EDTA). The pH of the buffer solution was adjusted to 7.4 with a Sartorius pH meter (glass electrode). The

prepared Tris-KCl buffer was stored at +4 °C. AS1411 aptamer solution was prepared with Tris-KCl buffer (pH: 7.4). After 5 minutes of incubation at 95 °C, it was slowly cooled down to room temperature. It was kept at +4 °C for at least one night before use. 150  $\mu$ M Bismarck Brown Y and 150  $\mu$ M Palladium solutions were prepared in Tris-KCl buffer (pH: 7.4). UV-Vis spectrum scanning and absorbance measurements were performed with a Shimadzu 1800 UV-Vis spectrophotometer using a quartz cuvette. The circular dichroism spectrum was scanned with the Jasco J 815 spectrophotometer (Bilkent-UNAM). For capillary gel electrophoresis studies, a high-sensitivity LED-induced fluorescence detector Qsep100 capillary gel electrophoresis system was used with a high-resolution S1 cartridge.

### 2.2. UV-Vis spectroscopic titration

The interaction of AS1411 G-quadruplex DNA with BBY-Pd<sub>2</sub> in Tris-KCl buffer (pH: 7.4) was followed by a UV-Vis spectrophotometer. Quartz cuvettes (1 cm light path) were used in the experiments. The spectral measurements were made triplicate and against reagent blanks prepared under appropriate conditions. For spectrophotometric titration studies, the absorption spectrum of the BBY-Pd<sub>2</sub> solution was first scanned. Then, the spectrum was monitored by adding small portions of the AS1411 solution.

### 2.3. The conformational change of AS1411-circular dichroism spectroscopic experiments

The effect of BBY-Pd<sub>2</sub> on the AS1411 G-quadruplex conformation was investigated by CD spectroscopic experiments [18]. The G-quadruplex structure of AS1411 was determined by CD spectrophotometer (in Tris-KCl buffer, pH: 7.4). The interaction of BBY-Pd<sub>2</sub> with G-AS1411 and conformation changes were interpreted from the changes in the CD spectrum.

### 2.4. DNA polymerase stop assay

Han et al. (1999) protocol has been followed with some improvements [19]. For polymerization, PQ-80 oligonucleotide with AS1411 G-quadruplex DNA structure in the core of the strand was used as template DNA. After the template DNA molecule has interacted with the BBY-Pd<sub>2</sub> complex at different concentrations, its amplification was carried out with a Blue-ray turbocycler 2 thermal cycler. The template DNA (PQ-80, 0.1 mM) and primer (P18, 0.1 mM) in Tris-KCl buffer (10 mM Tris, 150 mM KCl, pH 8.0) were denatured by incubation at 95 °C for 5 min. The mixture, which was left to cool down, was kept at room condition for at least 15 minutes until it stabilized after the addition of the BBY-Pd<sub>2</sub> complex. dNTP (100  $\mu$ M), MgCl<sub>2</sub> (3  $\mu$ M) and Taq polymerase (2.5 U) was added to the medium and

amplified at 55 °C for 30 minutes. The polymerization was terminated by adding a stop buffer to the reaction product. Results were monitored using the Qsep100 capillary gel electrophoresis system with a high-resolution S1 cartridge.

### 3. Results

Because of the active role of DNA in cell proliferation, DNA-targeted ligands are important for cancer diagnosis and treatment [12]. G-quadruplex DNAs are one of the secondary structures of DNA that are exposed in important regions of the genome such as telomeres and oncogenes. These regions are rich in guanine and can form G-quadruplexes formed by stacking of G tetrads formed by four guanine bases binding by Hoogsteen hydrogen bonds [20]. After the discovery that these structures can be formed *in vivo*, intensive scientific studies have been carried out on the role, function, imaging, and targeting of these structures [21]. The interaction of G-quadruplex DNAs with planar ligands with a conjugated  $\pi$  system that can make  $\pi$ - $\pi$  interaction is very important. Preventing the folding of a G-quadruplex structure from relaxing with appropriate ligands will create disruptions in proliferation. Similarly, targeting these structures emerges as a method for cancer diagnosis and treatment, since their relaxation will lead to changes in related cellular processes. The synthesis of ligands with these properties is a very popular research topic [22]. The preparation of a ligand which capable of interacting with the G-quadruplex was the aim of this study.

#### 3.1. Formation of BBY-Pd complex

The formation of the complex between Palladium and BBY was checked by UV-Vis spectrophotometrically in two ways. In the first set of experiments, all solutions were diluted to equal volumes by adding increasing mole ratios of palladium to solutions containing the same amount of BBY. In the second set of experiments, Job's method was used, keeping the total mole fraction constant, and varying the mole ratios of the components. UV-Vis spectrophotometric results of both experimental sets are given in Fig. 2 and Fig. 3.

As can be seen from Fig. 2, BBY's spectrum consisted of a shoulder below 400 nm and a maximum wavelength above 400 nm. This spectrum started to change with the addition of Pd to the solution. The 0 to 1-fold addition of palladium resulted in hyperchromic and hypochromic effects in the shoulder and in the maximum wavelength of BBY itself. Further increasing the mole ratio caused a very distinct and severe peak to appear around 450 nm.

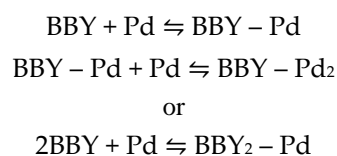
When the spectrum of the complex formed with palladium added with a 2-fold mole ratio is examined, it

is observed that the spectrum consisted of a sharp peak around 450 nm. On the other hand, the peaks obtained with palladium added 2.5 and 3 times more are flattened. In addition, when the spectra of equi-concentrated solutions prepared in 1:1 and 1:2 mole ratios were compared, it was observed that the spectrum obtained with a 1:2 mole ratio showed higher spectral stability which obviously increase the repeatability of the experimental results.

The UV-Vis spectra of solutions for Job's methods are shown in Fig. 2. As can be seen from the figure, the decrease in the mole fraction of BBY in the solution, that is, the increase in the mole fraction of Pd, led to the formation of a sharper single peak. This is in agreement with the data of the first set of experiments.

When the electronic spectra of the solutions prepared in 1:1 and 1:2 (BBY: Pd) mole ratios are compared, it can be said that the spectrum of the complex prepared with a 1:1 mole ratio is similar to the solution spectrum in which BBY is alone. In the 1:2 mole ratio, this is not valid. The observed spectrum is quite different from the spectrum of solutions containing BBY and palladium alone. The spectrum of BBY alone consists of a band between 350 – 470 nm. As the amount of Pd in the solution increases, a single and sharp peak occurs around 448 nm.

Job graphs were drawn from the absorbance values of 271, 301, 395, 448, and 459 (Fig. 4 for 459 nm). As can be seen, it is difficult to determine stoichiometry from the job graphs. Different complexes can be formed with the addition of Pd. Considering the chemical structure of BBY, it is thought that 1:1, 1:2, 2:1 or different higher-order complexes can be formed (Fig. 5).



The clarification of the exact complex formation mechanisms may be different and only be determined via docking studies and instrumental techniques.

In order to examine the effect of the complex concentration on the stability of the formed complexes, the spectra were examined by adding a buffer to the solutions prepared at both 1:1 and 1:2 ratios. As can be seen in Fig. 6, changes are observed in the electronic spectrum of the 1:1 complex with dilution. In the figure, a peak at 450 nm and a shoulder of ~400 nm is observed at 50  $\mu\text{M}$  concentration. After the addition of buffer solution, the peak at ~400 nm becomes more dominant due to the effect of dilution.

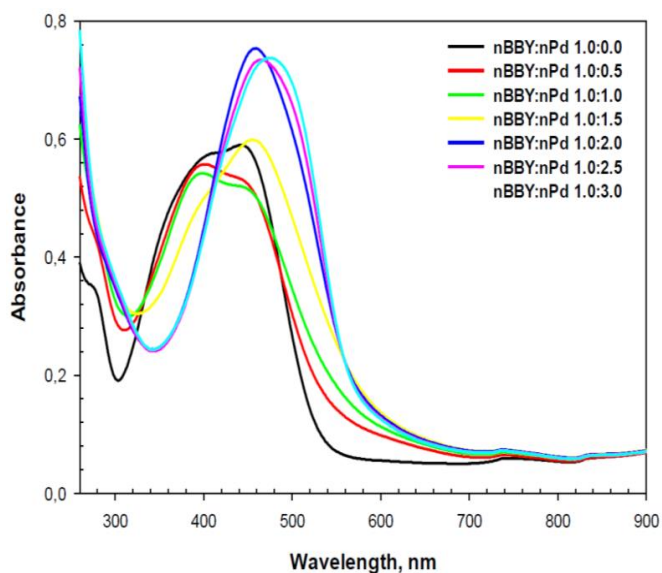


**Figure 2.** Electronic spectra of Bismarck Brown Y and Pd (Bismarck Brown Y concentration is constant and Pd concentrations are varied, pH 7.4 Tris buffer, 150 mM KCl)

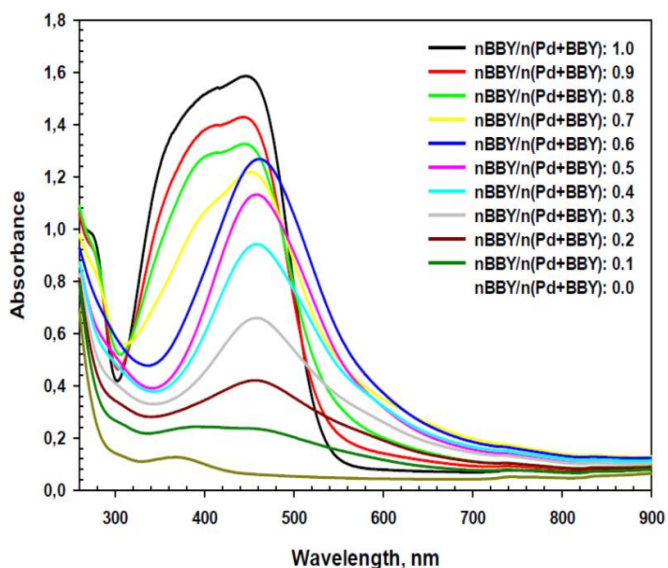


**Figure 3.** Electronic spectra of Bismarck Brown Y and Pd for Job's Experiments (both Bismarck Brown Y and Pd concentrations were varied, pH 7.4 Tris buffer, 150 mM KCl)

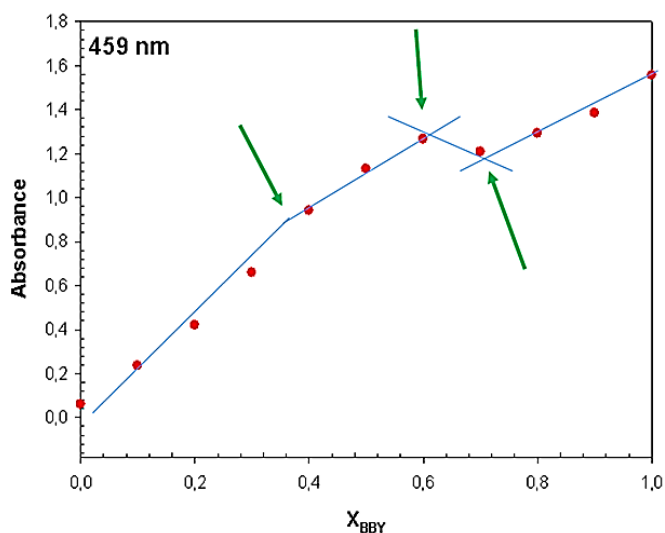


**Figure 4.** Job's diagram for the absorbance values at 459 nm (pH 7.4 Tris buffer, 150 mM KCl)

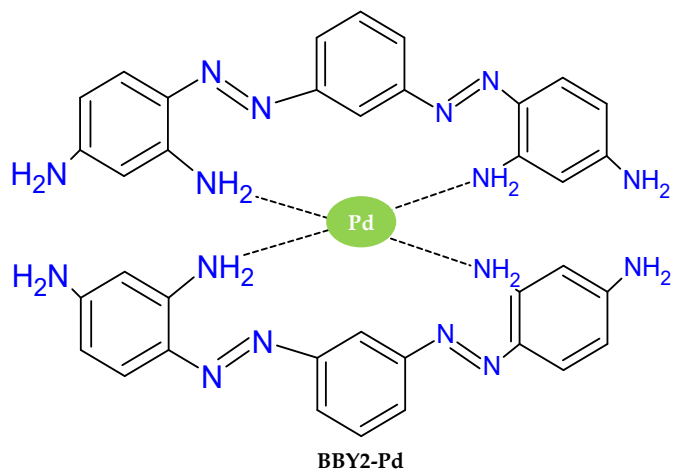
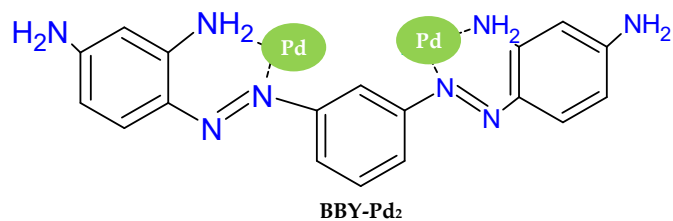
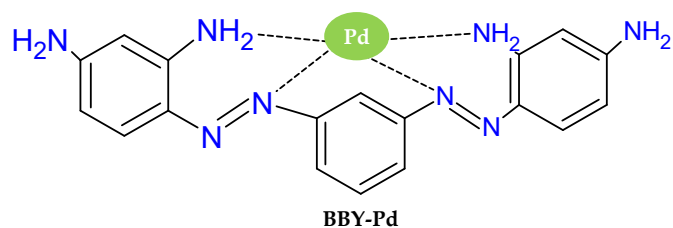


**Figure 5.** Possible 1:1, 1:2 and 2:1 BBY: palladium complex

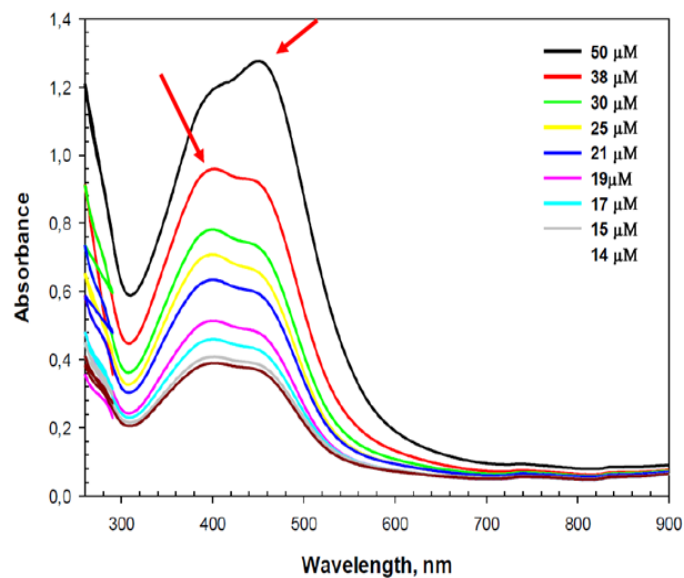


**Figure 6.** Effect of dilution on BBY-Pd complex (pH 7.4 Tris buffer, 150 mM KCl)

So, it can be concluded that some simple factors such as dilution thus affect the stability of the 1:1 complex. The dilution of the complex formed at a ratio of 1:2 did not cause any significant spectral change (Fig. 7). No shift was observed in the maximum wavelength up to 25  $\mu\text{M}$ .

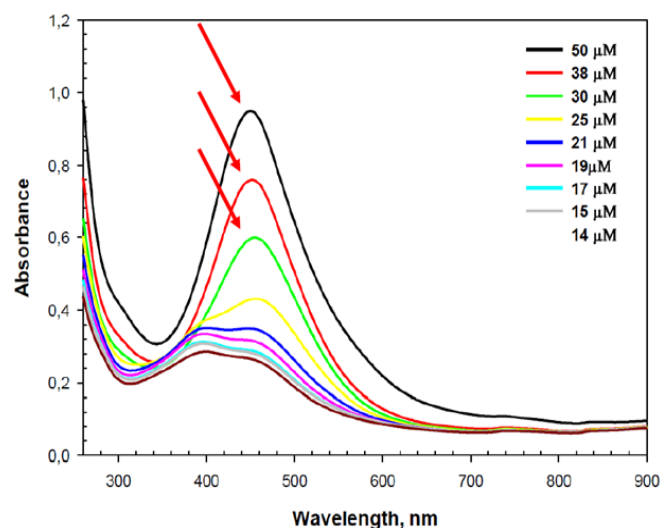


Figure 7. Effect of dilution on BBY-Pd<sub>2</sub> complex (pH 7.4 Tris buffer, 150 mM KCl)

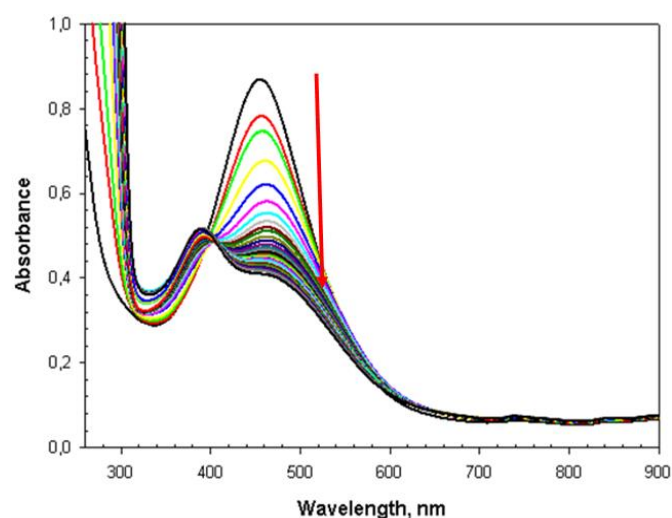


Figure 8. The UV-Vis spectrophotometric titration of the BBY-Pd<sub>2</sub> complex with AS1411 (pH 7.4 Tris buffer, 150 mM KCl)

### 3.2. Investigation of the interaction of BBY-Pd<sub>2</sub> with AS1411

#### 3.2.1. Spectroscopic titration

The interaction of the BBY-Pd<sub>2</sub> complex with AS1411 was performed by spectrophotometric titration method. The change in the spectrum was observed by adding small aliquots of concentrated AS1411 to the BBY-Pd<sub>2</sub> complex.

Fig. 8 shows the electronic spectrum of the titration of the BBY-Pd<sub>2</sub> complex with AS1411. The addition of AS1411 caused a hypochromic effect. On the other hand, the binding constant  $K_B$  was calculated from the absorbance data and was found to be  $4.38 (\pm 1.96) \times 10^4 \text{ M}^{-1}$ ; this value is in agreement with the binding constants of the biomolecule-ligand interaction reported in the literature [23]. Li et al., investigated the interaction of the BBR-Eu(III) complex with DNA. They found that The binding constants of the BBR-Eu(III) complex with DNA are  $K_{298.15\text{K}}^\theta = 1.58 \times 10^4 \text{ L/mol}$  and  $K_{308.15\text{K}}^\theta = 9.35 \times 10^4 \text{ L/mol}$ .

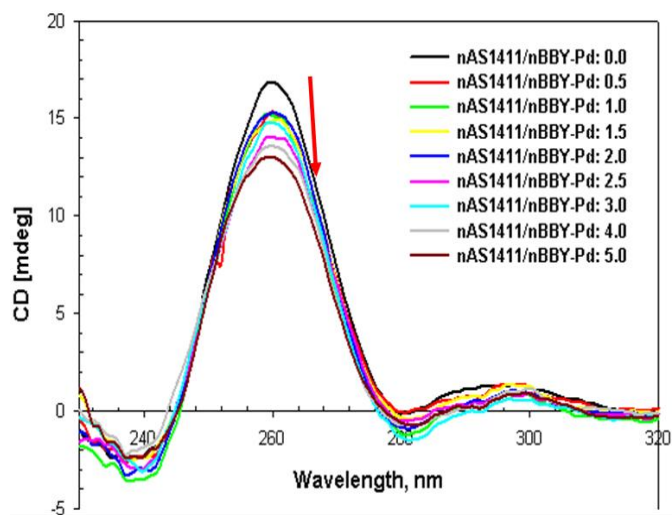


Figure 9. Effect of BBY-Pd<sub>2</sub> on AS1411 CD spectrum (pH 7.4 Tris buffer, 150 mM KCl)

They concluded that the interaction mechanism of the BBR-Eu(III) complex with DNA includes groove binding and intercalative binding [20].

Alzeer et al., investigated guanidinium-modified zinc phthalocyanine Zn-DIGP with a G-quadruplex DNA from the c-Myc promoter for the development of a high-affinity G-quadruplex fluorescent probes and transcriptional regulators. They found the  $K_D \leq 2 \text{ nM}$  for the interaction between Zn-DIGP and c-Myc G-quadruplex DNA [24]. Jain et al. synthesized four compounds having the 1,3-phenylene-bis(piperazinyl benzimidazole) unit as a basic skeleton, and their

interactions with the 24-mer telomeric DNA sequences from *Tetrahymena thermophila* d(T<sub>2</sub>G<sub>4</sub>)<sub>4</sub> have been investigated [25]. They found that EtBzEt binds strongly to the G-quadruplex DNA showing a dissociation constant ( $K_D$ ) of  $5.32 \times 10^5 \text{ M}^{-1}$ , while for duplex DNA, the  $K_D$  was only  $6.0 \times 10^3 \text{ M}^{-1}$ , indicating the weaker binding of the ligand with the duplex DNA. They did not detect any significant binding with CT-DNA in absorption titrations.

#### 3.2.2. Effect of complex on the conformation of AS1411

The effect of complex binding on the conformation of AS1411 was investigated by CD spectroscopy. In order to affect the dilution of AS1411's CD spectrum, solutions were prepared in separate tubes and the final AS1411 concentration in each tube was kept the same. As can be seen from Fig. 9, the CD spectrum of AS1411 consisted of a sharp, positive peak around 260 nm and a negative peak around 240 nm which obviously show that AS1411 has a parallel conformation under the studied experimental conditions [26]. The increasing amount of BBY-Pd<sub>2</sub> resulted in the hypochromic effect on the peak

around 260 nm. It is obvious that BBY-Pd<sub>2</sub> caused the relaxation of the G-quadruplex structure of AS1411 (Fig. 9).

### 3.2.3. DNA polymerase stop assay

The effect of the complex on DNA polymerization was studied to further prove the interaction. G-quadruplex conformation induced template DNA with AS1411 core was amplified by DNA polymerase enzyme at different BBY-Pd<sub>2</sub> concentrations. It was observed that the polymerization of template DNA decreased in the presence of the complex (Fig. 10).

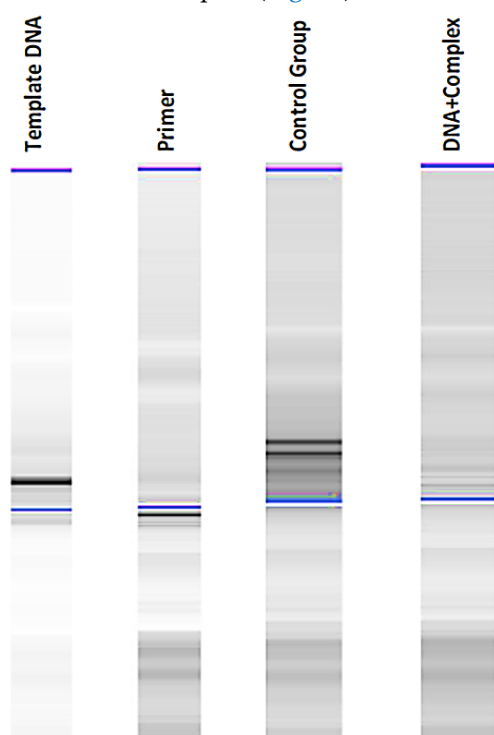


**Figure 10.** Capillary gel electrophoresis for DNA polymerase stop assay.

## 4. Conclusions

The main motivation of the study was to prepare a ligand that can interact with G-quadruplex DNA and be prepared in a very practical way. BBY was complexed with palladium in aqueous solution. Preliminary studies have shown that the compounds can form different complexes with different stoichiometric ratios in solution. However, due to the low reproducibility and environmental factors such as dilution causing stability problems in the 1:1 complex, the studies were carried out with the complex prepared at 1:2 stoichiometric ratios. The formed complex interacts with AS1411 and the binding constant for this interaction was obtained. The obtained constant was found to be almost at the same level as the data in the literature. On the other hand, the effect of the prepared complex on the AS1411 conformation was investigated and it was observed that

it relaxed the G-quadruplex structure. Another part of the study was to investigate the effect of the prepared complex on AS1411 amplification. The polymerization products of the AS1411 G-quadruplex were investigated. It was observed that the interaction of the complex with AS1411 caused a decrease in the polymerisation product.

As a result, we can conclude that the complex between BBY and palladium can be formed quickly and simply in a single step in a solution environment. The resulting complex at a stoichiometric ratio of 1:2 is stable under experimental conditions. 1:2 complex interacts with AS1411 G-quadruplex structure. The interaction constant is comparable to ligand-G-quadruplex DNA interactions in the literature. Interaction AS1411 relaxes the G-quadruplex DNA structure. Interaction of ligand interferes the AS1411 amplification.

Therefore, the complex between BBY and palladium has the potential for cancer treatment by supporting further studies. It is an important advantage that the synthesis is easy, and the ligand is cheap.

## Acknowledgement

This work was supported by the project TÜBİTAK 2209-A (application number 1919B012006536).

Esra Bağda is the principal author.

## References

- [1] World Health Organization, WHO report on cancer: setting priorities, investing wisely and providing care for all, (2020).
- [2] C. Schiliro, B.L. Firestein, Mechanisms of metabolic reprogramming in cancer cells supporting enhanced growth and proliferation, *Cells*, 10(5), 2021, 1056.
- [3] A.R. Yadav, S.K. Mohite, Cancer-A silent killer: An overview, *Asian Pharm Res*, 10(3), 2020, 213–216.
- [4] M.A. Khan, M. Tania, J. Fu, Epigenetic role of thymoquinone: impact on cellular mechanism and cancer therapeutics, *Drug Discov Today*, 24(12), 2019, 2315–2322.
- [5] T. Das, D. Panda, P. Saha, J. Dash, Small molecule driven stabilization of promoter G-quadruplexes and transcriptional regulation of c-MYC, *Bioconjugate Chem*, 29(8), 2018, 2636–2645.
- [6] E. Bağda, E. Bağda, The recent studies about the interaction of phthalocyanines with DNA, *Turkish Anal Chem*, 3(1), 2021, 9–18.
- [7] L. Hassani, Z. Fazeli, E. Safaei, H. Rastegar, M. Akbari, A spectroscopic investigation of the interaction between c-MYC DNA and tetrapyridinoporphyrazinatozinc (II), *J Biol Phys*, 40(3), 2014, 275–283.
- [8] D. Bhattacharyya, G. Mirihana Arachchilage, S. Basu, Metal cations in G-quadruplex folding and stability, *Front Chem*, 4, 2016, 38.
- [9] Q. Li, J.F. Xiang, H. Zhang, Y.L. Tang, Searching drug-like anticancer compound (s) based on G-quadruplex ligands, *Curr Pharm Design*, 18(14), 2012, 1973–1983.
- [10] Z. Shen, K.A. Mulholland, Y. Zheng, C. Wu, Binding of anticancer drug daunomycin to a TGGGGT G-quadruplex DNA probed by all-atom molecular dynamics simulations: Additional pure groove binding mode and implications on designing more selective G-quadruplex ligands, *Mol Model*, 23(9), 2017, 1–11.

- [11] A. Awadasseid, X. Ma, Y. Wu, W. Zhang, G-quadruplex stabilization via small-molecules as a potential anti-cancer strategy, *Biomed Pharmacother*, 139, 2021, 111550.
- [12] Q. Cao, Y. Li, E. Freisinger, P.Z. Qin, R.K. Sigel, Z.W. Mao, G-quadruplex DNA targeted metal complexes acting as potential anticancer drugs, *Inorg Chem Front*, 4(1), 2017, 10–32.
- [13] R. Yazdian-Robati, P. Bayat, F. Oroojalian, M. Zargari, M. Ramezani, S.M. Taghdisi, K. Abnous, Therapeutic applications of AS1411 aptamer, an update review. *Int Biol Macromol*, 155, 2020, 1420–1431.
- [14] J. Carvalho, J.L. Mergny, G.F. Salgado, J.A. Queiroz, C. Cruz, G-quadruplex, Friend or Foe: The Role of the G-quartet in Anticancer Strategies, *Trends Mol Med*, 26(9), 2020, 848–861.
- [15] J. Figueiredo, J. Lopes-Nunes, J. Carvalho, F. Antunes, M. Ribeiro, M.P.C. Campello, A. Paulo; A. Paiva, G.F. Salgado, J.A. Queiroz, J.L. Mergny, C. Cruz, AS1411 derivatives as carriers of G-quadruplex ligands for cervical cancer cells, *Int Pharm*, 568, 2019, 118511.
- [16] E. Krieg, M.M. Bastings, P. Besenius, B. Rybtchinski, Supramolecular polymers in aqueous media, *Chem Rev*, 116(4), 2016, 2414–2477.
- [17] Y. Liu, J. Li, M. Chen, X. Chen, N. Zheng, Palladium-based nanomaterials for cancer imaging and therapy, *Theranostics*, 10(22), 2020, 10057.
- [18] E. Bağda, E. Bağda, A. Kocak, M. Durmuş, Investigation of Binding behaviour of a water-soluble gallium (III) phthalocyanine with double-stranded and G-quadruplex DNA via experimental and computational methods, *Mol Struct*, 1240, 2021, 130536.
- [19] H. Han, L.H. Hurley, M. Salazar, A DNA polymerase stop assay for G-quadruplex-interactive compounds, *Nucleic acids research*, 27(2), 1999, 537–542.
- [20] A. Dey, K. Pandav, M. Nath, R. Barthwal, R. Prasad, Binding characterization of anthraquinone derivatives by stabilizing G-quadruplex DNA leads to an anticancerous activity, *Mol Ther-Nucl Acids*, 2022.
- [21] H.J. Lipps, D. Rhodes, G-quadruplex structures: in vivo evidence and function. *Trends Cell Biol*, 19(8), 2009. 414–422.
- [22] S.M. Haider, S. Neidle, G.N. Parkinson, A structural analysis of G-quadruplex/ligand interactions. *Biochimie*, 93(8), 2011, 1239–1251.
- [23] H. Li, Y. Tang, S. Lei, Z. You, T. Yang, S. Wang, A Spectroscopic Study of the Interaction Between the Bismarck Brown R-Eu (III) Complex and DNA, *Appl Spectrosc*, 85(4), 2018, 791–799.
- [24] J. Alzeer, B.R. Vummidi, P.J. Roth, N.W. Luedtke, Guanidinium-modified phthalocyanines as high-affinity G-Quadruplex fluorescent probes and transcriptional regulators, *Angew Chem Int Edit*, 48(49), 2009, 9362–9365.
- [25] A.K. Jain, V.V. Reddy, A. Paul, and S. Bhattacharya, Synthesis and evaluation of a novel class of G-quadruplex-stabilizing small molecules based on the 1, 3-phenylene-bis (piperazinyl benzimidazole) system, *Biochemistry*, 48(45), 2009, 10693–10704.
- [26] Z. Bagheri, B. Ranjbar, H. Latifi, M.I. Zibaii, T.T. Moghadam, A. Azizi, Spectral properties and thermal stability of AS1411 G-quadruplex, *Int Biol Macromol*, 72, 2015, 806–811.



# Determination of LC-MS/MS phenolic profile, antioxidant activity and $\alpha$ -glucosidase enzyme inhibition of *Linum mucronatum* Bertol. subsp. *armenum* (Bordz.) P.H.Davis

Fatma KILIÇ<sup>1</sup> , Zeynep AKAR<sup>2\*</sup> 

<sup>1</sup> Gümüşhane University, Department of Biotechnology, Graduate Education Institute Gümüşhane University, 29000, Gümüşhane, Türkiye

<sup>2</sup> Gümüşhane University, Department of Genetics and Bioengineering, Faculty of Engineering and Natural Sciences, 29000, Gümüşhane, Türkiye

## Abstract

Plants include compounds having high antioxidant activity such as flavonoids, phenolics, and carotenoids. Antioxidant defense mechanisms play an important role in the prevention and treatment of oxidative stress diseases in humans. In the study, was performed to evaluate the antioxidant and  $\alpha$ -glucosidase inhibitory effects of the flower and leaf parts of *Linum mucronatum* subsp. *armenum*. The antioxidant activities of the extracts were determined using six antioxidant activity determination assays (iron(III) reducing/antioxidant power (FRAP), DPPH radical scavenging activity, copper(II) reducing antioxidant activity (CUPRAC), ABTS radical scavenging capacity, total flavonoid content, and total phenolic content). While, the methanol extract showed the highest activity for the flower part, ethanol extracts of leaf part showed the highest antioxidant activity in the DPPH, FRAP and CUPRAC tests. The highest activity values in both flower and leaf parts were measured in acetone extract with  $SC_{50} = 0.287$  mg/mL and  $SC_{50} = 0.163$  mg/mL in ABTS test, respectively. Lowest activity values of solvent extracts were measured in hexane extracts in all tests. Phenolic compounds of the plant were identified using LC-MS/MS. These phenolics are kaempferol, vanillin, protocatechuic acid, caffeic acid, *p*-coumaric acid, *p*-OH benzoic acid, salicylic acid, quercetin and rutin. The leaf and flower parts have  $\alpha$ -glucosidase enzyme inhibitor effect. It was determined that the leaf part of the plant ( $IC_{50} = 4.53$  mg/mL) have higher enzyme inhibition than in the flower ( $IC_{50} = 6.10$  mg/mL). As a result, it was determined that the plant showed the biological activity. The results will contribute to the studies on the biological activity of the other plant.

**Keywords:** Antioxidant activity,  $\alpha$ -glucosidase, phenolic, *Linum*

## 1. Introduction

Oxidative stress, which take place because of an imbalance between antioxidants and free radicals in the human body, can negatively affect human health in many ways [1,2]. Especially, free radicals defect structure of cellular components such as nucleic acids, proteins and membrane phospholipids [3]. These radicals having unpaired electrons are highly unstable. To become stable, take electrons from other molecules and at the same time, oxidize the molecules. Thus, they cause the formation of another free radical [4]. Therefore, they are the major pathogens that cause various diseases in human such as diabetes, cancer, and neurodegenerative disorders [5]. Antioxidants known to prevent oxidative stress that may occur in the human body with the effect of free radicals [6]. There are mechanisms to prevent oxidative stress in the human body with antioxidants occurs endogenously or

supplied externally from foods and supplements [7,8]. Recently, synthetic antioxidant compounds have been added to foodstuffs to protect food from reactive oxygen damages such as lipid oxidation during their processing and storage [9]. However, some synthetic antioxidant compounds such as BHA (butylated hydroxyanisole) and BHT (butylated hydroxytoluene) have been shown to have toxic effects on humans [10]. Today, because of that there is a greater tendency towards natural antioxidants rather than synthetic antioxidants that cause adverse health effects [11]. Plants are the most important source of natural antioxidants [12,13]. Antioxidants obtained from plants are effective in the prevention of many disorders such as diabetes and cancer [14]. One of the approaches used in the treatment of diabetes is to inhibit enzyme of alpha glucosidase for delay glucose absorption [15]. Plants

**Citation:** F. KILIÇ, Z. AKAR, Determination of LC-MS/MS phenolic profile, antioxidant activity and  $\alpha$ -glucosidase enzyme inhibition of *Linum mucronatum* Bertol. subsp. *armenum* (Bordz.) P.H.Davis, Turk J Anal Chem, 4(2), 2022, 123–131.

 <https://doi.org/10.51435/turkjac.1196786>

**\*Author of correspondence:** zeynep\_iskefiyeli@hotmail.com

**Tel:** +90 (456) 233 10 00→1965

**Fax** +90 (456) 233 10 75

**Received:** October 31, 2022

**Accepted:** November 30, 2022

contain hypoglycemic agents and 1200 plant species have been reported to have hypoglycemic activity. Therefore, it is important to use natural  $\alpha$ -amylase and  $\alpha$ -glucosidase inhibitors obtained from plant sources in the control of hyperglycemia [16]. One of the most common research topics is also the biological activities of plant compounds against various diseases, especially their antioxidant properties.

Because of that there are not enough studies on biochemical properties, The present study was focused some biochemical properties of the leaf and flower parts of *Linum mucronatum* Bertol. subsp. *armenum* (Bordz.) P.H.Davis (it is called sarıkamuşketeni in Turkish) which is distributed in the Gümüşhane province of Türkiye. In the present study, it was aimed to identify the antioxidant activity potential in various solvent extracts of flowers and leaves of the plant. It was applied to determine antioxidant activity of the leaves, flower parts, tests having different mechanisms such as iron(III) reducing/antioxidant power (FRAP), ABTS<sup>•+</sup> radical scavenging capacity, (DPPH) radical scavenging activity, copper(II) reducing antioxidant activity (CUPRAC), total flavonoid content and total phenolic content. Additionally, the phenolic profile of the plant parts was identified using LC-MS/MS and the inhibition of  $\alpha$ -glucosidase enzyme were determined.

## 2. Material and methods

### 2.1. Preparation of extracts

*L. mucronatum* subsp. *armenum* was collected from Bağlarbaşı district of the Gümüşhane province in Black Sea Region of Türkiye in July 2021. It was stored in KTUB Herbaria (M. Gültepe 702). The plant is a non-shrub, herbaceous perennial with branching at the base. Flowering stems are erect or ascending, 10 – 35 cm long. These stems are keeled, spine straight and do not bear base leaves. Stem leaves oblong or oblanceolate, acuminate, 1 – 3 veined, 9 – 35 × 3 – 8 mm, stipules at leaf base. Inflorescence cymose, 7 and more flowered. Sepals lanceolate, 9 – 11 × 1.5 – 2.5 mm, keeled. It is membranous edged and ciliated at the tip. Petals yellow and base purple spotted, obovate, 19 – 33 × 8 – 11 mm, acute or obtuse. The filament tube is 3 – 4 mm and the filaments are 8–11 mm long at most. Anthers oblong 2 – 3 mm long, yellow in color. Staminode linear, up to 1 mm spherical ovary, linear stigma, capsule is 4 – 5 mm [17].

The flower and leaf parts of the plant were separated and dried at the room temperature. Then, the parts were powdered using a blender. Five solvents (methanol, ethanol, acetone, acetonitrile, and hexane) having different polarities were used for extraction. In the

extraction process, 5 g of powdered both flower and leaf were weighed into a 100 mL beaker and 50 mL solvent was added to the onto the samples [18]. These mixtures were extracted using a magnetic stirrer for 2 hours. After that the extracts were filtered and the its solvents were removed in the rotary evaporator device (Heildoph, Germany). Their concentrations were determined by adding solvents. The prepared extracts were kept closed at +4 °C.

### 2.2. Analyses

#### 2.2.1. Antioxidant activity

##### 2.2.1.1. DPPH radical scavenging activity

The DPPH<sup>•</sup> (1,1-diphenyl-2-picrylhydrazyl) radical assay is widely used in determining antioxidant activity of the substances [19]. In this method, antioxidants cause a decrease in intensity of the purple color from DPPH<sup>•</sup>. The antioxidant activity value is calculated based on this intensity decrease in the color. Firstly, 100  $\mu$ M DPPH radical solution was added onto 750  $\mu$ L of the sample. The solution was mixed with vortex, and it was kept at room temperature for 60 minutes. Then, Absorbances of the each mixture were determined at 517 nm with a UV-Vis spectrophotometer (UV-1800, Shimadzu, Japan). For comparison, the activity values in different concentrations of trolox antioxidant standard (starting from 0.005 mg/ml) were also determined under the same conditions. The absorbances of DPPH radical in different sample concentration were measured and graph was plotted with the concentrations corresponding to these absorbances. In the  $y = ax + b$  equation, the sample amount that cut in half DPPH<sup>•</sup> concentration was determined in  $\mu$ g/mL and the results were expressed as the SC<sub>50</sub> value. Lower SC<sub>50</sub> values indicate higher radical scavenging potential.

##### 2.2.1.2. Determination of iron (III) reduction / antioxidant power (FRAP)

In the method developed by Benzie and Strain [20], extracts of solvent of the leaf and flower parts were diluted at various concentrations (62.5 -125-250-500-1000  $\mu$ M). It was applied same procedure the antioxidant standard Trolox. First, 50  $\mu$ L of both sample and standard solution was pipetted to the tubes. In addition to this, 50  $\mu$ L of sample solvent and sample solutions were added to the sample and reagent blank tubes respectively. Then, 1.5 mL of FRAP solvent was transferred to the blank tubes. After that FRAP reagent (1.5 mL) was pipetted to the all tubes excluding the sample blank tubes and were vortexed. At the end of a 20 min period, the values of absorbance were spectrophotometrically measured at 595 nm. The results were computed in  $\mu$ M TEAC by comparing the standard Trolox.

### 2.2.1.3. Copper (II) reducing antioxidant activity (CUPRAC)

In the CUPRAC method developed by Apak et al. [21] was made some modification and applied to the samples. First, the neocuproine alcoholic solution (96% ethanol), Cu(II) chloride solution, analysis solutions and ammonium acetate buffer (pH = 7) in equal volumes were transferred to the test tube. The volume of the final solution was set to 4.1 mL with adding pure water. These tubes were capped and stored at room conditions for 30 minutes and the values of absorbance were spectrophotometrically measured at 450 nm. As in other tests, antioxidant standard trolox was studied at 6 different concentrations. The antioxidant capacities of the samples were determined based on values from the trolox graph, as  $\mu\text{M}$  TEAC in trolox equivalent.

### 2.2.1.4. ABTS<sup>•+</sup> radical scavenging capacity

This method [22] is one of the commonly used methods by researchers for the determination of antioxidant activity. First, to prepare the stock solution of ABTS (7 mM), solvent mixture (water:ethanol 1:5) was prepared and ABTS solution was formed by dissolving ABTS reagent in the mixture. The solution was then mixed with a 2.45 mM solution of potassium persulfate prepared with water:ethanol (3:1). The mixture was kept in the dark at room conditions for 18 hours and ABTS<sup>•+</sup> was formed and diluted to 1/40. Thus, it was adjusted to absorbance of 0.07 at 734 nm. The standard antioxidant trolox solution used for comparison with sample extracts of different concentrations was pipetted in triplicate and the same procedure was applied to the sample and the reagent blank. These were left for 20 minutes at the room temperature. Finally, the values of absorbance were determined at 734 nm. Then sample amounts that cut in half the ABTS<sup>•+</sup> concentration were computed in mg/mL and the results were reported as SC<sub>50</sub>.

### 2.2.1.5. Total phenolic content (TPC)

The phenolic substance contents of the leaf and flower parts of *L. mucronatum* subsp. *armenum* extracted using different solvents were measured using Folin-Ciocalteu reagent based on Slinkard and Singleton method [23], with some modifications. First, 50  $\mu\text{L}$  of extracts were diluted in distilled water (2.5 mL) and 0.2 N Folin-Ciocalteu (250  $\mu\text{L}$ ) of was transferred on the diluted extract. Then, 750  $\mu\text{L}$  of Na<sub>2</sub>CO<sub>3</sub> (7.5%) was pipetted onto the mixture and vortexed. After that the prepared tubes were stored for 120 min at room conditions and values of absorbance were measured at 765 nm spectrophotometrically.

Gallic acid antioxidant standard was prepared at various concentrations (62.5-125-250-500-1000  $\mu\text{g/mL}$ ). The phenolic compounds amounts were computed as

gallic acid equivalent (GAE  $\mu\text{g/mL}$ ) using the function of the line from the standard calibration graph.

### 2.2.1.6. Total flavonoid content (TFC)

The flavonoid contents of the leaf and flower parts of the *L. mucronatum* subsp. *armenum* were measured using the method developed by Fukumoto and Mazza [24]. As in the other tests, the measurements were carried out in triplicate. In addition, sample and reagent blanks were prepared. Samples in equal amounts (250  $\mu\text{L}$ ) were transferred into the tubes, then 2.1 mL of methanol was added to all the tubes. Finally, 50  $\mu\text{L}$  of 1M CH<sub>3</sub>COONH<sub>4</sub> (ammonium acetate) and 10% Al(NO<sub>3</sub>)<sub>3</sub>.9H<sub>2</sub>O (aluminum nitrate) were transferred to the tubes excluding the sample blank. After that, the mixtures were vortexed and stored at the room temperature for 40 min. The values of absorbance were read at 415 nm.

The antioxidant standard of quercetin was used simultaneously in the same conditions. Six different concentrations of quercetin (0.25 mg/mL) were prepared, and values of the absorbance were measured. Then, the standard calibration graph was drawn with the absorbance values corresponding to the concentration. According to the graph, the total flavonoid substance amounts of the samples were calculated in quercetin antioxidant equivalent (QAE mg/mL).

### 2.2.2. Determination of plant phenolic substance content using LC-MS/MS

Determination of phenolic content by LC-MS/MS was performed at Scientific Technical Application and Research Center, Hitite University. Analysis of phenolic substance content in leaf and flower parts of the *L. mucronatum* subsp. *armenum* was using LC-MS/MS (Thermo Scientific/Dionex Ultimate 3000-TSQ Quantum). Ethanol solvent was used for the extraction of plant parts. Column (ODS Hypersil 4.6\*250 mm, 5 $\mu\text{m}$ ) were used in the sample analyzes and a gradient program were applied with formic acid (0.1% in deionized water) in A reservoir and methanol (100%) in B reservoir. In addition, it was optimized with the column temperature to 30 °C, the mobile phase flow to 0.7 mL/min and 20  $\mu\text{L}$  of injection volume of standards and samples. The optimization of gradient program was carried out passing 100% in the A reservoir in 0–1 minutes, 5% A in 22 minutes for 3 minutes, and 100% in the B reservoir in 26 minutes for 8 minutes [17].

### 2.2.3. In vitro $\alpha$ -glucosidase enzyme inhibition

The  $\alpha$ -glucosidase enzyme inhibitory activities of the ethanol extracts of the leaf and flower parts of *L. mucronatum* subsp. *armenum* were measured according to the modified method of Yu et al. [25].

**Table 1.** Antioxidant activities and total phenolic content and total flavonoid content in different solvent extract of leaves and flowers of *L. mucronatum* subsp. *armenum*

Plant parts	Solvent	DPPHSC <sub>50</sub> (mg/mL)	FRAPTEAC ( $\mu$ M)	CUPRACTEAC ( $\mu$ M)	ABTSSC <sub>50</sub> (mg/mL)	TPC ( $\mu$ g/mL GAE)	TFC (mg/mL QAE)
Flower	Methanol (M)	0.12 $\pm$ 0.08	643 $\pm$ 2.11	0.20 $\pm$ 0.12	0.56 $\pm$ 0.15	803 $\pm$ 2.86	0.10 $\pm$ 0.05
	Ethanol (E)	0.17 $\pm$ 0.10	372 $\pm$ 1.17	0.16 $\pm$ 0.08	0.88 $\pm$ 0.21	450 $\pm$ 1.55	0.07 $\pm$ 0.04
	Acetonitrile (ACN)	0.14 $\pm$ 0.09	572 $\pm$ 1.82	0.18 $\pm$ 0.09	0.82 $\pm$ 0.20	564 $\pm$ 1.76	0.03 $\pm$ 0.01
	Acetone (A)	0.20 $\pm$ 0.11	340 $\pm$ 1.02	0.11 $\pm$ 0.03	0.29 $\pm$ 0.13	391 $\pm$ 1.21	0.04 $\pm$ 0.01
	Hexane (H)	1.58 $\pm$ 0.25	44 $\pm$ 0.54	0.07 $\pm$ 0.02	10.17 $\pm$ 1.21	17 $\pm$ 0.23	0.002 $\pm$ 0.01
Leaf	Methanol (M)	0.03 $\pm$ 0.03	570 $\pm$ 1.76	0.16 $\pm$ 0.08	0.22 $\pm$ 0.09	821 $\pm$ 2.12	0.13 $\pm$ 0.03
	Ethanol (E)	0.02 $\pm$ 0.02	645 $\pm$ 2.05	0.16 $\pm$ 0.09	0.21 $\pm$ 0.09	827 $\pm$ 2.09	0.10 $\pm$ 0.02
	Acetonitrile (ACN)	0.05 $\pm$ 0.06	530 $\pm$ 1.55	0.15 $\pm$ 0.07	0.30 $\pm$ 0.11	787 $\pm$ 1.87	0.10 $\pm$ 0.02
	Acetone (A)	0.05 $\pm$ 0.06	512 $\pm$ 1.32	0.14 $\pm$ 0.05	0.16 $\pm$ 0.09	758 $\pm$ 1.45	0.10 $\pm$ 0.02
	Hexane (H)	0.36 $\pm$ 0.13	58 $\pm$ 0.83	0.07 $\pm$ 0.01	8.43 $\pm$ 1.04	23 $\pm$ 0.41	0.001 $\pm$ 0.01

In the test, 650  $\mu$ L of phosphate buffer (0.1 M and pH: 6.8) was pipetted to the test tube. Then, 20  $\mu$ L of sample and 30  $\mu$ L of  $\alpha$ -glucosidase enzyme (*Saccharomyces cerevisiae*, lyophilized powder,  $\geq$  10 units/mg protein – Sigma Aldrich) prepared in phosphate buffer were added on the solution. After, the mixture was kept at 37 °C for 10 minutes and 75  $\mu$ L of substrate (4-Nitrophenyl- $\alpha$ -D-glucopyranoside) was added on to the mixture. Once again, it was incubated at 37 °C for 20 minutes, then 650  $\mu$ L of 1M Na<sub>2</sub>CO<sub>3</sub> was transferred to all tubes and the reaction was stopped. Absorbance values were measured at 405 nm at the UV/VIS spectrophotometer.

Acarbose (positive control) were used in different concentrations as the standard inhibitor. The measurements were made in triplicate, including reagents and sample blanks. The IC<sub>50</sub> values of acarbose and samples (sample concentration that cut in half the enzyme activity in the environment) were calculated. The lower the IC<sub>50</sub> value of the sample, the more effective is in enzyme inhibition.

### 3. Results

#### 3.1. Antioxidant activity

The antioxidant activities of the extracts prepared in 5 different solvents (methanol, ethanol, acetone, acetonitrile, hexane) of the leaves and flowers of the *L. mucronatum* subsp. *armenum* were determined using 6 different antioxidant activity determination methods (iron(III) reduction/antioxidant power (FRAP), DPPH radical scavenging activity, ABTS<sup>•+</sup> radical scavenging capacity, copper(II) reducing antioxidant activity (CUPRAC), total flavonoid content and total phenolic content tests) (Table 1). For DPPH test, while the methanol extract has the highest antioxidant activity (0.12 mg/mL) in the flower part, the highest value (0.017 mg/mL) in the leaf part were measured in ethanol extract. However, hexane extracts showed the lowest activity in both flower and leaf parts with 1.58 and 0.36 mg/mL, respectively. In addition, it was determined that

the DPPH radical scavenging activity values of the leaf part were higher than the flower in all solvents.

The activity values measured in the FRAP test were similar to the DPPH test results. The methanol extract showed the highest antioxidant activity (643  $\mu$ M TEAC) in the flower part, while hexane extract showed the lowest activity (44  $\mu$ M TEAC). On the leaf part, the highest and lowest activity values were determined 645  $\mu$ M TEAC in ethanol extract, 58  $\mu$ M TEAC in hexane extract, respectively. As in DPPH and FRAP, the ranking of activity values measured in the CUPRAC test is M>ACN>E>A>H in flower and E>M>ACN>A>H in leaf.

In ABTS radical scavenging activity, lower SC<sub>50</sub> values indicate higher radical scavenging potential. Unlike the other antioxidant activity tests, it is seen that the acetone extract has the highest antioxidant activity in both the flower (0.29 mg/mL) and leaf (0.163 mg/mL) parts. In addition, as in the other tests, hexane extracts of flower and leaf parts showed the lowest antioxidant activity as 10.17 mg/mL and 8.43 mg/mL, respectively.

**Table 2.** LC-MS/MS analysis of the phenolic compounds in the flower and leaf parts of *L. mucronatum* subsp. *armenum*

Phenolic Compounds	Flower ( $\mu$ g/mL)	Leaf ( $\mu$ g/mL)
Epicatechin	nd	nd
Catechin	nd	nd
Protocatechuic acid	0.41	nd
Protocatechuic aldehyde	nd	nd
Caffeic acid	0.86	0.22
Ferulic acid	nd	nd
Vanillin	0.34	0.44
Taxifolin	nd	nd
<i>p</i> -coumaric acid	1.41	1.92
Salicylic acid	0.45	nd
<i>p</i> -OH benzoic acid	0.39	nd
Rutin	1.19	0.42
Syringic acid	nd	nd
Quercetin	0.45	0.02
Rosmarinic acid	nd	nd
Kaempferol	0.26	nd
Resveratrol	nd	nd
Gallic acid	nd	nd
Ellagic acid	nd	nd
Oleuropein	nd	nd

nd: not detected

Unlike the others the ranking of activity values measured in the ABTS radical scavenging activity is A>M>ACN>E>H in flower and A>E>M>ACN>H in leaf.

The highest activity value of total phenolic content in the samples was measured in the methanol extract of flower part as 803  $\mu\text{g}/\text{mL}$  GAE and in the ethanol extract of the leaf as 821  $\mu\text{g}/\text{mL}$  GAE. In addition, hexane extract has the lowest amount of phenolic content in both flower (17  $\mu\text{g}/\text{mL}$  GAE) and leaf (23  $\mu\text{g}/\text{mL}$  GAE) parts. The ranking of activity values measured in the test was the same as in all other tests except ABTS radical scavenging activity. In determination of the total flavonoid content of the samples, it is seen that methanol extract has the highest activity in both the flower (0.098  $\text{mg}/\text{mL}$  QAE) and leaf (0.126  $\text{mg}/\text{mL}$  QAE) parts. Similar to all tests, the lowest activity values of flower and leaf were measured in hexane extract with 0.002 and 0.001  $\text{mg}/\text{mL}$  QAE, respectively. The ranking of activity values of the solvent extracts was different from the other tests, and it was M>E>A>ACN>H in flower and M>E>A>ACN>H in leaf.

### 3.2. LC-MS/MS analysis

Phenolic profiles of the leaf and flower parts were identified quantitatively using LC-MS/MS device in their ethanol extracts. In total 20 of phenolic acids and flavonoids compounds were examined and 9 of them were identified in the flower part (caffeic acid, protocatechuic acid, vanillin, salicylic acid, *p*-coumaric acid, rutin, *p*-OH benzoic acid, quercetin and kaempferol) and 5 of them (caffeic acid, vanillin, *p*-coumaric acid, rutin and quercetin) were detected in the leaf (Table 2). The flower part has richer diversity and amount of phenolic compound than the leaf. In addition, caffeic acid, vanillin, rutin and quercetin were detected in both leaf and flower parts of the plant and the highest amount of phenolic compounds in both flower and leaf parts was measured for *p*-coumaric acid with 1.410  $\mu\text{g}/\text{mL}$  and 1.923  $\mu\text{g}/\text{mL}$ , respectively. Also, the rutin was dominant in the leaf (1.923  $\mu\text{g}/\text{mL}$ ). Finally, while the total phenolic content of the flower part of the plant was measured with 5.496  $\mu\text{g}/\text{mL}$ , it was determined as 3.028  $\mu\text{g}/\text{mL}$  in the leaf part.

### 3.3. $\alpha$ -Glucosidase inhibitor effect

The  $\alpha$ -glucosidase inhibition activities ( $\text{IC}_{50}$ ) of ethanol extracts of the flower and leaf parts of *L. mucronatum* subsp. *armenum* and were determined as  $6.10 \pm 0.21$  and  $4.53 \pm 0.12$  respectively (Fig. 1). I added, acarbose activity was measured as  $0.70 \pm 0.06$   $\text{mg}/\text{mL}$ . The lower the  $\text{IC}_{50}$  value is more effective the enzyme inhibition. Therefore,

the enzyme inhibition of the leaf is higher than the flower.

## 4. Discussion

### 4.1. Antioxidant activity

Plants are rich in antioxidants, and it has further increased their importance in research in the field of health and functional food [26]. The activities of natural antioxidants are closely related to their functions. There are many applications for the use of plants with antioxidant activity in food and nutrition fields [27]. The studies about the determination of biological activity and chemical composition of members of the genus *Linum* generally focused on *Linum usitatissimum* L., which is called flaxseed and is the type species of the *Linum* genus [28–30]. However, phenolic content analysis, antioxidant activity determination and enzymatic activity studies have not been conducted on *L. mucronatum* subsp. *armenum*.

Antioxidant activities of solvents extracts in different polarities (methanol, ethanol, acetonitrile, acetone and hexane) of flowers and leaves of *L. mucronatum* subsp. *armenum* were determined using 6 methods. The methanol extract showed the highest antioxidant activity in flowers for all tests except ABTS radical scavenging activity. However, highest antioxidant activity in the leaves was determined in ethanol extract in all tests except tests of ABTS radical scavenging activity and total flavonoid content. In addition, different results were measured for each solvent in the same activity tests. The polarities of the solvents are effective on extraction of phytochemicals [31]. In a previous study, DPPH, ABTS, total antioxidant content, total phenol and flavonoid contents in methanolic extracts of leaf and fruit part extracts of *Linum arboretum* L. were carried out by Yıldız et al. [32] and  $\text{IC}_{50}$  values of leaf parts were calculated for DPPH and ABTS tests as 106.55 and 1144.8  $\mu\text{g}/\text{mL}$ . In the same study, while the total phenol content was measured as 56.96  $\mu\text{g}$  GA  $\text{mg}^{-1}$  and total flavonoid 426.49  $\mu\text{g}$  catechin  $\text{mg}^{-1}$  in the leaf part.

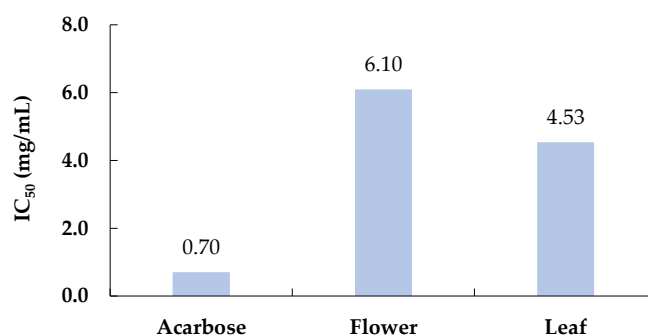


Figure 1.  $\text{IC}_{50}$  values of  $\alpha$ -glucosidase enzyme inhibition of acarbose and flower and leaf parts of the *L. mucronatum* subsp. *armenum*

The DPPH values in leaf part of *L. arboreum* were similar to the values (124 µg/mL) in methanolic extracts of *L. mucronatum* subsp. *armenum* (Table 1). However, in the present study, values of ABTS (555 µg/mL) and total phenolic content (803 µg GAE mL) were significantly higher than the values measured in *L. arboreum*, while the total flavonoid content value (98 µg/mL QAE) was determined in the very low amount. In another study, DPPH (IC<sub>50</sub>) values, total phenol and flavonoid contents of *L. arboreum* were determined as 85.1 µg/mL, 40.7 and 55.4 µg/mg in the herbal methanolic extract [33]. While DPPH values were similar to the results in the present study, the total phenolic and flavonoid content values were significantly lower. Many factors are effective on antioxidant activity values in plants; For example, individual genetic diversity, part of the plant analyzed, post-harvest handling, stage of maturity, variety, climatic conditions, environmental modification processing, and storage [18,34]. FRAP, CUPRAC, total phenolic content and total flavonoid content values measured in same solvent extracts of leaf and flower parts were determined similar to each other. However, this situation was not observed in both DPPH and ABTS measurements. For example, while the DPPH value is 0.17 mg/mL in leaf ethanol extracts, it is 0.02 mg/mL in flowers. Likewise, the ABTS value ethanol extracts, was measured as 0.88 mg/mL in the leaf and 0.21 mg/mL in the flower. It can be explained by the fact that the flowers have high antioxidant activity due to their more pigmentation [35].

#### 4.2. LC-MS/MS analysis

Phenolic compound composition and amounts in the flower and leaf parts of *L. mucronatum* subsp. *armenum* were determined using LC-MS/MS device. The total phenolic content and phenolic composition of the flower was higher than the leaf based on used the phenolic standards (Table 2). *p*-coumaric acid, an organic compound belonging to the hydroxycinnamic acid class [36] was the phenolic compound having the highest amount in both flower and leaf parts with 1.41 and 1.92 µg/mL, respectively. *p*-coumaric acid is mostly found in the cell wall of grasses, fruits and vegetables in the form of esterified or free acid [37,38] In the development of therapeutic drugs, the main aim of most research groups is to use natural and organic compounds, which are known to have no harm or side effects against the environment, humans and all other organisms. *p*-coumaric acid inhibits the growth of bacterial pathogens [37,39] and can be used for these purposes. In addition, the antimelanogenic effects (natural skin lightening) of *p*-coumaric acid from plants have been demonstrated in a variety of experimental investigations, also including human studies [40]. In addition, rutin was determined by the highest amount in flower with 1.19 µg/mL. It is

also known as quercetin-3-O-rutinoside, and vitamin P is a flavonoid found in many foods, beverages, and vegetables. It has biological activity effects such as antioxidant, anti-inflammatory, anti-diabetic, nephroprotective, gastroprotective, neuroprotective and hepatoprotective [41,42]. In both leaf and flower parts of the plants, other phenolic compounds such as caffeic acid having various bioactivity, which is present in many food sources including blueberry, coffee drinks, apple and cider [43,44] and vanillin the main component of natural vanilla, which is common used as an aroma and flavor enhancer in foods [45], and quercetin, which is a powerful antioxidant that protects the plant against biotic and abiotic stress factors were also detected. *p*-coumaric acid and vanillin in both flower and leaf ethanolic extracts of *L. mucronatum* subsp. *armenum* were also detected in *L. usitatissimum* [46].

#### 4.3. $\alpha$ -Glucosidase inhibitor effect

Enzymes, consist of a long chain of amino acids joined by peptide bonds, are biological catalysts in the protein structure responsible for numerous biochemical reactions occurring in the cell [47,48]. Therefore, enzymes are compounds that are necessary for the survival of organisms. Although enzymes are only synthesis in cells, many of them can leave cells and continue to function *in vitro*. Because of these properties, enzymes are used in industry and food production processes, bioremediation and medicine. For example,  $\alpha$ -glucosidase, an important enzyme in the treatment of diabetes, catalyzes the last step of the digestion of carbohydrates [15]. Therefore,  $\alpha$ -glucosidase inhibitors are a class of oral drugs. Thus, in type 2 diabetes, the absorption of carbohydrates from the intestine is reduced by the inhibitor effect and it slowed down the rate of glucose pass into blood in the postprandial state [49]. These type inhibitors have been reported from plant and microbial sources [50]. Plants have an important place among all organisms in terms of showing  $\alpha$ -glucosidase enzyme inhibition. Benella et al. [49] emphasized that natural products isolated from medicinal plants that inhibit  $\alpha$  glucosidase strongly. Within the genus *Linum*, enzyme activity determination studies were mostly carried out on *L. usitatissimum* which is widely known and cultivated. Some of the enzymes studied in this species are as follows: Alkalase [51],  $\beta$ -glucosidase enzyme [52],  $\alpha$ -amylase and  $\alpha$ -glucosidase [53], However, there are no studies on the inhibition of  $\alpha$ -glucosidase enzyme of *L. mucronatum* subsp. *armenum*. In the present study, *In vitro*  $\alpha$ -glucosidase enzyme inhibition was investigated. It was determined that the enzyme inhibition IC<sub>50</sub> value of the leaf (4.53 mg/mL) was higher than in the flower (6.10 mg/mL). Many studies have been carried out to determine the  $\alpha$ -glucosidase enzyme inhibition of plants.

Benella et al. [49], 47 of plant species belonging to 29 families were evaluated in terms of  $\alpha$ -glucosidase enzyme inhibition, and it was reported that their  $IC_{50}$  values varied between 0.9  $\mu\text{g}/\text{mL}$  and 17  $\text{mg}/\text{mL}$ . In other a study, Lawag et al. [54], inhibitor activities of 6 plant species for the same enzyme were reported  $IC_{50}$  values (0.08 and 519.86  $\mu\text{g}/\text{mL}$ ). Assefa et al. [55] classified the natural  $\alpha$ -glucosidase inhibitor compounds with  $IC_{50}$  values according to the data obtained from the literature and it was reported that quercetin ( $IC_{50}$ : 7  $\mu\text{M}$ ) and protocatechuic acid ( $IC_{50}$ : 85.1  $\mu\text{g}/\text{mL}$ ). These both the compounds were identified in leaf and flower ethanolic extracts of the *L. mucronatum* subsp. *armenum*. In addition, it was reported that *p*-coumaric acid [56], caffeic acid [57], rutin [58] phenolics showed significantly  $\alpha$ -glucosidase inhibitor activity. These compounds were identified both the leaf and flower parts of *L. mucronatum* subsp. *armenum*

## 5. Conclusions

Antioxidant activities of the extracts of the leaf and flower of *L. mucronatum* subsp. *armenum* prepared in five different solvents were measured using six different antioxidant activity tests. Extracts have high antioxidant activity. Activity values of leaf and flower parts were different from each other in all solvent extracts due to solvent polarity. In the flower part of the plant, the activity values of the methanol extracts are the highest in all tests except ABTS test (highest value in acetone solvent). The highest activity values in the leaf part were measured in ethanol extracts for all tests, except ABTS (highest value in acetone solvent) and total flavonoid content (highest value in methanol solvent). However, the lowest activity values of both leaf and flower were measured in hexane solvent extract in all tests. When the activity values of the leaf and flower parts were evaluated together, the activity of the leaf part was determined to be higher in all tests except CUPRAC. Vanillin, quercetin, caffeic acid, rutin, *p*- and coumaric acid phenolics were identified in LC-MS/MS analyzes of ethanol extracts of both leaf and flower parts. In addition, *p*-coumaric acid was the compound with the highest amount in both parts. Finally, the total phenolic content of the flower part and leaf part was measured using LC-MS/MS as 5.496  $\mu\text{g}/\text{mL}$  and 3.028  $\mu\text{g}/\text{mL}$ , respectively. The  $\alpha$ -glucosidase inhibition activities ( $IC_{50}$ ) of ethanol extracts of the leaf and flower parts of *L. mucronatum* subsp. *armenum* were determined as  $4.53 \pm 0.12$  and  $6.10 \pm 0.21$  respectively. The results indicate that, leaf and flower parts of the *L. mucronatum* subsp. *armenum* have antioxidant activity and  $\alpha$ -glucosidase enzyme inhibition. Therefore, *L. mucronatum* subsp. *armenum* can also be evaluated as antibacterial,

antifungal, cytotoxic and other enzyme activities. Determine the biological activities of other species, subspecies, and varieties in *Linum* genus, which has a rich taxon diversity in our country will contribute to the design of new biotechnological products.

## Acknowledgement

This study was supported by Gümüşhane University Scientific Research Projects Coordination Unit (GÜBAP), Project no: 21.E0102.07.02. The author also would like to thank Dr. Bülent AKAR for collection of the plant and Dr. Mutlu GÜLTEPE for identification of the plant.

## References

- [1] J. Finaud, G. Lac, E. Filaire, Oxidative stress, Sports Med, 36(4), 2006, 327–358.
- [2] V. Lobo, A. Patil, A. Phatak, N. Chandra, Free radicals, antioxidants and functional foods: Impact on human health, Pharmacogn Rev, 4(8), 2010, 118–126.
- [3] L. Gate, J. Paul, G.N. Ba, K.D Tew, H. Tapiero, Oxidative stress induced in pathologies: the role of antioxidants, Biomed Pharmacother, 53(4), 1999, 169–180.
- [4] Ş. Gökpinar, T. Koray, E. Akçiçek, T. Göksan, Y. Durmaz, Algal Antioksidanlar, E. U. Su Ürünleri Dergisi, 23, 2006, 85–89.
- [5] V. Calabrese, C. Cornelius, A.T. Dinkova-Kostova, E.J. Calabrese, M.P. Mattson, 2010. Cellular stress responses, the hormesis paradigm, and vitagenes: novel targets for therapeutic intervention in neurodegenerative disorders, Antioxid Redox Sign, 13(11), 2010, 1763–1811.
- [6] A.H. Goldfarb, Antioxidants: role of supplementation to prevent exercise-induced oxidative stress, Med Sci Sport Exer, 25(2), 1993, 232–236.
- [7] L.A. Pham-Huy, H. He, C. Pham-Huy, Free radicals, antioxidants in disease and health, Int J Biomed Sci, 4(2), 2008. 89–96.
- [8] S.E. Fernández-Bravo, (2022). Antioxidants in Dentistry: Oxidative Stress and Periodontal Diseases, Lipid Oxidation in Food and Biological Systems, Editor: C. Bravo-Diaz, 2022, Switzerland, Springer Cham.
- [9] F. Shahidi, P. Ambigaipalan, Phenolics and polyphenolics in foods, beverages and spices: Antioxidant activity and health effects—A review, J Funct Foods, 18, 2015, 820–897.
- [10] V. Sindhi, V. Gupta, K. Sharma, S. Bhatnagar, R. Kumari, N. Dhaka, Potential applications of antioxidants—A review, J Pharm Res, 7(9), 2013, 828–835.
- [11] M. López-Pedrouso, J.M. Lorenzo, D. Franco, Advances in natural antioxidants for food improvement, Antioxidants, 11(9), 2022. 1825.
- [12] D.E. Pratt, Natural Antioxidants From Plant Material, Phenolic Compounds in Food and Their Effects on Health II, Editors: M.T. Huang, C.T. Ho, C.Y. Lee, 1992, USA, Am Chem S.
- [13] Z. Akar, Ç. Demir, O. Alkan, Z. Can, B. Akar, LC-MS/MS and RP-HPLC-UV analysis and antioxidant activities of *Arum italicum* Miller edible and nonedible tuber parts, J Anatol Environ Animal Sci, 6(3), 2021, 294–301.
- [14] C. Nirmala, M.S. Bisht, H.K. Bajwa, O. Santosh, Bamboo: A rich source of natural antioxidants and its applications in the food and pharmaceutical industry, Trends Food Sci Tech, 77, 2018. 91–99.
- [15] S. Kumar, S. Narwal, V. Kumar, O. Prakash,  $\alpha$ -glucosidase inhibitors from plants: A natural approach to treat diabetes. Phcog Rev, 5(9), 2011. 19–29
- [16] R. Tundis, M.R. Loizzo, F. Menichini, Natural products as  $\alpha$ -amylase and  $\alpha$ -glucosidase inhibitors and their hypoglycaemic

- potential in the treatment of diabetes: an update, *Mini-Rev Me. Chem*, 10(4), 2010, 315–331.
- [17] Ö. Yılmaz, Türkiye'deki *Linum* L. (Linaceae) türleri üzerinde taksonomik araştırmalar, Doktora Tezi, Uludağ Üniversitesi Fen Bilimleri Enstitüsü, 2009.
- [18] Z. Akar, Chemical compositions by using LC–MS/MS and GC–MS and antioxidant activities of methanolic extracts from leaf and flower parts of *Scabiosa columbaria* subsp. *columbaria* var. *columbaria* L, *Saudi J Biol Sci*, 28(11), 2021, 6639–6644.
- [19] W. Brand-Williams, M.E. Cuvelier, C.L.W.T. Berset, Use of a free radical method to evaluate antioxidant activity, *LWT - Food Sci Tech*, 28(1), 1995, 25–30.
- [20] I.F. Benzie, J.J. Strain, The ferric reducing ability of plasma (FRAP) as a measure of “antioxidant power”: the FRAP assay, *Anal Biochem*, 239(1), 1996, 70–76.
- [21] R. Apak, K. Güçlü, M. Özyürek, S.E. Karademir, Novel total antioxidant capacity index for dietary polyphenols and vitamins C and E, using their cupric ion reducing capability in the presence of neocuproine: CUPRAC method, *J Agric Food Chem*, 52(26), 2004, 7970–7981.
- [22] R. Re, N. Pellegrini, A. Proteggente, A. Pannala, M. Yang, C. Rice-Evans, Antioxidant activity applying an improved ABTS radical cation decolorization assay, *Free Radic Biol Med*, 26(9–10), (1999), 1231–1237.
- [23] K. Slinkard, V.L. Singleton, Total phenol analysis: automation and comparison with manual methods, *Am J Enol Viticult*, 28(1), 1977, 49–55.
- [24] L. R., Fukumoto, G. Mazza, Assessing antioxidant and prooxidant activities of phenolic compounds, *J Agric Food Chem*, 48(8), 2000, 3597–3604.
- [25] Z. Yu, Y. Yin, W. Zhao, J. Liu, F. Chen, Anti-diabetic activity peptides from albumin against  $\alpha$ -glucosidase and  $\alpha$ -amylase, *Food Chem*, 135(3), 2012, 2078–2085.
- [26] M. Loi, C. Paciolla, Plant antioxidants for food safety and quality: Exploring new trends of research, *Antioxidants*, 10(6), 2021, 972.
- [27] D. Dziki, R. Różyło, U. Gawlik-Dziki, M. Świeca, Current trends in the enhancement of antioxidant activity of wheat bread by the addition of plant materials rich in phenolic compounds, *Trends Food Sci Tech*, 40(1), 2014, 48–61.
- [28] W. Fedeniuk, R.C.G. Biliaderis, Composition and physicochemical properties of linseed (*Linum usitatissimum* L.) mucilage, *J Agric Food Chem*, 42(2), 1994, 240–247.
- [29] A.J. Jhala, L.M. Hall, Flax (*Linum usitatissimum* L.): current uses and future applications, *Aust J Basic Appl Sci*, 4(9), 2010, 4304–4312.
- [30] X. Li, J. Li, S. Dong, Y. Li, L. Wei, C. Zhao, J. Li, X. Liu, Y. Wang, Effects of germination on tocopherol, secoisolaricresinol diglucoside, cyanogenic glycosides and antioxidant activities in flaxseed (*Linum usitatissimum* L.), *Int J Food Sci Tech*, 54(7), 2019, 2346–2354.
- [31] H. Nawaz, A.M. Shad, N. Rehman, H. Andaleeb, N. Ullah, Effect of solvent polarity on extraction yield and antioxidant properties of phytochemicals from bean (*Phaseolus vulgaris*) seeds, *Brazilian J Pharm Sci*, 56, 2020, e17129.
- [32] G. Yıldız, C. Aktürk, M. Özerkan, Ö. Yılmaz, Free radical scavenging activity and antioxidant contents of *Linum arboreum* L. (Linaceae), *KSU J Agric Nat*, 22 (1), 2019, 16–23.
- [33] Z. Sultan, *Linum arboreum* üzerinde farmakognozik çalışmalar, Master Thesis, Ankara University, Institute of Health Sciences, 2020.
- [34] S. Sreelatha, P.R. Padma, Antioxidant activity and total phenolic content of *Moringa oleifera* leaves in two stages of maturity, *Plant Foods Hum Nutr*, 64(4), 2009, 303–311.
- [35] S. Benvenuti, E. Bortolotti, R. Maggini, Antioxidant power, anthocyanin content and organoleptic performance of edible flowers, *Scientia Horti*, 199, 2016, 170–177.
- [36] N. Schultheiss, M. Roe, S.X.M. Boerrigter, Cocrystals of nutraceutical *p*-coumaric acid with caffeine and theophylline: polymorphism and solid-state stability explored in detail using their crystal graphs, *Cryst Eng Comm*, 13(2), 2011, 611–619.
- [37] Z. Lou, H., Wang, S. Rao, J. Sun, C. Ma, J. Li, *p*-Coumaric acid kills bacteria through dual damage mechanisms, *Food Control*, 25(2), 2012, 550–554.
- [38] H. Boz, *p*-Coumaric acid in cereals: presence, antioxidant and antimicrobial effects, *Int J Food Sci*, 50(11), 2015, 2323–2328.
- [39] M. Matejczyk, R. Swislocka, M. Kalinowska, G. Widderskp, W. Lewandowski, A. Jablonska-Trypuo, S.J. Rosochacki, *In vitro* evaluation of biological activity of cinnamic, caffeic, ferulic and chlorogenic acids with use of *Escherichia coli* K-12 recA: gfp biosensor strain, *Acta Pol Pharm*, 74(3), (2017). 801–808.
- [40] Y.C. Boo, *p*-Coumaric acid as an active ingredient in cosmetics: A review focusing on its antimelanogenic effects, *Antioxidants*, 8(8), 2019, 275.
- [41] H. Hosseinzadeh, M. Nassiri-Asl, Review of the protective effects of rutin on the metabolic function as an important dietary flavonoid, *J Endocrinol Invest*, 37(9), 2014, 783–788.
- [42] A. Ghorbani, Mechanisms of antidiabetic effects of flavonoid rutin, *Biomed Pharmacother*, 96, 2017, 305–312.
- [43] C. Magnani, V.L.B. Isaac, M.A. Correa, H.R.N. Salgado, Caffeic acid: a review of its potential use in medications and cosmetics, *Anal Methods*, 6(10), 2014, 3203–3210.
- [44] F. Armutcu, S. Akyol, S. Ustunsoy, F.F. Turan, Therapeutic potential of caffeic acid phenethyl ester and its anti-inflammatory and immunomodulatory effects, *Exp Ther Med*, 9(5), 2015, 1582–1588.
- [45] A.K. Sinha, U.K. Sharma, N. Sharma, A comprehensive review on vanilla flavor: extraction, isolation and quantification of vanillin and others constituents, *Int J Food Sci Nutr*, 59(4), 2008, 299–326.
- [46] H. Han, H. Yılmaz, I. Gülçin, Antioxidant activity of flaxseed (*Linum usitatissimum* L.) shell and analysis of its polyphenol contents by LC-MS/MS, *Rec Nat Prod*, 12(4), 2018, 397–402.
- [47] S. Kermasha, M.N. Eskin, Selected industrial enzymes, *Enzymes*, Editors: S. Kermasha, M.N. Eskin, 2021, Academic Press.
- [48] C. López-Otín, J.S. Bond, Proteases: multifunctional enzymes in life and disease, *J Biol Chem*, 283(45), 2008, 30433–30437.
- [49] W. Benalla, S. Bellahcen, M. Bnouham, Antidiabetic medicinal plants as a source of  $\alpha$ -glucosidase inhibitors, *Curr Diabetes Rev*, 6(4), 2010, 247–254.
- [50] S. Ganesan, S. Raja, P. Sampathkumar, K. Sivakumar, T. Thangaradjou, Isolation and screening of  $\alpha$ -glucosidase enzyme inhibitor producing marine actinobacteria, *Afr J Microbiol Res*, 5(21), 2011, 3437–3445.
- [51] C. Wei, K., Thakur, D., Liu, J. Zhang, Z. Wei, Enzymatic hydrolysis of flaxseed (*Linum usitatissimum* L.) protein and sensory characterization of Maillard reaction products, *Food Chem*, 263, 2018, 186–193.
- [52] M.A. Fieldes, K.E. Gerhardt, Developmental and genetic regulation of  $\beta$ -glucosidase (linamarase) activity in flax seedlings, *J Plant Physiol*, 158, 2001, 977–989.
- [53] M. Bhat, S.S. Zinjarde, S.Y. Bhargava, A.R. Kumar, Joshi, B.N. Antidiabetic Indian plants: a good source of potent amylase inhibitors, *Evid-Based Compl Alt*, 2011, 810207.
- [54] I.L. Lawag, A.M. Aguinaldo, S. Naheed, M. Mosihuzzaman,  $\alpha$ -Glucosidase inhibitory activity of selected Philippine plants, *J Ethnopharmacol*, 144(1), 2012, 217–219.
- [55] S.T. Assefa, E.Y. Yang, S.Y. Chae, M. Song, J. Lee, M.C. Cho, S. Jang,  $\alpha$ -Glucosidase Inhibitory Activities of Plants with Focus on Common Vegetables, *Plants*, 9(1), 2019, 2.
- [56] K. Pei, J. Ou, J. Huang, S. Ou, *p*-Coumaric acid and its conjugates: dietary sources, pharmacokinetic properties and biological activities, *J Sci Food Agric*, 96(9), 2016, 2952–2962.
- [57] G. Oboh, O.M. Agunloye, S.A. Adefegha, A.J. Akinyemi, A.O. Ademiluyi, Caffeic and chlorogenic acids inhibit key enzymes linked to type 2 diabetes (*in vitro*): a comparative study, *J Basic Clin Physiol Pharmacol*, 26(2), 2015, 165–170.

- [58] S. Dubey, A. Ganeshpurkar, A. Ganeshpurkar, D Bansal, N. Dubey, Glycolytic enzyme inhibitory and antiglycation potential of rutin, *Future J Pharm Sci*, 3(2), 2017, 158–162.